UAB
Universitat Autònoma de Barcelona

# Characterization of the secretome of adipose tissues in adipocyte-specific PGC-1α/β knockout mice and its implication in the control of glucose homeostasis

**Marc Velilla Cajo**

# Characterization of the secretome of adipose tissues in adipocyte-specific PGC-1α/β knockout mice and its implication in the control of glucose homeostasis

***Marc Velilla Cajo***

*Doctoral Thesis*

*Barcelona, 2023*

Laboratory of Metabolism and Obesity
Unit of Diabetes and Metabolism
Vall d'Hebron Research Institute

Department of Biochemistry and Molecular Biology
Autonomous University of Barcelona

# Characterization of the secretome of adipose tissues in adipocyte-specific PGC-1α/β knockout mice and its implication in the control of glucose homeostasis

***Marc Velilla Cajo***

Thesis submitted for the Degree of Doctor in Biochemistry, Molecular Biology and Biomedicine

Barcelona, 2023

Josep A. Villena Delgado
*Thesis director*

Miquel Vila Bover
*Tutor*

Marc Velilla Cajo

# ACKNOWLEDGMENTS / AGRAÏMENTS

"*I en l'acceptació del canvi hi resideix l'alegria de la vida*"

Un canvi que ara culmino. Han estat mesos, anys, de lluitar per una causa, d'adaptar-me als condicionants, de ser resistent i resilient. Ara toca creuar la línia, aixecar al cap i abandonar-me a la incertesa d'un futur que desitjo ja encarar. No sé quant he après de ciència durant aquesta travessa, però m'emporto el coneixement de la vida viscuda durant aquest temps, les experiències acumulades i les persones trobades. La tesis, només per això, ja val la pena haver-la fet.

Escric per recordar i complaure'm d'aquest període, així que vull citar i agrair a totes les persones que, amb major o menor intensitat, m'han acompanyat durant la tesis i me l'han fet una mica més plaent.

**Pep,** moltes gràcies per haver-me dirigit tot aquest temps i per haver-me ensenyat, més enllà de la bona ciència, el rigor de la feina ben feta, a ser autònom i coordinar tasques importants i el gaudir de l'aprenentatge. La teva confiança al triar-me pel projecte em va obrir la porta a totes les experiències viscudes a posteriori, fet que sempre t'agrairé. **Rosi,** has jugat molts papers durant la meva estança al laboratori, tant des de la vessant més acadèmica i científica com la més humana i emocional. Et dec moltes hores al meu costat ensenyant-me, ajudant-me a tirar els experiments endavant i, fent equip, hemos llevado a los DKO a lo más alto ;). Més enllà de la ciència, el que realment m'emporto d'haver-te conegut i treballat amb tu és tot el teu afecte, la teva bondat i l'amistat que hem creat dins i fora del lab. De tu he après moltes coses, més de les que segurament t'hagi agraït, però sé que, on vagi, les teves lliçons vitals m'acompanyaran i em serviran de far. Amb tot, et trobaré a faltar Rosi. Acabant la triada del 144, **Maria,** saps que vas ser, ets i seràs un gran suport en els meus projectes laborals i vitals. Ets la meva millor amiga i, de cada conversa, riure, llàgrima o malestar que hàgim pogut compartir, n'hem tret un moment íntim. Vaig venir al laboratori en bona manera per la teva presència, però me n'alegro de que la nostra amistat s'hagi forjat tant fortament fora de la ciència. Tens un amic al teu costat que t'acompanyarà fins al darrer moment.

Moltes persones boniques han passat pel laboratori durant la meva estança. M'agradaria fer-vos un escrit a tots, ja que n'he après de cada un de vosaltres, cadascú a la seva manera, però després d'escriure la tesis m'he quedat buit de paraules. Us agraeixo els bons moments compartits, la paciència amb mi, el haver-me acompanyat en aquest viatge i el poder ara escriure-us aquestes línies, ja que són la prova de l'afabilitat compartida i del record que us tinc a tots. En ordre alfabètic: **Aleix, Andrea, Belén, Caio, Clàudia, Ingrid, Isabella, Júlia, Laura, Lucía, Meri i Pedro**, moltes gràcies a tots i a totes.

Dels veïns també se'n gaudeix, sobretot quan compartiu tants espais, hores i moments plegats. **Patri,** t'agraeixo la proximitat que vas donar-me des del moment zero, l'oferiment de suport i les petites converses que, de forma improvisada, hem tingut sobre afers de la vida.

**Huguito,** o pseudomarc segons qui et miri, trobaré a faltar les nostres converses, la proximitat trobada durant aquests anys i el temps que ens hem donat en tants moments. Ets una gran persona i me n'alegro moltíssim d'haver compartit aquesta època de la nostra vida. A distància i sense veure'ns tant, però continuarem mantenint la bonica amistat i sent còmplices amb l'altre. **Anna,** sento que, amb més temps junts i en unes altres circumstàncies, encara podríem haver-nos unit més. Ets una gran persona i tens molt potencial, així que enyoraré la teva proximitat, vitalitat i el teu respecte cap als demés. **Jordi,** trobaré a faltar els riures compartits, les anades d'olla i els moments casuals trobats per gaudir plegats. M'has cuidat, literalment, i m'has fet sentir com a casa dins del laboratori. Per últim, **David,** estic content d'haver-te conegut i pogut passar bons moments al teu costat, ja que penso que tens molt a dir i a compartir. Del vostre laboratori també vull anomenar en **Joel,** que des de la distància del temps, et recordo com un gran company i, quan ens hem retrobat, com una bonica persona amb qui he connectat.

Dins del VHIR m'agradaria mencionar moltes més persones que, molt o poc, m'han regalat un somriure, un bon dia o amb els qui he tingut i tinc una bonica amistat. Sabeu qui sou, però vull mencionar a la **Marta Barber,** a **l'Adri,** a la **María Dema** i a tots els demés companys i companyes que m'heu alegrat els dies al VHIR. Així mateix, gràcies a **l'Andrés,** la **Eulàlia**, la **Rosa** i altres membres d'estructura per ajudar-me en molts moments i fer-me sentir a gust.

El doctorat no només és una feina o un aprenentatge acadèmic, si no que transcendeix les parets del laboratori i te l'emportes a casa, on el mastegues i el comparteixes amb els teus. **Natasha,** t'agraeixo molt la comprensió, la estima i el suport que m'has donat durant tots aquests mesos. Ets la meva companya de viatge, però de vegades en el trajecte ens trobem amb obstacles que costen d'assimilar. Hem viscut una temporada de lluita enfront d'adversitats alienes, començant per la tesis i acabant per d'altres de personals. Tu hi has estat en totes de forma incommensurable. Saps tot el que sento de boca, però vull deixar escrit que has estat, ets i desitjo que siguis, la qui m'acompanya en totes les etapes de la meva vida. Amb tu, també vull recordar a la **Debbie**, al **Fèlix** i a la **Eileen,** que s'han preocupat en molts moments per mi, m'han cuidat i m'han fet gaudir oblidant les penes del doctorat.

**Papes,** gràcies a vosaltres he arribat fins aquí. M'heu donat les eines i l'educació per avançar acadèmicament, però sobretot m'heu ensenyat uns valors que m'han fet créixer com a individu i dels quals n'estic ben orgullós. Heu estat allà durant tot el recorregut de la tesis i, des de la distància, m'heu donat forces per avançar. Aquest doctorat és tant vostre com meu, així que espero que us sentiu orgullosos d'ell com jo ho estic de vosaltres. **Iaio, iaies,** no esteu ni ho sabeu, però en tot el camí m'heu acompanyat. Us he anat perdent mentre m'anava fent doctor, però això m'ha servit per recordar-vos encara més i trobar-vos a faltar. **Tiet, Dídac, Ona, Gemma,** sou la meva família i una estima imprescindible per donar valor humà a la meva vida més enllà de la feina.

A tots els meus amics i amigues, a tots els qui heu estat al meu costat durant aquesta etapa i m'heu donat sentit a la lluita, sabeu que sou molt importants per mi i que formeu part de la meva vida més enllà d'aquest doctorat. **Àlex, Marc, Robert, Sergi, Viktoria,** amics íntims i quasi germans, aquest moment de goig el comparteixo amb vosaltres, com tant d'altres en vull compartir al llarg del nostre viatge. **Bart, Clara, Ivette, Manuel, Mar, Omar,** gràcies també

per acompanyar-me, poder compartir amb tots vosaltres aquesta etapa i celebrar l'amistat que ens uneix.

No vull deixar d'agrair també a totes les persones, entitats i casuístiques que m'han dificultat tirar endavant la tesis. Podria haver-la fet sense certs maldecaps, però això dona més valor al fet de que l'hagi aconseguit acabar. Enfront del got mig buit, posa-li aigua.

En definitiva, gràcies a tothom que ha estat al meu costat, durant el doctorat i en general a la meva vida. Penso que no em deixo a ningú, però si és el cas, sento tenir tanta mala memòria i espero ser disculpat.

# TABLE OF CONTENTS

# ABBREVIATIONS

| | |
|---|---|
| **18F-FDG** | fluorine 18-fluorodeoxyglucose |
| **12,13-diHOME** | 12,13-dihydroxy-octadecenoic acid |

## A

| | |
|---|---|
| **AC** | adenylate cyclase |
| **Aco2** | aconitase 2 |
| **AdipoQ** | adiponectin |
| **Adrb33** | adrenergic beta3 receptor |
| **AKT/PKB** | serine-threonine kinase 1/protein kinase 1 |
| **ANGPTL8** | angiopoietin-like 8 |
| **ANOVA** | analysis of variance |
| **Arx** | aristaless related homebox |
| **AT** | adipose tissues |
| **ATF3** | activating transcription factor 3 |
| **ATF6** | activating transcription factor 6 |
| **ATM** | adipose tissue macrophages |
| **ATP** | adenosine triphosphate |
| **ATP5B** | ATP synthase f1 subunit B |
| **Atp5b** | ATP synthase 5b |
| **AU** | arbitrary units |
| **AUC** | area under the curve |

## B

| | |
|---|---|
| **BAT** | brown adipose tissue |
| **BCA** | bicinchoninic acid |
| **BMI** | body mass index |
| **BMP4** | bone morphogenetic protein 4 |
| **BMP7** | bone morphogenetic protein 7 |
| **BMP8b** | bone morphogenetic protein 8b |
| **BSA** | bovine serum albumin |

## C

| | |
|---|---|
| **CAM** | carbamidomethylation |
| **cAMP** | cyclic adenosine monophosphate |
| **Ccl2** | C-C motif chemokine ligand 2 |
| **Ccl7** | C-c motif chemokine ligand 7 |
| **Cdc11/Itgax** | integrin subunit alpha x |
| **cDNA** | complementary DNA |
| **CEEA** | animal testing ethics committee |
| **Cfd** | complement factor D |
| **Chop/Ddit3** | damage inducible transcript 3 |
| **Cidea** | cell death inducing DFFA like effector A |

| | |
|---|---|
| **Cox7a1** | cytochrome c oxidase subunit 7a1 |
| **Coxii** | cytochrome c oxidase subunit ii |
| **Coxiv** | cytochrome c oxidase subunit iv |
| **CREB** | cAMP responsive element binding protein |
| **CT** | computerized tomography |
| **Cxcl14** | C-X-C motif chemokine ligand-14 |
| **Cycs/Cytc** | cytochrome c |
| **Cypa** | cyclophilin A |

## D

| | |
|---|---|
| **DAG** | diacylglycerols |
| **DAPI** | 4',6-diamidino-2-phenylindole |
| **DAVID** | database for annotation, visualization and integrated discovery |
| **DEPC** | diethyl pyrocarbonate |
| **Dio2** | deiodinase-2 |
| **DM** | diabetes mellitus |
| **DMEM** | dulbecco's modified eagle medium |
| **DMSO** | dimethyl sulfoxide |
| **DNA** | deoxyribonucleic acid |
| **dNTP** | deoxynucleotide triphosphates |
| **DTT** | Dithiothreitol |

## E

| | |
|---|---|
| **EBF2** | early B-cell factor 2 |
| **EBP** | CCAAT/enhancer-binding proteins |
| **ECM** | extracellular matrix |
| **EDTA** | ethylenediaminetetraacetic acid |
| **eIF2** | eukaryotic initiation factor 2 |
| **ELISA** | enzyme linked immunosorbent assay |
| **EOS** | empirical observability score |
| **EPDR1** | ependymin-related protein 1 |
| **ER** | endoplasmic reticulum |
| **ERRα** | estrogen-related receptor α |
| **ERRγ** | estrogen-related receptor γ |

## F

| | |
|---|---|
| **FA** | formic acid |
| **FABP4** | fatty acid-binding protein 4 |
| **FBS** | foetal bovine serum |
| **FC** | fold change |
| **FFA** | free fatty acids |
| **FFAR** | free fatty acids receptor |
| **FGF2** | fibroblast growth factor 2 |
| **FGF21** | fibroblast growth factor 21 |

| | | |
|---|---|---|
| | **Foxo1** | forkhead box O1 |
| | **FSTL1** | follistatin like-1 |
| **G** | | |
| | **GA** | glutaraldehyde |
| | **Gapdh** | glyceraldehyde-3-phosphate dehydrogenase |
| | **Gcg** | glucagon |
| | **Gck** | glucokinase |
| | **GDF8** | growth differentiation factor 8 |
| | **GDM** | gestational diabetes mellitus |
| | **GIP** | gastric inhibitory peptide |
| | **GLP-1** | glucagon-like peptide 1 |
| | **Glp-1r** | GLP-1 receptor |
| | **Glut1** | glucose transporter 1 |
| | **Glut2** | glucose transporter 2 |
| | **GSIS** | glucose-stimulated insulin secretion |
| | **gWAT** | gonadal WAT |
| **H** | | |
| | **HBSS** | hanks balanced salt solution |
| | **HEPES** | 4-(2-hydroxyethyl)-1-piperazineethanesulfonic acid |
| | **HFD45** | high-fat diet 45% Kcal from fat |
| | **HFD60** | high-fat diet 60% Kcal from fat |
| | **HHEX** | haematopoietically expressed homeobox |
| | **Hox9** | homebox 9 |
| | **Hprt1** | hypoxanthine phosphoribosyltransferase 1 |
| | **HSL** | hormone sensitive lipase |
| **I** | | |
| | **IAA** | iodoacetamide |
| | **Iapp** | islet amyloid polypeptide |
| | **IC** | insulin content |
| | **IDIBELL** | biomedical research institute of bellvitge |
| | **IGFBP2** | insulin-like growth factor-binding protein 2 |
| | **Igfbp3** | insulin-like growth factor-binding protein 3 |
| | **IKKβ** | inhibitor of NF-κB kinase |
| | **IL-1β** | interleukin 1β |
| | **IL-6** | interleukin 6 |
| | **IL-6R** | IL-6 receptor |
| | **Ins1** | insulin 1 |
| | **Ins2** | insulin 2 |
| | **IpGTT** | intraperitoneal GTT |
| | **IpITT** | intraperitoneal ITT |

| | | |
|---|---|---|
| | **IR** | insulin resistance |
| | **IRE-1** | inositol requiring enzyme 1 |
| | **IRS-1** | insulin receptor substrate 1 |
| | **IRS-2** | insulin receptor substrate 2 |
| | **IRX1/2** | iroquois homebox 1 and 2 |
| | **iWAT** | inguinal WAT |
| **J** | **JNK1** | c-Jun N-terminal kinase |
| **K** | **KAT2A** | lysine acetyltransferase 2A |
| | **KRBH** | krebs-ringer bicarbonate hepes |
| **L** | **LCFA** | long-chain fatty acids |
| | **LC-MS/MS** | liquid chromatography–mass spectrometry |
| | **Lhx8** | lim homebox 8 |
| | **LTQ** | linear and quadruple ion trap |
| **M** | **Mafa** | MAF BZIP transcription factor A |
| | **Mafb** | MAF BZIP transcription factor B |
| | **MCP-3** | monocyte chemoattractant |
| | **Mdh2** | malate dehydrogenase 2 |
| | **Meox2** | mesenchyme homebox 2 |
| | **mRNA** | messenger RNA |
| | **mtDNA** | mitocondrial DNA |
| | **MUNC** | syntaxin binding protein |
| | **MYF5** | myogenic factor 5 |
| | **MYOD** | myogenic differentiation D |
| **N** | **NAFLD** | non-alcoholic fatty liver disease |
| | **NCBI** | national center for biotechnology information |
| | **Nd2** | NADH:Ubiquinone oxidoreductase core subunit 2 |
| | **Ndufb9** | ADH:Ubiquinone oxidoreductase subunit B9 |
| | **NE** | norepinephrine |
| | **NEFA** | non-esterified fatty acids |
| | **NEUROD1** | neuronal differentiation 1 |
| | **NGF** | nerve growth factor |
| | **NGN3** | neurogenin 3 |
| | **NKX6.1** | NK6 homebox 1 |
| | **Nos2** | nitric oxid synthase 2 |

| | |
|---|---|
| **NRF1/2** | nuclear respiratory factors 1 and 2 |
| **NRG4** | neuroregulin 4 |

## O

| | |
|---|---|
| **OD** | optical density |
| **OGTT** | oral GTT |

## P

| | |
|---|---|
| **Pax4** | paired box 4 |
| **Pax6** | paired box 6 |
| **PBS** | phosphate buffer saline |
| **PC1** | principal component 1 |
| **PC2** | principal component 2 |
| **PCA** | principal component analysis |
| **PCR** | polymerase chain reaction |
| **Pcsk1** | proprotein convertase subtilisin/kexin type 1 |
| **Pcsk2** | proprotein convertase subtilisin/kexin type 2 |
| **Pdk1** | pyruvate dehydrogenase kinase 1 |
| **Pdk4** | pyruvate dehydrogenase kinase 4 |
| **PDX1** | pancreatic and duodenal homebox 1 |
| **PERK** | PKR-like ER kinase |
| **PET** | positron emission tomography |
| **PFA** | paraformaldehyde |
| **PGC-1α/Ppargc1a** | PPARG co-activators 1 alpha |
| **PGC-1β/Ppargc1b** | PPARG co-activators 1 beta |
| **PGC-1α/β-FAT-DKO** | double-knockout mice for PGC-1α/β in adipose tissues |
| **PI-3K** | phosphatidylinositol 3-kinase |
| **PK** | proteinase K |
| **PKA** | protein kinase A |
| **PKC** | protein kinase C |
| **PM** | post meridiem |
| **PP** | pancreatic polypeptide |
| **PPARα** | peroxisome-proliferator activated receptor α |
| **PPARγ** | peroxisome proliferator activated receptor γ |
| **PPARδ** | peroxisome-proliferator activated receptor δ |
| **PRC** | PPARγ related co-activator |
| **PRDM16** | PR/SET domain 16 |
| **PRM** | parallel reaction monitoring |
| **PSS** | predicted suitability score |

## R

| | |
|---|---|
| **RAB27** | ras-related protein 28 |
| **RAB3** | ras-related protein 3 |
| **RBP4** | retinol-binding protein 4 |

| | |
|---|---|
| **RCDC** | reducing agent and detergent compatible |
| **RER** | rough endoplasmic reticulum |
| **RIM** | synaptic membrane exocytosis |
| **RIPA** | radio-immunoprecipitation assay |
| **RNA** | ribonucleic acid |
| **ROI** | region of interest |
| **ROS** | reactive oxygen species |
| **RP** | reserve pool |
| **RPM** | revolutions per minute |
| **RPMI** | roswell park memorial institute |
| **RRP** | ready releasable pool |
| **RT** | reverse transcriptase |
| **RT-qPCR** | reverse transcription quantitative PCR |

## S

| | |
|---|---|
| **SAGE** | serial analysis of gene expression |
| **Sdhb** | succinate dehydrogenase subunit B |
| **SDS** | sodium dodecyl sulfate |
| **SEM** | standard error of the mean |
| **SFM** | serum free media |
| **SNAP25** | synaptosome associated protein 25 |
| **SPARC** | secreted protein acid and cysteine rich |
| **Sst** | somatostatin |
| **SSTR** | somatostatin receptor |
| **STX** | syntaxin |
| **Stx1a** | syntaxin 1A |
| **SVF** | stromal vascular fraction |
| **Syp** | synaptophysin |

## T

| | |
|---|---|
| **T1D** | type 1 diabetes |
| **T2D** | type 2 diabetes |
| **TAE** | tris-acetate-EDTA |
| **TAG** | triglycerides |
| **TCA** | tricarboxylic acid |
| **Tcf21** | transcription factor 21 |
| **TEM** | transmission electron microscopy |
| **TFAM** | mitochondrial transcription factor A |
| **TFB1M** | mitochondrial transcription factor B1 |
| **TFB2M** | mitochondrial transcription factor B2 |
| **TGN** | trans-golgi network |
| **TLR4** | toll-like receptors 4 |
| **TNFR** | TNFα receptor |
| **TNFα** | tumor necrosis factor α |
| **Tris-HCl** | Tris(hydroxymethyl)aminomethane hydrochloride |

| | | |
|---|---|---|
| **U** | **UAB** | autonomous university of Barcelona |
| | **Ucp1** | uncoupling protein 1 |
| | **UCSC** | university of California Santa Cruz |
| | **Unc13b** | unc-13 homolog B |
| | **UPR** | unfolded protein response |
| | **Uqcrq10** | ubiquinol-cytochrome c reductase subunit 10 |
| | **UTIP** | unity of pancreatic islets transplants |
| **V** | **VAMP** | vesicle associated membrane protein |
| | **Vamp2** | vesicle associated membrane protein 2 |
| | **VEGFA** | vascular endothelial growth factor A |
| | **VERSEDA** | vertebrate secretome database |
| | **VGCC** | voltage-gated calcium channels |
| | **VHIO** | vall d'Hebron oncology institute |
| | **VHIR** | vall d'Hebron research institute |
| **W** | **WAT** | white adipose tissue |
| | **WNT** | wingless and int |
| | **WT** | wild type |
| **X** | **Xbp1** | x-box binding protein 1 |
| **Z** | **ZFP** | zinc finger protein |
| | **Zic1** | zic family member 1 |

# ABSTRACT

The development of metabolic diseases such as obesity and *type 2 diabetes (*T2D*)* is firmly correlated with the loss-of-function of *white adipose tissue (WAT)*, in agreement with its regulatory role on energy balance and glucose homeostasis. By contrast, *brown adipose tissue (*BAT*)* mass and function inversely correlate with WAT accretion and insulin resistance. Recently, BAT has emerged as an endocrine organ secreting a myriad of molecules that are involved in health and disease. To gain insight into the contribution of BAT to glucose homeostasis, in a previous study from our lab we generated an adipocyte-specific mouse model devoid of PGC-1α/PGC-1β, the master regulators of mitochondriogenesis and brown adipocyte differentiation (PGC-1α/β-FAT-DKO mice). Adipose tissues from these mice displayed an impaired mitochondrial biogenesis and oxidative capacity. Despite being cold intolerant, they did not develop obesity or insulin resistance. When fed a *high-fat diet (*HFD*)* with a 45% of Kcal from fat, PGC-1α/β-FAT-DKO mice were prone to glucose intolerance despite preserving insulin sensitivity.

To further explore glucose intolerance in PGC-1α/β-FAT-DKO mice, we subjected them to a diet with a higher content of fat (HFD60 or 60% Kcal from fat). PGC-1α/β-FAT-DKO mice gained more weight over time, which correlated with an accumulation of fat in BAT. Moreover, fat deposition in BAT was accompanied by the up-regulation of classical WAT markers, thereby indicating a process of "whitening" of the tissue. These mice preserved insulin sensitivity but developed severe glucose intolerance independently of body weight gain. However, basal and glucose-stimulated serum c-peptide levels were decreased in PGC-1α/β-FAT-DKO mice. Altogether, these data pointed towards a pancreatic defect involving insulin secretion.

Morphometric analysis of pancreatic islets by immunofluorescence and transmission electron microscopy did not reveal differences in β-cell mass, islet size or the maturation of β-cell insulin granules between PGC-1α/β-FAT-DKO and Wt control mice. Similarly, gene expression analysis of pancreatic islets did not unmask a dysregulation in the expression of genes encoding for proteins involved in the secretion of insulin in pancreatic β-cells. The assessment of insulin secretion directly on isolated pancreatic islets indicated that responsiveness to glucose was preserved in PGC-1α/β-FAT-DKO mice despite having lower serum insulin levels.

Impaired glucose homeostasis in PGC-1α/β-FAT-DKO mice suggested the establishment of an adipose-pancreatic crosstalk. To study this relation, we performed a proteomic study of adipose tissues secretome. *Untargeted* proteomics revealed notable differences between Wt and PGC-1α/β-FAT-DKO mice in BAT but not in WAT. *Targeted* proteomics allowed us to discern the proteins differently secreted by BAT from PGC-1α/β-FAT-DKO mice that could exert an endocrine role on pancreas. *In vitro* analysis of resistin, however, did not clarify its contribution to the regulation of insulin secretion.

Taking together, our data indicate that the lack of PGC-1s alters BAT endocrine function, ultimately leading to altered glucose homeostasis as a result of a, yet unmasked, pancreatic defect.

# RESUM

El desenvolupament de malalties metabòliques com ara la obesitat i la diabetis tipus 2 es relaciona fermament amb la pèrdua de funció del teixit adipós blanc, d'acord amb el seu rol en el balanç energètic i la homeòstasis de la glucosa. Pel contrari, la massa i la funció del teixit adipós marró es relacionen inversament amb la acreció del WAT i la resistència a la insulina. Recentment, el teixit adipós marró ha emergit com un òrgan endocrí capaç de secretar un conjunt de molècules involucrades en la salut i en la malaltia. Per aprofundir en la contribució del teixit adipós marró a la homeòstasis de la glucosa, en un estudi previ del nostre laboratori vam generar un model animal específic de teixit adipós en el qual vam suprimir els PGC-1α/PGC-1β, reguladors primordials de la mitocondriogènesis i de la diferenciació del teixit adipós marró (ratolins PGC-1α/β-FAT-DKO). Els teixits adiposos d'aquests ratolins mostraven una biogènesis mitocondrial i funció oxidativa deteriorades. Tot i ser intolerants al fred, aquests animals no desenvolupaven obesitat o resistència a la insulina. Quan se'ls va alimentar amb una dieta rica en grassa (45% Kcal provinents de la grassa), els ratolins PGC-1α/β-FAT-DKO mostraven una tendència a ser intolerants a la glucosa, encara que mantenien la sensibilitat a la insulina.

Per tal d'aprofundir en l'estudi de la intolerància a la glucosa en els ratolins PGC-1α/β-FAT-DKO, els vam alimentar amb una dieta amb un major contingut de grassa (60% Kcal provinents de la grassa). Els ratolins PGC-1α/β-FAT-DKO van guanyar més pes amb el temps de dieta, relacionant-se amb una acumulació de grassa en el teixit adipós marró. A més, la deposició de grassa en aquest teixit es va acompanyar d'una sobreexpressió de marcadors típics de teixit adipós blanc, indicant un procés de blanquejament del teixit. Aquests ratolins preservaven la sensibilitat a la insulina però van desenvolupar una severa intolerància a la glucosa, la qual era independent del pes corporal. No obstant, els nivells basals i estimulats per glucosa en sèrum del pèptid c estaven disminuïts en els ratolins PGC-1α/β-FAT-DKO. En conjunt, aquestes dades senyalaven cap a un defecte pancreàtic en la secreció d'insulina.

L'anàlisi morfomètric dels illots pancreàtics per immunofluorescència i microscòpia electrònica de transmissió no van revelar diferències en la massa de cèl·lules beta, el nombre d'illots o la maduració dels gränuls d'insulina en les cèl·lules beta entre els ratolins PGC-1α/β-FAT-DKO i els control. De forma similar, l'anàlisi de l'expressió gènica dels illots pancreàtics no va revelar una desregulació en la expressió de gens codificants per proteïnes involucrades en la secreció d'insulina en les cèl·lules beta pancreàtiques. L'avaluació de la secreció d'insulina directament en illots pancreàtics aïllats va mostrar que la resposta a la glucosa estava preservada en els ratolins PGC-1α/β-FAT-DKO tot i tenir menor nivells d'insulina en sèrum.

La alteració en la homeòstasis de la glucosa en els ratolins PGC-1α/β-FAT-DKO suggeria la presencia d'una comunicació adiposa-pancreàtica. Per tal d'estudiar-la, vam dur a terme un estudi proteòmica del secretoma dels teixits adiposos. La proteòmica no dirigida va revelar diferències notables entre els ratolins control i els PGC-1α/β-FAT-DKO en el teixit adipós marró, però no en el blanc. La proteòmica dirigida ens va permetre discernir les proteïnes

diferentment secretades pel teixit adipós marró dels ratolins PGC-1α/β-FAT-DKO que podrien exercir un rol endocrí sobre el pàncrees. Els estudis *in vitro* de la resistina, no obstant, no van clarificar la contribució d'aquesta en la regulació de la secreció d'insulina.

Les nostres dades indiques que la falta dels PGC-1s altera la funció endocrina del teixit adipós marró, alterant finalment la homeòstasis de la glucosa com a resultat d'un defecte pancreàtic encara per ésser descobert.

# 1. INTRODUCTION

## 1.1. Obesity-related type 2 diabetes (T2D)

In a world that concerns over malnutrition, obesity burden cannot be ignored. Considered now as an epidemic worldwide, obesity numbers are increasing sharply in middle- and high-income countries. In this regard, worldwide obesity has almost tripled since 1975 (1). This trend implied that in 2016 there was a 13% of adults over 18 years who developed obesity and a 39% who were overweight. In the same dangerous direction, over 340 million children and teenagers aged 5-19 were overweight or obese in 2016 (1). Hence, obesity is a problem socially tolerated and its incidence is increasing dramatically nowadays.

Far for being just an excessive accumulation of fat in adipose tissues, obesity is also considered a threat that can truly impair our health. In fact, obesity and overweight increase the risk for many serious diseases, like cardiovascular diseases, mental disorders, *non-alcoholic fatty liver disease* (NAFLD), many types of cancer and *type 2 diabetes* (T2D) (2). For this reason, eating balanced calorie-controlled diets and burning the excess of energy by practising exercise is essential to prevent the development of obesity and its related diseases.

One of the diseases that greater has grown with the rise of obesity is T2D. This disease represents more than 95% of all cases of diabetes and, in 2021, more than 500 million individuals suffered from it (Figure 1.1) (3). Also, T2D is a chronic disease that requires constant treatment and supervision, thereby promoting a high health expenditure by health care systems.

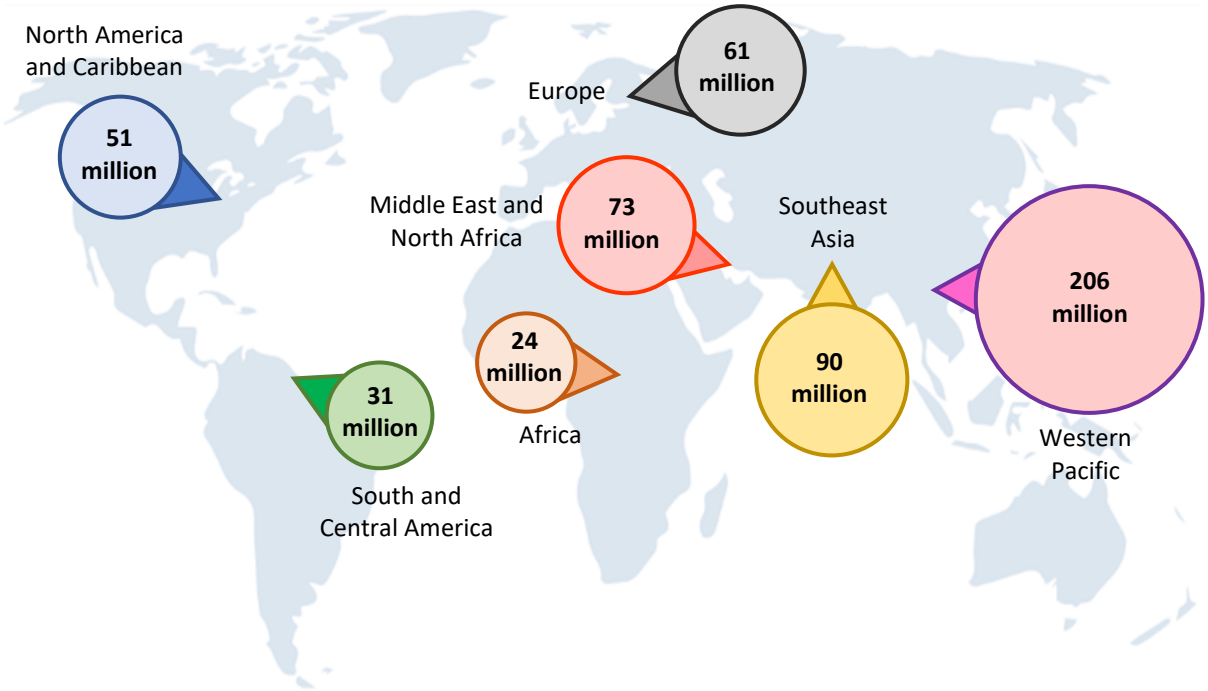


**Figure 1.1**. **Illustrative map of type 2 diabetes prevalence worldwide among adults in 2021**. Image adapted from (3).

*Diabetes Mellitus* (DM) is a chronic disease characterized by high sugar blood levels and impaired insulin secretion in response to glucose. Although T2D is the most prevalent type of diabetes and the one with a greater impact on health systems, it is not the only one. Originally known as insulin-dependent diabetes, ***Type 1 diabetes*** (T1D) comprises 2% of all diabetic

cases worldwide, especially amongst teenagers. T1D is characterized by a defective insulin production, mainly due to the autoimmune destruction of pancreatic β-cells. The impairment of insulin secretion conditionate T1D individuals to administrate a daily dose of insulin to balance their blood sugar levels. Despite the contribution of genetic, epigenetic and environmental factors to the development of the disease, the precise mechanisms behind T1D development remain to be fully understood. Viral infections, birth weight, altered microbiome, T2D or certain genetic mutations, however, have been linked to the activation of the immune system driving the autoimmune response that ultimate destroys pancreatic β-cells (4,5). A third common type of diabetes is ***gestational diabetes mellitus*** (GDM), which develops during pregnancy and usually disappears after giving birth. This condition affects 2% to 10% of pregnant women and is determined by a less efficient action of insulin due to an increase in body weight and the effect of hormones. After pregnancy, GDM can evolve towards T2D (6).

### 1.1.1 Hallmarks of type 2 diabetes

Pathophysiology of T2D is characterized by peripheral *insulin resistance* (IR) and the subsequent impairment of insulin secretion. IR comprises a deficient physiological response to insulin by the main regulators of glucose homeostasis (adipose tissues, liver and skeletal muscles) that impairs the capacity of these tissues to efficiently uptake glucose from blood. This incompetent insulin response results from a disruption in insulin signalling pathways in these tissues. The occurrence of both IR and defective insulin secretion appears to be driven by the adoption of modern lifestyles, characterized by hypercaloric diets and high rates of obesity and sedentarism (7), although genetic and epigenetic components also play a very relevant role.

Normal glucose tolerance is maintained by a balance between glucose uptake and insulin secretion. However, in certain individuals, environmental and genetic factors, throughout mechanisms that are not fully understood, induce IR in insulin-sensitive tissues, being these tissues less capable to respond to insulin. As a result, this blocking of insulin signalling leads to decreased glucose uptake by these tissues, reduced hepatic synthesis of glycogen and enhanced gluconeogenesis (8). The outcome of this process is an increase in glucose blood levels. Aside from hyperglycaemia, IR prompts lipolysis in adipose tissues, which results in the uncontrolled liberation of *free fatty acids* (FFA), also known as *non-esterified fatty acids* (NEFA), to the blood (9). Hyperglycaemia, hyperlipidaemia and low-grade chronic body inflammation reinforce IR (see paragraph 1.1.2) and force pancreatic β-cells to produce more insulin to counteract the cellular effects of IR. This increment in insulin secretion by pancreatic β-cells occurs concomitantly to an increase in β-cell mass. Despite the normalization of glucose levels as a result of β-cell compensation, long-term IR eventually exhausts the capacity of these cells to reverse hyperglycaemia (10,11). At this moment, β-cells fail and start to die, which ultimately results in a disbalance of glycaemia and in the development of T2D. The description of the impaired β-cell insulin secretion in diabetic and insulin resistant individuals will be treated in detail in section 1.2.

### 1.1.2 Mechanisms behind the development of insulin resistance

Many studies have provided plausible pathways by which IR appears in insulin-sensitive tissues. Yet, the molecular mechanisms that trigger the irresponsiveness of these tissues to insulin are not completely understood. Identifying these mechanisms is crucial for the design of new therapeutic strategies to prevent and treat T2D. So far, the main mechanisms identified are: lipotoxicity, *endoplasmic reticulum* (ER) stress, inflammation and mitochondrial dysfunction (Figure 1.2). However, other causes cannot be ruled out in the development of T2D. For instance, some recent studies have reported that gut microbiota is altered in diabetic individuals (12,13), opening the possibility for the transplantation of faecal microbiota to reverse IR and T2D. In this sense, faecal transplantation has proven to improve insulin sensitivity and the *body mass index* (BMI) in T2D patients through the colonization of their microbiota (14).

**Lipotoxicity** refers to the cellular stress derived from the accumulation of lipid intermediates, such as *diacylglycerols* (DAGs) and ceramides, in liver, skeletal muscle and adipose tissues (15,16). In physiological conditions, excess of dietary fatty acids enter the cells and are esterified to form fatty acyl-CoAs that are successively transferred to a glycerol backbone to finally produce triglycerides. The storage of excessive energy under the form of triglycerides mainly occurs in adipose tissues, but almost all tissues can store triglycerides, although much lower amounts. Chronic exposure to an overload of lipids, as it occurs in obesity, impairs storing capacity of adipocytes and other cell types (hepatocytes, muscle cells, etc.) leading to the intracellular accumulation of intermediates of lipid metabolism, such as DAGs and ceramides.

Intracellular accumulation of DAG has been shown to trigger the activation of isoforms of the *protein kinase C* (PKC), PKCδ and PKCθ, which phosphorylate and inhibit *insulin receptor substrate 1* (IRS-1). The inhibition of IRS-1 reduces the recruitment of *phosphatidylinositol 3-kinase* (PI-3K) and causes the inhibition of the downstream insulin signalling pathway. By its side, ceramides induce IR through the activation of another isoform of PKC, PKCζ, which in turn inhibits *serine/threonine kinase 1* (AKT) and impairs insulin signalling (17,18).

Empiric observations have also detected an activation of the immune system and a chronic elevation of pro-inflammatory cytokines in obese insulin resistant individuals and type 2 diabetic subjects (19,20). This **chronic low-grade inflammation** has been identified as another mechanism that generates IR. Indeed, in obese individuals, hypertrophic and dying adipocytes recruit *adipose tissue macrophages* (ATMs), which are characterized by the secretion of pro-inflammatory cytokines, such as *interleukin 6* (IL-6), *tumour necrosis factor alpha* (TNFα) or the *C-C motif chemokine ligand 2* (CCL2*)* (21,22). These adipokines can directly affect insulin-sensitive tissues and induce IR through the activation of inflammatory pathways that are mediated by the *c-Jun N-terminal kinase* (JNK1) and the *inhibitor of NF-κB kinase* (IKKβ) (23). These kinases act by phosphorylating the insulin receptor at inhibitory residues, resulting in the impairment of proper insulin signalling. Moreover, pro-inflammatory cytokines also disbalance lipidaemia, thereby aggravating lipotoxicity in insulin-responding tissues. In addition, these cytokines promote lipolysis in adipocytes via a decrease in stabilizing proteins

from lipids droplets. The released FFA can activate *toll-like receptors 4* (TLR4) and magnify the immune response (17).

**ER stress** has been also proposed as a mechanism involved in the onset of IR. ER is an important organelle that orchestrates the synthesis, folding and trafficking of a wide range of proteins. Under stress conditions, including the rapid increase of incorrectly folded proteins or viral infections, cells activate a homeostatic mechanism named *unfolded protein response* (UPR), aimed at reducing the pathogenic accumulation of proteins. In mammals, UPR is based on three ER transmembrane stress sensors: *PKR-like ER kinase* (PERK), *inositol requiring enzyme 1* (IRE-1) and *activating transcription factor 6* (ATF6) (16). Altogether, these sensors down-regulate the transcription of proteins, increase the folding ability of ER resident chaperones and facilitate the removal of misfolded proteins, all in aims to re-establish ER homeostasis (24). If UPR is insufficient to deal with unfolded or misfolded proteins, the cell ultimately undergoes apoptosis via activation of JNK1.

UPR helps the cell to adapt to the stress created by the abnormal protein accumulation, but when it is unproperly and steadily activated, it may lead to cellular dysfunction. In this regard, some studies have proven that UPR is activated in diabetic rodents and humans or in individuals that have IR (25,26). Although the exact link between UPR and IR remains uncertain, two mechanisms have proposed. The first mechanism involves the activation of JNK1 pathway via IRE-1, what results in the phosphorylation of IRS-1 at inhibitory residues (27). The second mechanism involves the activation of the PERK/eIF2/ATF3 signalling pathway, which ultimately leads to the inhibition of AKT and the impairment of the insulin signalling (28). Moreover, some other studies support that ER stress can also be induced by intracellular FFAs (29), providing an additional mechanism by which lipids can induce lipotoxicity and IR.

Finally, many studies have claimed that **mitochondrial dysfunction** also constitutes a major mechanism triggering IR. These organelles are known as the powerhouse of the cell, as they generate up to 90% of the energy required for the cell in the form of *adenosine triphosphate* (ATP) under aerobic conditions. Mitochondria oxidate different substrates, such as glucose, fatty acids or amino acids, which serve as sources of metabolic energy when required. However, in certain pathological conditions, such as in obesity, the number of mitochondria is reduced and their oxidative function impaired. In this situation, tissues have less capacity to oxidise lipids, amongst other nutrients, and this therefore causes the accumulation of intracellular lipid species. As previously described, these intermediates can cause lipotoxicity, blocking the insulin-signalling pathway and leading to the development of IR (17).

The hypothesis of mitochondrial dysfunction as a trigger of IR stems from studies reporting that muscle, adipose tissue and liver from insulin resistant or T2D individuals have reduced expression of mitochondrial genes involved in fatty acid oxidation and oxidative phosphorylation pathways. This reduction in gene expression is also accompanied by a decrease in mitochondrial mass and oxidative activity in these tissues (30,31). Moreover, data from *transmission electron microscopy* (TEM) have revealed that insulin resistant and diabetic subjects have less and smaller mitochondria in insulin-sensing tissues than healthy individuals (30,32). Number and size of mitochondria depend on mitochondrial biogenesis but also in

mitochondrial dynamics, which involves fission and fusion of mitochondria in order to adapt to new nutritional and physiological stimuli. In this sense, abnormal mitochondrial dynamics has been observed in T2D individuals (33,34).

Akin to the reduction in the mitochondrial function and dynamics, mitochondria are also related to the development of IR through the production of *reactive oxygen species* (ROS). Insulin stimulation leads to a spike in the production of hydrogen peroxide, which facilitate the autophosphorylation of the insulin receptor for the normal insulin downstream signalling cascade (35). However, when the generation of ROS is too high inside the cell, the opposite effect occurs and insulin signalling is blocked. In this regard, nutrient overload, inefficient oxidation of lipids, inflammation and ER stress in the context of T2D promote the excessive generation of ROS. In this situation, ROS activates IKKβ, PKC and JNK1 protein kinases, which in turn phosphorylate IRS-1/2 and inhibit their association with the insulin receptor, ultimately leading to the development of IR.

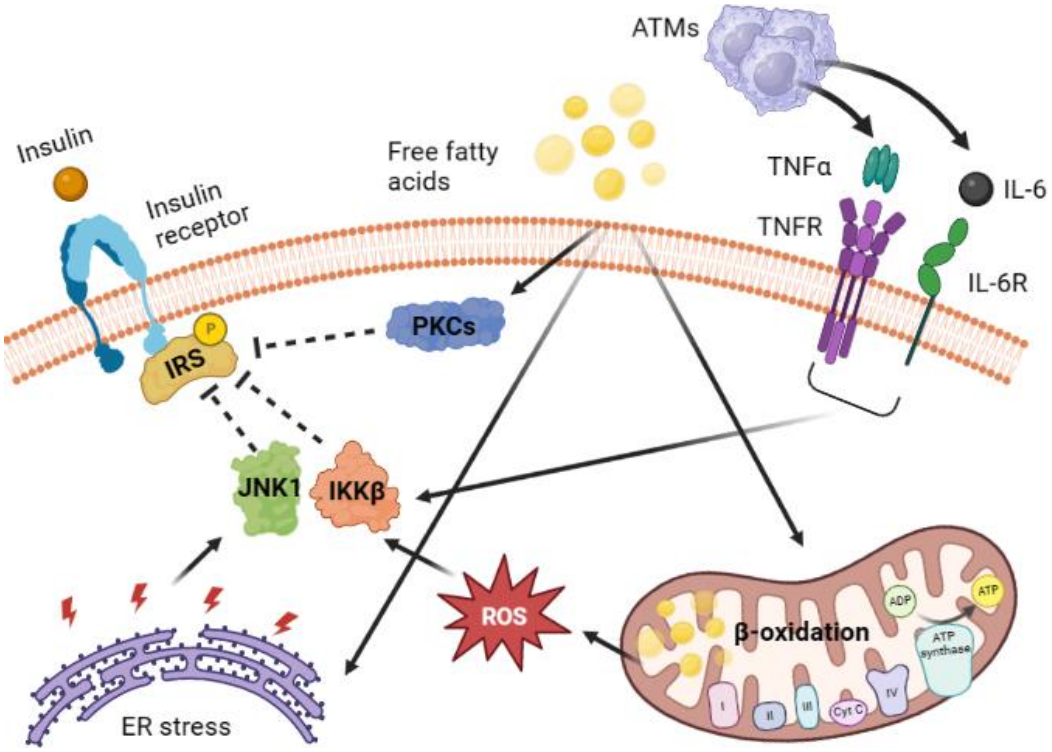


**Figure 1.2**. **Scheme of the principal mechanisms that promote IR**. IRS, Insulin Receptor Substrate; JNK1, c-Jun N-terminal Kinase 1; IKKβ, Inhibitor of NF-κB Kinase; PKC, Protein Kinase C; TNF-α, Tumor Necrosis Factor α; TNFR, TNF-α Receptor; IL-6, Interleukin 6; IL-6R, IL-6 Receptor; ATM, Adipose Tissue Macrophages; ROS, Reactive Oxidative Species. Figure adapted from (17).

However, the role of mitochondrial dysfunction in the development of IR is highly controversial and several studies have provided data that argue against it.

To study how mitochondrial dysfunction leads to IR and alters glucose homeostasis, a mouse model of impaired mitochondria was previously generated in our laboratory (36). For this, crucial regulators of mitochondria, the *PPARG co-activators 1 alpha and 1 beta* (PGC-1α and PGC-1β co-activators, respectively) were specifically depleted in adipose tissues (PGC-1α/β-FAT-DKO). These co-activators are members of the PGC-1 family (section 1.3.2.3) and they are

crucial to orchestrate mitochondrial function and biogenesis in high energy demanding tissues such as liver, skeletal muscle and adipose tissue.

Consistent with the role of PGC-1s, mice lacking both co-activators exhibited a 30-50% reduction in the basal expression of mitochondrial genes in WAT (Figure 1.3, A), as well as a decreased level in mitochondrial proteins. Examined by high-resolution respirometry, altered mitochondria in WAT from PGC-1α/β-FAT-DKO mice displayed a lower respiratory capacity. In a similar way, BAT from PGC-1α/β-FAT-DKO mice showed a down-regulation of mitochondrial genes (Figure 1.3, B) and a reduction in mitochondrial protein levels. These alterations were associated with an accumulation of triglycerides in brown adipocytes, leading to the acquisition of a WAT-like phenotype.

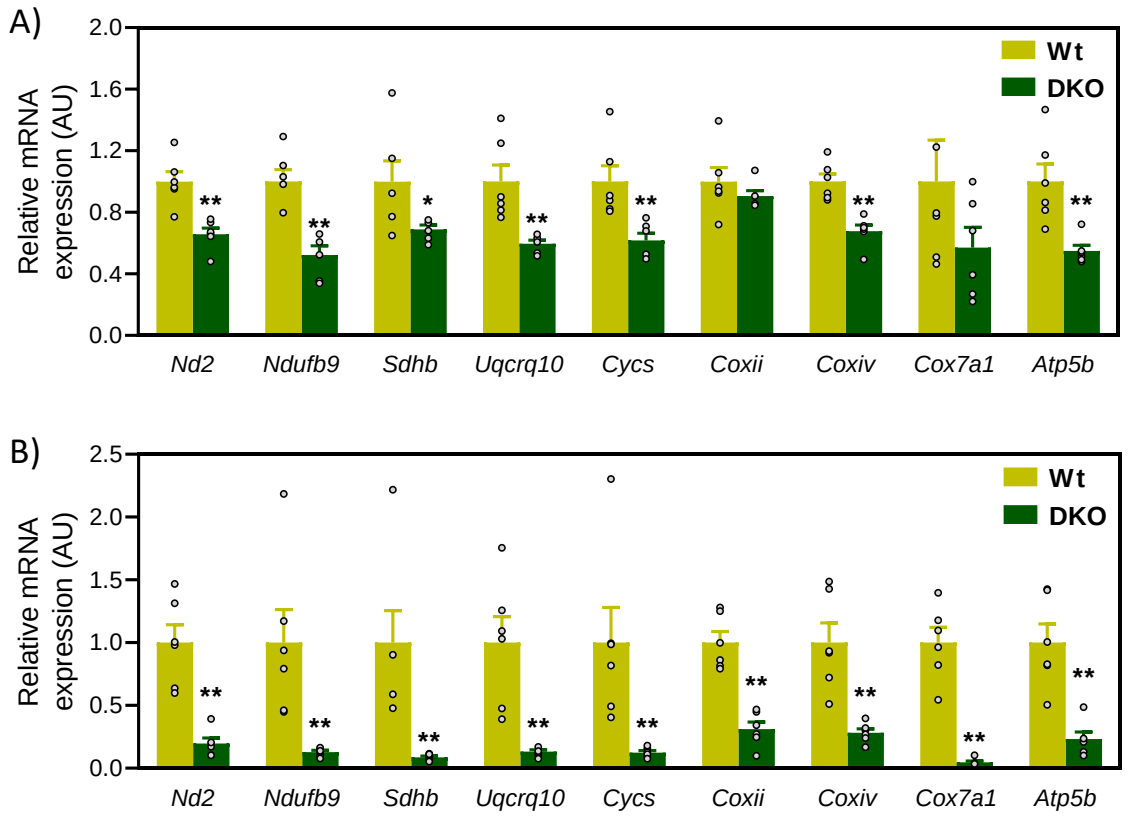


**Figure 1.3**. **Mitochondrial gene expression in adipose tissues.** Expression of genes from the OxPhos system in WAT (A) and in BAT (B) from Wt and PGC-1α/β-FAT-DKO. Nd2, NADH Dehydrogenase 2; Ndufb9, NADH:Ubiquinone Oxidoreductase Subunit B9; Sdhb, Succinate Dehydrogenase Subunit B; Uqcrq10, Ubiquinol-Cytochrome C Reductase Subunit 10; Cycs, Cytochrome C; Coxii, Cytochrome C Oxidase II; Coxiv, Cytochrome C Oxidase IV; Cox7a1, Cytochrome C Oxidase Subunit 7A1; Atp5b, ATP Synthase F1 Subunit Beta. Data obtained from (36).

Despite mitochondrial biogenesis was blunted in the adipose tissues from PGC-1α/β-FAT-DKO mice, body weight was preserved when these mice were fed with an obesogenic *high-fat diet* (HFD) (45% Kcal from fat). In agreement with this, weights of major organs such as WAT, BAT, liver and muscle were not altered. When glucose homeostasis was assessed, it was observed that PGC-1α/β-FAT-DKO mice were prone to glucose intolerance (Figure 1.4, A), but insulin sensitivity was preserved (Figure 1.4, B).

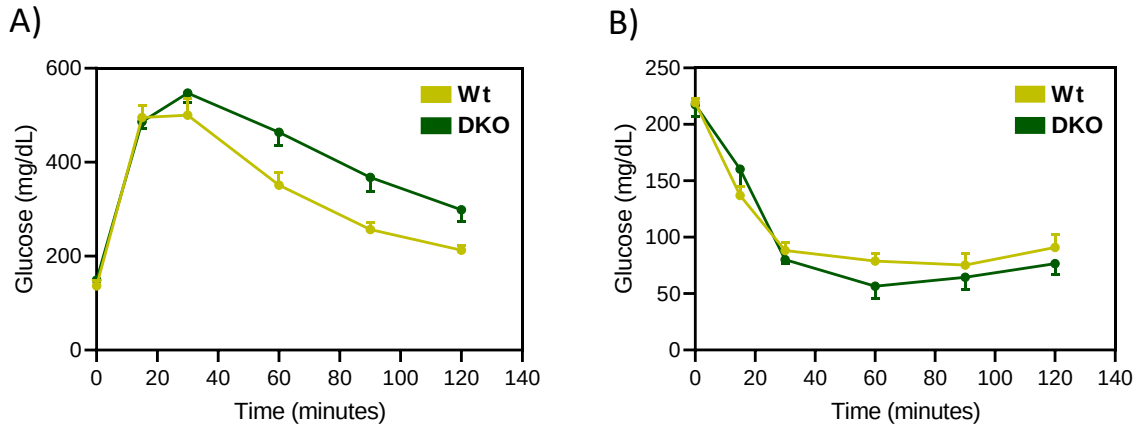


**Figure 1.4**. **Analysis of glucose homeostasis by glucose and insulin tolerance tests.** Evaluation of glucose clearance during the course of A) glucose and B) insulin tolerance tests (GTT and ITT, respectively) in Wt and PGC-1α/β-FAT-DKO mice fed a HFD (45% Kcal from fat). Mice of 8 weeks of age were fed a HFD for 3 months and then GTT and ITT were performed. Both tests were done intraperitoneally, with a dose of 2g glucose/kg mice for GTT and 0.9 U insulin/kg mice for ITT. Data obtained from (36).

These data indicated that adipose-specific mitochondrial dysfunction is not sufficient to promote IR in a context of diet-induced obesity, although some level of glucose intolerance was present.

## 1.2 The crucial role of pancreas in the regulation of glucose homeostasis

### 1.2.1 Physiology of pancreas

The pancreas is an organ with crucial functions in nutrient digestion and metabolism by means of two different pancreatic compartments referred as exocrine and endocrine pancreas (37) (Figure 1.5). The exocrine part of the pancreas is composed by numerous clusters of acinar cells that secrete enzymes for the digestion such as lipase and trypsin. The endocrine part is formed by pancreatic islets containing a variety of hormone-secreting cells that principally control glucose homeostasis. Although the exocrine part accounts for more than 95% of pancreas, both compartments are ubiquitously distributed through the organ.

Anatomically, pancreas is divided into head, body and tail by an arbitrary line. Histologically, its parenchyma has a lobular structure consisting of numerous clusters of acinar cells and, amongst them, pancreatic islets are distributed (38) (Figure 1.5).

#### 1.2.1.1 Pancreatic islet structure and cell composition

Pancreatic islets are highly vascularized and innervated mini-organs that orchestrate the endocrine secretion of pancreatic hormones. In mice, the number of pancreatic islets can scale up to 5000 (39). In comparison, healthy humans contain, approximately, from 3.2 to 14.8 million of pancreatic islets. Regarding their size, most islets have an area between 1000 and 10,000 $\mu m^2$, and contain, in average, 1500 cells (40,41).

Five different types of endocrine cells compose pancreatic islets: α-cells, which secrete glucagon; β-cells, which secrete insulin; δ-cells, which secrete somatostatin; γ-cells, which secrete *pancreatic polypeptide* (PP); and ε-cells, which secrete ghrelin (42). Unlike pancreatic islets from mice, which have a β-cell core and a peripheral area containing the other endocrine cell types, human islets from adult individuals comprise a more homogeneous distribution of cells (Figure 1.5). In terms of relative cell composition, 60% to 80% of cells are β-cells in mouse islets, followed by 15% to 20% of α-cells, less than 10% of δ-cells and 1% of the remaining γ-cells and ε-cells. By contrast, human islets contain less β-cells (50%), more α-cells (40%) and a similar percentage of δ-cells (10%), γ-cells and ε-cells (1%) (42). Notwithstanding the different contribution of each cell to total pancreatic cell population, both human and rodent pancreatic islets from the same pancreas display a high range of heterogeneity between them. Hereof, recent studies support the idea that cell composition varies depending on the location, size or even the function of the islet (43,44). In fact, it appears that small islets are composed mainly of β-cells, whereas large islets show a mix of cell populations (43). Similarly, some reports indicate an uneven distribution of human islets through the pancreas, which is plausible to be related to functional differences between pancreatic islets (45).

In close association with endocrine cells, pancreatic islets also contain capillaries, neuronal projections, immune cells and fibroblasts (46). These different cell populations are suggested to modulate the function of pancreatic islets. In this sense, vascular cells and neuronal processes are known to establish interactions with endocrine cells that coordinate the secretion of hormones in response to stimuli (46). To the same extent, resident immune cells in islets, which mainly belong to T cell and macrophage lineages, play crucial roles in the development and function of endocrine cells. In fact, early infiltration of macrophages is believed to promote islet plasticity and regeneration of pancreatic β-cells (47), whereas resident T cells are involved in the maintenance of islet cell homeostasis (48).

As previously introduced, pancreatic islets contain five types of endocrine cells that secrete hormones to control metabolism. Their specific functions are described below:

- **β-cells:** these are the cells that produce insulin. β-cells are the first endocrine cells to differentiate during human pancreatic morphogenesis, followed by α- and δ-cells differentiation (49). During the development of the endocrine lineage, β-cell identity is acquired by the expression of crucial transcriptional regulators such as *MAF BZIP transcription factor A* (*Mafa*), *neurogenin 3* (*Ngn3), pancreatic and duodenal homeobox 1 (Pdx1), NK6 homeobox 1 (Nkx6.1)* and *insulin* (*Ins*) (50). Therefore, differentiation is the main cellular driver that form pancreatic β-cells during pancreatic embryology (51). In adulthood, by contrast, β-cell mass is maintained mainly by replication, although neogenesis of pancreatic precursors and differentiation into fully functional pancreatic β-cells are still present (52,53). In the same way, trans-differentiation from pancreatic acinar cells, hepatocytes or other endocrine cells can also replace β-cell pool (54).

- **α-cells:** these cells are in charge of secreting glucagon, a hormone that opposes the action of insulin in the control of glucose homeostasis. Glucagon commands the mobilization of fuels (i.e., glucose and fatty acids) to different organs and tissues to supply nutrients to cells for their catabolic reactions. Differentiation and secretory function of these cells depend on the expression of selective markers, including *MAF BZIP transcription factor B (Mafb)*, *iroquois homebox 1 and 2* (*Irx1/2)*, *aristaless related homeobox* (*Arx*), *neuronal differentiation 1* (*Neurod1*) and *glucagon* (*Gcg)*. Pancreatic α-cells are intermingled with β-cells in human islets, thereby enhancing the bidirectional regulation between both populations (55). Moreover, they have the potential to transdifferentiate into β-cells (56).
- **δ-cells:** being the third most prevalent cell type in pancreatic islets, δ-cells are negative regulators of insulin, glucagon and polypeptide secretion (57). δ-cell fate is determined by the expression of *paired box 4 (Pax4)* and is maintained by the expression of *hematopoietically expressed homeobox* (*Hhex*) (58). Akin to α-cells, δ-cell can also transdifferentiate into β-cells (59).
- **γ- and ε-cells:** polypeptide and ghrelin, respectively, are the hormones secreted by these pancreatic cells. γ-cells make up 1-2% of total islet cell population and are more concentrated in the head of the pancreas. These cells have an important role in the pancreas-gut-brain axis in terms of intestinal function and satiety. In this regard, postprandial secretion of PP by pancreatic and intestinal endocrine cells causes a negative effect on energy balance, as it decreases food intake and gastric emptying and increases energy expenditure, via parasympathetic vagus nerve (60). Moreover, they inhibit glucagon secretion at low glucose concentrations, despite not affecting insulin secretion (61). Regarding ε-cells, ghrelin is increased during fasting and inhibits insulin secretion, both in human and rodents. At the same time, ghrelin is thought to be a regulator of glucagon, PP and somatostatin release (40).

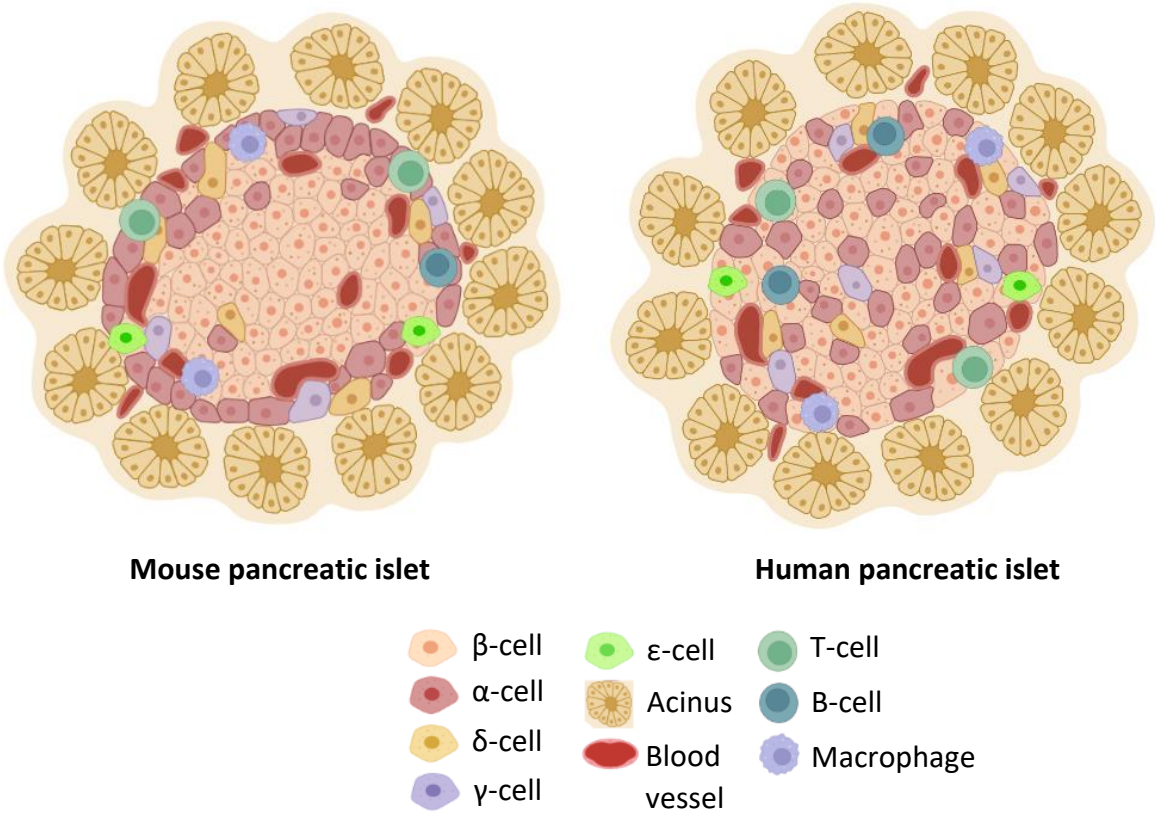


**Figure 1.5**. **Illustrative image of a mouse and a human pancreatic islet being surrounded by exocrine acinus.** Mouse pancreatic islet contains β-cells in the centre of the islet, whereas the other endocrine cells are found in the periphery. Contrary, human pancreatic islet consists of a mix of endocrine cells homogenously distributed throughout the islet. Both types of islets are composed by endocrine, immune and vascular cells.

### 1.2.2 Pancreatic islet regulation of glucose homeostasis

Glucose blood levels are constantly maintained in a specific range in order to supply cells of the body with the energy and the nutrients required for their functions. Low glucose levels, called hypoglycaemia, starve cells, whereas an excess of glucose, or hyperglycaemia, can be toxic. In the fasting state, glucose blood levels from healthy individuals are below 100 mg/dL. However, after eating a meal, this value almost doubles (62). Pancreas regulates glycaemic levels to adapt to different stimuli and conditions through the secretion of glucagon and insulin, which act in an opposite and a balanced manner.

#### 1.2.2.1 Control of insulin secretion in pancreatic β-cells

In β-cells, insulin is stored inside secretory vesicles in a crystalline form and forming a complex with zinc. This hormone is firstly synthesized as preproinsulin and then converted to proinsulin in the *rough endoplasmic reticulum* (RER) (Figure 1.6). In this moment, some RER cargo proteins, zinc and calcium are packed with insulin in its route to Golgi (63). However, it is in Golgi where more packaging events occur. In this organelle, proinsulin is sorted into immature granules, which are emanated from *trans-golgi network* (TGN) to continue with the subsequent granule maturation. To accomplish this task, immature granules become more acidic by means of an ATP-dependent proton pump. Acidification process facilitates the conversion of proinsulin to insulin and c-peptide by endoproteases PC1/3 and PC2 and

carboxypeptidase E (64). At this moment, insulin secretory granules exist as large dens-core structures with a clear region or halo surrounding the core. The dense core is generated by a condensation process involving calcium, zinc and the recently formed insulin. Mature insulin granule is finally generated when undesirable components yet found in the granule are packed and excreted in the form of a clathrin-coated bud (64).

Upon the stimulation by glucose or other secretagogues, such as certain amino acids and hormones, secretory granules containing insulin are released by β-cells. However, before the stimulation phase, there is a primary signal for insulin secretion that prepares the body for the incoming shot of glucose. This basal insulin signal is triggered by neurotransmitters released in response to the smell or sight of food and incretins, peptides released by gut when food is present (62). These potentiators of insulin secretion, like amino acids, fatty acids and incretins, can act at resting glucose blood levels, set at 4-5 mM in human and 7-10 mM in mouse. After a meal, however, glucose is the main trigger of insulin secretion, and all the other stimuli just potentiate it. In this regard, in both human and mice, insulin secretion is half-maximal at 10-12 mM glucose and saturates at concentrations of glucose above 20 mM (62).

Insulin secretion pathway starts when glycaemia increases and glucose is uptaken by pancreatic β-cells (Figure 1.7). In mice, the transport of glucose is mediated by the *glucose transporter 2* (GLUT2) receptor, whereas GLUT1 is the predominant receptor in human β-cells (65). Once inside the cell, glucose is phosphorylated by glucokinase or hexokinase IV, in a process that is the rate-limiting step in insulin secretion. Following phosphorylation, glucose is metabolized through glycolytic pathways. Most of the glucose transported into the cell that enters glycolysis proceeds into the Krebs cycle and is fully oxidized, with just a small percentage used for glycogen synthesis and others (66). The resulting net raise in intracellular ATP inhibits potassium channels located in the cell membrane and changes cell membrane potential. Specifically, the closure of $K^+$ channels leads to an increase in cell potential, which enough to fire a depolarization response in the cell membrane. This, in turn, promotes the opening of *voltage-gated calcium channels* (VGCC) and the entrance of calcium ion ($Ca^{2+}$) inside β-cells. Intracellular elevation of $Ca^{2+}$ concentration facilitates, then, the mobilization of the secretory insulin granules to cell membrane (62). β-cell exocytosis and insulin secretion are finally achieved by a highly regulated process that triggers the fusion of insulin granules with cell membrane. This process involves the interaction of proteins from both compartments, including: *ras-related protein 3 and 27 (Rab3, Rab27), regulating synaptic membrane exocytosis family (Rim), syntaxin family (Stx), vesicle associated membrane protein family (Vamp)* and *syntaxin binding protein family (Munc).* When glycaemia is further normalized, glucose metabolism inside β-cell is diminished and potassium channels return to their normal potential state, thereby decreasing insulin secretion (62).

Stimulation of insulin secretion by glucose adopts a biphasic pattern in terms of duration and intensity (Figure 1.6). In this regard, glucose elicits a 1$^{st}$ phase secretion, lasting less than 10 minutes, followed by a 2$^{nd}$ phase secretion, sustained up 2 hours in time. Moreover, 2$^{nd}$ phase has a lower peak in secreted insulin than the 1$^{st}$ phase (62,64). The biphasic secretion responds to the nature of different pools of secretory granules inside β-cells and not to a

change in the metabolic signal. In contrast, both phases are shaped by the biphasic rise in cytoplasmic calcium concentration ([$Ca^{2+}$]). In this sense, 1st phase is characterized by a rapid elevation of [$Ca^{2+}$] that mobilize insulin granules ready to be secreted, whereas 2nd phase requires more signals to participate and demands the mobilization of granules stored inside β-cell (62,64).

Mature insulin granules can be found in two different pools: *readily releasable pool* (RRP) and the *reserve pool* (RP), which accounts for 1st and 2nd insulin secretion phases respectively (Figure 1.6). In a normal β-cell, there are approximately 10,000 secretory insulin granules, but only a fraction (1-2%) of them, the RRP, is immediately available for release (67). In contrast to RP granules, RRP granules are biochemically prepared for release, as they are close or docked to cell membrane and are highly responsive to calcium and ATP signalling pathways. Under a stimulatory dose of glucose, these granules rapidly secrete their insulin content to control glucose homeostasis in the first minutes after the sugar ingestion. In turn, glucose promotes the replenishment of docked RRP granules and the mobilization of newcomers granules from the RP, a process that requires more time and new ATP production to be accomplished (64).

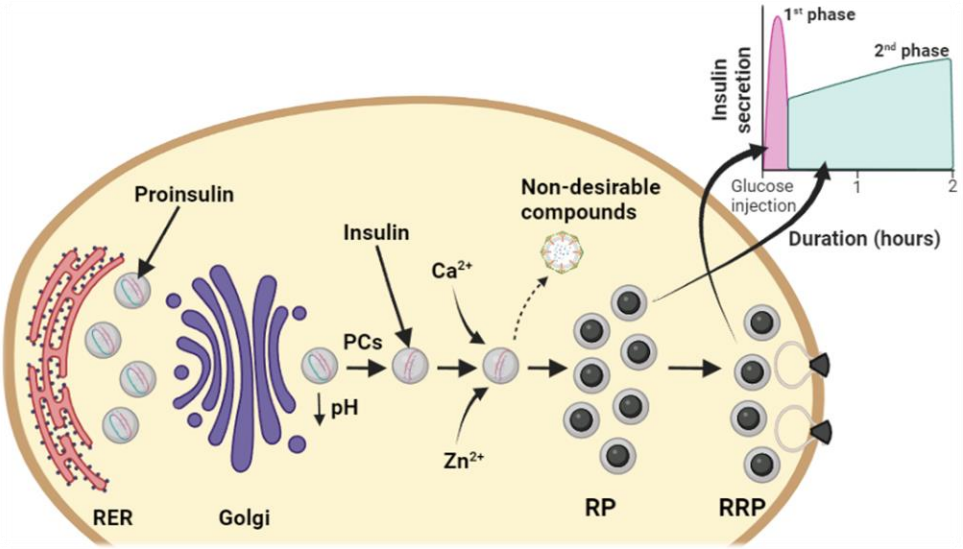


**Figure 1.6**. **Illustration of the process of insulin maturation inside secretory granules and its release in the 1st and 2nd insulin secretion phases.** Proinsulin is generated from preproinsulin in the RER and transported into Golgi apparatus. There, proinsulin is sorted into immature granules and subsequently matured to insulin by proconvertases 1, 2 and 3, which are activated by the acidic pH created by an ATP-dependent proton pump. Afterwards, insulin is concentrated into secretory granules by adding zinc, calcium and after excreting non-desirable compounds. Mature insulin granules are then prepared to be secreted (RRP) or stored within the cell (RP). RRP insulin granules account for the 1st phase insulin secretion and RP granules for the 2nd phase. RER, Rough Endoplasmic Reticulum; PCs, Proconvertases 1, 2 and 3; $Zn^{2+}$, Zinc ion; $Ca^{2+}$, Calcium ion; RP, Reserve Pool insulin granules and RRP, Ready-Releasable Pool insulin granules. Figure adapted from (64).

#### 1.2.2.2 Modulators of β-cell insulin secretion

Glucose is the main inducer of insulin secretion in pancreatic β-cells. However, the amino acid leucine, certain drugs (e.g., sulfonylureas) and non-esterified fatty acids (albeit only weakly) can also be initiators of insulin release. Other agents, by contrast, are capable only to potentiate or inhibit insulin secretion in the presence of a substimulatory glucose

concentration (3 mM or above), but they cannot induce directly insulin secretion on their own. For this reason, they are referred as modulators of insulin secretion. There exist many of them, being either nutritional signals (fatty acids, amino acids), hormonal signals (leptin, prolactin, growth hormone, insulin, glucagon, *glucagon-like peptide 1* (GLP-1), *gastric inhibitory peptide* (GIP), somatostatin or neural signals (acetylcholine, adrenaline) (Figure 1.7).

**Amino acids** are molecules capable to increment insulin secretion. Different from leucine, which is capable to induce insulin secretion by itself, other amino acids only potentiate the release of insulin triggered by glucose. In this sense, it is known that arginine, lysine, alanine and glutamate can be transported into β-cell and contribute to overall cell membrane depolarization and aperture of $Ca^{2+}$ channels (64). By contrast, leucine directly initiates insulin secretion by serving as a metabolic fuel and as an allosteric activator of glutamate dehydrogenase for Krebs cycle (68).

**NEFA** exerts both stimulatory and inhibitory actions in pancreatic β-cells, as an acute exposure promotes insulin secretion, but a chronic exposure seems to inhibit the process. The mechanisms accounting for NEFA potentiation of insulin secretion include stimulation of exocytosis and elevation of $Ca^{2+}$ levels once NEFA bind to their receptors (69). Chronically elevated NEFA, by contrast, seem to inhibit insulin secretion by decreasing insulin biosynthesis, β-cell glucose sensitivity and glucose-stimulated insulin secretion (70). Moreover, they can increase the basal rate of insulin secretion, thereby exhausting β-cell insulin stores, which cannot be replenished on time by proinsulin conversion (71). *Long-chain fatty acids* (LCFA) are the main saturated NEFA that impairs insulin secretion when chronically exposed, due to the induction of mitochondrial dysfunction and ER stress. By contrast, unsaturated fatty acids or short-chain saturated fatty acids do not reduce insulin secretion (72).

**GLP-1** and **GIP** are considered incretins, hormones released from the gut in response to the ingestion of food that modulate insulin secretion. GLP-1 is released from the enteroendocrine L-cells, whereas GIP is released by the enteroendocrine K-cells of the proximal small intestine and accounts for most of the incretin effect. Both hormones stimulate β-cell electrical activity and enhance exocytosis of insulin granules. They do so through the interaction of GLP-1 and GIP receptors with $G_s$ protein-coupled receptors, triggering an elevation of intracellular *3',5'-cyclic adenosine monophosphate* (cAMP) and $Ca^{2+}$ levels. GIP also promotes the closure of $K^+$ channels. In a similar way, glucagon released by α-cells also enhances insulin secretion by a cAMP-dependent mechanism and inhibits $K^+$ channels (62).

In contraposition to the stimulatory role of the previous modulators of insulin secretion, **somatostatin**, epinephrine and leptin act as inhibitors agonists of the β-cell secretory function. Somatostatin is a hormone locally released by pancreatic δ-cells and also by the gut. This hormone inhibits insulin secretion by supressing the inward depolarizing current and by activating a repolarizing current (62). At the same time, it also supresses insulin release by disrupting normal exocytosis (73). **Epinephrine** inhibits electrical activity and exocytosis in β-cells by a mechanism resembling that of somatostatin (62). As an example of crosstalk with other organs, adipose tissues-secreted **leptin** is believed to exert an inhibitory effect on

insulin secretion. Leptin promotes potassium channel trafficking to the cell membrane and increases its activity, which in turn decreases $Ca^{2+}$ intracellular levels and decreases insulin secretion (74).

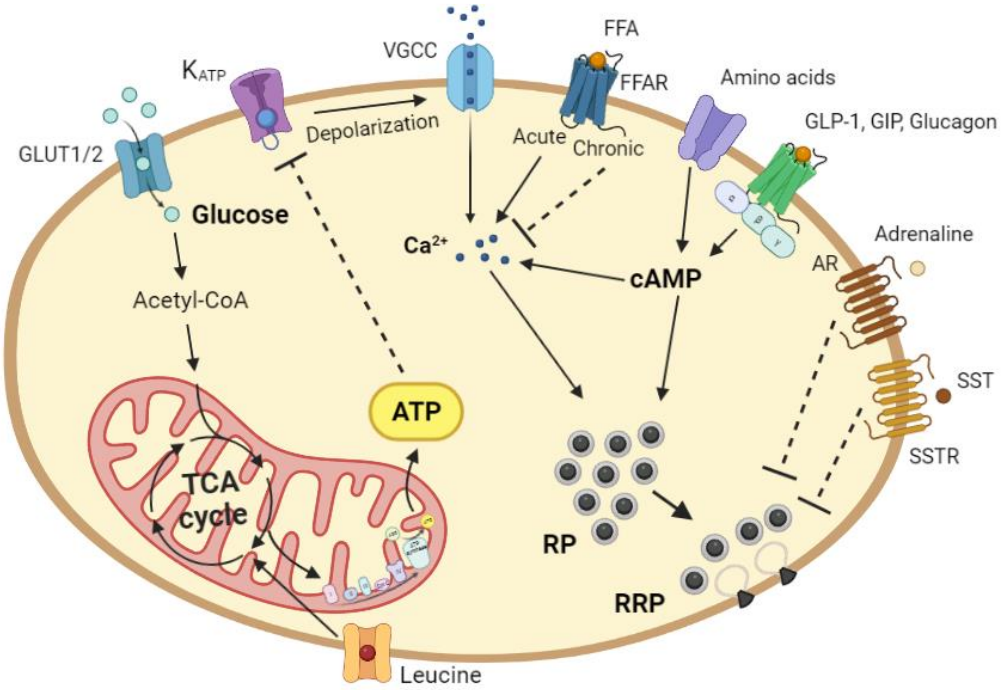


**Figure 1.7**. **Illustration of the mechanism of insulin secretion and its modulation by different molecules in pancreatic β-cells**. Glucose increases ATP though TCA cycle and the OxPhos system, leading to the closure of ATP-dependent potassium channels. This closure drives cell membrane depolarization, causing the opening of VGCC channels and the entrance of $Ca^{2+}$ inside the cell. Elevation of intracellular $Ca^{2+}$ by glucose and other molecules promotes the mobilization (RP) and the secretion (RPP) of insulin granules. Different modulators can potentiate or, by contrast, inhibit insulin secretion. GLUT1/2, Glucose-Transporter 1/2; TCA, Tricarboxylic Acid cycle; ATP, Adenosine Triphosphate; VGCC, Voltage-Gated Calcium Channel; FFA, Free fatty acids; FFAR, FFA receptor; GLP-1, Glucagon-Like Peptide-1; GIP, Gastric Inhibitory Polypeptide; cAMP, cyclic Adenosine Monophosphate; AR, Adrenaline Receptor; SST, Somatostatin; SSTR, Somatostatin Receptor; RP, Reserve Pool insulin granules and RRP, Ready-Releasable Pool insulin granules.

#### 1.2.2.3 Regulation of glucose homeostasis by insulin and glucagon

Pancreas regulates glycaemic levels to adapt to different stimuli and conditions through the secretion of, principally, glucagon and insulin. During sleep, exercise or in between meals, when glycaemic levels are low, **glucagon** is released from α-cells to restore glucose levels. To this aim, glucagon directly promotes hepatic glycogenolysis, which breaks down stored glycogen and increases glucose output. At the same time, this hormone enhances gluconeogenesis to increment the production of glucose for prolonged fasting and decreases glycolysis. Hence, glucagon boosts glucose production to fulfil energetic requirements in tissues like liver, adipose tissue and skeletal muscle (Figure 1.8). In the same extent, glucagon provides lipids to demanding tissues by increasing lipolysis in adipose tissues and their oxidation in liver. In a paracrine way, glucagon seems to regulate positively insulin secretion (75,76). Although seems counterintuitive, glucagon may up-regulate insulin secretion under high glucose concentrations to prevent an overshoot of glycaemia when recovering from a blood glucose drop (77).

During the fed state, **insulin** is secreted by pancreatic β-cells to reduce glycaemia and promote glucose uptake and storage (Figure 1.8). Insulin action relies primarily on the regulation of the main glucose responding tissues: liver, skeletal muscle and adipose tissue. In **liver**, insulin prompts the usage of glucose and the storage of the remaining in the form of glycogen. Also, excess of glucose is converted into fatty acids and *triglycerides* (TAG). Inversely, insulin down-regulates the net glucose production by inhibiting gluconeogenesis, and by reducing the breakdown of glycogen into glucose (78,79). Given the fact that 70% of blood glucose is directed to **skeletal muscle** to fulfil its high energy requirements, insulin triggers the rapid uptake and oxidation of glucose by this tissue. As in liver, uptaken glucose is converted to glycogen to be stored. Moreover, insulin promotes the anabolic synthesis of proteins to increase muscle mass, whereas inhibits proteolysis (80). **Adipose tissue** is mainly responsible for the storage of nutrients in the form of triglycerides in lipid droplets. Hence, insulin boosts lipogenesis in this tissue, at the same time that reduces the secretion of FFA by preventing lipolysis (80).

Aside from the well-known functions in triggering glucose uptake and oxidation, insulin has also other major physiological roles. Indeed, insulin is believed to be important in the bone development and maintenance (81), in kidney homeostasis (82), in the regulation of satiety and neural function in brain and in the functioning of endothelium vasculature (80).

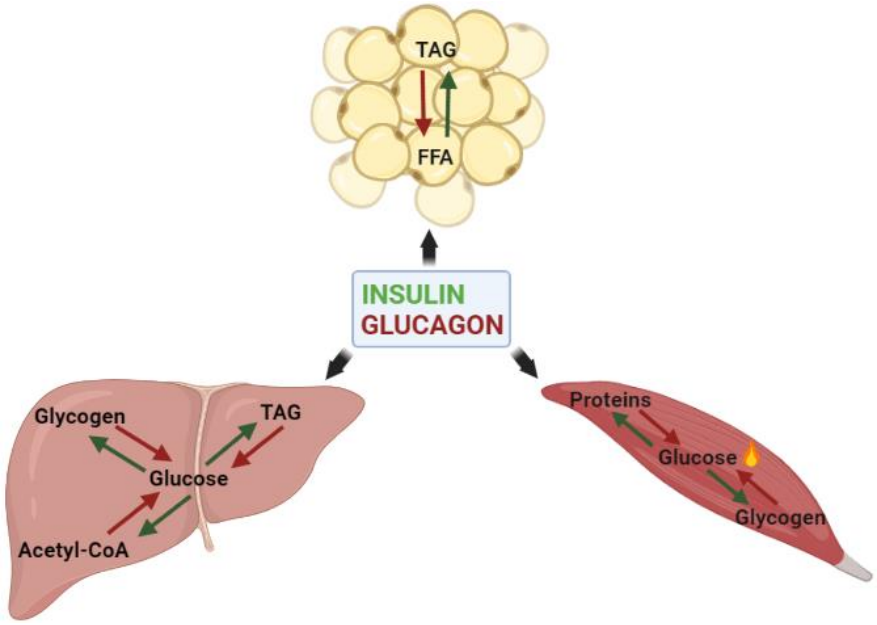


**Figure 1.8. Schematical representation of the pathways regulated by insulin and glucagon in the main glucose-responding tissues (liver, adipose tissue and skeletal muscle).** During the fed state, insulin promotes the storage of energy in the form of glycogen, proteins or triglycerides. In the fasting state, glucagon mobilizes the energy stores and supplies these tissues with glucose and fatty acids. TAG, Triglycerides; FFA, Free-Fatty Acids.

### 1.2.3 Pancreatic islet pathology in T2D

T2D is characterized by a reduction in β-cell capacity to secrete insulin and restore normoglycaemia (sections 1.1.1 and 1.1.2). In non-diabetic obese individuals, IR is counterbalanced by an increase in insulin secretion. β-cells adapt to IR not only through an increment in insulin production and release, but also they undergo a process of hyperplasia

and hypertrophy that is aimed at increasing circulating insulin levels. In diabetic individuals, though, there is a reduction in β-cell mass, which is principally caused by an increase in β-cell apoptosis. This reduction in β-cell mass is accompanied by a decrease in total pancreatic islet mass (83). However, many studies suggest that this reduction in β-cell mass is not sufficient to account for the diminished insulin secretion observed in diabetic patients. In fact, reports indicate that β-cell mass is only reduced by a maximum of 40% in diabetic individuals (84). Hence, even if T2D results in a mild decrease in insulin content and β-cell mass, this reduction is unlikely to be the main cause behind the impairment of insulin secretion.

In parallel to a decrease in β-cell mass, the course of diabetes has been also linked to an impaired-cell function, represented as a failure of β-cell to respond normally to a stimulated dose of glucose. Data from patients indicate 27% reduction in acute insulin response during the transition from normal to impaired glucose tolerance and 51% reduction in diabetic individuals (85). Although not completely understood, β-cell dysfunction appears to be caused by a defective response to glucose, which is translated into an impairment in insulin granules mobilization and secretion. In agreement with this, it is suggested that oxidative metabolism is reduced in T2D patients, thereby lowering the amounts of ATP necessary to depolarize the β-cell (86). Moreover, in diabetic individuals there is a loss of the biphasic insulin secretion. Specifically, 1$^{st}$ phase insulin release is absent in response to glucose, replaced by a slow insulin secretion process that resembles that from 2$^{nd}$ phase. The principal cause of the loss of biphasic response is a drop in β-cell electrical activity, manifested as a reduction in the stimulatory capacity of the sugar. However, the response is fully retained with other secretagogues like incretins or amino acids (62). Concomitant with a lower electrical activity, insulin secretory granules are also affected in T2D. In this regard, proinsulin-insulin ratio is increased in dysfunctional β-cells, which derives in a major secretion of secretory granules containing proinsulin instead of mature insulin (62). In addition to the alteration in the secretory granule content, the mobilization and exocytosis of these vesicles are also impaired in T2D individuals. On one side, there is a reduction in the rate of successful docking events, therefore reducing the number of insulin granules ready to be secreted (87). On the other side, the expression of proteins involved in the fusion of secretory granules with cell membrane is decreased in diabetic individuals. These proteins include STX1A, *synaptosome associated protein 25* (SNAP25), MUNC13 and synaptotagmin, and their down-regulation may involve a diminished capacity of insulin granules to fuse and secrete insulin (62).

Impaired β-cell function and decreased β-cell mass in the context of T2D are believed to be induced mainly by glucotoxicity and lipotoxicity. As explained, chronic hyperglycaemia exhausts insulin from secretory granules, thereby diminishing the amount of hormone secreted in response to a new dose of glucose. Regarding lipotoxicity, it has been shown that prolonged exposure to high levels of fatty acids promotes the conversion of proinsulin to insulin. Furthermore, hyperglycaemia and hyperlipidaemia exert a negative effect on β-cell function and β-cell mass by inducing an ER stress and promote inflammation (83,88).

Together with β-cell function and mass, α-cell function also appears to be affected in the context of T2D. In contrast to insulin secretion, glucagon secretion is increased in the fed state

in diabetic individuals (89). By contrast, glucagon secretion is impaired in hypoglycaemic conditions. It is unclear the exact mechanism that drives this increase, but it is believed that indirectly paracrine regulation by insulin is blunted in T2D. Hyperglycaemia might also have detrimental effects directly on α-cell. In this sense, it is though that hyperglycaemia impairs α-cell mitochondrial function, causes intracellular acidification and dysregulate potassium channels, thereby affecting glucagon secretion (90).

## 1.3 Adipose tissues

Far from its role as a lipid store, *adipose tissue* (AT) is gaining insight for its major role in nutrient homeostasis and as a regulator of metabolism. Currently, AT is classified into WAT and BAT (Figure 1.9), both of which exert different but coordinated functions to regulate glucose homeostasis and energy balance. Adipocytes are the structural units that compose primarily adipose tissues, and they are surrounded by the *stromal vascular fraction* (SVF), which is formed by other cell types such as pre-adipocytes, immune cells, fibroblasts and endothelial cells (91).

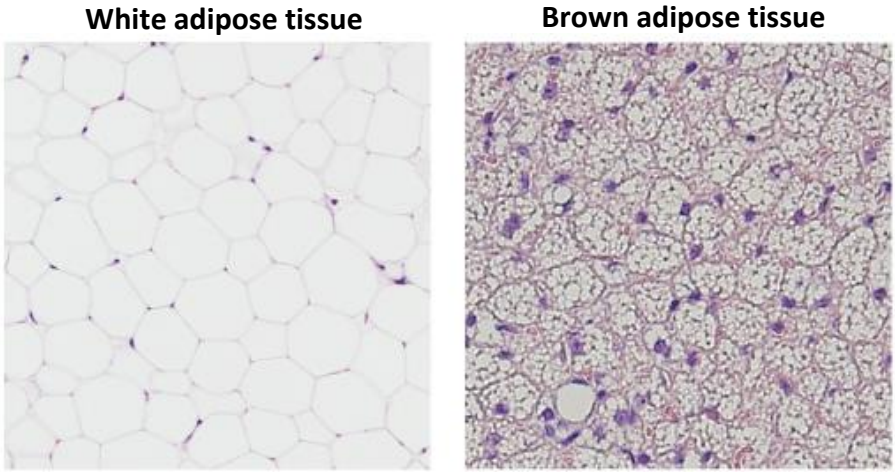


**Figure 1.9**. **WAT and BAT morphology.** White adipocytes contain a big lipid droplet with a nucleus in the lateral region. Brown adipocytes contain multiple small lipid droplets and a large number of mitochondria, which gives them a brownish aspect. Haematoxylin/eosin-stained images are obtained from (114).

### 1.3.1 White adipose tissue

White adipose tissue is the most abundant form of adipose tissue and it is widespread throughout the body. Apart from cushioning body parts exposed to mechanical stress and providing insulation in cold conditions, it has notorious functions in metabolism. White adipocytes possess a single, large lipid droplet that occupies most of the cell, and a relative low number of mitochondria and other organelles in the remaining space (91) (Figure 1.9). Despite its ubiquitous distribution, WAT accumulates in discrete locations, named depots. In this regard, anatomical location allows the differentiation of subcutaneous, beneath the skin, and visceral depots, located in the peritoneal cavity (Figure 1.10). In terms of quantity, subcutaneous white adipose tissue accounts for 80% of total WAT, although, in pathological

conditions such as obesity, the contribution of visceral WAT is much higher than that from subcutaneous WAT (92).

Remarkably, beyond their different anatomical localization, subcutaneous and visceral WAT depots exhibit notable functional differences and differential pathological implications. In mice, **subcutaneous WAT** is distributed in the posterior inguinal depot and in the anterior axillary or interscapular depot. In humans, subcutaneous fat is found in posterior lumbar, epidural, buttock and gluteal regions. More than any other depot, subcutaneous WAT is displayed as a metabolic "sink" for the lipid storage. This tissue primarily adapts to circulant lipids by generating new adipocytes (hyperplasia) and, in a lesser proportion, by expanding existing adipocytes (hypertrophy) (93). **Visceral WAT** represents less than 20% of overall adipose tissue in lean individuals, although it plays a capital role in the regulation of metabolism (94). In humans, visceral WAT is represented in the mesenteric, omental, retroperitoneal, perirenal, epicardial and mediastinal depots. In a similar way, mice contain mesenteric, retroperitoneal, perirenal, mediastinal and perigonadal visceral depots, but omental depot is barely present. In contrast to subcutaneous WAT, visceral adipocytes are more prone to undergo hypertrophy when exposed to an excess dose of lipids (92). Subcutaneous and visceral WAT depots display differential roles in the regulation of glucose homeostasis and energy balance. In this sense, visceral adiposity correlates with IR and an increased risk of cardiometabolic diseases, even in normal-weight individuals (93). By contrast, expansion of subcutaneous WAT is associated to a more favourable metabolic profile and insulin sensitivity (92). The reasons behind these discrepancies are complex and not fully understood, but they seem to be related to a differential response to overnutrition. In this sense, visceral WAT is more prone to immune cell infiltration and inflammatory cytokine production than subcutaneous fat (95). Inflammation in visceral depot is the result of the hypertrophic growth in this tissue, whereas hyperplasia observed in subcutaneous WAT negatively correlates with the development of this pathological condition. In turn, larger adipocytes undergo higher lipolysis rates, thereby releasing fatty acids that contribute to IR in distant organs (96).

Regardless of the anatomical location, WAT main function involves the storage of lipids in the form triglycerides in lipid droplets. In a fasted state, stimulatory signals (i.e., norepinephrine, glucagon) promote lipolysis in the lipid droplets, thereby releasing free fatty acids that reach circulation in order to supply fuel to other tissues. By contrast, in the fed state, the excess of nutrients not used are uptaken by WAT and re-stored. In particular, metabolites resulting from the metabolism of glucose and amino acids in adipocytes are used to esterify fatty acids with glycerol to form triglycerides by *de novo* lipogenesis, a process regulated by insulin (92).

In addition to its role as an energy storage depot, WAT is nowadays recognized as an **endocrine organ**. Through the secretion of a variety of molecules that exert signalling functions, WAT regulates nutritional homeostasis and energy balance, and modulates other physiological function, like reproduction or immunity. Secreted molecules by WAT are typically peptide hormones (usually referred as adipokines), although bioactive lipids (lipokines) and RNA molecules with signalling function have also been identified (97).

The most well-known adipokines are leptin, adiponectin and resistin**. Leptin** is exclusively expressed in adipocytes and circulating levels positively correlate with adiposity (97). The role of this hormone is the suppression of appetite and the promotion of energy expenditure (98). Hence, both in rodents and humans, lack of leptin or leptin receptor directly induces obesity and IR (99). Leptin supresses the appetite by repressing the orexigenic pathways in the hypothalamus and stimulating the anorexigenic pathways (98). Leptin also prompts the burning of energy by downregulating insulin signalling pathways in pancreas, liver and adipose tissues. Contrary, **adiponectin,** an adipocyte-specific hormone, has insulin-sensitizing and anti-inflammatory properties (100). In fact, adiponectin levels are decreased in obese rodents and humans (100). This hormone enhances glucose uptake and oxidation by liver and muscle, as well as it inhibits glucose production. In pancreas, adiponectin preserves insulin secretion and β-cell mass (97). Differently from leptin and adiponectin, **resistin** is secreted by adipocytes and adipose tissue macrophages in mice, but only by circulant monocytes and tissue macrophages in humans (101). It has been shown that resistin plasma levels correlate with obesity, and its presence favours the development of IR (93,97).

Aside from the typical adipose hormones previously described, white adipocytes also secrete many other hormones that are usually tight related with obesity and IR. Although they are not exclusively secreted by WAT, their secretion is modulated in this tissue under pathological conditions. For instance, the expression of ***retinol-binding protein 4*** **(RBP4)**, the main plasma carrier for retinol, is especially high in visceral WAT from adults with obesity and IR. In visceral WAT, RBP4 drives adipocyte hypertrophy and inflammation. This factor induces tissue-specific IR in skeletal muscle and adipocytes, but it also promotes systemic IR (97). Similarly, ***fatty acid-binding protein 4*** **(FABP4),** which it is highly released from adipocytes of obese and T2D individuals, increases gluconeogenesis in liver and promotes lipolysis in AT, thereby favouring the development of IR (97). In addition, **vaspin**, an insulin-sensitizing protease inhibitor, is more secreted by WAT from obese individuals and promotes IR (97). Contrary to the hormones up-regulated in WAT from obese and T2D individuals, other endocrine factors are down-regulated in white fat from these subjects. This is the case of omentin or adipsin. **Omentin**, an adipokine derived from the stromal vascular fraction of WAT, enhances insulin-stimulated glucose uptake in adipocytes, promotes weight loss and has anti-inflammatory effects. However, its expression in WAT and its serum levels are reduced in obese and diabetic subjects (93). In the case of **adipsin** (also known as complement factor D), a modulator of inflammatory status, its circulant levels in obese mice decline over time, suggesting a protective role in obesity. In this sense, it boosts glucose-dependent insulin secretion in murine pancreatic β-cells. By contrast, studies in humans indicate a proinflammatory role of adipsin and an increment in its circulating concentration in obese individuals (97).

Noteworthy, WAT from obese individuals prone to develop T2D is also the major source of classical pro-inflammatory cytokines, such as IL-6, TNF-α and *interleukin 1* beta (IL-1β) (93). As previously described (see section 1.1.2), the levels of these adipokines are positively correlated with adiposity, insulin levels, weight gain and IR. IL-6 is released from adipocytes subjected to high lipolysis rates, TNF-α is mainly secreted by pro-inflammatory macrophages that infiltrate WAT (93) and IL-1β is mostly produced by adipose macrophages and it promotes IR in adipose tissues (102).

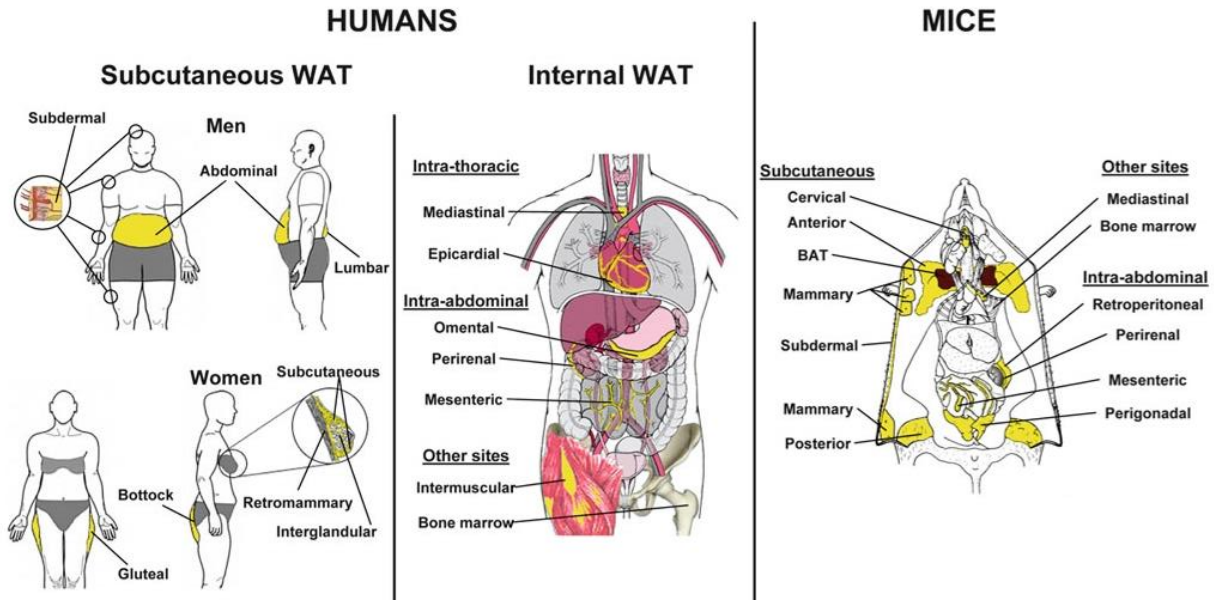


**Figure 1.10. Distribution pattern of WAT depots in human and mice**. Both species consist of white fat under the skin, subcutaneous WAT, and inside the internal cavities or visceral WAT. The main difference between species is that perigonadal WAT is only found in mice. Image obtained from (92).

### 1.3.2 Brown adipose tissue

Oppositely to white fat, BAT main function is the production of heat to maintain body temperature through a process known as non-shivering adaptive thermogenesis. BAT consists of brown adipocytes containing multilocular lipid droplets and an abundant number of mitochondria (Figure 1.9), which confers this tissue a brownish colour and a great oxidative capacity. Brown fat is highly vascularized and innervated by the sympathetic nervous system (103,104). Neglected for a long time in adult humans, BAT was considered almost exclusive from new-borns and small mammals such as rodents. However, relatively recent studies demonstrated by *$^{18}$F-fluorodeoxyglucose* ($^{18}$F-FDG)-PET/CT that functional brown fat is also present in adult humans (105-107).

BAT is anatomically distributed in very specific depots. In mice, BAT is found in interscapular, cervical, axillary, perirenal, mediastinal and mammary regions (108). In adult humans, this tissue is located in neck, supraclavicular, axillary, paravertebral, periaortic and suprarenal regions (109,110). BAT allocation along the principal blood vessels facilitates the rapid diffusion of heat generated through the body.

#### 1.3.2.1 “Beige” adipocytes in white adipose tissue

In rodents, prolonged cold exposure or adrenergic signalling induce the appearance of clusters of UCP-1$^{+}$ cells adopting a brown fat-like morphology amongst white adipocytes, in a process called “browning”. These cells, called “beige” or “brite” adipocytes, are found in much higher numbers in subcutaneous WAT rather than in visceral WAT (91). Despite the similarity with brown adipocytes, beige adipocytes share the same progenitor as white adipocytes, and are transdifferentiated directly from mature white cells or after the differentiation of the common precursor (111,112). Akin to brown adipocytes, beige adipocytes are capable of producing heat when it is required. Once heat production is no longer necessary, beige

adipocytes undergo a conversion back to an energy-storing white adipocyte, highlighting a remarkable adaptation capacity (91).

#### 1.3.2.2 Non-shivering thermogenesis

As previously mentioned, the main function of BAT is the generation of heat by means of non-shivering thermogenesis (Figure 1.11). At thermoneutral conditions, 23°C in humans and 28-30°C in mice, extra heat production is no necessary to sustain body temperature (113), as basal metabolism is sufficient to maintain it. However, at lower temperatures, generation of heat by specialized means is required. Given the fact that shivering thermogenesis by skeletal muscle is limited in time, BAT non-shivering thermogenesis raises as an efficient and long-lasting source of heat (114). In order to accomplish this mission, BAT contains a large number of mitochondria expressing *uncoupling protein 1 (Ucp1)*. This protein is unique from brown fat and its function and regulation are the same in rodents and humans (115). The presence of UCP1 provides singular characteristics to BAT mitochondria, as oxidation of substrates is not coupled to ATP synthesis in this organelle. As in normal ATP synthesis, the energy derived from the electron transport chain through the mitochondrial complexes is used to pump protons out of the mitochondrial matrix into the inter-membrane space. However, in this case proton gradient generated between compartments is not used by ATP-synthase to form ATP, but by UCP1 to dissipate energy in the form of heat (114).

Non-shivering thermogenesis is mainly regulated by the central nervous system (Figure 1.11). When faced a cold environment, the decrease in body temperature is sensed by the paraventricular and ventromedial nuclei of hypothalamus, which in turn innervate BAT through sympathetic nerve fibers (114). Sympathetic terminals release norepinephrine, which promotes brown adipocytes differentiation and activation through $\beta_1$- and $\beta_3$-adrenoreceptors. In brown cells, norepinephrine stimulation of β-adrenoreceptors activates G stimulatory (Gs) proteins, leading to the production of intracellular cAMP via the activity of *adenylate cyclase* (AC). Cyclic AMP acts as a second messenger that activates *protein kinase A (*PKA*)*, a downstream effector that triggers the pathways required for the thermogenic response. On the one hand, it phosphorylates the *hormone sensitive lipase* (HSL) and perilipin from the lipid droplets, thereby prompting lipolysis to supply fatty acids for the production of heat. On the other hand, PKA up-regulates the expression of the thermogenic genes *Ucp1* and *cAMP responsive element binding protein (Creb)* in collaboration with the PGC-1α transcriptional co-activator. In the same extent, long-term cold stimulation increases the expression of genes from the electron transport chain, *tricarboxylic acid cycle* (TCA*)* and beta-oxidation to increment the thermogenic capacity (114). To this aim, circulant nutrients such as glucose, amino acids, glutamate and NEFA are also uptaken by BAT to supply energy (116).

Non-shivering thermogenesis is modulated by a variety of factors and hormones (115). Insulin inhibits lipolysis and negatively affects thermogenesis, whereas glucagon administration increases whole-body oxygen consumption in rodents and humans. Regarding incretins, GLP-1 peptide has been shown to stimulate BAT activity and WAT browning, although the paper of GIP remains unclear. Importantly, thyroid hormones are crucial for BAT thermogenic function through the regulation of thermogenic genes (114).

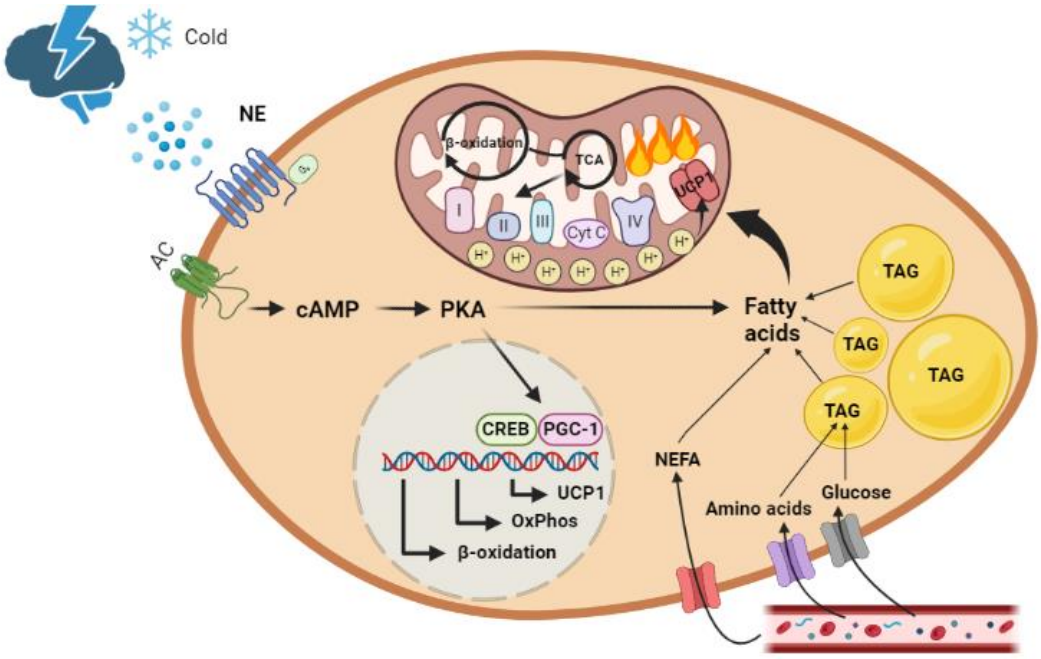


**Figure 1.11. Overview of the signalling pathways that control non-shivering thermogenesis in BAT**. Cold stimulus drives, through the effect of norepinephrine, the thermogenic response in brown adipocytes. This response accounts for the mobilization of circulatory fuels, the lipolysis of triglycerides from lipid droplets and the up-regulation of thermogenic genes. AC, Adenylate Cyclase; NE, Norepinephrine; cAMP, cyclic Adenosine Monophosphate; PKA, Protein Kinase A; CREB, cAMP Responsive Element Binding protein; PGC-1, PPARγ co-activator 1; UCP1, Uncoupling Protein 1; OxPhos, Oxidative Phosphorylation; TAG, Triglycerides; NEFA, Non-esterified Fatty Acids; TCA, Tricarboxylic Acid cycle. Image adapted from (111,115,116).

### 1.3.2.3 BAT development: the role of *Pparg* co-activators 1 (PGC-1s)

Both white and brown adipocytes arise from progenitor cells of the embryonic mesoderm, sharing the developmental origin with other tissues such as skeletal muscle or bone. At this point, the expression of specific morphogens commits mesodermal stem cells to the formation of BAT and muscle instead of WAT or bone (117). In this regard, the activation of the hedgehog and *wingless and int* (WNT)-signalling pathways, together with the participation of members from the *bone morphogenetic proteins* (BMPs) (BMP4/7) and FGF (FGF16/19) families, differentiate mesodermal progenitors to fibroblast-like brown adipogenic progenitors, which give raise to BAT and skeletal muscle cells. In mouse, these progenitors clearly originate brown fat cells at day 15.5 of the embryonic development. To differentiate from muscle cells, fibroblast-like adipogenic progenitors are subjected to a transcriptional control by *zinc finger proteins* (ZFPs) members such as Zfp423, which positively regulates the commitment of progenitors to the adipogenic lineage. For this, Zfp423 enhances the expression of the *Pparg* gene, a master regulator of adipogenesis. In turn, the expression of *Pparg* is also promoted by the expression of the *early B-cell factor 2* (EBF2) in differentiating brown adipocytes. But, most importantly, PPARγ is tightly regulated by PGC-1α throughout the differentiation into adipocytes, as PGC-1α is the main driver of the *Pparg* expression (Figure 1.12). Together with the tandem PGC-1α-PPARγ, *PR/SET domain* 16 (PRDM16) is also crucial to specify the differentiation of brown adipocytes. Apart from interacting with the family of *CCAAT/enhancer-binding proteins* (C/EBPs), which are essential to form mature adipocytes, PRDM16 down-regulates the expression of myogenic transcription factors such

as *myf5, myoD* and *myogenin*. Hence, the differentiation of brown adipocytes is principally driven by PRDM16 and the PGC-1α, which controls PPARγ.

PGC-1 family is composed by *PGC-1 related co-activator* (PRC), PGC-1β, PGC-1α and the short isoforms NT-PGC-1α and PGC-1α4. As any of these members possess histone acetyl transferase activity to modify gene expression, they serve as docking platforms for other proteins with histone acetyl transferase capacity (118), such as *lysine acetyltransferase 2A* (KAT2A). Despite the lack of the carboxy-terminal region, the truncated NT-PGC-1-α isoform retains the full capacity to enhance energetic metabolism as PGC-1α (119). PGC-1α4, by its side, shares the same sequence as the NT-PGC-1-α isoform and it is originated from an alternative promoter located upstream of the *Ppargc1a* gene (118).

PGC-1 co-activators integrate environmental and physiological signals in order to regulate transcription factors related to the energetic metabolism. Specifically, PGC-1α and PGC-1β respond to environmental cues that signal high energy demands (e.g., fasting, exercise, cold) by increasing mitochondrial biogenesis and function and fulfil the energy requirements. In this sense, PGC-1α regulates hepatic gluconeogenesis, muscular slow-twitch fiber conversion and adaptative thermogenesis in BAT (118). By its side, induction of PGC-1β is principally relevant in the liver, as this co-activator enhances *de novo* hepatic lipogenesis, resulting in an increase in the synthesis of fatty acids, triglycerides and cholesterol (120). PRC displays a similar expression pattern across different tissues and its role in adults remains unclear (121). In fact, *in vitro* studies indicate that PRC expression is elevated in proliferating cells. During cell proliferation, PRC member orchestrates mitochondrial biogenesis and function in association with the same transcription factors as PGC-1α (122,17).

Adipose tissues differ in the expression level of PGC-1s. Whereas BAT, a mitochondria-rich tissue, consists of high expression of PGC-1α and PGC-1β, WAT exhibits a lower expression of these co-activators. PGC-1α controls different mitochondrial pathways in BAT such as oxidative phosphorylation, tricarboxylic acid cycle or fatty acid oxidation, but it is only required for the regulation of non-shivering thermogenesis (Figure 1.12). Upon cold exposure, PGC-1α capitalizes the thermogenic response by inducing the expression *of Ucp1* and *deiodinase-2 (Dio2)*, the enzyme that produces $T_3$ hormone (123). Moreover, it enhances the activity of some transcription factors (thyroid hormone receptor, PPARγ, PRDM16, and others) that drive the thermogenic response (123). In WAT, by contrast, PGC-1α is not essential for mitochondrial gene expression, although it is needed for the differentiation of beige adipocytes in this tissue (124).

Due to the redundant role in mitochondrial biogenesis and function of both PGC-1α and PGC-1β co-activators, one of them can compensate the lack-of-function of the other. Hence, deletion of both co-activators results in higher metabolic alterations. For instance, PGC-1α activity is dispensable for the adaptation of muscle to exercise maybe through the compensation of PGC-1β (125). In a similar way, brown adipose PGC-1β expression may compensate the lack of PGC-1α-related regulation of mitochondria under housing temperature conditions. However, loss of both co-activators leads to a severe reduction in mitochondrial biogenesis and function (126) (see section 1.1.2). Functional redundancy of PGC-1 co-activators also plays an important role in the differentiation of beige and brown

adipocytes. In this sense, PGC-1α alone seems to be dispensable for the differentiation of these cells, but deletion of both co-activators causes a total loss of cell differentiation and mitochondria biogenesis (126).

PGC-1 co-activators orchestrate the increase in the mitochondrial biogenesis and function by increasing mitochondrial mass and gene expression through the regulation of essential nuclear and mitochondrial transcription factors such as NRFs, PPARs and ERRs (127) (Figure 1.12). ***Nuclear respiratory factors 1*** **and** ***2*** **(NRF1/2)** are transcription factors implicated in the regulation of the subunits of the OxPhos system, as well as in the import and assembly of mitochondrial proteins (128,129). Moreover, NRF1/2 also regulate the expression of ***mitochondrial transcription factor A*** **(TFAM)** and ***mitochondrial transcription factor B1 and B2*** **(TFB1M and TFB2M)**, which are essential factors involved in the replication and transcription of *mitochondrial DNA (mtDNA)* (130). ***Peroxisome-proliferator-activated receptors α*** **and** ***δ*** **(PPARα and PPARδ)** are responsible for the regulation of mitochondrial genes involved in lipid transport and oxidation (131,132). ***Estrogen-related receptors α*** **and** ***γ*** **(ERRα and ERRγ)** are known to be critical in many aspects of mitochondrial biogenesis. In this sense, ERRα regulates the expression of genes from the OxPhos system, tricarboxylic acid cycle and fatty acid oxidation. Moreover, this factor also controls the transcription of genes related to mitochondrial dynamics and mtDNA replication and transcription via TFAM activation. ERRγ binds, by its side, to the same regulatory elements than ERRα and, therefore, it regulates mitochondrial biogenesis in a similar way (127).

Many studies have highlighted the relation existing between mitochondrial dysfunction and the development of IR and type 2 diabetes (reviewed in section 1.1.2). In this regard, individuals suffering from IR and type 2 diabetes exhibit a decrease in mitochondrial mass and gene expression in different organs such as skeletal muscle and adipose tissue. The alteration in the mitochondrial parameters in these tissues has been also associated to a reduction in the expression levels of both PGC-1α and PGC-1β. This data leads to the notion that PGC-1s reduced activity contributes to the development of IR that precedes T2D (133,134). In fact, some polymorphisms in the *Ppargc1a* gene have been linked to T2D (135-137). In line with this, it has been observed that adipose tissue-specific PGC-1α deletion in mice fed a HFD resulted in IR in parallel to a decrease in mitochondrial gene expression (138). In opposition to this data, an adipose-specific PGC-1α knockout model generated in our laboratory has not exhibit signals of mitochondrial dysfunction or IR (124). Similarly, loss-of-function of PGC-1 co-activators in skeletal muscle has led to conflicting results. Some studies indicate that reduced expression of PGC-1α in muscle of T2D individuals is associated with the disruption of glucose homeostasis (139,140). In other studies, however, specific deletion of PGC-1α, PGC-1β or both co-activators simultaneously do not correlate with IR despite showing mitochondrial dysfunction (125). Tissue-specific overexpression of PGC-1 co-activators have not clarified neither their contribution to the onset of IR and T2D. In this sense, whereas PGC-1α overexpression is correlated with IR in some studies (141), other reports claim for the opposite (142). In a preliminary study from our laboratory (see section 1.1.2; 36), adipose-specific deletion of both PGC-1α and PGC-1β resulted in impaired mitochondrial function in this tissue. Although a certain grade of glucose intolerance was observed, insulin sensitivity was preserved in these mice.

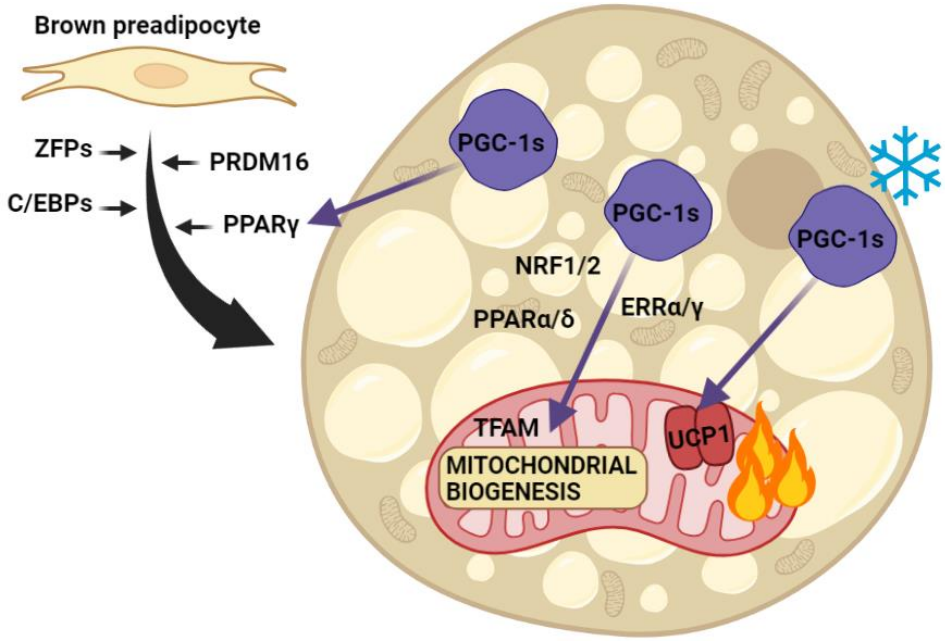


**Figure 1.12**. **PGC-1s regulation of brown adipocyte differentiation and functions.** PGC-1s are crucial for the differentiation of brown adipocytes, as well as for their thermogenic function and for the regulation of mitochondrial biogenesis. ZFPs, Zinc Finger Proteins; C/EBPs, CCAAT/Enhancer-Binding Proteins; PRDM16, PR/SET Domain 16; PPARγ, Peroxisome Proliferator-Activated Receptor γ; PGC-1s, PPARγ Co-activators 1; NRF1/2, Nuclear Respiratory Factors 1 and 2; PPARα/δ, Peroxisome Proliferator-Activated Receptors α and δ; ERRα/γ, Estrogen-Related Receptors α and γ; TFAM, Mitochondrial Transcription Factor A; UCP1, Uncoupled Protein 1. Image adapted from (117,118).

#### 1.3.2.4 Brown adipose tissue and the control of glucose homeostasis and energy balance

Given the amount of energy expended during the thermogenic process, it is evident that BAT activation plays an important role in the energy balance. In fact, numerous studies indicate that the amount of BAT is inversely correlated with the BMI, whereas individuals with detectable brown fat show a lower index of obesity and a higher energy expenditure (143-145). Parallelly, obesity is also associated with a reduction in BAT thermogenic capacity (146).

BAT activity is proven to reduce hyperlipidaemia and counteract obesity, thereby improving insulin sensitivity and lowering the risk to develop T2D (147,148). The amelioration in whole-body glucose homeostasis and insulin sensitivity is driven also in healthy individuals after cold exposure (149). On one side, brown fat is a highly oxidative tissue that uptakes and burns lipids in a rapid and efficient manner. Therefore, it promotes triglycerides and fatty acids clearance from plasma to replenish intracellular reserves or oxidize them to carry on thermogenesis (149). In a similar way, circulant glucose is also decreased to supply energy to this tissue (150). The role of BAT as a glucose sink contributes to the glycaemic control and the improvement of glucose homeostasis. This effect is amplified by the hypolipidemic action of BAT, what contributes to prevent ectopic accumulation of lipids in insulin-sensitive tissues, therefore reducing lipotoxicity, a process with detrimental actions on insulin sensitivity.

#### 1.3.2.5 BAT as a secretory organ

The fact that traditionally WAT cytokines such as leptin are poorly secreted by BAT, have contributed to neglect the secretory capacity of brown fat for a long-time. Nowadays, however, a myriad of BAT secreted adipokines are being discovered. The uncovering of these molecules is gaining attention for their role as regulators of metabolism. However, to date, none of these molecules are found to be exclusively secreted by BAT, and therefore they are referenced as preferentially secreted by BAT in comparison to WAT or other tissues (151). Moreover, despite some factors are secreted by non-adipose cells such as immune or vascular cells from the SVF of BAT, some studies have provided evidence that activated brown adipocytes directly secrete factors that can act as batokines in mice (152-154). In humans, by contrast, information about BAT secretome is still scarce and, therefore, most conclusions are provided by studies made with rodents. Nevertheless, recent reports have also highlighted the importance of several human batokines in health and disease (155).

Akin to other secretory tissues, it has been observed that, in rodents, most BAT secrete factors have autocrine and paracrine actions. On one side, BAT secretes molecules that promote its activity and functioning. In this sense, ***neuroregulin 4*** **(NRG4)** (151)***, nerve growth factor*** **(NGF)** (156) **and** ***fibroblast growth factor 2*** **(FGF2)** (157) released from BAT target nerve endings promote their outgrowth, thereby increasing sympathetic innervation in this tissue to fulfil its thermogenic function. Apart from enhancing its own innervation, BAT also secretes factors to prompt its vascularization. In this regard, ***bone morphogenesis protein 8b*** **(BMP8b)** secreted by brown adipocytes, which sensitises these cells to the noradrenergic stimulus via NRG4 induction, also favours the growth of capillaries in this tissue (151). Similarly, ***vascular endothelial growth factor A*** **(VEGFA)** is secreted by brown adipocytes to promote vascularization (158).

On the other side, BAT also secretes factors with the potential to impact brown adipocyte differentiation and commitment. Specially, BMPs have strong effects on these pathways. **BMP7**, which is produced by the SVF of BAT, is capable to induce brown adipogenesis trough the activation of PRDM16 and PGC-1α. BMP7 also enhances mitochondrial activity and lipid metabolism in fully activated brown adipocytes. Moreover, BMP7 promotes BAT recruitment and therefore induces weight loss by increasing energy expenditure (159). **BMP4** promotes the differentiation of brown-like adipocytes in WAT (160). Differentiation of BAT is also inhibited by factors secreted by this tissue. In this regard, the secretion of the ***growth differentiation factor 8*** **(GDF8)** or myostatin by BAT, negatively regulates brown adipocytes differentiation and thermogenic function, as well as inhibits the browning of WAT (161). **Follistatin**, another BAT adipokine induced when faced cold temperatures, counteracts myostatin effects by inhibiting this factor and allowing the differentiation of brown adipocytes (160).

Importantly, BAT secreted factors can directly regulate the immune system within the tissue. **IL-6**, considered a pro-inflammatory cytokine, exerts the opposite effects in BAT. In this tissue, its up-regulated when stimulated with cold, and then it activates the alternative anti-inflammatory M2 macrophages (162). Moreover, IL-6 promotes brown adipocytes activity and WAT browning (160). Similarly, the ***chemokine C-X-C motif chemokine ligand-14***

**(CXCL14)** is secreted by brown adipocytes in response to noradrenergic stimulation and it promotes the recruitment and activation of M2 macrophages (151).

BAT also secretes molecules with the potential to act in an endocrine way. Nevertheless, studies addressing the endocrine role and physiological impact of batokines are not conclusive and information is scarce. By far, the most well-known endocrine factor secreted by BAT is **FGF-21**. BAT secretes FGF-21 when stimulated by cold. In this situation, FGF-21 promotes glucose uptake and oxidation in glucose-sensing tissues, thereby improving glycaemia and lipidaemia (163,164). Moreover, FGF-21 enhances insulin sensitivity by expanding subcutaneous adipose tissue (165) and prevents the onset of diet-induced diabetes by activating the thermogenesis and the browning of WAT via PGC-1α (166, 167). In humans, it has been observed that cold exposure increases the plasma levels of FGF21, suggesting that enhanced BAT activity may improve glucose homeostasis by means of increasing FGF-21 (168). Finally, FGF-21 also has a strong cardioprotective effect (151). Despite the proven actions of FGF21, most of circulating FGF21 has a hepatic origin and, therefore, the contribution of FGF21 secreted by BAT to whole physiology has been questioned. Aside from FGF-21, many other factors secreted by BAT, some of which have an autocrine or paracrine effect, also target distant tissues. In this sense, myostatin secretion by BAT is known to negatively affect muscle insulin sensitivity, growth and functioning (161). Some other factors secreted by BAT have endocrine effects, such as ***angiopoietin-like 8*** **(ANGPTL8)**, which enhances pancreatic β-cell replication (160) or ***insulin-like growth factor-binding protein 2*** **(IGFBP2)**, which promotes bone remodelling (161).

#### 1.3.2.6 BAT recruitment and activation as a therapeutic strategy for obesity and diabetes

The relevance of BAT in the control of glucose homeostasis has opened a door to the development of therapeutic strategies based on enhancing BAT activity and mass for the treatment of obesity and diabetes. For instance, BAT activation through cold exposure in humans has been associated to improvements in body composition (169). However, this method of activation of BAT is uncomfortable and requires the strong commitment of patients, which it is not always easy. For this reason, the transplantation of BAT from healthy individuals to recipients suffering from obesity and T2D is gaining attention as a possible efficient mechanism to counteract these pathologies. In fact, some studies have investigated the potential of BAT transplantation to prevent obesity. In one study, BAT transplantation in recipient mice fed a HFD reduced body weight and adiposity in these mice, concomitantly to an improvement in glucose tolerance and insulin sensitivity (170). In another study made in a HFD mouse model, it was confirmed that transplanted BAT prevented weight gain and increased energy expenditure in recipient mice (171). In a similar way, transplantation of subcutaneous WAT in which browning was present resulted in an amelioration on glucose homeostasis in these mice (172).

The beneficial effects seen with BAT transplantation are not restricted to its thermogenic capacity. In fact, transplanted BAT usually involutes and loses part of its thermogenic capacity, but it still ameliorates body weight and glucose homeostasis in the recipients. Therefore, other additional factors seem to be behind the positive effects that transplanted BAT exerts

on energy balance and glucose homeostasis. In this regard, some studies have observed that the levels of some BAT secreted factors such as IL-6 and FGF-21 are modulated in recipients (173), thereby suggesting that batokines are likely to mediate the positive effects observed after the transplantation of BAT.

Some batokines have been identified or postulated as possible factors mediating BAT beneficial effects, as is the case of FGF-21, IL-6, IGF-1, NRG4 and VEGFA (174). Circulating **FGF-21** levels are increased in mice after BAT transplantation (173).

# 2. HYPOTHESIS & OBJECTIVES

## HIPOTHESIS AND OBJECTIVES

Previous studies in our laboratory aimed at defining the contribution of impaired mitochondrial function to the development of obesity and insulin resistance showed that mice with reduced mitochondrial mass as a result of the lack of co-activators PGC-1α and PGC-1β in adipose tissues did not exhibit changes in body weight or insulin sensitivity when fed a high fat diet with a 45% of the Kcal from fat. However, these mice exhibited a tendency towards the development of glucose intolerance and presented lower fasting insulin levels, pointing towards a defect in the pancreatic function. Moreover, adipose tissues, both white and brown, are known to control the activity of distant tissues by secreting a variety of molecules, including proteins, generically known as adipokines. Considering the mild glucose intolerance previously observed and the evidences pointing at a defect in β-cell function as the underlying cause of the glucose intolerance developed, I propose the hypothesis that *lack of PGC-1s co-activators in adipocytes alters their endocrine function and disrupts the crosstalk between adipose tissues and pancreas, leading to β-cell failure and the development of glucose intolerance.*

To prove this hypothesis and identify the molecules involved in the adipose tissues-pancreatic crosstalk, I propose the following objectives:

**Objective 1.** To precisely define the effects that impaired mitochondrial function in adipose tissues has on glucose homeostasis in mice lacking PGC-1 co-activators in adipose tissues.

**Objective 2.** To identify the mechanism causing pancreatic β-cells dysfunction in adipocyte-specific PGC-1α/β knockout mice.

**Objective 3.** Identify the protein or proteins secreted by white and brown adipose tissues that mediate the adipose-pancreatic crosstalk.

# 3. MATERIALS & METHODS

## 3.1 Animal studies

### 3.1.1 Description of adipose-specific PGC-1α/β double knockout mouse model

Adipose-specific PGC-1α/β double knockout mice (PGC-1α/β-FAT-DKO mice) were previously generated in the laboratory (36) by means of the *Cre/loxP* recombination system. With this gene editing technique, a specific genetic locus of interest is flanked with two *loxP* motifs, a target nucleotide sequence consisting of 34 bp (ATAACTTCGTATANNNTANNNTATACGAAGTTAT). These regions are recognized by the *Cre* recombinase enzyme, allowing the deletion of the genes only in those cells expressing *Cre*.

To obtain PGC-1α/β-FAT-DKO mice, mice with exons 4-5 of *Ppargc1a* and *Ppargc1b* genes flanked by *loxP* sites (*Ppargc1a*$^{flox/flox}$ /*Ppargc1b*$^{flox/flox}$) were crossed with transgenic mice that overexpress *Cre* recombinase under the adipose-specific promoter of *AdipoQ* gene (AdipoQ-Cre mice) (Figure 3.1)

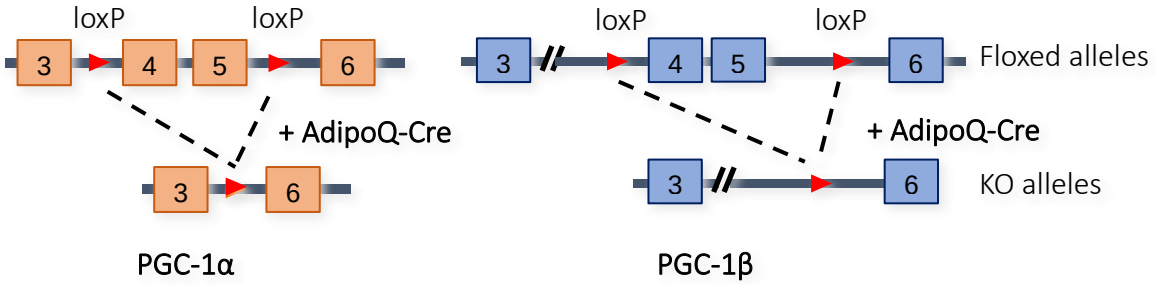


**Figure 3.1**. **Scheme of PGC-1α/β-FAT-DKO mice generation.** Deletion of *Ppargc1a* and *Ppargc1b* was performed by *Cre* recombinase, which recombines *loxP* sites flanking exons 4 and 5 of these genes. Cre recombinase was expressed under the control of adiponectin promoter and, therefore, recombination was specific from adipose tissue (36).

### 3.1.2 Mice genotyping

At 21 days postpartum, mice were weaned, earring and genotyped to differentiate between Wt and PGC-1α/β-FAT-DKO mice. For this, a small piece of tail was digested and DNA was isolated. Then, a *polymerase chain reaction* (PCR) was performed in order to identify *Ppargc1a* and *Ppargc1b* Wt and floxed alleles. A second PCR determined the presence of the *AdipoQ*-Cre transgene. These procedures are explained in detail below.

#### 3.1.2.1 DNA extraction

Total DNA was extracted from the mice tails by *Proteinase K* (PK) (Canvax) digestion, which disrupts the tissue and facilitates the release of nucleic acids. For this, 1-2 mm of tail were cut and digested overnight at 40°C with constant shaking in 500 µL of PK digestion buffer (0.5% SDS, 0.1 M NaCl, 0.05 M Tris-HCl pH 8, 3 mM EDTA, 3U/mL PK). Then, DNA was isolated by chloroform-ethanol extraction and precipitation. To do this, 75 µL of 8 M potassium acetate and 500 µL of chloroform were added to the digestion mix, followed by a vortex of the samples. Once vortexed, samples were stored at 80°C for one hour. Then, samples were centrifuged at 13,000 rpm for 5 min at room temperature to recover the DNA-containing aqueous phase. Nucleic acids were precipitated with 1 mL of 100% ethanol and samples were

centrifuged at 13,000 rpm for 5 min at 4°C. With this, we obtained a small DNA pellet. Samples were subsequently washed with 500 µL of 70% ethanol, air-dried and re-suspended in miliQ water. For better resuspension, samples were incubated at 40°C during 10 min with constant shaking. Concentrations were measured with a NanoDrop ND-2000 spectrophotometer and the purity of the samples was determined based on 260/280 and 260/230 ratios. Pure and uncontaminated DNA samples show a 260/280 ratio of 1.8 and a 260/230 ratio of 2.0-2.2 approximately.

#### 3.1.2.2 PCR

To identify mice carrying *loxP* motifs flanking *Ppargc1a* and *Ppargc1b* genes, specific primers flanking *loxP* sites between exons 3 and 6 were used. Similarly, the presence of the *AdipoQ*-Cre transgene was also determined.

To amplify the target DNA, a mix containing 100-200 ng of DNA, forward and reverse specific primers (Table 3.1), Taq DNA polymerase enzyme and a specific buffer was prepared (final concentration is resumed in Table 3.2).

| | Sequence |
|---|---|
| ***Ppargc1a floxed allele*** | |
| **Forward primer** | CACGCTTCATCCCATCTCTGT |
| **Reverse primer** | CAATTGTCAGCTCCCAACTGTCT |
| ***Ppargc1b floxed allele*** | |
| **Forward primer** | GGCTACCGTGCTGCACTGTT |
| **Reverse primer** | ACAGATGCCCTTTAAGGTGACATA |
| ***Cre* transgene** | |
| **Forward primer** | GACGAAATCCATCGCTCGACCAG |
| **Reverse primer** | GACATGTTCAGGGATCGCCAGGCG |

**Table 3.1. Specific primers used for genotyping.** Sequences of primers used to detect *Ppargc1a/Ppargc1b* floxed alleles and *Cre* transgene. Expected fragments lengths are also indicated.

| Component | Final concentration |
|---|---|
| **Water** | |
| **10X PCR buffer** | 2 mM $MgCl_2$ |
| **dNTP mix (10 mM each)** | 200 µM (of each dNTP) |
| **Forward primer (10 µM)** | 0.52 µM |
| **Reverse primer (10 µM)** | 0.52 µM |
| **Taq DNA polymerase (5U/µL)** | 0.05 U/µL |

**Table 3.2. Master mix composition for PCR amplification.** Final concentrations are indicated.

A GenAmp PCR System 2400 (Perkin Elmer) thermocycler was used for the reaction, which took place in optimized times and temperatures for each of the genes amplified (Table 3.3).

**A. *Ppargc1a/Ppargc1b* genotyping**

| Step | Temperature | Time | Cycles |
|---|---|---|---|
| Denaturation/Activation | 94°C | 2 min | 1 |
| Denaturation | 94°C | 30 sec | 35 |
| Annealing | 60°C | 30 sec | |
| Extension | 72°C | 45 sec | |
| Final extension | 72°C | 5 min | 1 |
| Cooling | 4°C | ∞ | 1 |

**B. *Cre* genotyping**

| Step | Temperature | Time | Cycles |
|---|---|---|---|
| Denaturation/Activation | 94°C | 5 min | 1 |
| Denaturation | 94°C | 45 sec | 30 |
| Annealing | 64°C | 45 sec | |
| Extension | 72°C | 45 sec | |
| Final extension | 72°C | 10 min | 1 |
| Cooling | 4°C | ∞ | 1 |

**Table 3.3. PCR steps to genotype *Ppargc1a/Ppargc1b* (A) and *Cre* (B) genes.**

### 3.1.2.3 Agarose gel electrophoresis

DNA amplification products were separated by size in agarose gel containing *Tris-Acetate-EDTA* (TAE) buffer (40 mM Tris, 20 mM acetic acid, 1 mM EDTA). Percentage of agarose to resolve *Cre* amplified DNA was set to 1%, whereas for *Ppargc1a* and *Ppargc1b* it was necessary 2% of agarose. The DNA intercalating agent ethidium bromide was added to stain nucleic acids, which were visualized using an UV transilluminator.

The size of the amplicons expected in each PCR reactions is as follows:

*Ppargc1a*:

487 bp band → *Ppargc1a*$^{+/+}$ mouse

487 and 555 bp bands → *Ppargc1a*$^{flox/+}$ mouse

555 bp band → *Ppargc1a*$^{flox/flox}$ mouse

*Ppargc1b*:

166 bp band → *Ppargc1b*$^{+/+}$ mouse

166 and 234 bp bands → *Ppargc1b*$^{flox/+}$ mouse

234 bp band → *Ppargc1b*$^{flox/flox}$ mouse

AdipQ-Cre:

596 bp → *Cre*$^{+}$ mouse

No band → *Cre*$^{-}$ mouse

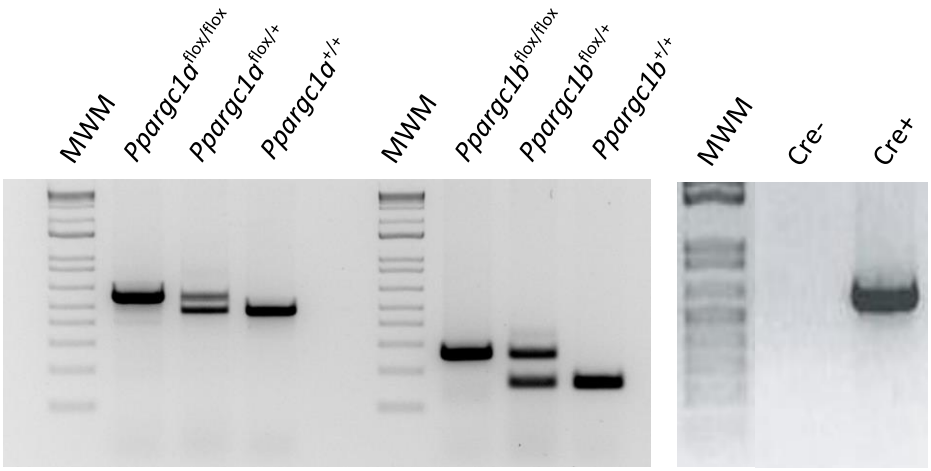


**Figure 3.2**. **Gel electrophoresis of DNA amplified products.** *Ppargc1a* and *Ppargc1b* genotypes to identify loxP flanked regions (*left*) and Cre genotype showing the Adiponectin-Cre transgene (*right*).

### 3.1.3 Mice housing conditions

Unless indicated differently, mice were bred and raised at 21°C on a 12 h light/dark cycle in the conventional clean area of *Vall d'Hebron Research Institute* (VHIR) animal facility.

For mouse breeding, adult *Ppargc1a*$^{flox/flox}$/*Ppargc1b*$^{flox/flox}$/adipoQ-Cre$^{-}$ (Wt) females were mated with adult *Ppargc1a*$^{flox/flox}$/*Ppargc1b*$^{flox/flox}$/adipoQ-Cre$^{+}$ (PGC-1α/β-FAT-DKO) males. This breeding strategy resulted on a heterogeneous offspring of *Ppargc1a*$^{flox/flox}$/*Ppargc1b*$^{flox/flox}$/adipoQ-Cre$^{-}$ (Wt) and *Ppargc1a*$^{flox/flox}$/*Ppargc1b*$^{flox/flox}$/ adipoQ-Cre$^{+}$ (PGC-1α/β-FAT-DKO) mice.

Three weeks after birth, mice were weaned and separated in cages according to their sex. Mice were distributed in cages containing 4-6 individuals/cage, placing the same number of Wt and PGC-1α/β-FAT-DKO mice within the same cage whenever possible. Mice were fed *ad libitum* to food and water. Depending on the experiment, mice were given a standard laboratory diet (Chow) (SAFE 150 Scientific Diets; 21% calories from proteins, 12.6% calories from fat, 66.4% calories from carbohydrates) or a (HFD) (Research Diets; 20% calories from protein, 60% calories from fat, 20% calories from carbohydrates).

All procedures involving animals were conducted according to the European Union Ethical Guidelines and approved by the Animal Experimentation and Ethics Committee of Vall d'Hebron Research Institute (ID 68/16 CEEA).

### 3.1.4 Assessment of glucose homeostasis

#### 3.1.4.1 Measurement of body weights

Body weights from mice were measured once a week to follow body weight gain. The measure was obtained the same week, at the same time and under the same environmental conditions.

#### 3.1.4.2 Basal glucose levels

Basal glucose levels of mice were measured after 5-6 h of fasting from the tail vein's blood using a glucometer (Contour XT, Bayer).

#### 3.1.4.3 Intraperitoneal glucose tolerance test

*Intraperitoneal glucose tolerance tests* (IpGTT) were performed in mice fasted for 6 h. Mice were tilted with their head toward the ground and injected with a load of D-glucose (G8644, Sigma) in their peritoneal cavity by means of a 25G needle and a syringe. Dose of glucose was different between mice fed a standard Chow diet (2 g/kg) and those fed a HFD diet (1-2 g/kg). A drop of blood from the tail was obtained and glucose levels were determined by using a glucometer (Contour XT, Bayer) at 0, 5, 15, 30, 60, 90 and 120 min after the intraperitoneal injection.

#### 3.1.4.4 Oral glucose tolerance test

*Oral glucose tolerance tests* (OGTT) were performed in mice fasted for 6 h. Mice received 2.5 g/kg body weight of D-glucose (G8644, Sigma) solution delivered by oral gavage. Blood glucose levels were determined from the tail at 0, 5, 15, 30, 60, 90 and 120 min after glucose administration, as described in section 3.1.4.3.

#### 3.1.4.5 Intraperitoneal insulin tolerance test

*Intraperitoneal insulin tolerance tests* (IpITT) were conducted to determine whole body insulin sensitivity. After fasting mice for 5 h, an insulin bolus was administered intraperitoneally to mice. *Actrapid* human insulin from Novo Nordisk® dissolved in saline solution (0.1-0.2U/mL) was used and injected to Chow (0.85 U/kg) and HFD (1 U/kg) fed mice. Glucose levels were measured in blood at 0, 5, 15, 30, 60, 90 and 120 min post-injection, as described in section 3.1.4.3.

### 3.1.5 Serological analysis

Blood from Wt and PGC-1α/β-FAT-DKO mice was collected from the tail of 5 h fasted mice. A small cut in the tip of the tail was done for the extraction of blood with a Microvette capillary tube (Sarstedt). Extracted blood was stored on ice and, prior to serum collection, kept at room temperature for 30 min. Then, blood samples were centrifuged at 3000 rpm for 10 min at 4°C. Serum was collected and stored at -20°C for further use.

#### 3.1.5.1 Cholesterol determination

Total cholesterol was quantified with commercial kit based on the Trinder colorimetric method (FAR diagnostics). In this protocol, esterified cholesterol is firstly hydrolysed into free cholesterol and fatty acid by cholesterol esterase. Then, free cholesterol is oxidized into cholestene-3-one by cholesterol oxidase, forming hydrogen peroxide. When peroxidase is present, hydrogen peroxide reacts with hydroxybenzoate and 4-aminoantipyrine producing a coloured complex. The intensity of colour can be measured at λ= 550 nm, being proportional to the concentration of total cholesterol present in the specimen. A cholesterol solution (200 mg/dL) was used as a standard and absorbance was read with a Spectra Max 340 spectrophotometer.

#### 3.1.5.2 Non-esterified fatty acids (NEFA) determination

FFA were assessed colorimetrically with the NEFA-HR kit (Wako Chemicals GmbH). In this method, NEFA are converted to Acyl-CoA, AMP and pyrophosphoric acid by Acyl-CoA synthetase, in the presence of coenzyme A and adenosine 5-triphosphate disodium salt. Next, Acyl-CoA is transformed to 2,3-trans-Enoyl-CoA and hydrogen peroxide by Acyl-Coa oxidase. When peroxidase is present, hydrogen peroxide contributes to the oxidative condensation of 3-Methyl-N-Ethyl-N-(β-Hydroxyethyl)-Aniline with 4-aminoantipyrine, producing a blue/purple pigment that can be measured at λ= 550 nm. In this final reaction, absorbance is proportional to NEFA concentration in the sample. 1 mmol/L NEFA solution was used as a standard and absorbance was read with a Spectra Max 340 spectrophotometer.

#### 3.1.5.3 Triglycerides determination

*Triglycerides* were evaluated using a commercial kit based on the Trinder colorimetric method (FAR diagnostics). The technique relies on the generation of products from TAG hydrolysis and in their later quantification. Firstly, triglycerides are converted into glycerol and fatty acids by lipoprotein-lipase. Glycerol is then transformed into glycerol-3-phosphate by glycerol kinase, and this product is oxidized by glycerol-phosphate-oxidase into hydroxyacetone phosphate, producing hydrogen peroxide. When peroxidase is present, hydrogen peroxide reacts with ethyl-sulphopropyl-toluidine and 4-aminophenazone to form a coloured complex, whose intensity of colour at λ= 550 nm is directly proportional to TAG concentration. The coloured product was measured colorimetrically using a Spectra Max 340 spectrophotometer and a TAG solution (200 mg/dL) was used as a standard.

#### 3.1.5.4 Insulin and C-peptide determination

Insulin and C-peptide were quantified in serum from fasted mice at basal state (no glucose administered) and during the course of both an intraperitoneal and an oral GTT (at 0, 5 and 15 min). Insulin was determined by using an Ultra-Sensitive Mouse Insulin ELISA Kit (Crystal Chem) and C-peptide with Mouse C-peptide ELISA Kit (Crystal Chem).

#### 3.1.5.5 Measurement of Adiponectin, Fstl1, glucagon, haptoglobin, leptin, MCP-3, SPARC and resistin

*Adiponectin* was determined in serum by ELISA using Mouse Adiponectin ELISA Kit (Crystal Chem). *Follistatin Like-1* (FSTL1) was measured with Mouse FSTL1 ELISA Kit (Ray Bio®). Glucagon was evaluated with Mouse Glucagon ELISA Kit (Crystal Chem). Haptoglobin was assayed with Mouse Haptoglobin ELISA Kit (Crystal Chem). Leptin was quantified with Mouse Leptin ELISA Kit (Crystal Chem). *Monocyte Chemoattractant Protein 3* (MCP-3) was assessed by Mouse MCP-3 Instant ELISA Kit (Invitrogen). *Secreted Protein Acidic And Cysteine Rich* (SPARC) was evaluated with Mouse SPARC ELISA Kit (Novus Biologicals) and *resistin* was determined by ELISA Mouse Resistin ELISA Kit (Thermo Scientific). All quantifications were performed in serum from 6 h fasted mice.

### 3.1.6 Acute cold exposure

For acute cold exposure experiments, 8-week-old Wt and PGC-1α/β-FAT-DKO mice were first acclimated at thermoneutrality (28-30°C) for 2 weeks. After the acclimation period, mice were individually caged with free access to food and water but with no environmental enrichment elements or bedding. A control group was maintained at thermoneutrality throughout the duration of the experiment, whereas cold-exposed mice were kept at 4°C for a maximum of 5 h. Core body temperature was monitored every hour for a period of 5 h, starting at 2 PM, with a rectal probe. Mice whose temperature dropped below 25°C were euthanized and they were not included for the experiment. After cold treatment, survivor mice were weighed and euthanized by cervical dislocation to obtain their tissues.

### 3.1.7 Tissue collection

After each experiment, mice were euthanized by cervical dislocation. Tissues and organs, including inguinal and gonadal WAT, BAT, liver, thymus, pancreas and soleus and gastrocnemius muscles were collected, weighed and quickly frozen in liquid nitrogen in order to analyse RNA, DNA and protein. For histological analysis, a piece of fresh tissue of approximately 0.5 $cm^3$ was collected and fixed for 12-24 h (depending on the tissue) with 4% paraformaldehyde (PFA) for posterior processing (see section 3.3).

## 3.2 Gene expression analysis

In order to quantify gene expression from tissue samples, total RNA was isolated by isopropanol precipitation or with a column-based purification kit. Then, isolated RNA was reverse transcribed to *complementary DNA* (cDNA) and quantified by *real time-quantitative PCR* (RT-qPCR).

### 3.2.1 Total RNA isolation

To prevent degradation of RNA by RNases, RNase-free solutions and material were used. Solutions were prepared using 0.1% *diethyl pyrocarbonate* (DEPC) treated water, a chemical that irreversibly inactivates RNases and other enzymes by modifying -NH, -SH and -OH groups.

#### 3.2.1.1 RNA isolation of adipose tissues and pancreatic islets by organic extraction with NZyol

Total RNA was isolated from samples by means of NZYol (Nzytech) reagent. NZYol contains phenol and ammonium thiocyanate that aid in disrupting cells and exposing cellular components while preserving RNA integrity. In association with chloroform, NZYol separates homogenized samples into organic and RNA-containing aqueous phases.

RNA was extracted from 50-100 mg of tissue. Tissue samples were homogenized in 0.5-1 mL of NZYol reagent, using a rotor-stator homogenizer (Ultra-Turrax IKA T25) or a hand-held mini-homogenizer for tissues containing elevated RNA concentrations, such as BAT (MiuLab, MT-13K). In order to separate phases, 200 µL of chloroform per mL of NZYol were added, followed by a 20 min centrifugation at 13,000 rpm and 4°C. RNA remained in the upper aqueous phase,

while DNA and proteins were retained in the interphase and in the lower organic phase. Then, the aqueous phase was recovered and transferred to a new tube, and one volume of isopropanol was added to precipitate RNA. After 10 min of centrifugation at 13,000 rpm and 4°C, the pelleted RNA was washed with 1 mL of 75% ethanol. The RNA pellet was again recovered through a centrifugation of 5 min at 9,500 rpm and 4°C. Then, RNA pellet was dried out and dissolved in RNase-free water. Finally, samples were incubated for 10 min at 55-60°C with constant shaking to dissolve the RNA in water. RNA samples were stored at -20°C for further analysis.

#### 3.2.1.2 RNA isolation from fatty tissues with GeneJet RNA Purification Kit

Excessive amount of lipids from tissues containing high amount of fat (i.e., WAT) can interfere with RNA isolation and subsequent enzymatic reactions. Hence, RNA extraction from WAT was performed by using a kit based on silica gel column (GeneJet RNA Purification Kit).

Tissues were firstly disrupted in 1 ml of NZYol with a homogenizer. To eliminate most part of the lipids, samples were centrifuged for 10 min at 12,000 rpm and 4°C. The fatty layer on the top was discarded and 200 µL of chloroform/mL NZYol were added and samples centrifuged at 12,000 rpm and 4°C during 10 min. The aqueous phase containing the RNA was then transferred to a new tube and mixed with one volume of 70% ethanol. Following, the mix was transferred to a RNA spin column from the Kit to extract RNA. The column was washed according to manufacturer's instructions and RNA was finally eluted by adding RNase-free water onto the column. RNA samples were stored at -20°C for further analysis.

### 3.2.2 RNA quality control

Following RNA isolation from samples, RNA concentration and purity were determined by UV absorption in a NanoDrop ND-2000 spectrophotometer. RNA concentration in the solution is evaluated by the *Optical Density* (OD) at 260 nm, in which an $A_{260}$ of 1.0 is translated to 40 µg/mL of RNA.

The purity of the isolated RNA is determined by comparing the absorbance of RNA to the absorbances of other molecules present in the samples, that is, proteins, phenol and other contaminants.

To assess RNA integrity of isolated RNA, 400 ng of RNA were run on a 1.2% agarose gel in TAE. The intercalating agent ethidium bromide was used to visualize the RNA. Total RNA samples migrated in the agarose gel at 90 V for 20 min, allowing the detection of the 5S, 18S and 28S rRNAs subunit bands (Figure 3.3). By contrast, if RNA is degraded, the bands do not appear and a RNA smear is visualized instead. 5S rRNA band is lost when RNA extraction method is performed using silica gel columns, as it is not retained in the filter of the column and therefore it is eluted.

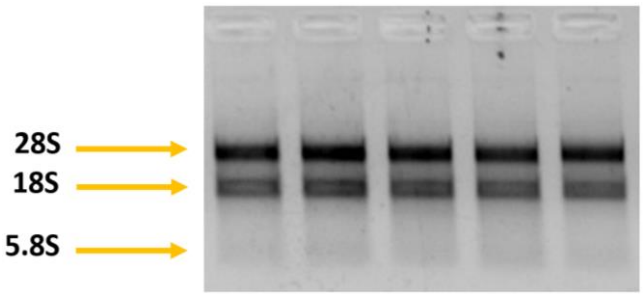


**Figure 3.3 RNA electrophoresis to check its integrity.** The presence of well-defined 28S and 18S bands indicates that the RNA is not degraded. 5.8S subunit is also visible when RNA is obtained by the NZyol method.

### 3.2.3 Reverse transcription

To quantify gene expression by RT-qPCR, mRNA must be first transcribed into cDNA. The reaction is performed by *reverse transcriptase* (RT) enzyme, which is able to create a single-stranded DNA from a RNA template. For our studies, we used oligo(dT) primers (Invitrogen) targeting the poly(A) tail as a primer for reverse transcription which was performed with a commercial kit (SuperScript II Reversa Transcriptase, Invitrogen). In the first step, 200-400 ng of RNA were mixed with 0.12 mM Oligo(dT)$_{12\text{-}18}$ primers and DEPC-treated water. The resulting mix was heated at 65°C for 10 min to break RNA secondary structure and then chilled to 4°C to allow primer annealing. Next, a master mix containing the reverse transcriptase enzyme was added to the samples (Table 3.4) and incubated at 42°C for 50 min to allow cDNA extension, followed by an incubation at 70°C for 15 min to inactivate RT. Finally, DEPC water was added to samples containing 400 ng of DNA to get all concentration at 10 ng/µL. Samples were then stored at -20°C until required for RT-qPCR.

| Component | Final concentrations |
|---|---|
| Buffer 5x | 1x |
| DTT (0.1 M) | 10 mM |
| dNTP mix (10 mM) | 0.5 mM |
| SuperScript II RT (200 U/µL) | 2.5 U/µL |

**Table 3.4. Master mix composition for reverse transcription**. Final concentrations of all the reagents from the master mix are indicated.

### 3.2.4 Real-time quantitative PCR

RT-qPCR was used to quantify the expression of target genes with a relative quantification method. As reference genes, we used *Cyclophilin A* (*CypA*) for adipose tissues and *Hypoxanthine Phosphoribosyltransferase 1* (*Hprt1*) for pancreatic samples.

To conduct the qPCR, SYBR green fluorochrome was used. Also, pre-designed specific primers for each target gene (Supplementary Table 1) were purchased (KiCqStart® Primers, Sigma). SYBR green was mixed with 0.5 µM Forward primer, 0.5 µM Reverse primer, DEPC water and 2 µL of cDNA. SDS 7000 (Applied Biosystems) and LightCycler480 (Roche) detection systems were indistinctly used with the conditions shown in (Table 3.5). Relative gene expression was analysed with the $2^{-\Delta\Delta CT}$ method normalised to a reference gene.

| Step | Temperature | Time | Cycles |
|---|---|---|---|
| Initial activation | 50°C | 2 min | 1 |
| DNA polymerase activation | 95°C | 10 min | 1 |
| Denaturation | 95°C | 20 sec | 40 |
| Annealing | 60°C | 20 sec | |
| Extension | 72°C | 34 sec | |
| Dissociation curve | 95°C | 15 sec | 1 |
| | 60°C | 1 min | |
| | ΔT° | +0.2°/sec | |
| | 95°C | 15 sec | |
| Cooling | 4°C | ∞ | 1 |

**Table 3.5. Thermocycler conditions to determine gene expression by qPCR.**

## 3.3 Histological analysis

Small fragments of inguinal WAT, gonadal WAT, liver and interscapular BAT were obtained for histological analysis. Complete pancreas was also dissected (see section 3.5.1). After extraction, tissue fragments were fixed for 24 h with 4% PFA. Then, tissues were washed in PBS and embedded in paraffin. Paraffin blocks were made by the CIBER ICTS-NanBiosis platform (located at VHIR) or, in the case of the pancreas, by the *Unity of Pancreatic Islets Transplants* (UTIP, Idibell).

Four µm thick sections of tissues were obtained with a microtome (Leica Biosystems), placed in poly-l-lysine coated slides (Epredia) and stored at RT.

### 3.3.1 Haematoxylin/eosin staining

Aqueous Harris haematoxylin at 0.5% and 0.25% alcoholic eosin (LEYCA) were used. First, paraffinized samples were soften by incubating them for 1 h at 65°C. Then, sections were deparaffined with xylene (2 rounds, 5 min) and hydrated with decreasing concentrations of ethanol (2 rounds of absolute ethanol, 96% ethanol, 70% ethanol, 50% ethanol and distilled water; 5 min each). Following hydration, samples were stained for 5 min with Harris haematoxylin and washed with tap water. To be stained with the hydrophobic eosin, samples were then dehydrated by increasing concentrations of ethanol solutions (50% ethanol and 70% ethanol; 5 min each). Eosin (0.25%) staining was performed during 30 sec and samples were then washed with 96% ethanol, 2 rounds of absolute ethanol and 2 rounds of xylene, 5 min each. Finally, the slides were mounted with DPX mounting media (Sigma).

Following staining and mounting, specimens were visualized using an ECLIPSE Ts2R microscope (Nikon) and images of representative fields at 4x, 10x and 20x were taken.

### 3.3.2 Quantification of adipocytes in histological stained sections

To measure areas of adipocytes in inguinal and gonadal WAT, ImageJ (NIH) software was used. Analysis was performed from 3 randomly fields at 10x of 3 Wt and 3 PGC-1α/β-FAT-DKO mice.

## 3.4 Proteomic studies to identify the secretome of adipose tissues

### 3.4.1 *Shotgun* or *Untargeted* proteomics

*Shotgun* proteomics consists of the inferential analysis of the proteins composing a sample by detecting the peptides released from the proteins through proteolysis. After peptide fractionation, the mixture is subjected to *liquid chromatography coupled to mass spectrometry analysis* (LC-MS/MS). Tandem mass spectra resulting from this technique are compared with theoretical tandem mass spectra from protein databases, thereby assigning proteins to peptides. As peptides are shared by more than one protein, identified proteins must be further curated and scored to be correctly determined (175).

#### 3.4.1.1 Sample preparation and trypsin digestion

To analyse the proteins secreted by adipose tissues that could modulate systemic glucose homeostasis, adipose tissues (BAT, gonadal WAT and inguinal WAT) from Wt and PGC-1α/β-FAT-DKO mice that had been fed a HFD for 12 weeks were collected and the explants were incubated in *dulbecco's modified eagle medium* (DMEM) (Thermo Fisher Scientific) to obtain their secretome (Figure 3.4). Specifically, 4-5 Wt and PGC-1α/β-FAT-DKO male mice subjected to a HFD diet for 3 months were euthanized and their adipose tissues removed and pulled. Adipose tissues were minced with scissors (1-2 $mm^3$) and washed twice in 20-30 ml of phenol red-free DMEM supplemented with antibiotics. Then, a 100 μm filter mesh was used to collect the tissue pieces, which were washed again twice with 10 ml of phenol-free DMEM medium and incubated in 5 ml of media for 2 h in a 6 cm-diameter culture dish. Afterwards, tissue was collected using a 100 μm filter mesh and washed twice with phenol red-free media. Finally, 700 mg of BAT, gonadal WAT and inguinal WAT were incubated in 5 ml of serum-free, phenol red-free DMEM media supplemented with antibiotics during 24h. After incubation, the conditioned media was collected, centrifuged for 5 min at 1000 rpm to remove any residual piece of tissue or debris, filtered through a 20 μm filter mesh and stored at -80°C for further analysis.

The proteins present in the conditioned media from adipose tissues were identified *by* shotgun proteomics in collaboration with the Proteomics Service of the *Vall d'Hebron Oncology Institute* (VHIO). Upon its arrival, conditioned media were concentrated by ultrafiltration using a 3 kDa cut-off Amicon Ultra filter (Merck Millipore) to a final volume of 40 μL, and buffer was exchanged to 6 M Urea in 50 mM ammonium bicarbonate. Then, protein content was quantified using the *reducing agent and detergent compatible* (RCDC) protein assay (BioRad) and 10 μg of each protein extract were taken for digestion with trypsin. Previous to tryptic digestion, samples were reduced and alkylated. Both reactions helped in breaking disulphide protein bonds and preventing their new formation by modifying covalently cysteine -SH groups. Reduction was achieved by adding *dithiothreitol* (DTT) to a final concentration of 10 mM for 1 h at RT, whereas alkylation was achieved by adding 20 mM of the alkylating agent *iodoacetamide* (IAA) for 30 min at RT in dark conditions. *carbamidomethylation* (CAM) reaction resulting from IAA addition was quenched by adding N-acetyl-L-cysteine to a final concentration of 35 mM and incubated for 15 min at RT in dark conditions. Then, samples were diluted with 50 mM of ammonium bicarbonate to a final

concentration of 1 M Urea. To perform digestion, modified porcine trypsin (Promega Gold) was added in a ratio of 1:10 (w/w) and the mix was incubated overnight at 37°C. The reaction was stopped with *formic acid* (FA) to a final concentration of 0.5% and the digest product was stored at -20°C until further analysis.

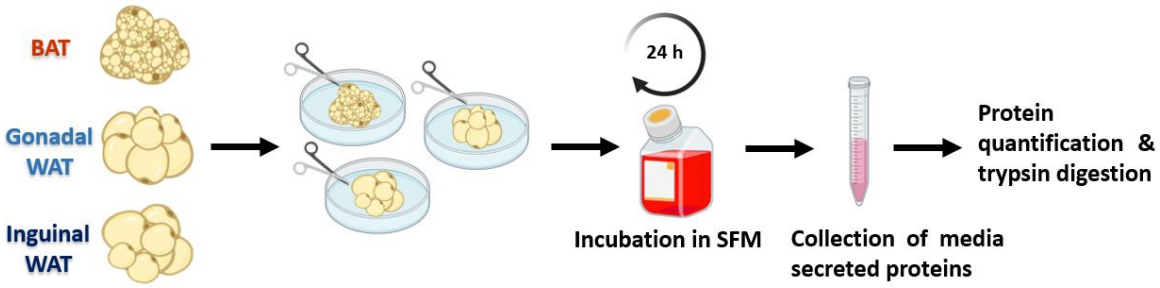


**Figure 3.4. Workflow for the collection and digestion of adipose tissues secreted proteins.**

#### 3.4.1.2 Liquid chromatography – mass spectrometry for label-free differential proteomic analysis

Digested samples were analysed with a linear ion trap Velos-Orbitrap *mass spectrometer* (MS) (Thermo Fisher Scientific). Peptide mixtures were fractionated by on-line nanoflow liquid chromatography using an EASY-nLC 1000 system (Proxeon Biosystems, Thermo Fisher Scientific) with a two-linear-column system. Samples were firstly loaded onto a trapping guard precolumn (Acclaim PepMap 100 nanoviper, Thermo Fisher Scientific) at 4 µL/min in order to separate sample components from impurities. Then, samples were eluted from the analytical column (with Reprosil Pur C18-AQ, Dr. Maisch). The elution was achieved by using a mobile phase composed of 0.1% FA (Buffer A) and 100% acetonitrile with 0.1% FA (Buffer B), and applying a linear gradient from 5 to 35% of Buffer B for 120 min at a flow rate of 300 nL/min. Once eluted, samples were ionized by applying a voltage of 1.9 kV to a stainless-steel nano-bore emitter (Proxeon, Thermo Fisher Scientific), connected to the end of the analytical column, on a Proxeon nano-spray flex ion source.

The *linear ion trap or quadruple ion trap* (LTQ)-Orbitrap Velos mass spectrometer was operated in data-dependent mode. The 20 most abundant ions were selected for collision-induced dissociation fragmentation in the LTQ when their intensity surpassed the threshold of 1000 counts, excluding singly charged ions. Accumulation of ions for both MS and MS/MS scans was performed in the linear ion trap. The maximum ion accumulation time was 500 and 200 ms in the MS and MS/MS modes, respectively. The normalized collision energy was set to 35%, and one microscan was acquired per spectrum. Ions subjected to MS/MS with a relative mass window of 10 ppm were excluded from further sequencing for 20 s. For all precursor masses a window of 20 ppm and isolation width of 2 Da was defined. Orbitrap measurements were performed enabling the lock mass option (m/z 445.120024) for survey scans to improve mass accuracy.

#### 3.4.1.3 Protein identification and quantitative differential analysis

Progenesis® QI for proteomics software v3.0 (Nonlinear dynamics, UK) was used to analyse MS data in default settings. The LC-MS runs from samples were automatically aligned to a selected reference run (Wild-type sample) and chromatograms were manually reviewed and adjusted. Only features within the 400 to 1500 m/z range, 15 to 130 min retention time and with positive charges between 2 to 4 were considered for identification and quantification. Peak lists were generated from Progenesis® and analysed using the Mascot search engine (v2.2, Matrix Science, UK) in order to identify proteins from MS spectrums. Protein identification was achieved using the SwissProt-human database. Based on the probability of Mascot score, significant threshold for peptide identification was set to $P \leq 0.05$ and minimum Mascot score of 20. Label-free protein abundance quantification was based on the sum of the peak areas within the isotope boundaries of peptide ion peaks. Only unique peptides were used for protein quantification. Statistical analysis was performed using Progenesis software. Proteins displaying greater than 2-fold change, and $P \leq 0.05$ (*t*-test) on the pairwise comparison between Wt and PGC-1α/β-FAT-DKO samples were considered significantly differential. Displayed proteins were evaluated and plotted with *Principal Component Analysis* (PCA) to differentiate between tissues and genotypes.

### 3.4.2 Workflow for the detection of actively secreted proteins

Proteins identified in the conditioned media from adipose tissues accounted for those that were actively secreted by adipocytes but also for proteins that were accidentally released to the media. For the identification of the genuine secreted proteins, an accurate bioinformatic analysis was applied to proteins detected by *shotgun* proteomics.

Proteins differentially identified in conditioned media of adipose tissues were filtered by peptide count (>1), confidence score (>25), *P*-value (<0.05) and Fold Change (FC≥ 2). Likewise, known mitochondrial and nuclear proteins were eliminated. After this first filtration, 667 proteins were differentially found in the conditioned media of Wt and PGC-1α/β-FAT-DKO mice, whereas differential content in media from Wt and PGC-1α/β-FAT-DKO mice was limited to 18 and 2 proteins in gonadal WAT and inguinal WAT, respectively.

In order to determine whether the protein found in the conditioned media were effectively secreted, they were evaluated with the *Vertebrate Secretome Database* (VerSeDa, from CIC bioGUNE's Genome Analysis Platform) (176). This repository was created to identify probabilistic secreted proteins across a wide variety of vertebrates and includes data from *National Center for Biotechnology Information* (NCBI), *Ensembl* genome browser and *University of California Santa Cruz* (UCSC) genome browser. It is built on the predictions obtained from different publicly available software tools, including TargetP, SignalP, SecretomeP) and it detects secreted proteins via classical and non-classical pathways. SignalIP (predicts the presence and location of a signal peptide cleavage site) and TargetP (predicts the subcellular location of eukaryotic proteins) were set at 0.8 cut-off, whereas SecretomeP (predicts non-classical protein secretion) cut-off was determined at 0.7.

Secreted proteins identified were analysed using the *Database for annotation, visualization and integrated discovery* (DAVID) Bioinformatic Database functional annotation tool (177),

which groups proteins in functional categories, providing some information about their cellular function.

### 3.4.3 *Targeted* proteomics

#### 3.4.3.1 Assessment of selected protein concentrations in serum of Wt and PGC-1α/β-FAT-DKO mice

Proteins identified as differentially secreted by adipose tissues of Wt and PGC-1α/β-FAT-DKO mice were quantified in serum of these mice by either *targeted* proteomics or ELISA**.** Detectable concentration limits of *targeted* proteomics oscillate from 0.1 to 1 mg/L, hence, candidate circulating proteins had to be in this range to be detected using this technique. Therefore, first, serum concentrations of each protein were searched in two main repositories: PeptideAtlas and The Human Protein Atlas. PeptideAtlas (Institute for Systems Biology) (178) is a publicly compendium of peptides identified with tandem mass spectrometry proteomic experiments in several organisms, including mouse and human. It gives data from proteins, best peptides for protein identification and protein concentrations by seeking in different established databases. The Human Protein Atlas (179), by contrast, intents to map only human protein in a variety of tissues and systems, integrating various omics technologies. By using both repositories, a list of quantifiable proteins by *targeted* proteomic in mouse serum was obtained. Proteins below the sensitivity of LC-MS/MS were evaluated by ELISA. Serum collection for *targeted* proteomics and ELISA was performed as stated in section 3.1.5.

#### 3.4.3.2 Selection of best peptides for *targeted* proteomic analysis

Quantification of proteins in serum by *targeted* proteomics requires the selection of the peptides most likely to be easily identified and quantified by the technique. In this sense, a variety of parameters, accounting from chemical properties of peptides to the probability of detecting the peptide in a sample, are considered. Firstly, the four most abundant peptides from each protein detected by *shotgun* proteomics were selected regarding to their normalized abundances. Then, these peptides were searched in the PeptideAtlas repository in aims to discover the probability to detect them in our samples. Bioinformatic parameters considered to define probability included: *N obs* (total number of observations in all modified forms and charge states), *empirical observability score* or EOS (measures how many samples a particular peptide is seen in relative to other peptides from the same protein) and *predicted suitability score* or PSS (combines publicly algorithms to define how good the peptide is). The higher values for all three parameters defined the suitability of that peptide in our samples. Finally, selected peptides were assessed for chemical properties that impede proper analysis by *targeted* proteomics. In this sense, peptides that contain methionine, tryptophan, asparagine in N-terminal region, glutamine, that were too long (>25 aa) or did not have a lysine or arginine as a last residue, were disregarded and replaced by better candidates.

#### 3.4.3.3 Liquid chromatography – *Targeted* mass spectrometry analysis

Protein content in serum samples was firstly quantified using the RCDC kit (BioRad). Next, 10 µg of each protein extract were mixed with 6 M Urea in 50 mM ammonium bicarbonate.

Selected peptides (Supplementary Table 2) were purchased from Thermo Fisher Scientific (PEPotec SRM Peptide Libraries, grade 3). All cysteines were carbamidomethylated to avoid their oxidation and the formation of disulphide bridges, which difficult the proteomic analysis. Moreover, peptides were labelled with a stable-isotope residue, either a lysine or an arginine. These labelled peptides (from now on named heavy peptides) had well-defined chemical properties and, therefore, they were used as standards to quantify serum endogenous samples (from now on named light peptides). Quantification is extrapolated from correlative concentration response curves between heavy/light peptides. For the quantification experiment, a known amount of internal heavy peptides (ranging from 20-48000 fmol/µg of tryptic digest) were mixed with sample digests. Then, 500 ng of the mixtures were analysed by a linear ion trap Velos-Orbitrap mass spectrometer (Thermo Fisher Scientific). Instrument control was performed using Xcalibur software package, version 2.2.0 (Thermo Fisher Scientific). Peptide mixtures were fractionated by on-line nanoflow liquid chromatography using an EASY-nLC 1000 system (Proxeon Biosystems, Thermo Fisher Scientific) with a two-linear-column system. Digested samples were firstly loaded onto a trapping guard precolumn (Acclaim PepMap 100 nanoviper, Thermo Fisher Scientific) at 4 µL/min. Then, samples were eluted from the analytical column (with Reprosil Pur C18-AQ, Dr. Maisch) by using a mobile phase composed of 0.1% FA (Buffer A) and 100% acetonitrile with 0.1% FA (Buffer B), and applying a linear gradient from 0 to 35% of Buffer B for 120 min at a flow rate of 300 nL/min. Once eluted, samples were ionized by applying a voltage of 1.9 kV to a stainless-steel nano-bore emitter (Proxeon, Thermo Fisher Scientific), connected to the end of the analytical column, on a Proxeon nano-spray flex ion source.

The LTQ Orbitrap Velos mass spectrometer was operated in *parallel reaction monitoring* (PRM) mode. In this mode, peptide-derived ions that enter the mass spectrometer are fragmented in a collision cell linear ion trap, generating multiple fragments. These fragments (also named transitions) are parallelly monitored inside an Orbitrap instrument, giving as a result a full MS/MS spectrum from target peptides (Figure 3.5). Accumulation of ions for MS/MS was performed with an AGC target value of 5000. The maximum ion accumulation time was 50 ms. The normalized collision energy was set to 38% and one microscan was acquired per spectrum. For all precursor masses an isolation width of 2 Da was defined.

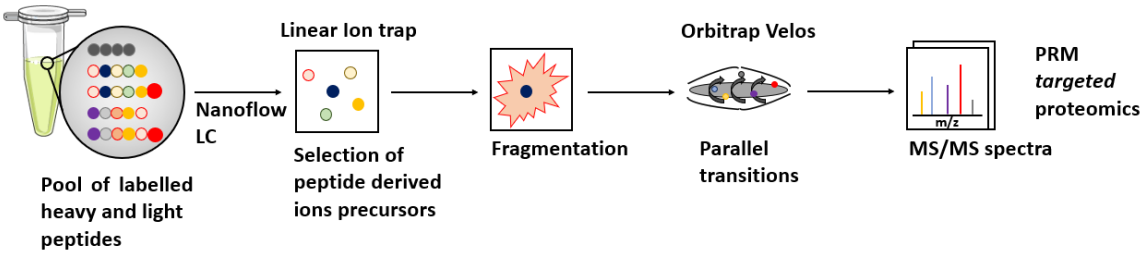


**Figure 3.5. Schematic representation of *targeted* data acquisition PRM method.**

Raw data was imported to Skyline (MacCoss Lab Software) software to analyze the results. To quantify each peptide, the 5 highest intensity transitions were used. For peptides giving significant amounts of two different charge state ions, signals were acquired for both. Protein concentrations were calculated from samples regarding L/H peptides correlation and data was further analyzed statistically.

## 3.5 Pancreatic studies

### 3.5.1 Immunofluorescent analysis of pancreatic islets

Pancreatic islets were evaluated by immunofluorescence to uncover morphometric differences in islets from PGC-1α/β-FAT-DKO mice compared to Wt littermates. To this aim, paraffin sections of whole pancreas at different depths were stained with antibodies against insulin, glucagon or somatostatin, to identify β-cells, α-cells and δ-cells, respectively.

Pancreas slides were obtained as it is described in section 3.3. When cutting paraffin blocks with the microtome, pancreas was positioned horizontally in order to cut the head, the body and the tail of the tissue in each slide. Moreover, three distinct depths were considered from each pancreas. In this sense, several slides were obtained from one depth, while trimming at least 150 µm until the next batch of slides were cut.

For immune-staining, slides were first incubated for 1 h at 65°C. Next, slides were deparaffinated with xylene (3 cycles, 5 min each), 100% ethanol (2 cycles, 2 min each), 95% ethanol (2 min), 90% ethanol (2 min), 70% ethanol (2 min) and distilled water (2 cycles, 2 min each). Following deparaffination, antigen retrieval was conducted in citrate buffer 40 mM pH 6 (stock solution of 400 mM containing 0.099 M citric acid and 0.41 M sodic citrate dihydrate) heated in a microwave (defrost mode, 2 cycles, 7 min each). This crucial step serves to reverse epitope masking and restore epitope-antibody recognition, usually lost during the fixation process. Without it, background increases and staining may become less specific. After a couple of washing steps with PBS (5 min each), cells were permeabilized with a solution containing 1% X-100 Triton (Sigma) in PBS. Following this, samples were blocked with 10% horse serum in PBS for 1 h at room temperature to limit possible non-specific binding of antibodies to cell proteins. After another wash step with PBS, samples were incubated with primary antibodies diluted in PBS (Table 3.6).

Staining ran in parallel in contiguous slides (insulin + glucagon; insulin + somatostatin) due to the limited capacity of combining antibodies. Therefore, mouse monoclonal anti-insulin antibody was combined with rabbit polyclonal anti-glucagon antibody or rabbit polyclonal anti-somatostatin antibody for staining somatostatin. In both cases, samples were incubated overnight at 4°C. Next day, samples were washed with PBS (2 cycles, 5 min each in agitation) and incubated for 1 h at room temperature with secondary antibodies: goat anti-mouse Alexa Fluor™ 555 antibody for insulin and donkey anti-rabbit Alexa Fluor™ 488 for glucagon or somatostatin). Then, samples were washed with PBS (2 cycles, 5 min each in agitation) and incubated with *4',6-diamidino-2-phenylindole* (DAPI) (Thermo Fisher Scientific) (1/1000 dilution in PBS 1X) for 10 min to stain cellular nuclei. Finally, samples were washed again and mounted with DAKO mounting media to fix coverslips on samples.

| Type | Name | Dilution | Reference |
|---|---|---|---|
| Primary | Mouse monoclonal anti-insulin | 1/1000 | Ab8304 (Abcam) |
| Primary | Rabbit polyclonal anti-glucagon | 1/400 | PA5-88091 (Invitrogen) |

| | | | |
|---|---|---|---|
| Primary | Rabbit polyclonal anti-somatostatin | 1/400 | PA5-97200 (Invitrogen) |
| Secondary | Goat anti-mouse Alexa Fluor 555 | 1/400 | A21127 (Invitrogen) |
| Secondary | Donkey anti-rabbit Alexa Fluor 488 | 1/400 | A21206 (Invitrogen) |

**Table 3.6. Antibodies used for the immunofluorescent staining of main pancreatic islet cell subpopulation.**

### 3.5.2 Insulin secretion studies in pancreatic islets

Insulin secretion studies in pancreatic islets were conducted with the help of the *Diabetes, Nutrition and Endocrinological Diseases* group at *the Biomedical Research Institute of Bellvitge* (IDIBELL) and with the group of *Translational Research in Diabetes, Lipids and Obesity from Clinic Hospital of Barcelona*.

#### 3.5.2.1 Isolation of pancreatic islets

Mice were euthanized by cervical dislocation and the bile duct was rapidly cannulated with a 26G needle through which 2 mL of a collagenase solution (1.5 mg/mL of Collagenase P in *Hanks Balanced Salt Solution* (HBSS) was injected. Pancreata were then placed into a non-adherent falcon (Corning) containing 1 mL of 3.0 mg/mL collagenase solution and digested at 37°C with agitation (90 rpm) for 8 min. Once uniformly homogenized, digestion was stopped by adding HBSS supplemented with 1% *bovine serum albumin* (BSA). Then, digested pancreata were centrifuged for 3 min at 100 g and 4°C, washed with Hanks-BSA and filtrated with a laboratory strainer (mesh size of 100 µm). Filtered tissue was again centrifuged for 3 min at 100 g and 4°C and then it was subjected to a density gradient created by the mixture of different Histopaque media. Histopaque 1119 (GranuloSep GSM 1119, HIMEDIA) was first added and homogenized with HBSS medium, creating a density of 1.119 g/mL. Following, Histopaque 1089 (1:1 mix of Histopaque 1119 and Histopaque 1077 (HiSep LSM 1077, HIMEDIA)) was added carefully to the superficial phase of the density gradient. As its density was 1.089 g/mL, it remained above Histopaque 1119 medium. Last, Hanks-BSA was also poured carefully above Histopaque 1089 to create three distinct density phases. After centrifugation during 20 min at 800 g and room temperature (acceleration 4, deacceleration 4), pancreatic islets remained in the interphase between Hanks-BSA and Histopaque 1089. Subsequently, islets were recovered, centrifuged for 5 min at 500 g and 4°C and washed twice with Hank's medium. At that moment, islets were fished and transferred to plates containing *Roswell Park Memorial Institute* (RPMI) 1640 medium supplemented with 10% *foetal bovine* serum (FBS), streptomycin/penicillin and L-glutamin (Figure 3.6). Four replicates consisting in 10 islets/plate were prepared for each animal, whereas the remaining islets were kept for RNA isolation. Plates were incubated in RPMI medium overnight at 37°C to facilitate the recovery of islets from the isolation protocol before an assay of insulin secretion in response to glucose was conducted.

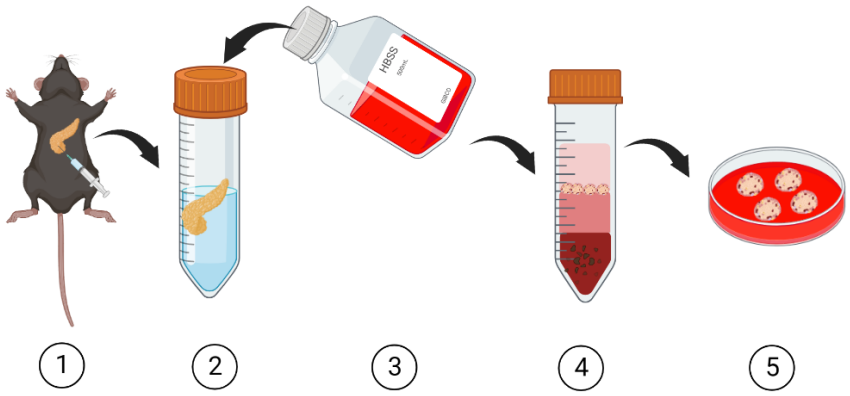


**Figure 3.6. Schematic representation of pancreatic islets isolation.** 1) Pancreata were firstly cannulated and perfused with collagenase and 2) digested for 8 min agitation at 37°C. 3) Digestion was stopped with HBSS supplemented with 1% BSA. 4) Pancreata components were filtered and moved to a 3-gradient phase (histopaque 1119, 1089 and HBSS-BSA). After centrifugation, isolated pancreatic islets were recovered in cell culture dishes containing RPMI 1640 medium.

#### 3.5.2.2 Glucose-stimulated insulin secretion (GSIS) assay

For GSIS assay, ten pancreatic islets per condition were firstly preincubated for 1 h at 37°C in *Krebs-Ringer Bicarbonate Hepes* (KRBH) (115 mM NaCl, 24 mM $NaHCO_3$, 5 mM KCl, 1 mM $MgCl_2$ 2.5 mM $CaCl_2 \cdot 2\ H_2O$, 10 mM HEPES and 0.5 g BSA, pH 7.4) containing 2.8 mM glucose. Then, islets were placed into special vials in which $CO_2$ exchange and humidity were optimized and pancreatic islets were visible with the magnifier. In these vials, incubation with 1 mL of 2.8 mM glucose KRBH (basal) or 1 mL of 20 mM glucose KRBH (stimulated) took place for 1 h at 37°C. Afterwards, medium was collected from the vials (taking care not to take islets) and stored at -80°C for subsequent analysis of insulin content. Islets were fished and stored in 400 µL of PBS to analyse insulin content and total DNA. For this, pancreatic islets were sonicated (3 cycles of 10 sec, amplitude 90). On one side, 300 µL of the lysate were centrifuged for 5 min at 1000 rpm and 4°C, and the supernatant containing the DNA was stored at -80°C until quantification by fluorimetry (see section 3.5.2.3 for detailed protocol). On the other side, the remaining 100 µL of the islet lysate were mixed with 300 µL of an acid-ethanol solution (2 mL of 37% HCl and 98 mL of 100% ethanol) and incubated overnight at 4°C to obtain intracellular insulin. Next day, samples were centrifuged for 15 min at 3,500 rpm and 4°C and the supernatant was stored at -80°C for further analysis on insulin.

#### 3.5.2.3 Fluorometric quantification of DNA from pancreatic islets

Normalization of secreted insulin and insulin content from pancreatic islets during the GSIS is crucial to avoid misleading results resulting from different islet size and β-cell content in each of them. Therefore, insulin absolute values were referred to DNA concentration in the samples. Due to the small quantity of islets isolated to perform a GSIS, DNA concentration is too low to be directly measured in pancreatic islets sonicated solution with a Nanodrop instrument. Instead, more sensitive and specific fluorimetry allows the detection of low concentrated DNA samples.

To be measured by fluorimetry, samples containing pancreatic islet DNA obtained in section 3.5.2.2 were mixed with Hoechst 33342, a fluorescent dye that binds to DNA and referred to

a standard (Herring sperm) with known DNA concentration. DNA concentration is directly proportional to the fluorescence of the standard, so a linear correlation is established. DNA concentration from samples can be then extrapolated from the fluorescence detected.

Lysate samples were mixed with a buffer containing 4 M NaCl, 0.07 M $Na_2HPO_4 \cdot 2H_2O$ and 3.98 mM EDTA $\cdot 2H_2O$. Herring sperm was prepared by diluting it in PBS to create a standard concentration curve of 5, 2.5, 1, 0.5, 0.25, 0.125 and 0.05 µg/mL of DNA. Hoechst 33342 stock solution was diluted to 3.33 µg/mL concentration with DNA buffer. Once reagents were prepared, 50 µL of sample or standard and 75 µL of Hoechst solution were pipetted into a Nunc™ Delta treated microplate (Thermo Fisher Scientific). Values were quantified with TECAN SPARK® multimodal plate reader at 360 nm excitation and 460 nm emission wavelengths. Concentration values of samples were inferred from the standard curve generated when DNA from Herring sperm was stained with Hoechst 33342.

#### 3.5.2.4 Quantification of secreted insulin and insulin content by ELISA

Secreted insulin during GSIS and insulin content in pancreatic islets were quantified from media with an Ultra-Sensitive Mouse Insulin ELISA Kit (Crystal Chem). Wide and High range assays (0.1-12.8 ng/mL and 1-64 ng/mL, respectively) were used and samples were diluted accordingly to fit the standard curve (usually 1/4 for stimulated secretion and 1/250 for insulin content). Absolute quantified values were then normalized by total DNA concentration.

### 3.5.3 Ultrastructural analysis of β-cell morphology by transmission electron microscopy

To study the ultrastructure of pancreatic β-cells and, particularly, insulin granules content and distribution, pancreatic islets were isolated and processed for transmission electron microscopy visualization.

#### 3.5.3.1 Isolation of pancreatic islets

After euthanizing mice by cervical dislocation, pancreata were rapidly cannulated to infuse with 2 mL of 2 mg/mL of collagenase (Collagenase P; Boehringer Mannheim Biochemicals) directly through the pancreatic duct. Pancreata were then placed in tubes with m199 medium (Invitrogen) supplemented with 10% FBS. Digestion was fostered by incubating the tubes at 37°C for 9 min, agitating them every 2 min. Once finished, the digestion was stopped by adding cold m199 medium without FBS. After this, 3 cycles of centrifugation (2,500 rpm, 1 min) were alternated with a replacement of m199 medium without FBS, which helped in washing the digested tissue. Subsequently, the medium containing the digested pancreata was filtered by a laboratory colander and recentrifuged at 2,500 rpm for 1 min. The pellet was resuspended with 10 mL of ficoll (Histopaque-1119; Sigma) and a gradient was created by adding m199 medium without FBS with the aim of separating pancreatic islets by density. Islets moved to the upper phase of this gradient by means of a centrifugation cycle of 2,500 rpm at 4°C and for 15 min, without stop. The supernatants containing the pancreatic islets were then obtained by decantation, centrifuged 1 min at 2,500 rpm and resuspended with m199 medium with 10% FBS. 2 more cycles of centrifugation at 2,500 rpm for 1 min contributed to the wash of the islets. Finally, the medium was poured onto a Petri dish and the pancreatic islets were picked individually amongst the exocrine residues of pancreas by

means of a laboratory magnifier. Independently of the experimental groups, between 80-150 pancreatic islets were obtained.

#### 3.5.3.2 Samples preparation for transmission microscopy

Sample processing and visualization by TEM microscopy was performed at the Microscopy Service of the *Autonomous University of Barcelona* (UAB). Pancreatic islets previously isolated were fixated with a combination of 2.5% glutaraldehyde (GA) and 4% paraformaldehyde (PFA) in 0.1 M phosphate buffer (pH = 7.4) overnight at 4°C. After washing the specimens 5 times (5 min each) with sterile water, they were incubated in 1% of osmium tetroxide in water for 2 h at 4°C. Another round of 6 washes with sterile water (5 min each) was followed by an incubation of samples in 1% uranyl acetate in sterile water for 2 h at 4°C. After 2 more washes with sterile water for 10 min, samples were dehydrated by successively incubating them in ethanol 30 % for 20 min, ethanol 50% for 20 min and ethanol 70% overnight. Next day, the dehydration process followed with an incubation in ethanol 90% during 30 min, ethanol 96% during 30 min and 3 cycles of ethanol 100% for 30 min). Once dehydrated, specimens were embedded in a mix of EPON® 812 epoxy resin and ethanol for various cycles: EPON/Ethanol 1/3 for 2 h, EPON/Ethanol 1/1 for 2 h, EPON/Ethanol 3/1 for 2 h, pure EPON for an overnight inclusion and pure EPON for 6 h. Finally, specimens were placed in molds with new pure EPON and polymerized at 60°C for 24-48 h.

Following specimen embedding in EPON resin, semithin (1 µm) and ultrathin (40 nm) sections from regions of interest in each specimen were obtained using an ultramicrotome (Leica EM UC7). Ultrathin sections were subsequently visualized by TEM microscopy (JEOL JEM-1400) and images of pancreatic β-cells containing insulin granules at 2,500x, 6,000x, 12,000x and 25,000x magnification were captured. At 6,000x magnification, quantification and localization of insulin granules within β-cells were performed in 14-21 cells/mouse from 3 Wt and 3 PGC-1α/β-FAT-DKO mice. Insulin granules were classified regarding their grade of maturity, based on the shape and colour of the insulin crystallized core, and they were quantified. This process was replicated for insulin granules located less than 500 nm far away from cell membrane, which are granules more prone to be secreted. Data were obtained with ImageJ (NIH) software.

## 3.6 *In vitro* studies

### 3.6.1 Culture of INS-1 832/3 rat insulinoma cell line

INS-1 832/13 cell line is a derivative of the INS-1 cell line, which was originally established from an x-ray induced insulinoma in rat (180). The INS-1 832/13 line is a subclone of INS-1 that was transfected with a CMV promoter-human insulin expression plasmid carrying a geneticin (G418)-resistance marker for selection. INS-1 832/13 have an enhanced secretory responsiveness to glucose and a robust GSIS that do not decrease over time compared to the original INS-1 cells (181). INS-1 832/13 cells used in this study were kindly provided by the *group of Diabetes, Nutrition and Endocrinological Diseases in the Biomedical Research Institute of Bellvitge* (IDIBELL).

#### 3.6.1.1 Thawing frozen INS-1 cell stocks from liquid nitrogen

To thaw frozen INS-1 832/13 cells, cryogenic vials were removed from liquid nitrogen and rapidly incubated in water bath at 37°C with gentle shaking. Once thawed, the content of the cryogenic tube was transferred to a conical centrifuge tube containing prewarmed proliferation RPMI-1640 medium (Corning™) supplemented with 10% *fetal bovine serum* (FBS), Antibiotic-Antimycotic Penicillin-Streptomycin (Sigma, 10,000 units/mL), 1 mM sodium pyruvate, 10 mM HEPES and 50 µM 2-mercaptoethanol). After 2 cycles of centrifugation at 1,300 rpm for 5 min and replacement of medium between cycles, the pellet containing the cells was resuspended in medium and transferred into a highly adherent Nunclon Delta 10 cm dish. Cells were maintained at 37°C and 5% of $CO_2$ and, the next day, medium was aspirated to remove non-attached cells and it was replaced with fresh proliferating medium.

#### 3.6.1.2 Subculture of proliferating INS-1 832/13 cells

INS-1 832/13 cells were maintained in proliferation medium, at 37°C and 5% of $CO_2$. When cells reached 70-80% confluence, they were recovered and reseeded into new dishes at lower density. For this, proliferation medium was firstly removed and cells were rinsed with PBS. Then, 2.5 mL of trypsin-EDTA (Sigma) were added to the cells and incubated at 37°C for 4 min. Once detached, proliferation medium was added to the cells in order to neutralise the enzyme. Cells were then collected and distributed in a new dish at a density of 50,000 cells/$cm^2$.

#### 3.6.1.3 Preparation of frozen stocks of INS-1 832/13 cells

To obtain frozen stocks, 70-80% confluent INS-1 832/13 cells were washed and detached from the plate with trypsin. Once detached, cells were centrifuged in proliferation medium at 1,500 rpm for 5 min (2 cycles), resuspended and counted using a Neubauer chamber. Then, proliferation medium was removed and cells were resuspended in freezing medium (RPMI-1640 supplemented with 20% FBS, 10% DMSO and 1X Antibiotic-Antimycotic). Cell suspension, 1x$10^6$ cells/mL approximately, was transferred to cryogenic tubes (1 mL/tube), placed in a freezing container (Mr. Frosty™, Thermo Fisher Scientific) to freeze them slowly (-1°C/minute) and stored at -80°C. Next day, vials were stored until use in liquid nitrogen.

#### 3.6.1.4 Glucose-stimulated insulin secretion assay in INS-1 832/13 cell line

100,000 cells/$cm^2$ INS-1 cells were seeded in 12 well-plates containing proliferation medium, and their insulin secretion capacity was assayed when cells reached 90% of confluency. *Hepes Balanced Salt Solution* (HBSS) was used for the assay (114 mM NaCl, 4.7 mM KCl, 1.2 mM $KH_2PO_4$, 1.16 mM $MgSO_4 \cdot 7H_2O$, HEPES 20 mM, $CaCl_2$ 2.5 mM, 25.5 mM $NaHCO_3$ and 0.2% BSA), adjusting its pH to 7.2 with HCl and filtering it with 0.22 µm filter before use. Cells were first washed twice with 1 mL/well of HBSS + 2.8 mM of glucose (Sigma) and then preincubated for 120 min at 37°C and 5% $CO_2$ with 1 mL/well of this medium. Afterwards, cells were incubated for 60 min with 1 mL/well of HBSS + 2.8 mM of glucose (basal) or HBSS + 16.7 mM of glucose (glucose-stimulated). Parallelly, KCl and leucine were used as positive controls for insulin secretion due to their potent role as insulin secretagogues (182). For each experiment, all treatments were performed in triplicate. Post-incubation, medium with secreted insulin

was collected from each condition, centrifuged for 5 min at 12,000 rpm and 4°C to eliminate cells and cellular debris and the supernatant stored at -20°C for further analysis.

Because secreted insulin was normalized to intracellular insulin content, this was also determined. To release the insulin contained within insulin granules from INS-1 832/13 cells, cells were exposed to an overnight incubation with 1 mL/well of acid-ethanol (1.5% HCl/75% ethanol). Next day, cells were harvested and sonicated (cycle 1, 80 amplification, 3 cycles of 10 seconds each). The lysate was then centrifuged for 5 min at 12,000 rpm and 4°C and the supernatant stored at -20°C for further analysis.

Secreted insulin in the culture media and cell insulin content were measured by Ultra-Sensitive Mouse Insulin ELISA Kit (Crystal Chem), which presents 100% crossreactivity with rat insulin. Wide Range Assay (0.1 – 12.8 ng/mL) was used and absolute values were normalised to total DNA or protein content measured in section 3.6.1.6.

#### 3.6.1.5 GSIS assay in INS-1 832/13 cells treated with resistin

To evaluate the role of resisting in regulating insulin secretion, a GSIS was conducted in INS-1 832/13 cells previously exposed to either 50 ng/mL or 500 ng/mL of recombinant mouse resistin (R&D Systems) for 24 h (183-185). Resistin in the culture media was maintained throughout the assay. As described in 3.6.1.4, GSIS was performed with basal and stimulated HBSS medium with or without resistin treatments, together with the use of leucine and KCl as controls for insulin secretion. Secreted medium was recollected, processed and stored at -20°C for further analysis. Insulin content was extracted by an acid-ethanol overnight incubation, sonicated and stored at -20°C for further analysis. Secreted insulin and insulin cell content were measured as described in section 3.6.1.4.

#### 3.6.1.6 Cell counting and DNA and protein extraction from INS-1 832/13 cells

In parallel to the assessment of insulin secretion in INS-1 832/13 cells when exposed to different treatments, another non-treated 12-well plate was used to normalise insulin secretion and insulin content to DNA content. Cells were quantified with the Neubauer Chamber and seeded the same day and in the same number as for the insulin secretion assay. The day of the GSIS, cells were detached and quantified in quadruplicates and the other wells were used for DNA/protein isolation. To do so, cells were harvested in PBS, centrifuged for 5 min at 2,000 rpm and 4°C and pellets were stored.

For DNA extraction, pellets were resuspended in 40-50 µL of PBS, sonicated (cycle 1, 80 amplification, 3 cycles of 10 seconds each) and centrifuged for 15 min at 12,000 rpm and 4°C. Supernatants were then collected and directly measured by a NanoDrop ND-2,000 spectrophotometer.

Proteins were extracted with *radio-immunoprecipitation assay* (RIPA) buffer (50 mM Tris-HCl pH 8, 150 mM NaCl, 1% Triton x-100, 0.5% sodium deoxycholate, 0.1% sodium dodecyl sulphate, 10 mM sodic glycerophosphate, 1 mM sodic pyrophosphate, 1 mM sodic orthovanadate, 1 mM phenylmethanesulfonylfluoride and commercial protease inhibitors (Sigma). Pellets were resuspended with 60 µL of RIPA and then sonicated (cycle 1, 80 amplification, 3 cycles of 10 seconds each). Lysates were centrifuged for 15 min at 12,000 rpm

and 4°C and supernatants containing the solubilized proteins were recovered. Protein concentration was determined following *bicinchoninic acid* (BCA) Protein Assay (Pierce) instructions and by using Spectra-max 340 plate reader. Once quantified, samples were stored at -20°C.

## 3.7 Statistical analysis

Results shown in figures and tables are expressed as mean ± SEM. When appropriate, *Student's test* or *analysis of* variance (ANOVA) test followed by a Tukey's multiple comparison post hoc analysis were applied to assess significative differences amongst groups. Statistical analysis was performed with GraphPad Prism 9 software and differences between conditions were considered significative when $P \leq 0.05$.

# 4. RESULTS

## 4.1. Characterization of PGC-1α/β-FAT-DKO mice

### 4.1.1 Generation of PGC-1α/β-FAT-DKO mouse model

An adipocyte-specific knockout mouse model lacking transcriptional co-activators PGC-1α and PGC-1β (PGC-1α/β-FAT-DKO) was previously generated in our laboratory (36). This tissue-specific loss-of-function mouse model was generated by homologous recombination using the *Cre/loxP* technology, and fat specificity was achieved by using the adiponectin promoter as a driver of the *Cre* expression. As previously reported (36), a noticeable decrease in the expression of *Ppargc1a* and *Ppargc1b* genes was observed in adipose tissues, both in inguinal WAT and BAT, from PGC-1α/β-FAT-DKO mice (Figure 4.1).

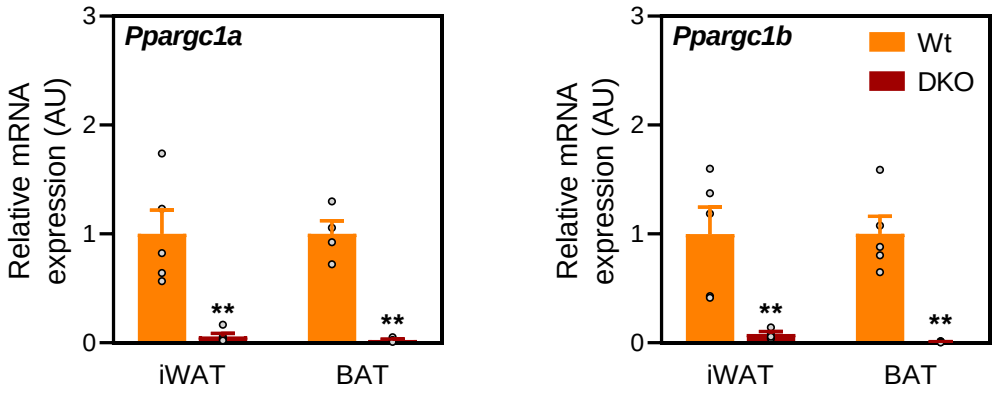


**Figure 4.1. mRNA expression of *Ppargc1a* and *Ppargc1b* genes in inguinal WAT and BAT from Wt and PGC-1α/β-FAT-DKO mice.** Male mice of 13 of weeks of age fed a regular chow diet and housed at 21°C were used. mRNA expression levels were determined by RT-qPCR. Student's t-test method was applied. Results are expressed as mean ± SEM (n=4-5 animals/group). * Indicates statistical significance of the comparison between Wt and PGC-1α/β-FAT-DKO mice ** $P \leq 0.01$.

As previously described, lack of PGC-1s in inguinal (subcutaneous) and gonadal (visceral) WAT depots and in BAT from 13-week-old male mice fed a regular chow diet and housed at 21°C led to a significant reduction in the expression of mitochondrial genes encoding for proteins of the OxPhos system in inguinal WAT (Figure 4.2) and in BAT (Figure 4.3, A). Also, accordingly to the importance of PGC-1s in non-shivering thermogenesis, deletion of both co-activators in BAT resulted in a severe reduction in the expression of the *uncoupling-protein 1* (*Ucp1*) gene (Figure 4.3, B). Somehow surprisingly, contrarily to the pattern observed for *Ucp1*, the expression of the gene encoding for the brown adipocyte-specific *adrenergic* β*3 receptor (Adrb3)* was not reduced in conditional knockout mice (Figure 4.3, B). Instead, its expression was increased by two-fold.

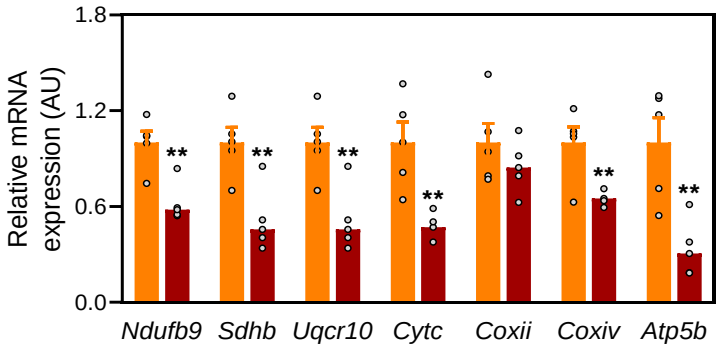


**Figure 4.2. mRNA expression of mitochondrial genes related to the OxPhos system in inguinal WAT from Wt and PGC-1α/β-FAT-DKO mice.** Male mice of 13 weeks of age fed a regular chow diet and housed at 21°C were used. mRNA expression levels were determined by RT-qPCR. Student's t-test method was applied. Results are expressed as mean ± SEM (n=5 animals/group). * Indicates statistical significance between the comparison of Wt and PGC-1α/β-FAT-DKO mice ** $P \leq 0.01$

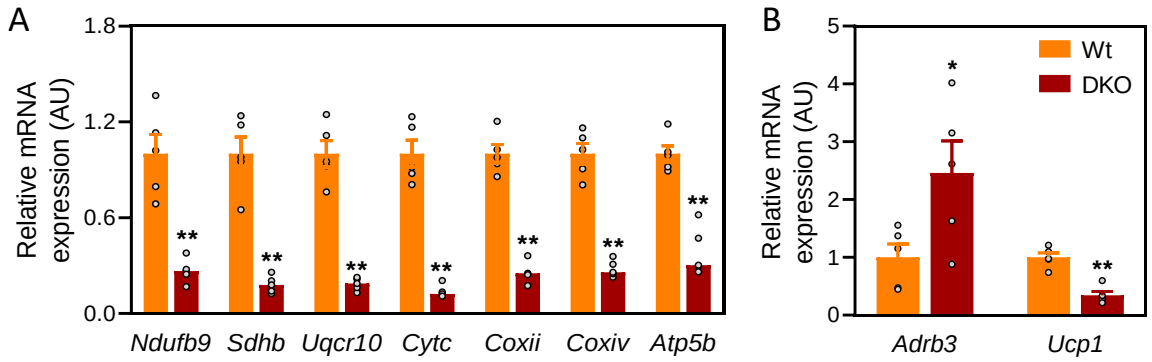


**Figure 4.3. mRNA expression of mitochondrial genes related to the OxPhos system and non-shivering thermogenesis in BAT from Wt and PGC-1α/β-FAT-DKO mice.** Male mice of 13 weeks of age fed a regular chow diet and housed at 21°C were used. mRNA expression levels of A) genes encoding for proteins of OxPhos system and B) thermogenic genes was determined by RT-qPCR. Student's t-test method was applied. Results are expressed as mean ± SEM (n=5 animals/group). * Indicates statistical significance of the comparison between Wt and PGC-1α/β-FAT-DKO mice * $P \leq 0.05$; ** $P \leq 0.01$.

### 4.1.2 Evaluation of non-shivering thermogenesis in Wt and PGC-1α/β-FAT-DKO mice subjected to an acute cold exposure

#### 4.1.2.1 Evolution of body temperature after exposure to an acute cold

Since genes related to the OxPhos system and the thermogenic process were down-regulated in BAT from PGC-1α/β-FAT-DKO mice (section 4.1.1), we analysed the capacity of these mice to sustain their body temperature when they faced an acute cold. For this, 10-week-old Wt and PGC-1α/β-FAT-DKO male mice fed a regular chow diet were exposed to cold (4°C) for 5h after being acclimated at thermoneutrality (30°C) for two weeks.

Prior to cold exposure, at thermoneutral conditions, Wt and PGC-1α/β-FAT-DKO mice had similar body temperature (Figure 4.4, A). However, when exposed to cold, PGC-1α/β-FAT-DKO mice failed to sustain normal body temperature (Figure 4.4, B) and rapidly became hypothermic, whereas Wt were able to maintain it. These results indicate that mice deficient in PGC-1α/β co-activators specifically in adipose tissues have impaired non-shivering

thermogenesis, an aspect of this mouse model that had not been directly addressed in previous studies.

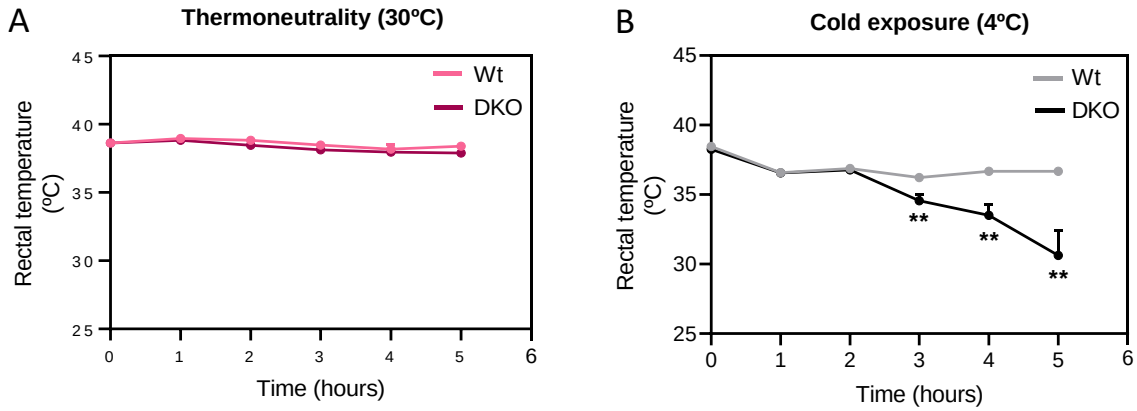


**Figure 4.4. Analysis of body temperature in Wt and PGC-1α/β-FAT-DKO mice fed a regular chow diet and maintained at thermoneutrality (30°C) or subjected to 5 h of cold exposure (4°C).** Ten-week-old male mice were used. A) Body temperature at thermoneutrality (30°C) and B) during an acute cold exposure (4°C) in mice previously acclimated at thermoneutrality for two weeks. Mice were individually caged with no food and exposed to cold for 5h. Body temperature was measured every hour using a digital thermometer with a rectal probe. Student's t-test method was applied. Results are expressed as mean ± SEM (n=5-6 animals/group). * Indicates statistical significance between the comparison of Wt and PGC-1α/β-FAT-DKO mice ** *P*≤ 0.01.

### 4.1.2.2 Effects of cold exposure on body and tissue weight

Cold-induced thermogenesis relies on the oxidation of fatty acids mobilized from the BAT itself but also, and primarily, from those mobilized from WAT. Despite the failure in the maintenance of proper body temperature when exposed to cold, no major changes in body weight in Wt and PGC-1α/β-FAT-DKO mice were observed. In fact, body weight was only reduced by 4.6% in Wt and 3.9% in PGC-1α/β-FAT-DKO mice upon cold exposure, although the results did not reach statistically significance (Figure 4.5).

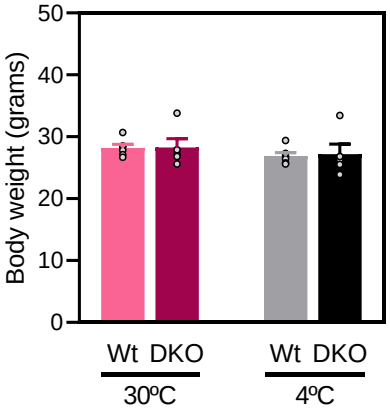


**Figure 4.5. Body weight of Wt and PGC-1α/β-FAT-DKO mice fed a regular chow diet and maintained at thermoneutrality (30°C) or subjected to 5 h of cold exposure (4°C).** Ten-week-old male mice were used. After being acclimated for two weeks at thermoneutrality (30°C), mice were kept at 4°C for 5 h. Graph depictures body weight immediately before and after cold exposure. ANOVA test followed by a Tukey's multiple comparison post hoc analysis was applied. Results are expressed as mean ± SEM (n=5-6 animals/group).

However, cold exposure notably reduced the weight of inguinal WAT depot by approximately 25% (in both Wt and PGC-1α/β-FAT-DKO mice) and weight of gonadal WAT depot by

approximately 33% in Wt and 31% in PGC-1α/β-FAT-DKO mice, although the results did not reach statistical significance (Figure 4.6). By contrast, the cold-induced adipose weight loss was more exacerbated in BAT (a reduction of approximately 64% in Wt and 47% in PGC-1α/β-FAT-DKO mice), although no differences were found between genotypes. Liver, soleus and gastrocnemius tissue weight did not change by the effect of the temperature nor the genotypic effect.

These data suggest that lipid mobilization in response to cold, which serve as substrates for thermogenesis, is not significantly affected by the loss of PGC-1s co-activators in WAT, and only marginally in BAT.

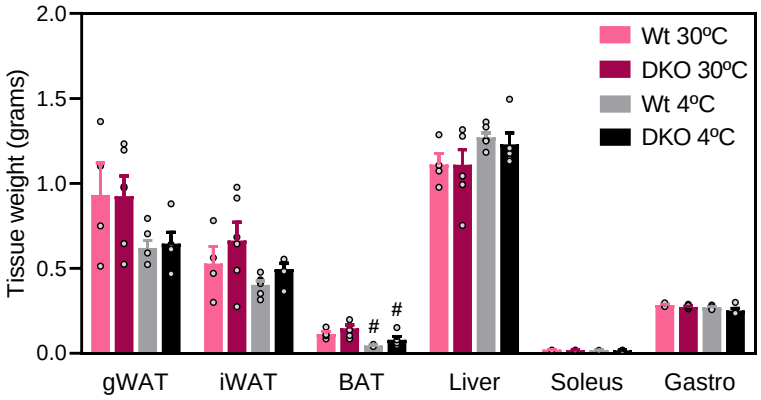


**Figure 4.6. Weight of tissues from Wt and PGC-1α/β-FAT-DKO mice fed a regular chow diet and maintained at thermoneutrality (30°C) or subjected to 5 h of cold exposure (4°C).** Ten-week-old male mice were euthanized and gonadal WAT, inguinal WAT, BAT, liver, soleus and gastrocnemius muscles were collected and weighted. ANOVA test followed by a Tukey's multiple comparison post hoc analysis was applied. Results are expressed as mean ± SEM (n=5-6 animals/group). # Indicates statistical significance between environmental temperature conditions. # $P \leq 0.05$.

#### 4.1.2.3 Gene expression analysis in BAT of Wt and PGC-1α/β-FAT-DKO mice in response to cold

An appropriate thermogenic response to cold relies on proper induction of genes involved in non-shivering thermogenesis. Therefore, we analysed gene expression in BAT from Wt and PGC-1α/β-FAT-DKO male mice acclimated at 30°C or after 5 h of being exposed to cold (4°C). Firstly, we assessed *Ppargc1a* and *Ppargc1b* expression levels. As expected, mutant mice had lower expression of PGC-1s-encoding genes than Wt counterparts. Cold exposure increased the expression of both genes in Wt mice, although the increment was much greater in *Ppargc1a*, consistent with its role as principal mediator of non-shivering adaptive thermogenesis. This response was severely blunted in PGC-1α/β-FAT-DKO mice (Figure 4.7).

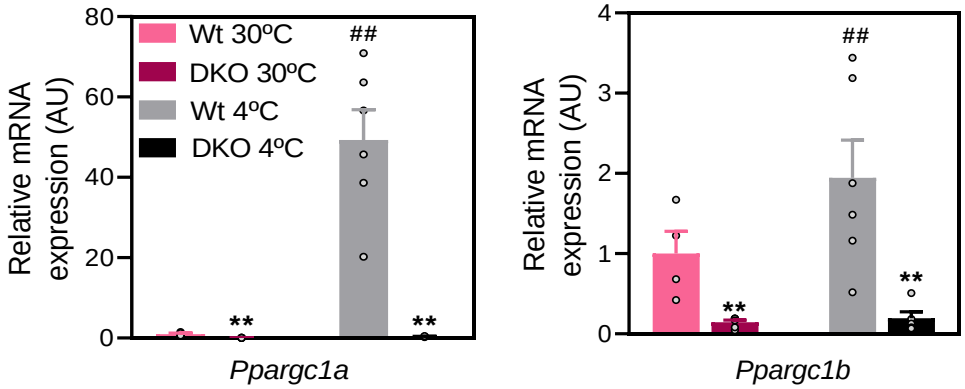


**Figure 4.7. Relative mRNA expression levels of *Ppargc1a* and *Ppargc1b* genes in BAT from Wt and PGC-1α/β-FAT-DKO mice maintained at thermoneutrality (30°C) or subjected to 5 h of cold exposure (4°C).** Ten-week-old male mice fed a regular chow diet were acclimated for two weeks at thermoneutrality or exposed to cold for 5h after the acclimation period. mRNA levels in BAT were determined by RT-qPCR. ANOVA test followed by a Tukey's multiple comparison post hoc analysis was applied. Results are expressed as mean ± SEM (n= 5-6 animals/group). * Indicates statistical significance between Wt and PGC-1α/β-FAT-DKO mice; # Indicates statistical significance between temperature treatments. **,## *P*≤ 0.01.

The expression of mitochondrial genes was also evaluated (Figure 4.8). Specifically, genes from the OxPhos system complex I (*Ndufb9*), complex II (*Sdhb*), complex III (*Uqcr10*), *Cycs*, complex IV (*Coxiv, Cox7a1*), complex V (*Atp5b*) and TCA (*Aco2*) were tested. The expression of *Uqcr10* and *Coxiv* was significantly, but mildly, up-regulated by cold in both Wt and PGC-1α/β-FAT-DKO mice, whereas the expression of *Ndufb9, Sdhb* and *Atp5b* was only up-regulated by cold in PGC-1α/β-FAT-DKO mice. However, the fold induction of these genes by cold was very modest (less than two-fold). Consistent with the known role of PGC-1s in the transcriptional regulation of the expression of these genes, their expression was significantly reduced in PGC-1α/β-FAT-DKO mice, both at thermoneutrality and after cold exposure.

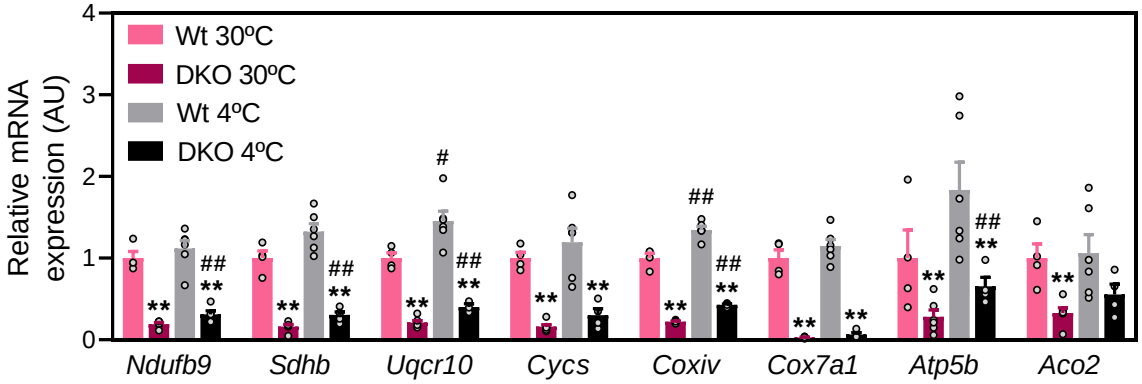


**Figure 4.8. Relative mRNA expression levels of mitochondrial genes in BAT from Wt and PGC-1α/β-FAT-DKO mice maintained at thermoneutrality (30°C) or subjected to 5 h of cold exposure (4°C).** Ten-week-old male mice were fed a regular chow diet and acclimated to 30°C during 2 weeks before being exposed to cold for 5h. mRNA levels were determined by RT-qPCR. ANOVA test followed by a Tukey's multiple comparison post hoc analysis was applied. Results are expressed as mean ± SEM (n=5-6 animals/group). * Indicates statistical significance between Wt and PGC-1α/β-FAT-DKO mice; # Indicates statistical significance between temperature treatments. *,# *P*≤0.05; **,## *P*≤ 0.01.

We then evaluated the gene expression of some of the main thermogenic mediators in BAT from Wt and PGC-1α/β-FAT-DKO mice. Essentially, we measured the expression of *Adrb3, Ucp1* and *Cell death inducing DFFA like effector A* (*Cidea*) (Figure 4.9). In agreement with their role as mediators of heat production, acute cold exposure significantly increased the expression of all genes in Wt mice. However, only the induction of *Ucp1* and *Cidea* genes by cold was blunted in PGC-1α/β-FAT-DKO mice. Contrarily, compared to Wt mice, *Adrb3* expression was notoriously up-regulated in PGC-1α/β-FAT-DKO mice, both at thermoneutrality and after cold exposure. The increase is analogous to that observed at normal housing temperature (21°C) (Figure 4.3).

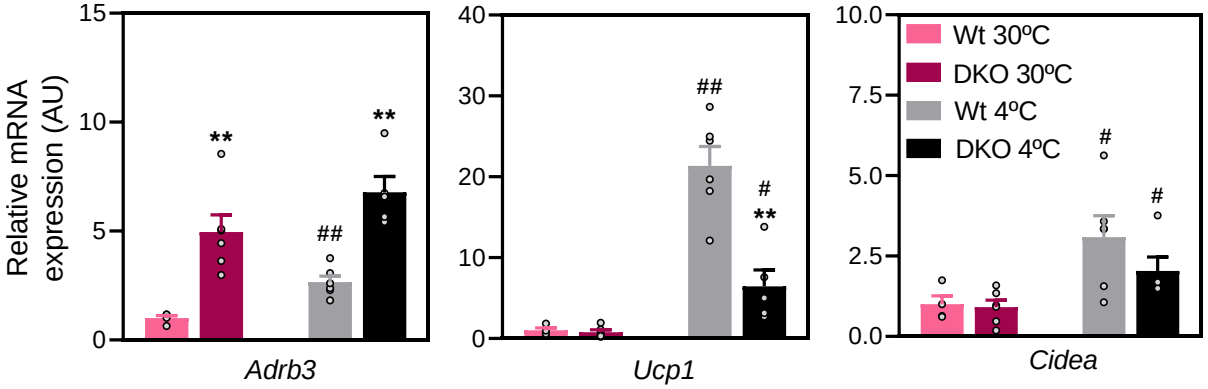


**Figure 4.9. Relative mRNA expression levels of *Adrb3*, *Ucp1* and *Cidea* in BAT of Wt and PGC-1α/β-FAT-DKO mice maintained at thermoneutrality (30°C) or subjected to 5 h of cold exposure (4°C).** Ten-week-old male mice were fed a regular chow diet and acclimated to 30°C during 2 weeks before being exposed to cold for 5h**.** mRNA levels in BAT were determined by RT-qPCR. ANOVA test followed by a Tukey's multiple comparison post hoc analysis was applied. Results are expressed as mean ± SEM (n=5-6 animals/group). * Indicates statistical significance between Wt and PGC-1α/β-FAT-DKO mice; # Indicates statistical significance between temperature treatments. *,# $P \leq 0.05$; **,## $P \leq 0.01$.

Hence, the lack of PGC-1α/β co-activators in BAT from mice results in a reduction in the expression of *Ucp1* and mitochondrial genes, all of which are required to sustain non-shivering adaptive thermogenesis.

### 4.1.3 Physiological characterization of PGC-1α/β-FAT-DKO mice fed a regular chow diet

Mitochondrial dysfunction in adipose tissues is suggested to impair systemic insulin sensitivity and reduce energy expenditure by these tissues, leading to the onset of type 2 diabetes and obesity. Since lack of PGC-1s co-activators in adipose tissues leads to a reduction in the expression of mitochondrial genes, both in WAT and BAT (Figures 4.2 and 4.3), we aimed to explore whether deletion of *Ppargc1a* and *Ppargc1b* genes could impair whole energy balance and glucose homeostasis. For this, Wt and PGC-1α/β-FAT-DKO male mice housed at 21°C and fed a regular chow diet were monitored until the age of 13 weeks. During this time, energy balance and glucose homeostasis were assessed.

### 4.1.3.1 Analysis of body and tissue weight in PGC-1α/β-FAT-DKO mice

To determine the effects on energy balance resulting from the lack of PGC-1s in adipose tissues, body weight of Wt and PGC-1α/β-FAT-DKO mice was monitored weekly. As shown in Figure 4.10, no differences in body weight were found between Wt and PGC-1α/β-FAT-DKO mice when fed a regular chow diet (Figure 4.10, A). Consistent with this, the weight of major tissues barely varied between genotypes, with the exception of gonadal WAT, which was mildly, but significantly decreased in PGC-1α/β-FAT-DKO mice (Figure 4.10, B). These data suggest that specific deletion of PGC-1s in adipose tissues of male mice fed a regular chow diet does not alter net energy balance in PGC-1α/β-FAT-DKO mice.

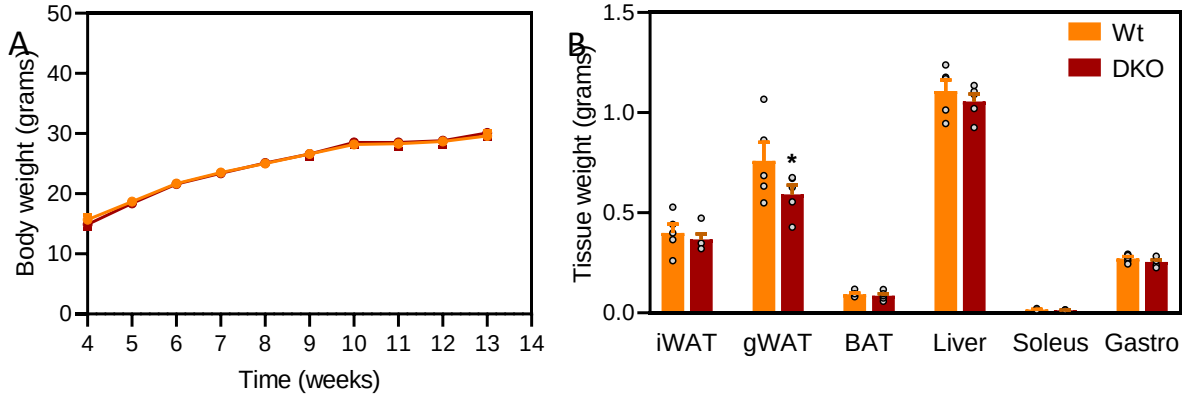


**Figure 4.10. Assessment of body and tissue weight of PGC-1α/β-FAT-DKO mice.** Male mice were housed at 21°C and fed a regular chow diet until the age of 13 weeks. A) Body weight of was followed weekly until week 13. B) The main depots of WAT (inguinal and gonadal), interscapular BAT, liver and skeletal soleus and gastrocnemius muscles were collected at 13 weeks of age and weighted. Student's t-test was applied. Results are expressed as mean ± SEM (n=5 animals/group). * Indicates statistical significance of the comparison between genotypes. * $P \leq 0.05$.

### 4.1.3.2 Evaluation of histological changes in adipose tissues of PGC-1α/β-FAT-DKO mice fed a regular chow diet

Given the importance of PGC-1s in regulating mitochondrial biogenesis in adipose tissues, the morphology of the adipocytes in inguinal WAT and BAT was assessed in PGC-1α/β-FAT-DKO mice and Wt littermates. To this aim, histological sections from these tissues were stained with haematoxylin/eosin and analysed. As seen in Figure 4.11, no gross morphological differences were evident, although white adipocytes appeared bigger in inguinal WAT from PGC-1α/β-FAT-DKO mice. By contrast, brown adipocytes of interscapular BAT from PGC-1α/β-FAT-DKO mice contain bigger lipid droplets than their Wt counterparts, thereby resembling white adipose tissue.

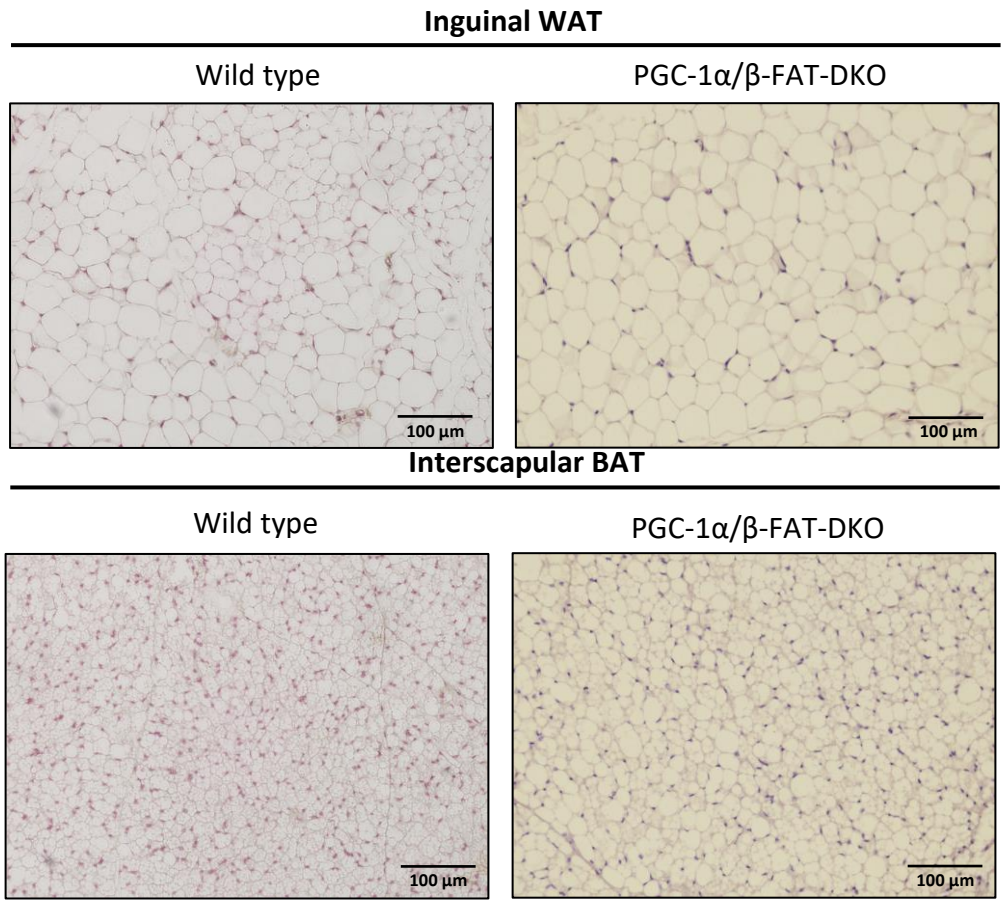


**Figure 4.11. Histological sections of inguinal WAT and interscapular BAT from Wt and PGC-1α/β-FAT-DKO mice.** Male mice were housed at 21°C and fed a regular chow diet until the age of 13 weeks. Then, mice were euthanised, tissues collected and histological sections stained with haematoxylin/eosin.

The quantitative analysis of the previous images revealed that the average adipocyte area in inguinal WAT from PGC-1α/β-FAT-DKO mice was approximately 29% bigger than that from Wt mice, although it did not reach statistical significance (Figure 4.12, A). This difference was represented in the area distribution pattern of the adipocytes between genotypes (Figure 4.12, B).

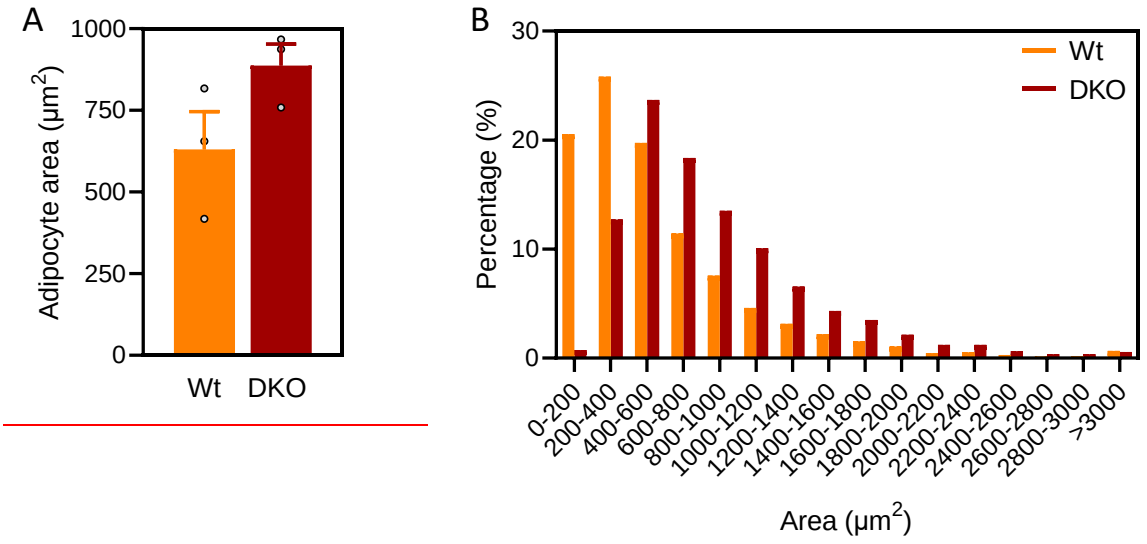

**Figure 4.12. Adipocyte area quantification and size distribution in inguinal WAT of PGC-1α/β-FAT-DKO mice.** Male mice of 13 weeks of age were housed at 21°C and fed a regular chow diet. Adipocytes area were quantified using the Image J software in three random fields of histological sections stained with hematoxylin/eosin from three different mice of each experimental group at 13 weeks of age. B) Size distribution of adipocytes from inguinal WAT of Wt and PGC-1α/β-FAT-DKO mice. In A) student's t-test was applied. Results are expressed as mean ± SEM (n=3 animals/group).

### 4.1.3.3 Analysis of glucose homeostasis in PGC-1α/β-FAT-DKO mice

Reduced mitochondrial mass and function in WAT and impaired BAT thermogenic activity have been associated with an altered glucose homeostasis, particularly with insulin resistance and type 2 diabetes. For this reason, we evaluated glucose tolerance by means of an oGTT and insulin sensitivity by an ipITT in mice fed a chow diet.

Oral GTT was performed in male mice of 11 weeks of age. As shown in Figure 4.13 A, no differences were observed between Wt and PGC-1α/β-FAT-DKO mice. Likewise, as assessed by ipITT, whole body insulin sensitivity was preserved in PGC-1α/β-FAT-DKO mice, which exhibit similar glucose clearance rates than their Wt counterparts (Figure 4.13, B). These results indicate that the specific disruption of PGC-1α/β co-activators in adipose tissues is not enough to alter glucose homeostasis, despite the reduction in mitochondrial gene expression in adipose tissues and the disruption of non-shivering thermogenesis.

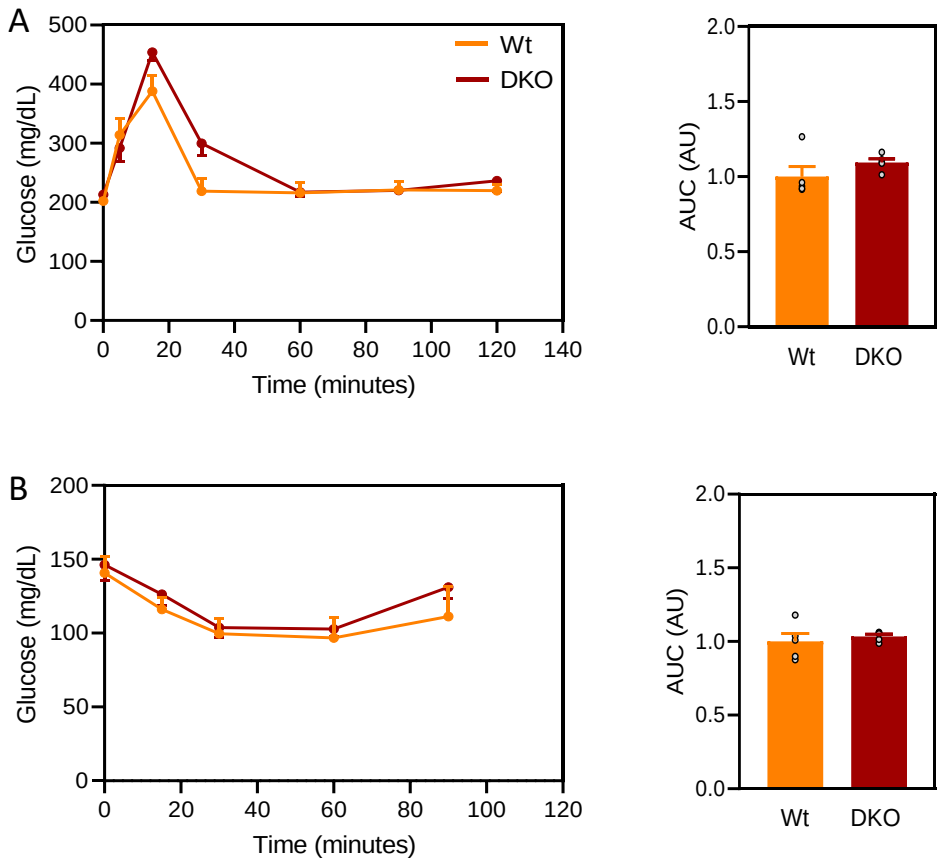


**Figure 4.13. Evaluation of glucose tolerance and insulin sensitivity in Wt and PGC-1α/β-FAT-DKO mice.** Male mice of 11 weeks of age and fed a regular chow diet were used. A) For the oGTT, glucose was delivered orally (2.5 g/kg) to Wt and PGC-1α/β-FAT-DKO mice and blood glucose levels were measured at 0, 15, 30, 60, 90 and 120 min after administration. B) For the ipITT, insulin (0.75 U/kg) was injected intraperitoneally to Wt and PGC-

1α/β-FAT-DKO mice and blood glucose levels were measured at 0, 15, 30, 60, 90 and 120 min after administration. Glucose tolerance and insulin sensitivity were estimated as the *area under the curve (*AUC*)* of the glucose excursion during the oGTT and ipITT. Student's t-test was applied. Results are expressed as mean ± SEM (n=5 animals/group).

#### 4.1.3.4 Biochemical determination of serum parameters PGC-1α/β-FAT-DKO mice

Adipose-specific PGC-1s deletion resulted in deficient non-shivering thermogenesis by BAT (section 4.1.2) and reduced mitochondrial gene expression in both WAT and BAT. Given the fact that lipids constitute a major substrate to sustain BAT thermogenesis, we aimed at investigating to which extent disruption of *Ppargc1a* and *Ppargc1b* expression in adipose tissues altered the serological lipid profile in these mice. For this, triglycerides, NEFA and cholesterol were quantified in serum of Wt and PGC-1α/β-FAT-DKO male mice at the age of 13 weeks (Table 4.1). Results indicated that serum of PGC-1α/β-FAT-DKO mice contained a mild, but statistically significant, increase in NEFA concentration compared to Wt mice, but not in TAG or cholesterol. This increase was independent of glucose and c-peptide levels, which were similar between Wt and PGC-1α/β-FAT-DKO mice, consistent with preserved glucose homeostasis.

| Parameter | Wt | PGC-1α/β-FAT-DKO |
|---|---|---|
| **Glucose (mg/dL)** | 202.4 ± 6 | 213.2 ± 7.1 |
| **C-peptide (ng/mL)** | 1.93 ± 0.07 | 2.27 ± 0.28 |
| **TAG (mg/dL)** | 55.6 ± 3.81 | 60.5 ± 4.31 |
| **NEFA (mg/dL)** | 0.79 ± 0.12 | 1.18 ± 0.06* |
| **Cholesterol (mg/dL)** | 107.18 ± 4.24 | 97.7 ± 6.52 |

**Table 4.1. Quantification of glucose, c-peptide and lipids in serum of Wt and PGC-1α/β-FAT-DKO mice.** Twelve-week-old male mice fed a regular chow diet were used. Serum was collected via tail cut after 5 h of fasting. Glucose was determined in serum with a glucometer and c-peptide by ELISA. TAG and total cholesterol were determined using a commercial kit based on the Trinder colorimetric method. NEFA were measured colorimetrically with the ACS-ACOD method. Student's t-test was applied. Results are expressed as mean ± SEM (n=5-6 animals/group). * Indicates statistical significance of the comparison between genotypes. * $P \leq 0.05$.

## 4.2. Contribution of adipose tissues from PGC-1α/β deficient mice to energy balance and glucose homeostasis when fed a high-fat diet

Previous work from our laboratory showed that PGC-1α/β-FAT-DKO mice challenged with an obesogenic diet rich in fat (HFD45) had preserved insulin sensitivity, although they showed some tendency to develop glucose intolerance. However, the alteration in glucose tolerance was modest and results did not reach statistical significance (36). To further explore the extent of which lack of PGC-1s co-activators could lead to alterations in glucose homeostasis, we decided to challenge PGC-1α/β-FAT-DKO mice with a diet containing a greater amount of fat (60% kcal from fat). Therefore, at the age of 8 weeks, mice started receiving a HFD60 until the age of 20 weeks (3 months of HFD) to assess energy balance and glucose homeostasis.

### 4.2.1 Gene expression analysis in inguinal WAT and interscapular BAT from Wt and PGC-1α/β-FAT-DKO mice fed a HFD60

Firstly, adequate deletion of PGC-1α/β specifically in adipose tissues of 24 to 26-week-old male mice fed for 4 months with a HFD60 was evaluated by RT-qPCR (Figure 4.14). Analysis of gene expression confirmed that *Ppargc1a* and *Ppargc1b* genes were down-regulated in inguinal WAT and BAT from PGC-1α/β-FAT-DKO mice compared to Wt control mice.

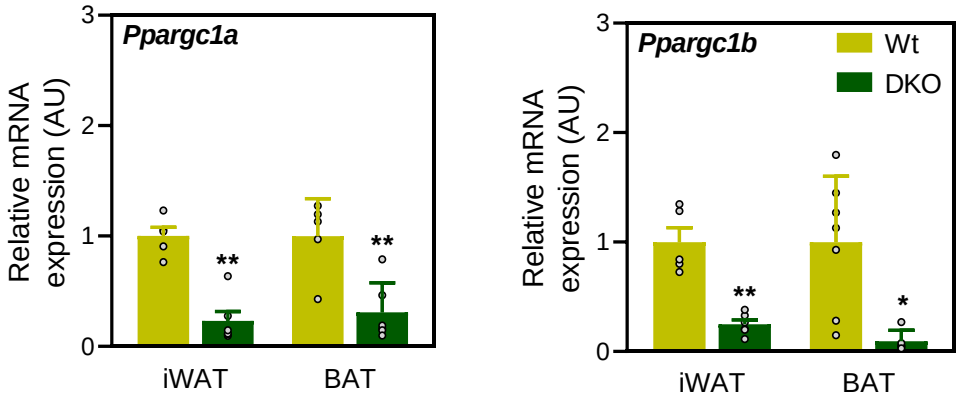


**Figure 4.14. Expression of *Ppargc1a* and *Ppargc1b* genes in inguinal WAT and BAT from Wt and PGC-1α/β-FAT-DKO mice fed a HFD60.** At the age of 8 weeks, male mice were given a HFD60 for 4 months. Mice were euthanized at the age of 24-26 weeks and mRNA levels of PGC-1α and PGC-1β in inguinal WAT and BAT were determined by RT-qPCR**.** Student's t-test was applied. Results are expressed as mean ± SEM (n=5-6 animals/group). * Indicates statistical significance between genotypes. * $P \leq 0.05$; ** $P \leq 0.01$.

### 4.2.2 Effects of the lack of PGC-1s co-activators on WAT gene expression in PGC-1α/β-FAT-DKO mice fed a HFD60

Analysis of gene expression in inguinal WAT was conducted in male mice of 24-26 weeks of age fed a HFD60 for 4 months. The effect of the diet was evaluated by comparing these mice with another group of age-matched mice fed a regular chow diet.

A previous study from our lab done in mice fed a HFD45 reported a decrease in mitochondrial gene expression in PGC-1α/β-FAT-DKO mice compared to Wt counterparts. These genes included the OxPhos system, TCA cycle and fatty acid transport and oxidation pathways (36). Reduced mitochondrial gene expression was accompanied by a decrease in mitochondrial protein levels and a decline in mitochondrial respiration. To confirm that reduced mitochondrial gene expression was also present under the effect of HFD60, we evaluated the expression of genes encoding from components of the OxPhos system. As with the HFD45, deletion of PGC-1s in inguinal WAT resulted in a decrease in the expression of these genes (Figure 4.15).

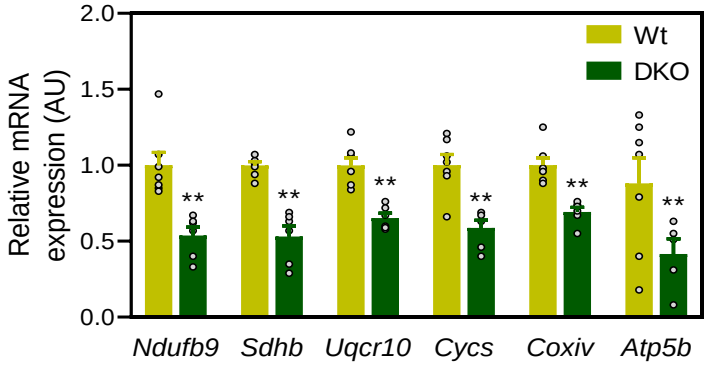


**Figure 4.15. Expression of mitochondrial genes related to the OxPhos system in inguinal WAT from Wt and PGC-1α/β-FAT-DKO mice fed a HFD60.** At the age of 8 weeks, male mice were given a HFD60 for 4 months. Mice were euthanized at the age of 24-26 weeks and mRNA levels of mitochondrial genes from the OxPhos system in inguinal WAT were determined by RT-qPCR**.** Student's t-test was applied. Results are expressed as mean ± SEM (n=5-6 animals/group). * Indicates statistical significance between genotypes. * *P*≤0.05; ** *P*≤ 0.01.

We firstly assessed whether lack of PGC-1s co-activators and the consequent reduction in mitochondrial mass and function was accompanied by a loss of adipose identity. For this, we analysed the expression of markers considered to be specific for white adipocytes, such as *insulin-like growth factor-binding protein 3* (*Igfbp3*) gene (186). As seen in Figure 4.16, A, HFD60 did not alter the expression of this WAT marker in comparison to chow diet. Despite 64% of reduction in the expression of *Igfbp3* in PGC-1α/β-FAT-DKO mice fed a regular chow diet and 22% reduction under the effect of HFD60, differences were not statistically significant. The expression of other WAT markers, like *Tcf21* or *Hox9* was also assessed, but their expression levels appear too low to be detected, even by RT-qPCR (data not shown).

Although they are not white adipocyte-specific, the expression of adiponectin, leptin and resistin was also evaluated, as they encode for the three most important and best characterized adipokines secreted by WAT. HFD60 appeared to increase *Leptin* expression level in Wt mice (3.15 ± 0.69 *arbitrary* units or AU), but not in PGC-1α/β-FAT-DKO mice, although it did not reach statistical significance. However, expression levels of *Leptin* were already high in WAT of PGC-1α/β-FAT-DKO mice fed a chow diet. No effect of diet or genotype was observed in the expression of *AdipoQ* or *Resistin.* (Figure 4.16, B).

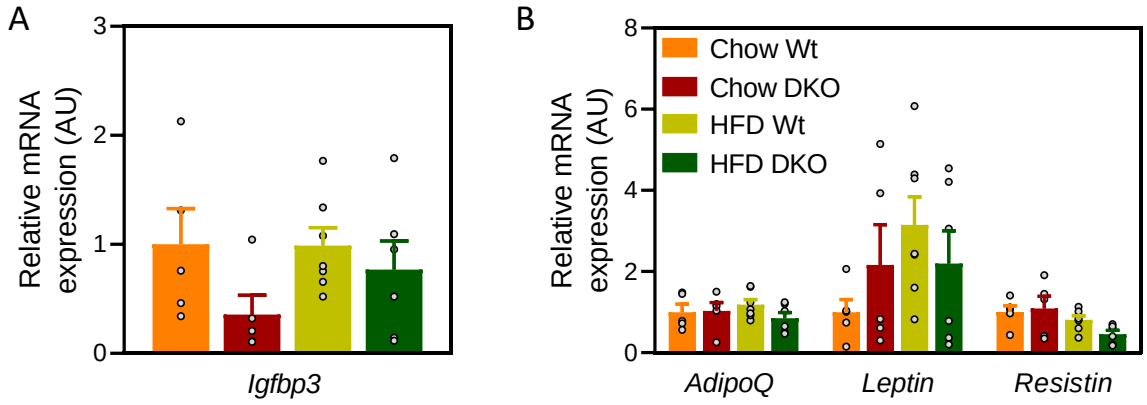


**Figure 4.16. Relative mRNA expression levels of *Igfbp3, AdipoQ, Leptin* and *Resistin* in inguinal WAT of Wt and PGC-1α/β-FAT-DKO mice fed a HFD60.** At the age of 8 weeks, male mice were given a HFD60 for 4 months. In

parallel, another cohort of age-matched mice were fed a regular chow diet. Mice were euthanized at the age of 24-26 weeks and mRNA levels in inguinal WAT were determined by qPCR. ANOVA test followed by a Tukey's multiple comparison post hoc analysis was applied. Results are expressed as mean ± SEM (n=5-7 animals/group).

WAT inflammation is a major hallmark of obesity and it is tightly related to the onset of IR. Therefore, the expression of some pro-inflammatory genes was evaluated (Figure 4.17). On the one side, we observed that the effect of HFD60 was not homogenous amongst all pro-inflammatory markers analysed. HFD60 robustly increased, both in Wt and PGC-1α/β-FAT-DKO mice, the expression of *Cd11c*, a marker of M1 polarized macrophages, although it did not reach statistical significance due to individual variation. However, the expression of *C-C Motif Chemokine Ligand 2* (*Ccl2*), *Nitric Oxide Synthase 2* (*Nos2*) and *Tumour Necrosis Factor alpha* (*Tnfa*), cytokines also associated to M1 macrophage polarization, was not altered by the HFD60. Contrary to what it was expected, compared to chow diet, HFD60 down-regulated the expression of pro-inflammatory genes such as *C-C Motif Chemokine Ligand 7* (*Ccl7*), *Complement factor d* (*Cfd*) and *Interleukin 1 beta* (*Il1b*), although differences were only statistically significant concerning *Cfd* and *Il1b* expression in Wt mice. On the other side, PGC-1s deficiency significantly reduced the expression of *Cfd* in mice fed a regular chow diet, but not when fed a HFD60. In a similar way, *Ccl2, Ccl7, Il1b* and *Tnfa* expression levels were reduced in PGC-1α/β-FAT-DKO mice fed a regular chow diet, but these results did not reach statistical significance. No differences in gene expression between Wt and PGC-1α/β-FAT-DKO mice were observed when mice were fed a HFD60, except for *Cfd*.

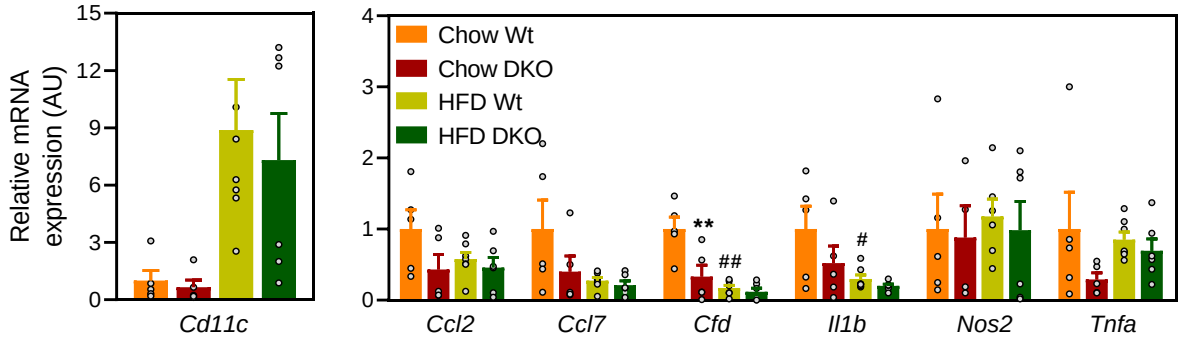


**Figure 4.17. Analysis of the expression of pro-inflammatory genes in inguinal WAT from Wt and PGC-1α/β-FAT-DKO mice.** At the age of 8 weeks, male mice were given a HFD60 for 4 months. In parallel, another cohort of age-matched mice were fed a regular chow diet. Mice were euthanized at the age of 24-26 weeks and mRNA levels in inguinal WAT were determined by qPCR. ANOVA test followed by a Tukey's multiple comparison post hoc analysis was applied. Results are expressed as mean ± SEM (n=5-7 animals/group). * Indicates statistical significance of the comparison between Wt and PGC-1α/β-FAT-DKO mice; # Indicates statistical significance of the comparison between diets. *, # $P \leq 0.05$; **, ## $P \leq 0.01$.

In summary, gene expression analysis shows that lack of PGC-1s does not change the identity of WAT or its inflammatory status, which, based on the expression of *Cd11c,* appears to be increased by HFD60 in Wt and PGC-1α/β-FAT-DKO mice.

### 4.2.3 Effects of the lack of PGC-1s co-activators on BAT gene expression in PGC-1α/β-FAT-DKO mice fed a HFD60

Previous results obtained from mice fed a HFD45 showed that brown adipocytes of interscapular BAT from PGC-1α/β-FAT-DKO mice adopted a WAT-like phenotype. To gain

insight into this "whitening" process as a result of the loss of PGC-1s co-activators, we analysed the expression of several white - and brown adipocyte-specific markers in BAT.

Gene expression of *Igfbp3* was primarily measured to evaluate a possible gain of WAT identity in BAT from PGC-1α/β-FAT-DKO mice. Also, although they are expressed at lower levels in brown adipocytes compared to white adipocytes, *AdipoQ* and *Leptin* genes were assessed as classical white adipokines. As shown in Figure 4.18, compared to chow diet, HFD60 increased the expression of *Igfbp3 AdipoQ* and *Leptin* both in Wt and PGC-1α/β-FAT-DKO mice. However, deletion of PGC-1s dramatically increased the expression of *Igfbp3, AdipoQ* and *Leptin* in all conditions, supporting the notion that PGC-1s deficiency induces the "whitening" of brown adipocytes.

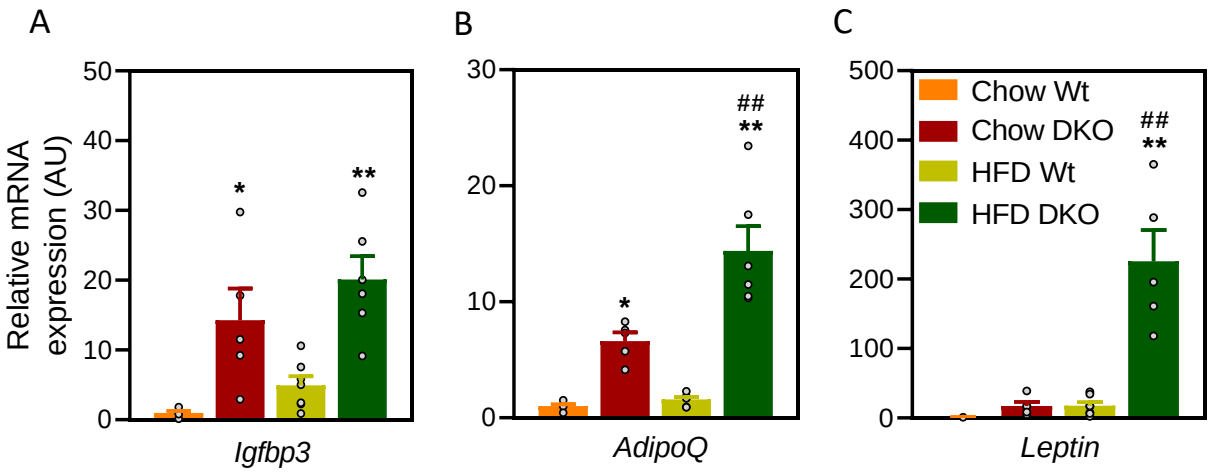


**Figure 4.18. Analysis of the expression of white adipocyte identity markers in BAT from Wt and PGC-1α/β-FAT-DKO mice.** At the age of 8 weeks, male mice were given a HFD60 for 4 months. In parallel, another cohort of age-matched mice were fed a regular chow diet. Mice were euthanized at the age of 24-26 weeks and mRNA levels in BAT were determined by RT-qPCR. ANOVA test followed by a Tukey's multiple comparison post hoc analysis was applied. Results are expressed as mean ± SEM (n=5-7 animals/group). * Indicates statistical significance of the comparison between Wt and PGC-1α/β-FAT-DKO mice; # Indicates statistical significance of the comparison between diets. *, # $P \leq 0.05$; **, ## $P \leq 0.01$.

Changes in brown adipocyte identity was also evaluated by analysing the expression of genes considered BAT-specific, such as the *Ucp1* or genes that are very highly expressed in BAT compared to WAT, like *Pyruvate Dehydrogenase Kinase 4* (*Pdk4*) or transcription factors like *Lim Homebox 8* (*Lhx8*), *Mesenchyme Homebox 2* (*Meox2*), *Prdm16* and *Zic Family Member 1* (*Zic1*) (186). In general, the gene expression analysis indicated that lack of PGC-1s, regardless of the nutritional condition, up-regulated the expression of BAT markers, what can be viewed as an attempt of PGC-1α/β-FAT-DKO mice to compensate for the thermogenic dysfunction of brown adipocytes by increasing brown adipogenesis (Figure 4.19).

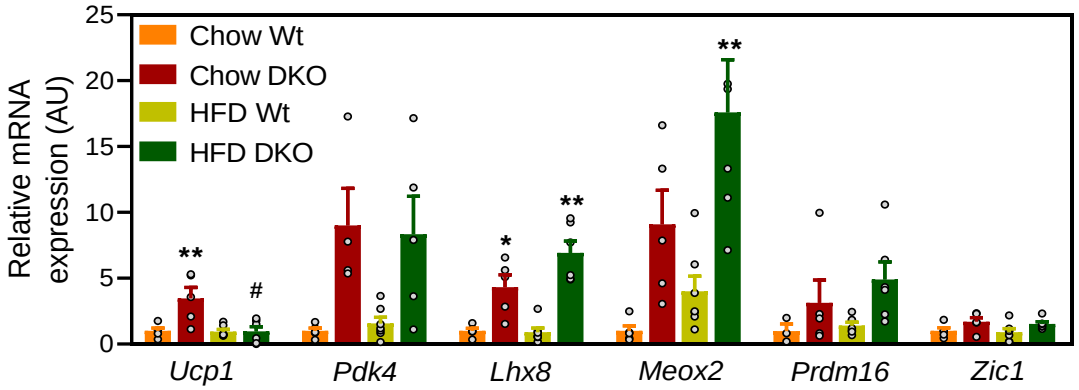


**Figure 4.19. Analysis of gene expression of brown fat markers in BAT from Wt and PGC-1α/β-FAT-DKO mice.** At the age of 8 weeks, male mice were given a HFD60 for 4 months. In parallel, another cohort of age-matched mice were fed a regular chow diet. Mice were euthanized at the age of 24-26 weeks and mRNA levels in BAT were determined by RT-qPCR**.** ANOVA test followed by a Tukey's multiple comparison post hoc analysis was applied. Results are expressed as mean ± SEM (n=5-7 animals/group). * Indicates statistical significance of the comparison between Wt and PGC-1α/β-FAT-DKO mice; # Indicates statistical significance of the comparison between diets. *, # $P \leq 0.05$; **, ## $P \leq 0.01$.

The effect of deleting PGC-1s co-activators on BAT inflammation was also assessed (Figure 4.20). Consistent with an increased inflammatory state, HFD60 was observed to up-regulate the expression of *Ccl2* and *Ccl7* genes in Wt and PGC-1α/β-FAT-DKO mice, although the results did not reach statistical significance due to the high variability amongst individuals. This pattern of regulation by HFD60 differed from the one in inguinal WAT, in which HFD60 appeared to down-regulate the expression of most of the pro-inflammatory genes analysed (mainly *Cfd* and *Il1b*). Remarkably, regardless of the diet, deletion of PGC-1α/β co-activators induced the expression of inflammatory genes. Of note, the induction of *Cfd* by the deletion of the PGC-1s was notably high in both diets, being significantly increased by more than 10-fold. With regard to the rest of the genes, the expression of *Ccl2*, *Ccl7* and *Il1b* (this only under chow diet) was mildly increased in PGC-1α/β-FAT-DKO mice, although differences did not reach statistical significance.

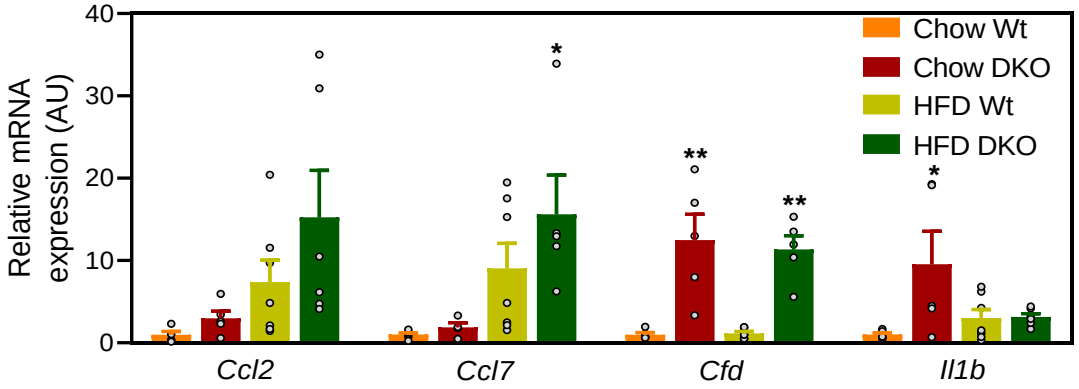


**Figure 4.20. Analysis of the expression of pro-inflammatory immune genes in BAT from Wt and PGC-1α/β-FAT-DKO mice.** At the age of 8 weeks, male mice were given a HFD60 for 4 months. In parallel, another cohort of age-matched mice were fed a regular chow diet. Mice were euthanized at the age of 24-26 weeks and mRNA levels in BAT were determined by RT-qPCR. ANOVA test followed by a Tukey's multiple comparison post hoc

analysis was applied. Results are expressed as mean ± SEM (n=5-7 animals/group). * Indicates statistical significance of the comparison between Wt and PGC-1α/β-FAT-DKO mice; * *P*≤0.05; ** *P*≤ 0.01.

### 4.2.4 Physiological characterization of PGC-1α/β-FAT-DKO mice fed a HFD60

Adipose-specific deletion of PGC-1s co-activators did not result in an impairment of energy balance when mice were fed a regular chow diet (section 4.1.3.1). In the same direction, glucose tolerance did not vary and insulin sensitivity was also preserved (section 4.1.3.3). When these mice were exposed to a HFD45, a mild glucose intolerance appeared. However, insulin sensitivity was similar to that of Wt mice (36). We therefore re-evaluated energy balance and glucose homeostasis in Wt and PGC-1α/β-FAT-DKO mice when fed a greater high-fat diet, HFD60, to unmask possibly alterations in energy and glucose homeostasis in mutant mice.

#### 4.2.4.1 Analysis of body weight and adiposity in PGC-1α/β-FAT-DKO mice fed a HFD60

When fed for 3 months with a HFD60, PGC-1α/β-FAT-DKO male mice gained more weight than Wt controls. Differences started after two months of exposition to the obesogenic diet and continued since mice were euthanized, at 20 weeks of age (Figure 4.21, A). Higher body weight in PGC-1α/β-FAT-DKO male mice correlated with a mild, but significant, increase in the weight of gonadal WAT and BAT (Figure 4.21, B).

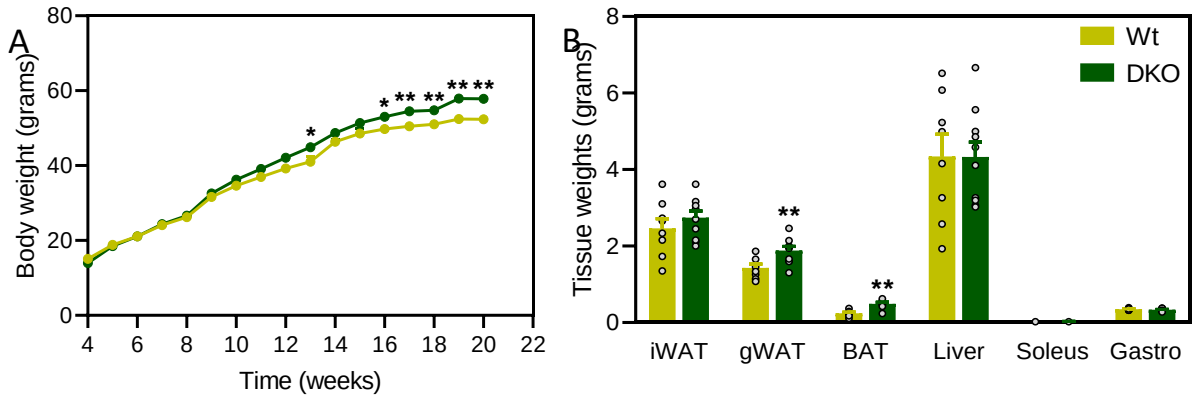


**Figure 4.21. Assessment of body and tissue weight in PGC-1α/β-FAT-DKO male mice fed a HFD60.** At the age of 8 weeks, male mice started receiving a HFD60. Mice were euthanized at the age of 20 weeks. A) Body weight was followed weekly throughout the experiment. B) Weight of the main depots of WAT (inguinal and gonadal), interscapular BAT, liver and skeletal soleus and gastrocnemius muscles collected at 20 weeks of age. Student's t-test was applied. Results are expressed as mean ± SEM (n=8-10 animals/group). * Indicates statistical significance of the comparison between genotypes. * *P*≤0.05; ** *P*≤ 0.01.

We also analysed the evolution of weight gain in Wt and PGC-1α/β-FAT-DKO females fed with a HFD60. Contrarily to male mice, PGC-1α/β-FAT-DKO females exhibited similar body weight than their Wt littermates after 3.5 months on a HFD60 (Figure 4.22, A). Consistently, weight of inguinal WAT, gonadal WAT, liver and skeletal muscles (soleus and gastrocnemius) was similar in Wt and PGC-1α/β-FAT-DKO females. However, although differences did not reach statistical significance, BAT of PGC-1α/β-FAT-DKO females was almost twice heavier than BAT

of Wt females (0.15 ± 0.03 grams in Wt and 0.31 ± 0.1 grams in PGC-1α/β-FAT-DKO females) (Figure 4.22, B).

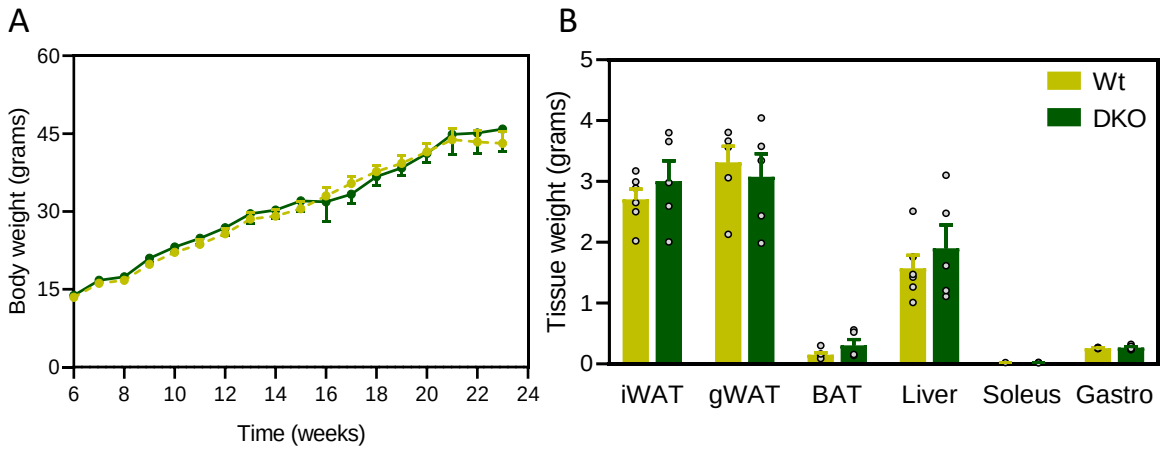


**Figure 4.22. Assessment of body and tissue weight from Wt and PGC-1α/β-FAT-DKO females fed a HFD60.** At the age of 8 weeks, female mice were given a HFD60 for 3.5 months. Mice were euthanized at the age of 23 weeks. A) Body weight was followed weekly throughout the experiment. B) Weight of the main depots of WAT (inguinal and gonadal), interscapular BAT, liver and skeletal soleus and gastrocnemius muscles at 23 weeks of age. Student's t-test was applied. Results are expressed as mean ± SEM (n=5-6 animals/group).

### 4.2.4.2 Morphological analysis of adipose tissues from PGC-1α/β-FAT-DKO mice fed a HFD60

The increment in body weight observed in PGC-1α/β-FAT-DKO male mice correlated with an increase in adipose tissues weight, specifically that of gonadal WAT and BAT. To analyse whether PGC-1s deletion in adipose tissues altered their structure beyond their weight, we performed a histological analysis. For this, histological sections from inguinal WAT, gonadal WAT and BAT from Wt and PGC-1α/β-FAT-DKO male mice were stained with hematoxylin/eosin (Figure 4.23). No gross morphological differences appeared between Wt and PGC-1α/β-FAT-DKO mice in inguinal or gonadal WAT. However, as previously observed when fed a chow diet or a HFD45 (36), BAT from PGC-1α/β-FAT-DKO mice fed a HFD60 appeared to have bigger adipocytes, usually containing a single big lipid droplet, that resemble white adipocytes.

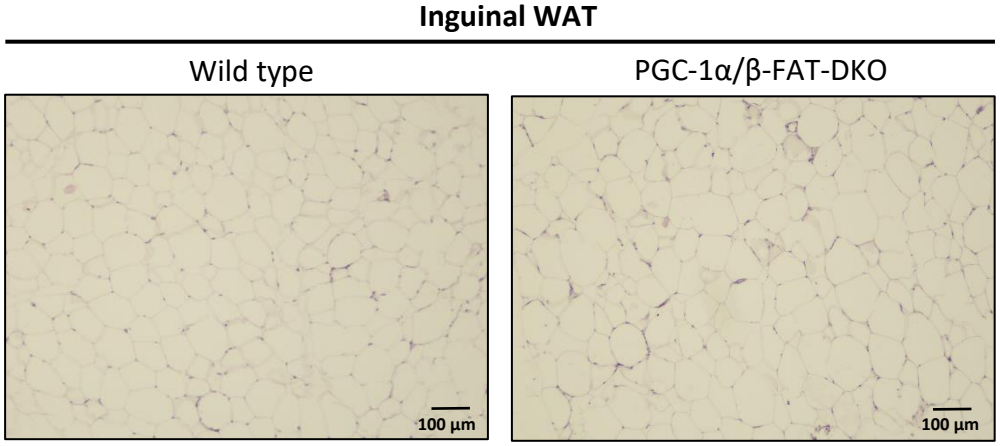

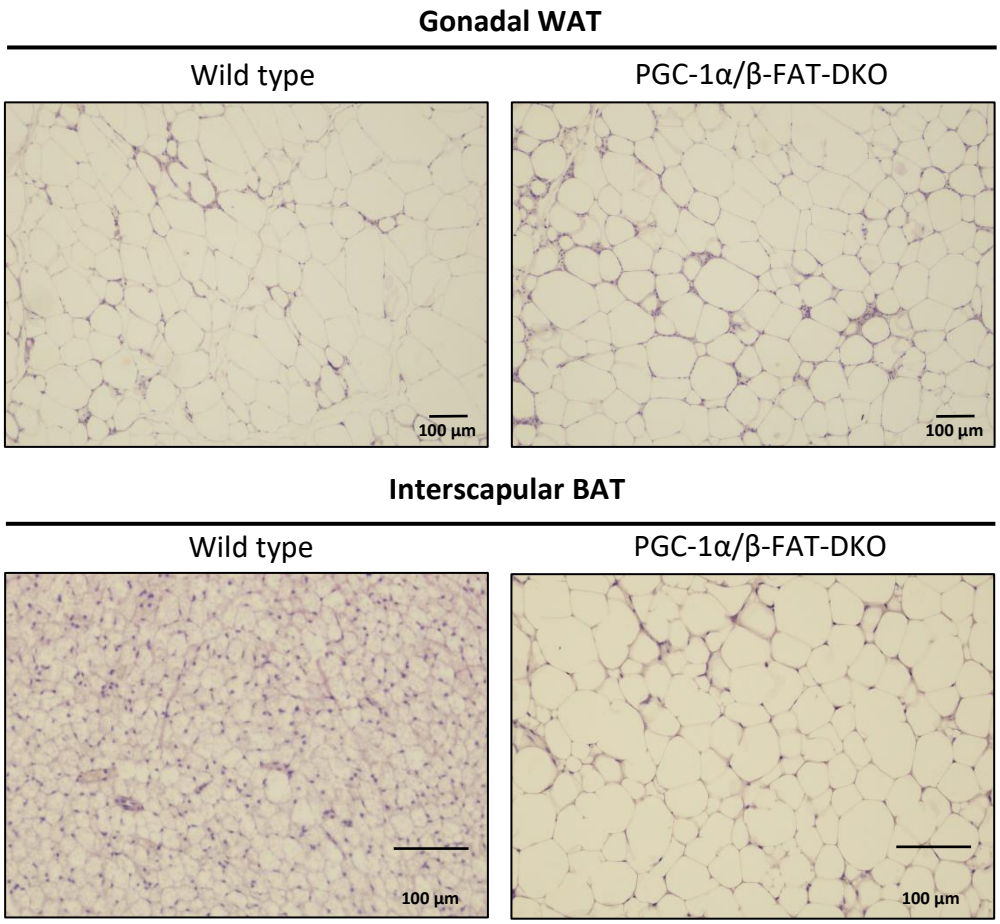


**Figure 4.23. Histological sections of inguinal WAT, gonadal WAT and interscapular BAT from Wt and PGC-1α/β-FAT-DKO mice fed a HFD60.** At the age of 8 weeks, male mice were given a HFD60 for 3 months. Mice were euthanized at the age of 20 weeks and histological sections were stained with haematoxylin/eosin.

Adipocyte's area from inguinal and gonadal WAT were then quantified to accurately identify differences between Wt and PGC-1α/β-FAT-DKO mice. Similar to what we observed in mice fed a regular chow diet, adipocyte mean area in inguinal WAT from PGC-1α/β-FAT-DKO male mice was bigger than in Wt mice (3,524 ± 396.4 $\mu m^2$ in Wt vs 4,925 ± 494.5 $\mu m^2$ in PGC-1α/β-FAT-DKO mice, *P*= 0.09). However, differences did not reach statistical significance (Figure 4.24). In contrast, the mean area of gonadal adipocytes was slightly smaller in PGC-1α/β-FAT-DKO mice, although it did not reach statistical significance (5,059 ± 1,097.7 $\mu m^2$ in Wt vs 4,204 ± 213.1 $\mu m^2$ in PGC-1α/β-FAT-DKO mice, *P*= 0.09)

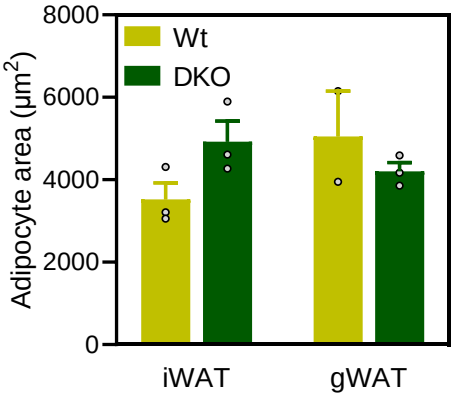


**Figure 4.24. Adipocyte area quantification in inguinal and gonadal WAT from Wt and PGC-1α/β-FAT-DKO mice fed a HFD60.** At the age of 8 weeks, male mice were given a HFD60 for 3 months. Mice were euthanized at the age of 20 weeks and histological sections were stained with hematoxylin/eosin. Mean adipocyte area was quantified in three random fields from 3 different mice of each experimental group. Student's t-test was applied. Results are expressed as mean ± SEM (n=3 animals/group).

The distribution of adipocyte size in inguinal and gonadal WAT depots was also evaluated. As seen in Figure 4.25, A, in inguinal WAT a higher abundance of small adipocytes was identified in Wt male mice, compared to PGC-1α/β-FAT-DKO mice. By contrast, on the gonadal depot (Figure 4.25, B), the size of adipocytes from Wt and PGC-1α/β-FAT-DKO mice followed a similar pattern of distribution, in agreement with their similar average size.

A

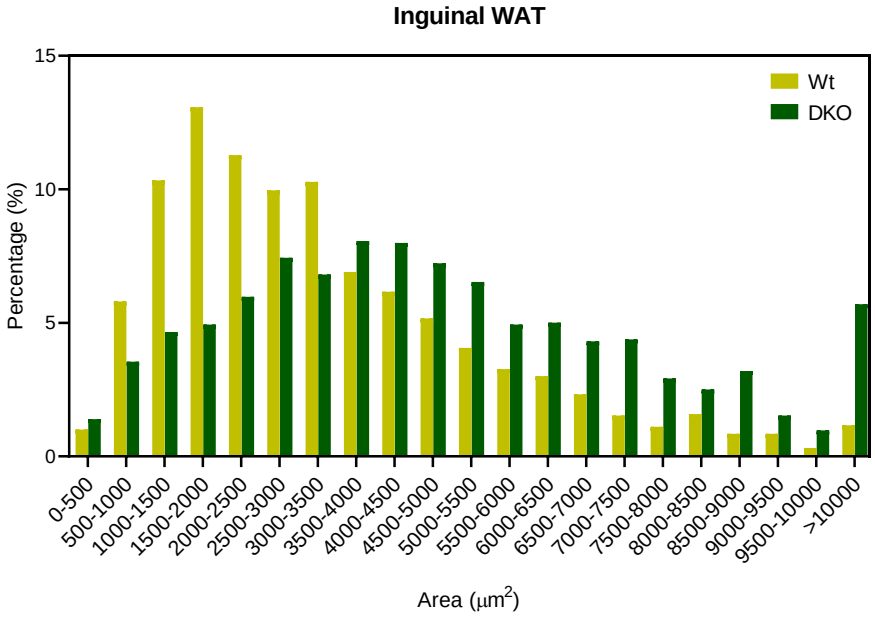

B

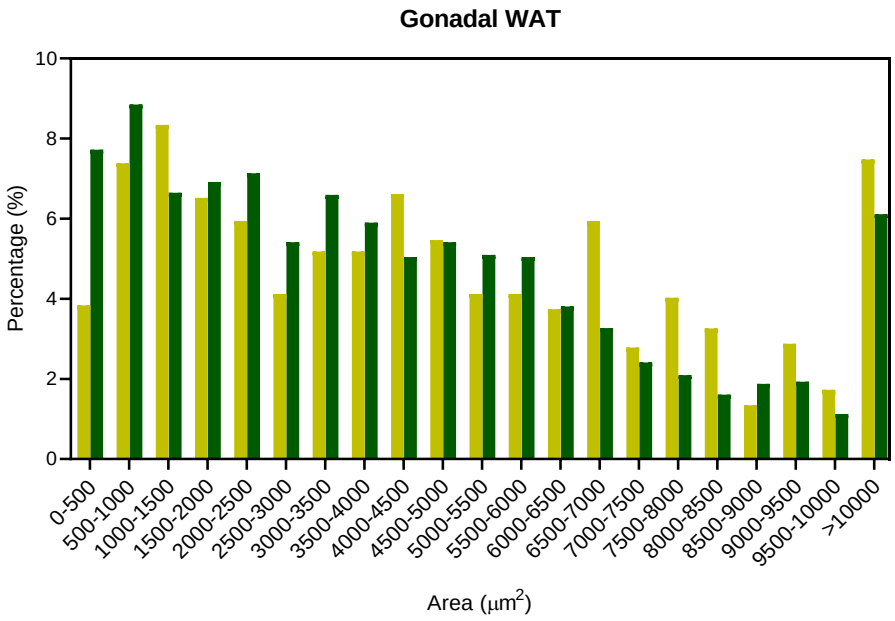


**Figure 4.25. Adipocyte size distribution in inguinal and gonadal WAT from Wt and PGC-1α/β-FAT-DKO mice fed a HFD60.** At the age of 8 weeks, male mice were given a HFD60 for 3 months. Mice were euthanized at the age of 20 weeks and histological sections were stained with hematoxylin/eosin. Adipocytes areas were quantified in three random fields from 3 different mice of each experimental group.

### 4.2.4.3 Analysis of glucose homeostasis and insulin sensitivity in PGC-1α/β-FAT-DKO mice fed a HFD60

The overtime follow-up analysis of glucose tolerance of mice fed a HFD60 revealed that glucose intolerance in PGC-1α/β-FAT-DKO mice appeared after 2 months on HFD60 and was sustained, and even worsened, at 3 months of age, when mice were euthanized (Figure 4.26, B and C, respectively).

A

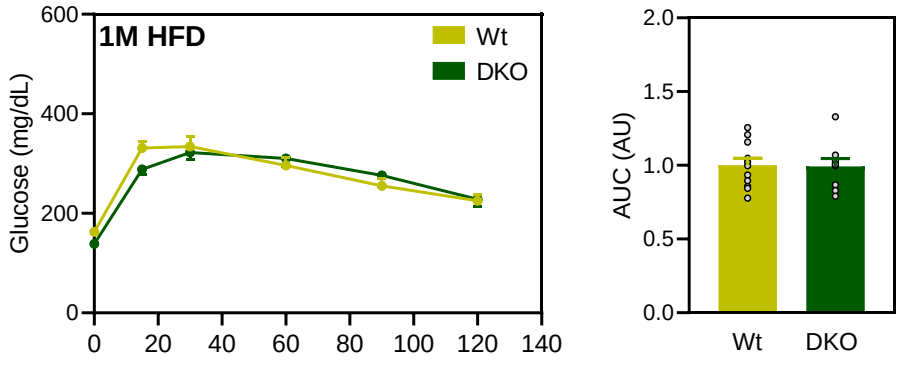

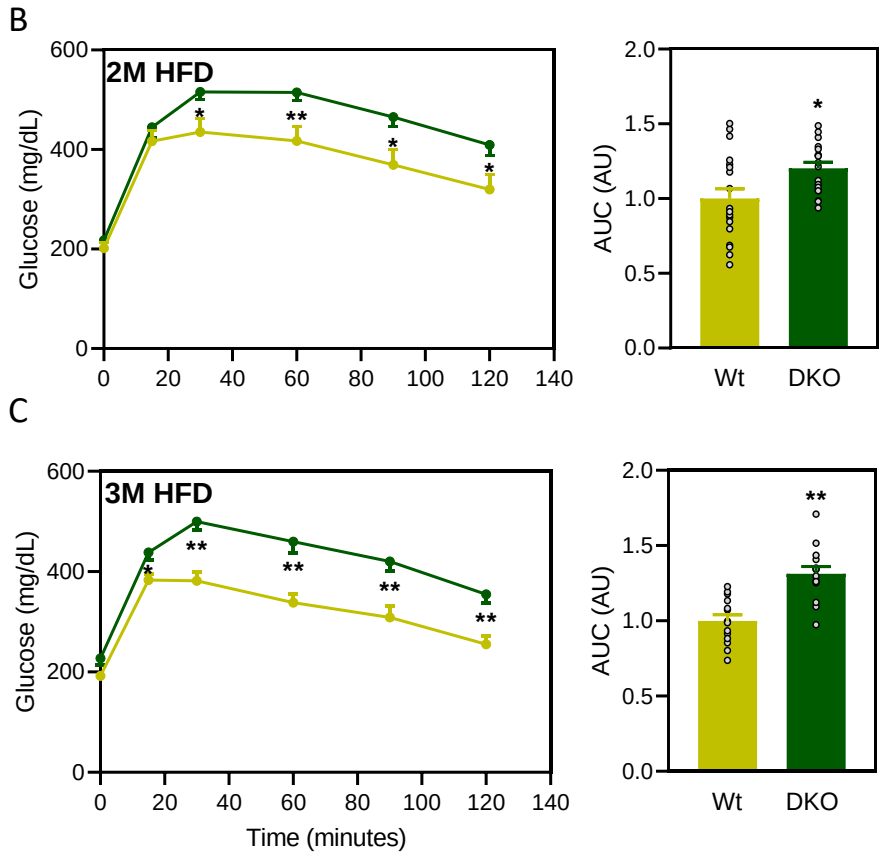


**Figure 4.26. Temporal evaluation of glucose tolerance in Wt and PGC-1α/β-FAT-DKO mice fed a HFD60.** At the age of 8 weeks, male mice were given a HFD60 for 1, 2 or 3 months. Intraperitoneal GTT were conducted in 12- (1 month of HFD60), 16- (2 months of HFD60) and 20-week-old (3 months of HFD60) mice fasted for 6 h. Glucose was delivered by an intraperitoneal injection (1 g/kg) to Wt and PGC-1α/β-FAT-DKO male mice and blood glucose levels were measured at 0, 15, 30, 60, 90 and 120 min after the administration. Glucose tolerance was estimated as the AUC of the glucose excursion during the ipGTT. Student's t-test was applied. Results are expressed as mean ± SEM (n= 9-19 animals/group). * Indicates statistical significance of the comparison between genotypes. * $P \leq 0.05$; ** $P \leq 0.01$.

Given the fact that PGC-1α/β-FAT-DKO mice became glucose intolerant after 2 months on a HFD60, insulin sensitivity was started to be evaluated at this timepoint. Despite exhibiting glucose intolerance, insulin sensitivity was preserved in PGC-1α/β-FAT-DKO mice 2 and 3 months after starting a HFD60 (Figure 4.27, A and B, respectively).

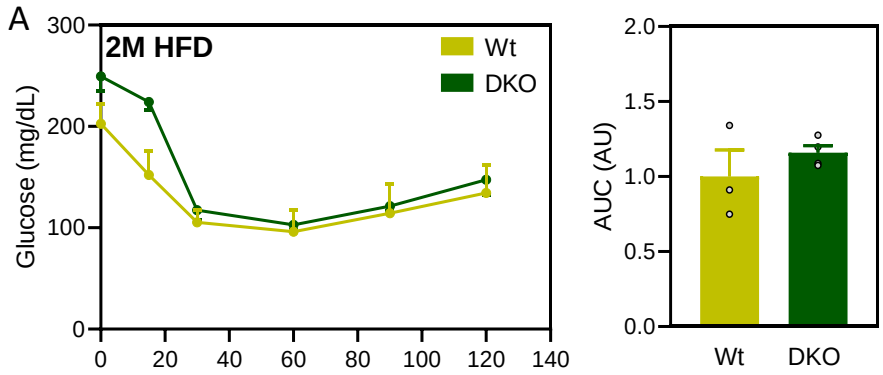

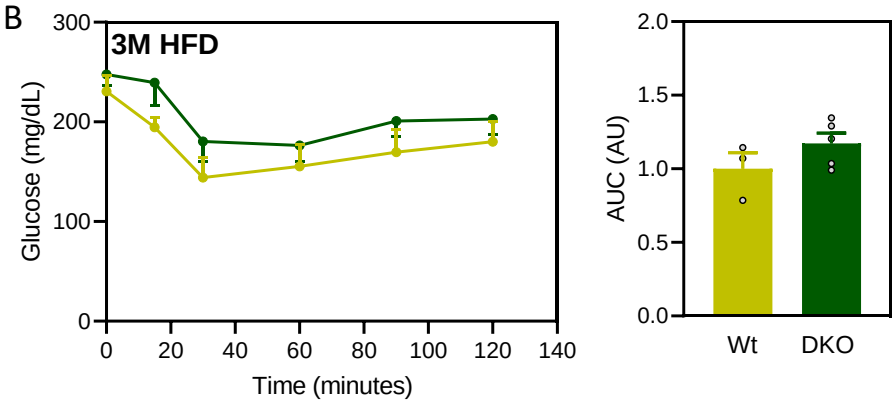


**Figure 4.27. Evaluation of insulin sensitivity in Wt and PGC-1α/β-FAT-DKO mice fed a HFD60.** At the age of 8 weeks, male mice were given a HFD60 for 2 or 3 months. ITT were performed in 16- (2 months of HFD60) and 20-week-old (3 months of HFD60) mice fasted for 6 h. Insulin (1 U/kg) was injected intraperitoneally to Wt and PGC-1α/β-FAT-DKO mice and blood glucose levels were measured at 0, 15, 30, 60, 90 and 120 min after administration. Insulin sensitivity was estimated as the AUC of the glucose excursion during the ipITT. Student's t-test was applied. Results are expressed as mean ± SEM (n= 3-5 animals/group).

Despite having a similar weight than their Wt littermates (Figure 4.22), glucose tolerance was impaired in PGC-1α/β-FAT-DKO females (Figure 4.28, A). As observed in PGC-1α/β-FAT-DKO males (Figure 4.27), glucose intolerance was not accompanied by insulin resistance, being insulin sensitivity from PGC-1α/β-FAT-DKO females comparable to that of Wt control females (Figure 4.28, B).

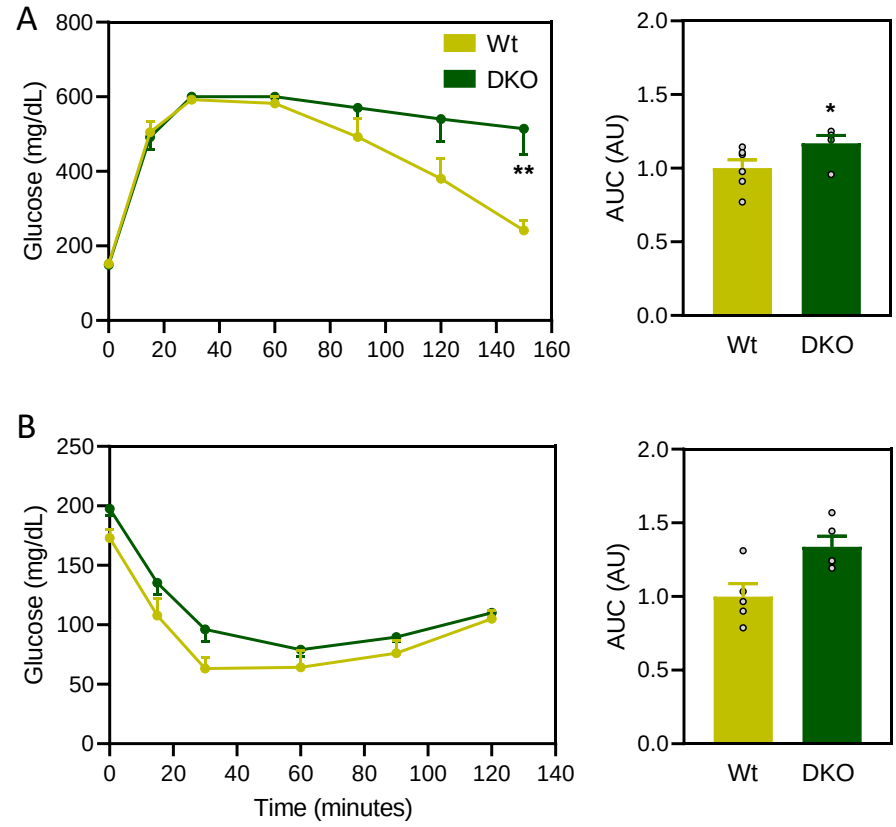


**Figure 4.28. Evaluation of glucose tolerance and insulin sensitivity in Wt and PGC-1α/β-FAT-DKO females fed a HFD60.** At 8 weeks of age, female mice were given a HFD60 for 3.5 months. GTT and ITT were done at 22-

week-old mice fasted for 6 h. Glucose (2 g/kg) or insulin (1 U/kg) were delivered by an intraperitoneal injection to Wt and PGC-1α/β-FAT-DKO mice and blood glucose levels were measured at 0, 15, 30, 60, 90 and 120 min after the administration. Glucose tolerance and insulin sensitivity were estimated as the AUC of the glucose excursion during GTT or ITT. Student's t-test was applied. Results are expressed as mean ± SEM (n= 5-6 animals/group). * Indicates statistical significance between genotypes. * $P \leq 0.05$; ** $P \leq 0.01$.

#### 4.2.4.4 Biochemical determination of serum parameters in PGC-1α/β-FAT-DKO mice fed a HFD60

Serum determination of metabolic parameters was performed in order to detect whether deletion of genes encoding for PGC-1s co-activators in adipose tissues lead to alterations in lipid homeostasis in response to a diet rich in fat. For this, triglycerides, NEFA and cholesterol were measured in serum of 5 h fasted mice. As shown in Table 4.2, a mild, but statistically significant, decrease in triglycerides in serum from PGC-1α/β-FAT-DKO mice compared to Wt controls was found. No major changes were observed regarding triglycerides or cholesterol concentration.

Apart from the lipidic metabolites, glucose, c-peptide and glucagon were also evaluated in serum from Wt and PGC-1α/β-FAT-DKO mice. Consistent with the altered glucose homeostasis, glycaemia was significantly higher in PGC-1α/β-FAT-DKO mice. Moreover, serum c-peptide concentration, a surrogate of insulin, was lower than in Wt mice. No changes were found in glucagon concentration.

| Parameter | Wt | PGC-1α/β-FAT-DKO |
|---|---|---|
| Glucose (mg/dL) | 194 ± 3.93 | 228 ± 7.81** |
| C-peptide (ng/mL) | 3.55 ± 0.23 | 2.27 ± 0.12** |
| Glucagon (pg/mL) | 27.01 ± 1.57 | 29.28 ± 2.30 |
| TAG (mg/dL) | 55.45 ± 1.71 | 50.6 ± 1.55* |
| NEFA (mg/dL) | 0.54 ± 0.02 | 0.57 ± 0.05 |
| Cholesterol (mg/dL) | 194.88 ± 3.14 | 189.05 ± 3.73 |

**Table 4.2. Analysis of lipidic metabolites and hormones in serum of PGC-1α/β-FAT-DKO mice fed a HFD60.** At 8 weeks of age, male mice were given a HFD60 for 3 months. Serum was collected via tail cut after 5 h of fasting in 20-week-old mice. Glucose was determined in serum with a glucometer. C-peptide and glucagon were determined in serum by ELISA. TAG and total cholesterol were determined using a commercial kit based on the Trinder colorimetric method. NEFAs were measured colorimetrically with the ACS-ACOD method. Student's t-test was applied. Results are expressed as mean ± SEM (n=9-13 animals/group). * Indicates statistical significance of the comparison between genotypes. * $P \leq 0.05$; ** $P \leq 0.01$.

#### 4.2.4.5 Analysis of energy balance and glucose homeostasis in weight-matched PGC-1α/β-FAT-DKO mice fed a HFD60

Considering that obesity is an underlying cause of impaired glucose homeostasis, we then evaluated whether higher body weight in PGC-1α/β-FAT-DKO mice (section 4.2.4.1) could be the cause of the glucose intolerance observed in these mice when fed a HFD60. For this, age and weight-matched (Figure 4.29, A) Wt and PGC-1α/β-FAT-DKO male mice fed a HFD60 for 2 months were analysed. Consistent with the lack of differences in body weight, no major

differences in the weight of the main fatty tissues (inguinal WAT and BAT), liver and skeletal muscles (soleus and gastrocnemius) were found. Still, a mild increase in the weight of gonadal WAT from PGC-1α/β-FAT-DKO mice compared to Wt mice was observed (1.34 ± 0.13 g in Wt and 1.91 ± 0.24 g in PGC-1α/β-FAT-DKO mice, *p*= 0.07), although this difference did not reach statistical significance (Figure 4.29, B).

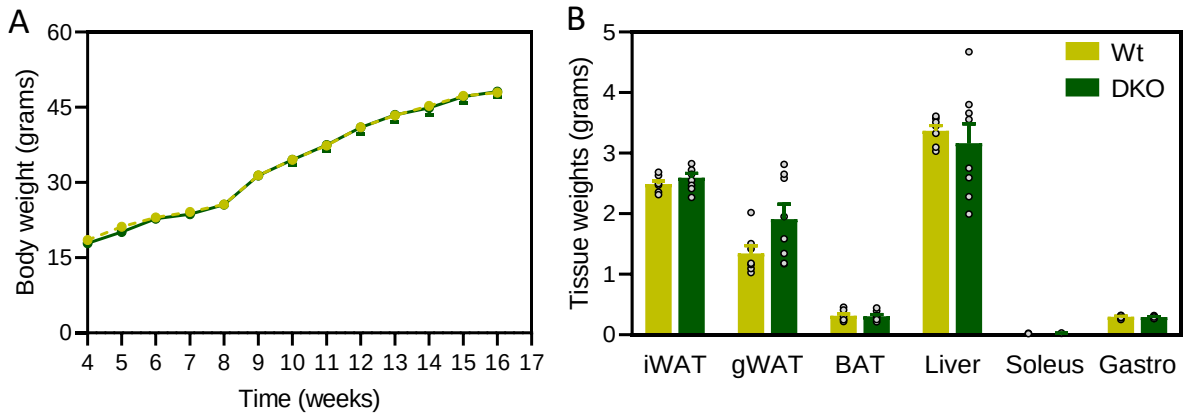


**Figure 4.29. Body and tissue weight from age- and weight-matched Wt and PGC-1α/β-FAT-DKO mice fed a HFD60.** At the age of 8 weeks, male mice were given a HFD60 for 2 months. Mice were euthanized at the age of 16 weeks. A) Body weight was followed weekly throughout the experiment. B) The main depots of WAT (inguinal and gonadal), interscapular BAT, liver and skeletal soleus and gastrocnemius muscles were collected and weighted. Student's t-test was applied. Results are expressed as mean ± SEM (n=7-8 animals/group).

Glucose tolerance in these mice was also evaluated (Figure 4.30). Despite similar body weight, we observed that PGC-1α/β-FAT-DKO mice became more glucose intolerant than Wt when exposed to HFD60. This indicates that the increased body weight observed in PGC-1α/β-FAT-DKO mice when a fed a high fat diet does not lie beneath the development of glucose intolerance in these mice.

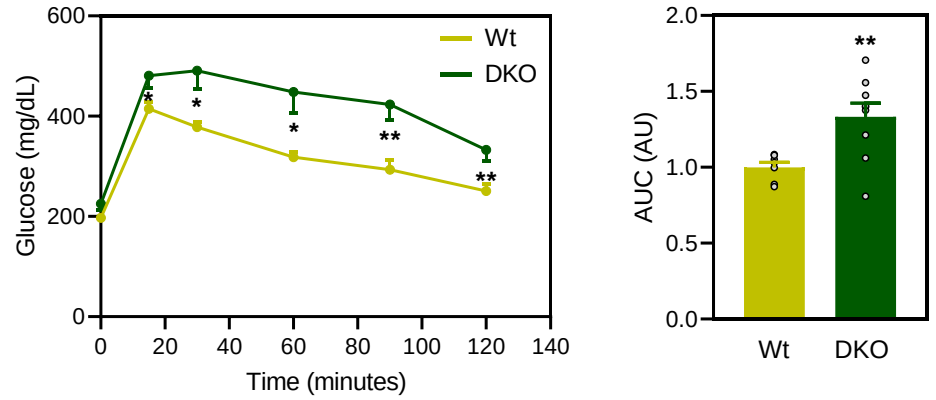


**Figure 4.30. Evaluation of glucose tolerance in age- and weight-matched Wt and PGC-1α/β-FAT-DKO mice fed a HFD60.** At the age of 8 weeks, male mice were given a HFD60 for 2 months. GTT was conducted at 16 weeks of age (2 months of HFD60). After 6 h of fasting, glucose (1 g/kg) was intraperitoneally delivered to Wt and PGC-1α/β-FAT-DKO mice and blood glucose levels were measured at 0, 15, 30, 60, 90 and 120 min after the administration. Glucose tolerance was estimated as the AUC of the glucose excursion during the GTT. Student's t-test was applied. Results are expressed as mean ± SEM (n= 7-9 animals/group). * Indicates statistical significance of the comparison between genotypes. * *P*≤0.05; ** *P*≤ 0.01.

#### 4.2.4.6 Analysis of insulin secretion in PGC-1α/β-FAT-DKO mice

Given the fact that insulin sensitivity is preserved in PGC-1α/β-FAT-DKO male mice when fed a HFD60, the glucose intolerance shown by these animals suggested a potential defect in insulin secretion. This hypothesis is reinforced by previous results from our laboratory showing that PGC-1α/β-FAT-DKO mice have lower serum basal insulin levels than their Wt littermates after 3 months of HFD60 feeding (36). Half-life of insulin in serum is relatively low and it is rapidly clear by liver and degraded. In order to rule out a differential removal of circulating insulin as the main cause of reduced insulin levels in PGC-1α/β-FAT-DKO mice, we decided to quantify serum levels of c-peptide. As shown in Figure 4.31, basal c-peptide serum levels were reduced PGC-1α/β-FAT-DKO mice after 1, 2 and 3 months of exposure to HFD60.

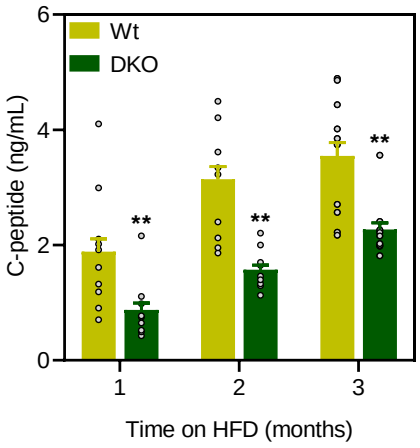


**Figure 4.31. Quantification of basal c-peptide serum levels in Wt and PGC-1α/β-FAT-DKO mice fed a HFD60.** At 8 weeks of age, male mice were given a HFD60 for 1 (12-week-old mice), 2 (16-week-old mice) or 3 months (20-week-old mice). Serum was collected via tail cut after 6 h of fasting and c-peptide was determined by immunoassay**.** Student's t-test was applied. Results are expressed as mean ± SEM (n= 18-20 animals/group). * Indicates statistical significance between genotypes. ** $P \leq 0.01$.

To better assess the dynamic secretion of insulin, c-peptide levels during the course of an oral GTT in Wt and PGC-1α/β-FAT-DKO male mice either fed a chow diet or a HFD60 were determined. Systematically, HFD60 prompted higher serum c-peptide levels in both Wt and PGC-1α/β-FAT-DKO mice compared to mice fed a regular chow diet throughout the months of dietary exposure, in agreement with the hyperinsulinemia normally associated with the HFD60-induced IR. In mice fed a chow diet, glucose administration induced similar secretion of insulin in Wt and PGC-1α/β-FAT-DKO mice. Of note, the levels of c-peptide secreted increased with age, what can be interpreted as the need of more insulin to counteract the IR developed with the age. Interestingly, in mice fed a HFD60, dynamic insulin secretion appears to be similar in Wt and PGC-1α/β-FAT-DKO mice, as assessed by c-peptide levels. However, at any given point of the GTT or time under HFD60, PGC-1α/β-FAT-DKO mice exhibited lower levels of c-peptide, being the differences statistically significant after 2 months on HFD60 (Figure 4.32, B).

The data regarding insulin secretion fit pretty well with the disturbances observed in glucose tolerance. Indeed, the lack of differences in insulin secretion between Wt and PGC-1α/β-FAT-DKO mice fed a chow diet are consistent with the lack of differences in glucose tolerance

observed in these mice (Figure 4.13, A). By contrast, when fed a HFD60, the reduced c-peptide serum concentration in PGC-1α/β-FAT-DKO mice, especially after 2 and 3 months on a HFD60, are consistent with the glucose intolerance observed in these mice (Figure 4.32, B and C, respectively).

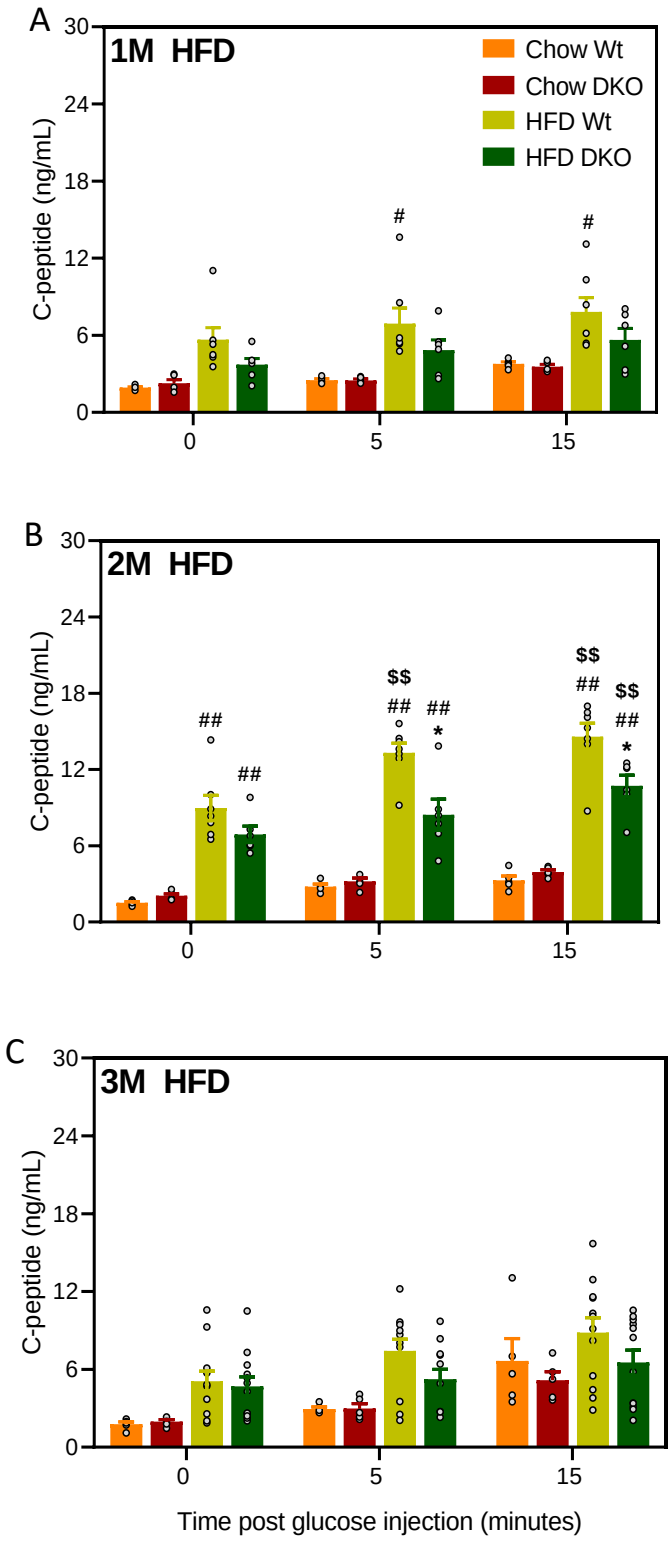


**Figure 4.32. C-peptide levels in serum of Wt and PGC-1α/β-FAT-DKO mice fed a regular chow diet or a HFD60 during the course an oral GTT.** At 8 weeks of age, male mice were given a HFD60. In parallel, another cohort of

age-matched mice were fed a regular chow diet. An oGTT was conducted at 12- (1 month of HFD60), 16- (2 months of HFD60) and 20-week-old (3 months of HFD60) mice fasted for 6 h. Blood samples were taken at 0, 5 and 15 min after an oral delivery (2.5g/kg) sand c-peptide was measure by ELISA. ANOVA test followed by a Tukey's multiple comparison post hoc analysis was applied. Results are expressed as mean ± SEM (n= 5-12 animals/group). * Indicates statistical significance of the comparison between Wt and PGC-1α/β-FAT-DKO mice; # Indicates statistical significance of the comparison between diets; $ Indicates statistical significance of the comparison between GTT time points. *,# ,$ $P \leq 0.05$; **,## ,$$ $P \leq 0.01$.

These data suggest that PGC-1α/β-FAT-DKO mice exposed to HFD60 have impair insulin secretion already after the first month on the HFD60 the diet, pointing towards a pancreatic defect on insulin secretion as the plausible cause of the glucose intolerance shown by these mice.

## 4.3. Study of the pancreatic functional and morphological alterations in PGC-1α/β-FAT-DKO mice fed a high-fat diet

As shown in previous sections, mice deficient of PGC-1α/β co-activators in adipose tissues were glucose intolerant but preserve insulin sensitivity. However, basal and glucose-dependent c-peptide serum concentrations were diminished in PGC-1α/β-FAT-DKO mice. These data pointed towards altered pancreatic insulin secretion as a potential mechanism involved in the development of glucose intolerance in PGC-1α/β-FAT-DKO mice.

### 4.3.1 Morphometric study of pancreatic islets from PGC-1α/β-FAT-DKO mice

A morphometric study of pancreatic islets was conducted in male mice after 1 (13 weeks of age) and 3 months (22 weeks of age) of HFD60 feeding. A 13-week-old, lean and insulin sensitive group of Wt and PGC-1α/β-FAT-DKO male mice fed a chow diet was also included in the study. Pancreatic islets mice were stained by immunofluorescence with antibodies against insulin, glucagon and somatostatin (Figure 4.33 for a representative staining with insulin and glucagon), allowing for the identification of β, α and δ cells, respectively.

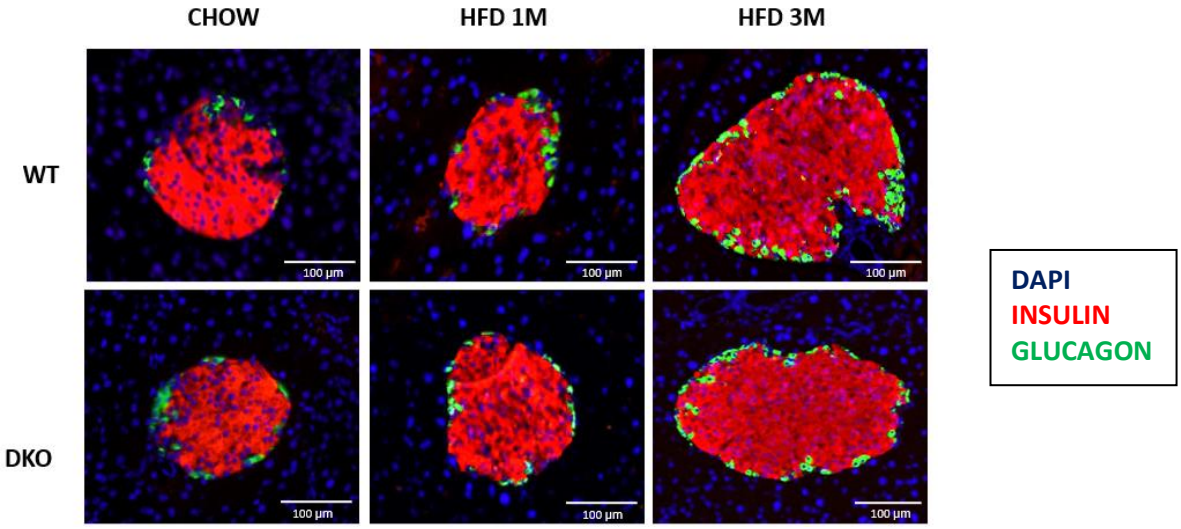

**Figure 4.33. Immunofluorescent staining of insulin and glucagon in pancreatic islets from Wt and PGC-1α/β-FAT-DKO mice fed a regular chow diet or exposed to a HFD60 for 1 or 3 months.** At 8 weeks of age, male mice were given a HFD60 for 1 or 3 months. Parallelly, a cohort of age-matched mice were fed a regular chow diet until the age of 13 weeks. Mice were euthanized at the age of 13 or 22 weeks, depending on the experimental group, and specific antibodies against insulin and glucagon were used to visualize β-cells (red) and α-cells (green), respectively. Double staining with insulin and glucagon were performed in pancreatic islets from 3 different pancreas depths.

As shown in Figure 4.34, A, the density of pancreatic islets increased after 3 months on a HFD60, indicating a hyperplasic response to compensate for the insulin resistance induced by the HFD60. These results were similar between genotypes, despite the fact that PGC-1α/β-FAT-DKO mice exhibited reduced circulating insulin levels and more glucose intolerance compared to Wt mice.

We then evaluated the mass of the main cell populations (α, β and δ-cells) in pancreatic islets. β-cell mass was significantly increased after 3 months of HFD60 feeding in both Wt and PGC-1α/β-FAT-DKO mice compared to 1 month of regular chow diet or HFD60 feeding (Figure 4.34, B). Analogous to the pattern observed for β-cell mass, α-cell mass significantly increased after 3 months of HFD60 in Wt and PGC-1α/β-FAT-DKO mice compared to 1 month of HFD60 (Figure 4.34, C). Contrarily, no significant differences were found between diets regarding δ-cell mass (Figure 4.34, D). Irrespectively of the effect that long-term HFD60 exposure had on pancreatic islets density and pancreatic cell masses compared to pancreas from mice fed a regular chow diet or a short-term HFD60, we could not find differences between Wt and PGC-1α/β-FAT-DKO mice with regard to the pancreatic islet cellular composition.

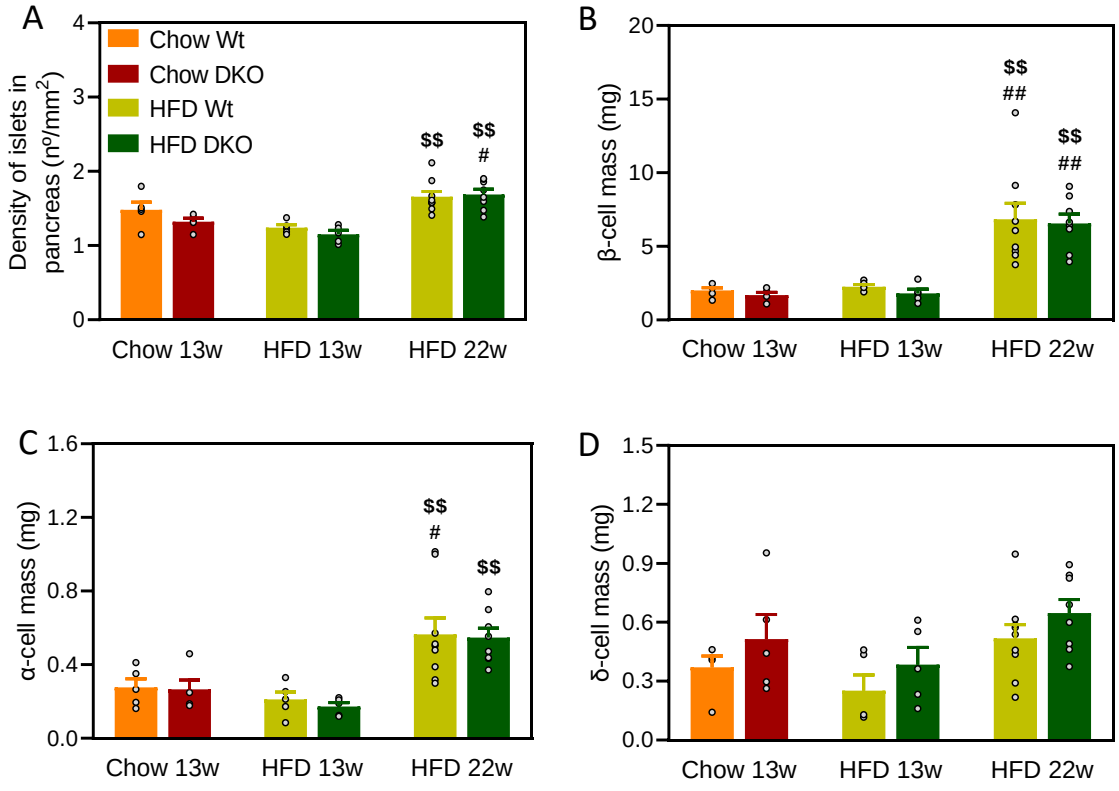


**Figure 4.34. Analysis of morphometrical parameters in pancreatic islets from Wt and PGC-1α/β-FAT-DKO mice fed a regular chow diet or exposed to a HFD60 for 1 or 3 months.** At 8 weeks of age, male mice were given a

HFD60 for 1 or 3 months. Parallelly, a cohort group of age-matched mice were fed a regular chow diet until week 13. Mice were euthanized at the age of 13 or 22 weeks, depending on the experimental group. A) Density of pancreatic islets, B) β-cell mass, C) α-cell mass and D) δ-cell mass from 3 different pancreas depths (except from δ-cell mass, 1 depth). ANOVA test followed by a Tukey's multiple comparison post hoc analysis was applied. Results are expressed as mean ± SEM (n=5-9 animals/group). # Indicates statistical significance of the comparison chow vs HFD60 3 months; $ Indicates statistical significance of the comparison HFD60 1 month vs HFD60 3 months. #, $ $P \leq 0.05$; ##,$$ $P \leq 0.01$.

### 4.3.2 Analysis of gene expression in pancreatic islets from PGC-1α/β-FAT-DKO mice in response to HFD60

Since c-peptide levels were robustly decreased in serum of PGC-1α/β-FAT-DKO mice (see section 4.2.4.6), we analysed the expression of key genes involved in cellular processes that have been proven essential for insulin synthesis and secretion. For this, pancreatic islets from 24 to 26-week-old male mice fed a regular chow diet or subjected to a HFD60 for 4 months were isolated and gene expression assessed by real-time qPCR.

First, we analysed the expression of **genes related to mitochondria**, knowing that it is a crucial organelle in the signalling pathway that drives insulin secretion in pancreatic β-cells. On one side, we confirmed that our mouse model was specific from adipose tissues and that genes encoding for PGC-1s were not depleted in pancreatic islets. For this, the expression of *Ppargc1a* and *Ppargc1b* genes was evaluated in pancreatic islets from Wt and PGC-1α/β-FAT-DKO mice (Figure 4.35, A). Analysis of the expression of both co-activators confirmed that their expression was not reduced in pancreatic islets from PGC-1α/β-FAT-DKO mice (*Ppargc1a* expression appeared increased by two-fold in PGC-1α/β-FAT-DKO mice fed a regular chow diet, but differences did not reach statistical significance). On the other hand, we also evaluated the expression of genes from the OxPhos system for their relevancy in increasing the ATP levels that trigger the closure of potassium channels in pancreatic β-cells (Figure 4.35, B). A very mild, but not statistically significant increase in the expression of some Oxphos genes (*Mdh2, Ndufb9, CyCs* or *Atp5b*) was observed in response to HFD60, regardless of the genotype. Despite these differences in response to diet, the expression levels of mitochondrial genes was not modulated in PGC-1α/β-FAT-DKO mice compared to Wt littermates in any dietary condition, suggesting that mitochondrial bioenergetics of pancreatic islets is not affected by the lack of PGC-1s co-activators in adipocytes.

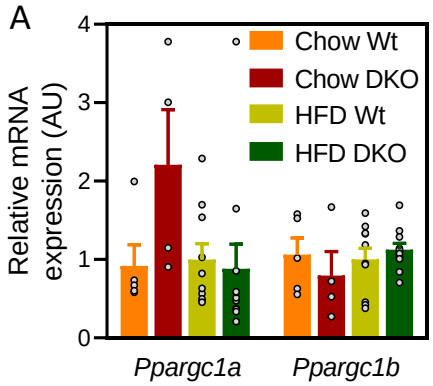

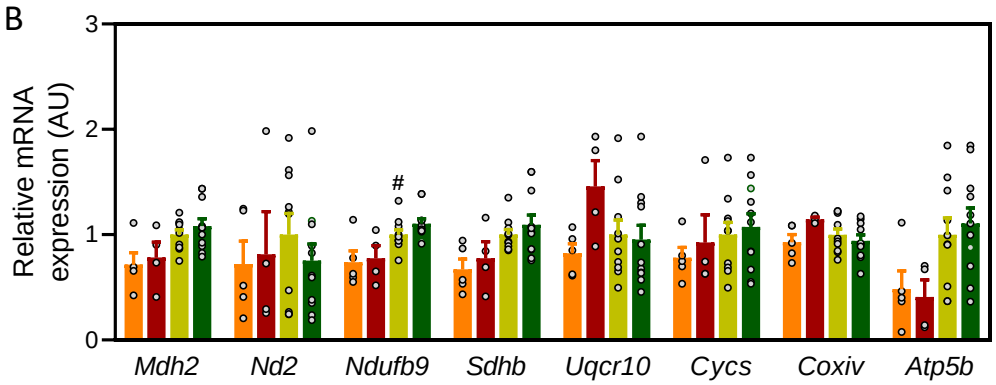


**Figure 4.35. Analysis of the expression of mitochondrial genes, including PGC-1s co-activators and components of the OxPhos system in isolated pancreatic islets from Wt and PGC-1α/β-FAT-DKO mice fed a regular chow diet or a HFD60.** At 8 weeks of age, male mice were given a HFD60 for 4 months. Parallelly, a cohort group of age-matched mice were fed a regular chow diet. Mice were euthanized at the age of 24-26 weeks and mRNA levels were determined by RT-qPCR. Gene expression of *Ppargc1a* and *Ppargc1b* co-activators and components of the OxPhos system (*Mdh2, Nd2, Ndufb9, Sdhb, Uqcr10, Cycs, Coxiv,* Atp5b) was assessed. ANOVA test followed by a Tukey's multiple comparison post hoc analysis was applied. Results are expressed as mean ± SEM (n=4-11 animals/group). # Indicates statistical significance of the comparison between diets between diets; # $P \leq 0.05$.

Next, we evaluated whether there was an impairment in the differentiation and maturity of pancreatic β-cells. For this, we analysed the expression of **genes that identify differentiated and mature β-cells**, such as *Forkhead box O1* (*Foxo1*), *Mafa*, *Nkx6.1* and *Paired Box 6* (*Pax6*) (Figure 4.36). No effects of the genotype or the diet were observed for most of the genes, with the exception of *Pax6,* whose expression was lower in PGC-1α/β-FAT-DKO mice fed a chow diet.

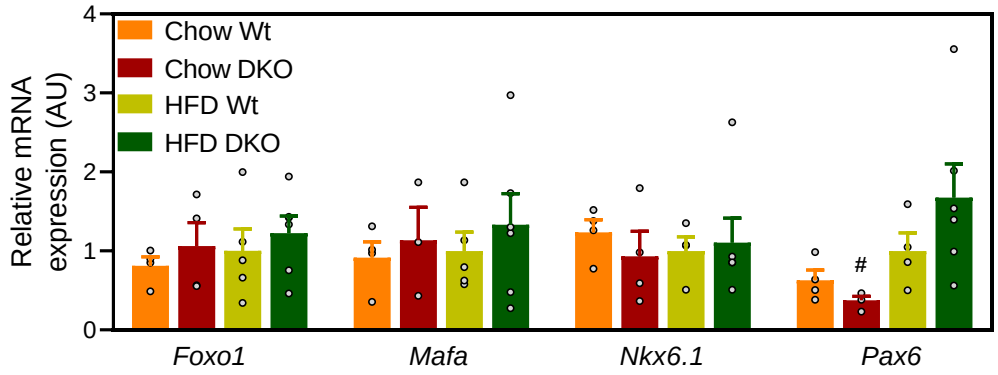


**Figure 4.36. Analysis of expression of markers for β-cell differentiation and maturity in pancreatic islets from Wt and PGC-1α/β-FAT-DKO mice fed a regular chow or a HFD60.** At 8 weeks of age, male mice were given a HFD60 for 4 months. Parallelly, a cohort group of age-matched mice were fed a regular chow diet. Mice were euthanized at the age of 24-26 weeks and mRNA levels were determined by RT-qPCR. The expression of *Foxo1, Mafa, Nkx6.*1 and Pax6 was evaluated. ANOVA test followed by a Tukey's multiple comparison post hoc analysis was applied. Results are expressed as mean ± SEM (n=3-6 animals/group).

We then assessed the expression of **markers of identity** for the main cells related to the endocrine function of pancreatic islets. Thus, we analysed the expression of *Ins1* and *Ins2* (insulin) genes to identify β-cells, *Gcg* (glucagon) expression for α-cells and *Sst* (somatostatin) expression for the identification of δ-cells. As seen in Figure 4.37, no differences were

observed in the expression of *Ins1* or *Gcg* genes. We detected only a mild, but statistically significant, increment in the expression of *Ins2* gene in pancreatic islets from PGC-1α/β-FAT-DKO mice fed a regular chow diet compared to HFD60 exposure. The expression of *Sst* appeared mildly reduced in animals fed a HFD60 regardless of the genotype, although it did not reach statistical significance.

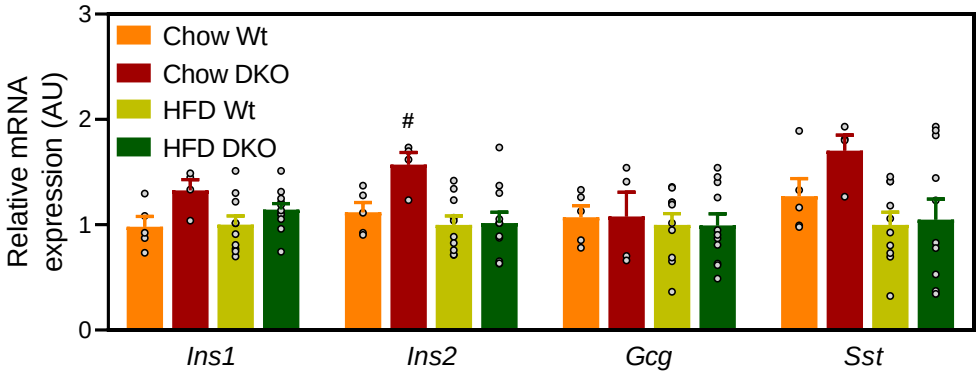


**Figure 4.37. Analysis of the expression of identity markers for pancreatic islets cell subpopulations in isolated pancreatic islets from Wt and PGC-1α/β-FAT-DKO mice fed a regular chow or a HFD60.** At 8 weeks of age, male mice were given a HFD60 for 4 months. Parallelly, a cohort group of age-matched mice were fed a regular chow diet. Mice were euthanized at the age of 24-26 weeks and mRNA levels were determined by qPCR. The expression of insulin (*Ins1, Ins2*), glucagon (*Gcg*) and somatostatin (*Sst*) genes was evaluated**.** ANOVA test followed by a Tukey's multiple comparison post hoc analysis was applied. Results are expressed as mean ± SEM (n=3-11 animals/group). # Indicates statistical significance of the comparison between diets; # $P \leq 0.05$.

At the transcriptional level, the expression of markers for the differentiation of pancreatic islets and markers for the identity of pancreatic islet cell populations were preserved in PGC-1α/β-FAT-DKO mice. For these reasons, we further explored other cellular pathways in pancreatic islets that could be altered and could lead to impaired β-cell function. In this sense, we quantified the expression of genes that coded for proteins implicated in the **transport and metabolism of glucose** in pancreatic β-cells**,** such as glucose transporters (*Glut1* and *Glut2*) and downstream enzymatic mediators of glycolysis, like *Glyceraldehyde-3-Phosphate Dehydrogenase* (*Gapdh*), *Glucokinase* (*Gck*) and *Pyruvate Dehydrogenase Kinase 1* (*Pdk1*). Moreover, we assessed the expression of the GLP-1 receptor (*Glp1r)* as a mediator of the effect of the incretin GLP-1 on insulin secretion by β-cells (Figure 4.38). We found that HFD60 appeared to up-regulate the expression of *Glp1r* and *Pdk1*, both in Wt and PGC-1α/β-FAT-DKO mice, although the results did not reach statistical significance. Nevertheless, no differences were found between Wt and PGC-1α/β-FAT-DKO mice, with the exception of *Glut1*, which was increased in PGC-1α/β-FAT-DKO compared to Wt mice, when animals were fed a regular chow diet. In any case, because *Glut1* expression is increased, it is rather unlikely to be blamed for the dysfunctional endocrine activity of β-cells.

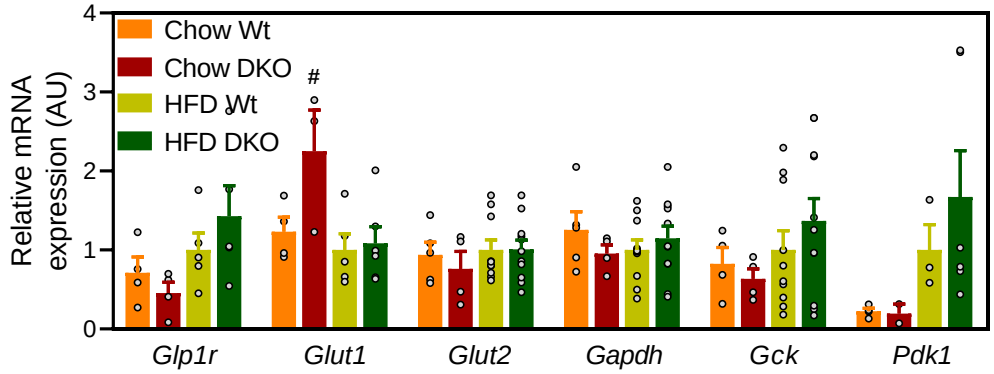


**Figure 4.38. Analysis of the expression of genes related to the transport and metabolism of glucose in pancreatic islets from Wt and PGC-1α/β-FAT-DKO mice fed a regular chow or a HFD60.** At 8 weeks of age, male mice were given a HFD60 for 4 months. Parallelly, a cohort group of age-matched mice were fed a regular chow diet. Mice were euthanized at the age of 24-26 weeks and mRNA levels were determined by qPCR. Expression of the Glp-1 receptor (*Glp1r*), glucose receptors (*Glut1, Glut2*) and glycolytic enzymes (*Gapdh, Gck, Pdk1*) was analysed. ANOVA test followed by a Tukey's multiple comparison post hoc analysis was applied. Results are expressed as mean ± SEM (n=3-11 animals/group). # Indicates statistical significance of the comparison between diets; # $P \leq 0.05$

Following, we evaluated the expression of genes that encode for proteins involved in the correct **packaging and folding of insulin** inside secretory granules. To this aim, we studied the expression of genes that code for the enzymes that convert proinsulin to insulin (*Proprotein Convertase Subtilisin/Kexin Type 1 and 2 (Pcsk1/2)) and* the expression of *Islet Amyloid Polypeptide* (*Iapp*), a hormone secreted concomitantly with insulin that also regulates insulin secretion (Figure 4.39). Gene expression analysis did not reveal changes in the expression of these genes as a result of the diet or by the lack of PGC-1s co-activators in adipose tissues.

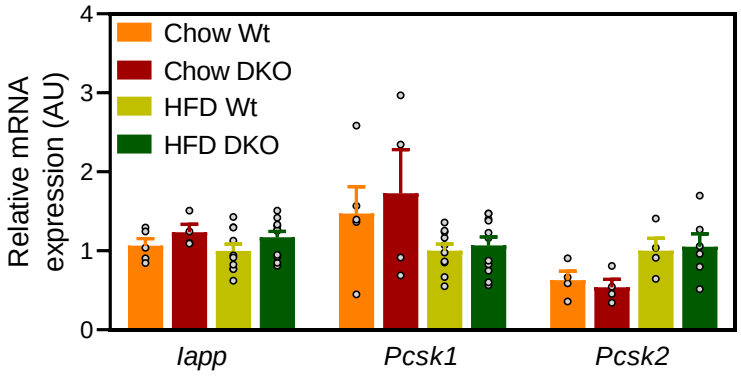


**Figure 4.39. Analysis of the expression of genes related to insulin maturation and folding inside secretory granules of pancreatic islets from Wt and PGC-1α/β-FAT-DKO mice fed a regular chow diet or a HFD60.** At 8 weeks of age, male mice were given a HFD60 for 4 months. Parallelly, a cohort group of age-matched mice were fed a regular chow diet. Mice were euthanized at the age of 24-26 weeks and mRNA levels were determined by qPCR. Expression levels of insulin co-secreted amylin *(Iapp*) and enzymes required for insulin formation *(Pcsk1, Pcsk2*) were assessed. ANOVA test followed by a Tukey's multiple comparison post hoc analysis was applied. Results are expressed as mean ± SEM (n=3-11 animals/group).

Then, we assessed the expression levels of genes related to the **fusion of insulin secretory granules with the cell membrane** (Figure 4.40). For this, we quantified the expression of

genes encoding for proteins of the cell membrane *Syntaxin 1A (Stx1a)* and *Unc-13 Homolog B (Unc13b)* and those encoding for proteins from the secretory granule membrane *Synaptophysin (Syp)* and *Vesicle Associated Membrane Protein 2 (Vamp2).* Gene expression analysis revealed no differences in their expression because of the effect of HFD60 or the lack of PGC-1s co-activators.

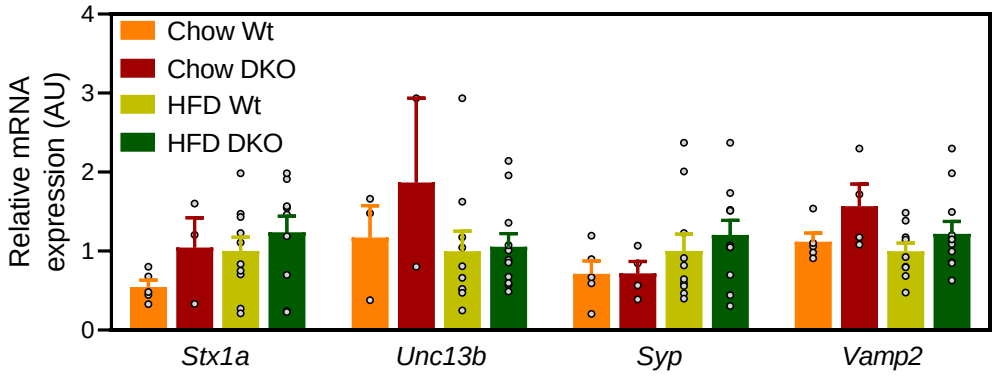


**Figure 4.40. Analysis of the expression of genes related to the fusion of secretory granules with cell membrane in pancreatic islets from Wt and PGC-1α/β-FAT-DKO mice fed a regular chow diet or a HFD60.** At 8 weeks of age, male mice were given a HFD60 for 4 months. Parallelly, a cohort group of age-matched mice were fed a regular chow diet. Mice were euthanized at the age of 24-26 weeks and mRNA levels were determined by qPCR. Expression levels of genes related to cell membrane *(Stx1a,* Unc13b) and secretory granule membrane *(Syp, Vamp2*) were evaluated. ANOVA test followed by a Tukey's multiple comparison post hoc analysis was applied. Results are expressed as mean ± SEM (n=3-11 animals/group).

In order to ascertain whether insulin was incorrectly unfolded and, therefore, abnormally accumulated inside the cell, we measured the expression of genes that encode for proteins of the **unfolded protein response**. To this aim, DNA *Damage inducible transcript 3 (Ddit3* or *Chop)* and *X-Box Binding Protein 1 (Xbp1)* expression levels were determined. As shown in Figure 4.41, A, HFD60 tended to up-regulate the expression of *Chop* and *Xbp1*, although differences were not statistically significant. Nevertheless, no differences were observed related to the genotype. Finally, we measured the expression of some **proinflammatory genes** to detect a differential inflammatory response affecting proper pancreatic islet function in PGC-1α/β-FAT-DKO mice when fed a HFD60. For this, the expression of *Ccl2* and *Il1b* was assessed (Figure 4.41, B). As for genes of the UPR, we did not find differences in *Ccl2* or *Il1b* expression attributable to a dietary or a genotypic effect.

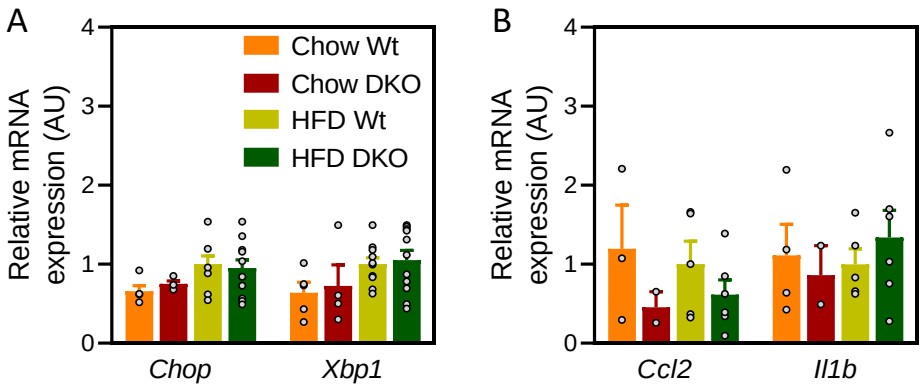

**Figure 4.41. Analysis of the expression of genes related to the *Unfolded Protein Response* (UPR) and immune system in pancreatic islets from Wt and PGC-1α/β-FAT-DKO mice fed a regular chow diet or a HFD60.** At 8 weeks of age, male mice were given a HFD60 for 4 months. Parallelly, a cohort group of age-matched mice were fed a regular chow diet. Mice were euthanized at the age of 24-26 weeks and mRNA levels were determined by qPCR. A) Genes from the UPR response (*Chop, Xbp1*) B) and genes from immune system in pancreatic islets (*Ccl2, Il1b*). mRNA levels were determined by qPCR**.** ANOVA test followed by a Tukey's multiple comparison post hoc analysis was applied. Results are expressed as mean ± SEM (n=3-11 animals/group).

Overall, results from the gene expression analysis indicate that there are not gross transcriptional alterations in pancreatic islets under any dietary condition that could explain the low insulin secretion observed in PGC-1α/β-FAT-DKO mice.

### 4.3.3 Evaluation by transmission electron microscopy of insulin granules ultrastructure in pancreatic β-cells from PGC-1α/β-FAT-DKO mice fed a HFD60

Three months of exposure to HFD60 significantly increased the density of pancreatic islets and the mass of α- and β-cells, both in Wt and in PGC-1α/β-FAT-DKO mice, compared to 1 month of HFD60 exposure or regular chow diet feeding. However, the lack of differences between Wt and PGC-1α/β-FAT-DKO mice in these parameters suggested possible alterations involving insulin secretion that were associated to defects in the content or maturation of insulin granules. Therefore, different subpopulations of insulin granules were assessed by TEM in pancreatic β-cells from Wt and PGC-1α/β-FAT-DKO male mice fed for 3 months with a HFD60.

Insulin granules were classified as immature (light insulin granule core with no halo), mature granules (dense crystalized insulin core with halo) and rod-shaped granules (very crystalized insulin core that adopts a rod form) (Figure 4.42, A). Mature granules containing fully crystallized insulin are the ones usually secreted when pancreatic β-cells are stimulated with glucose or other secretagogues. Data resulting from quantification of insulin granules revealed that PGC-1α/β-FAT-DKO mice had a mild but statistically significant decrease in the proportion of immature granules, whilst rod-shaped granules were mildly, but also significantly, increased in these mice compared to Wt mice (Figure 4.42, B). By contrast, no differential changes were detected in mature granules between genotypes.

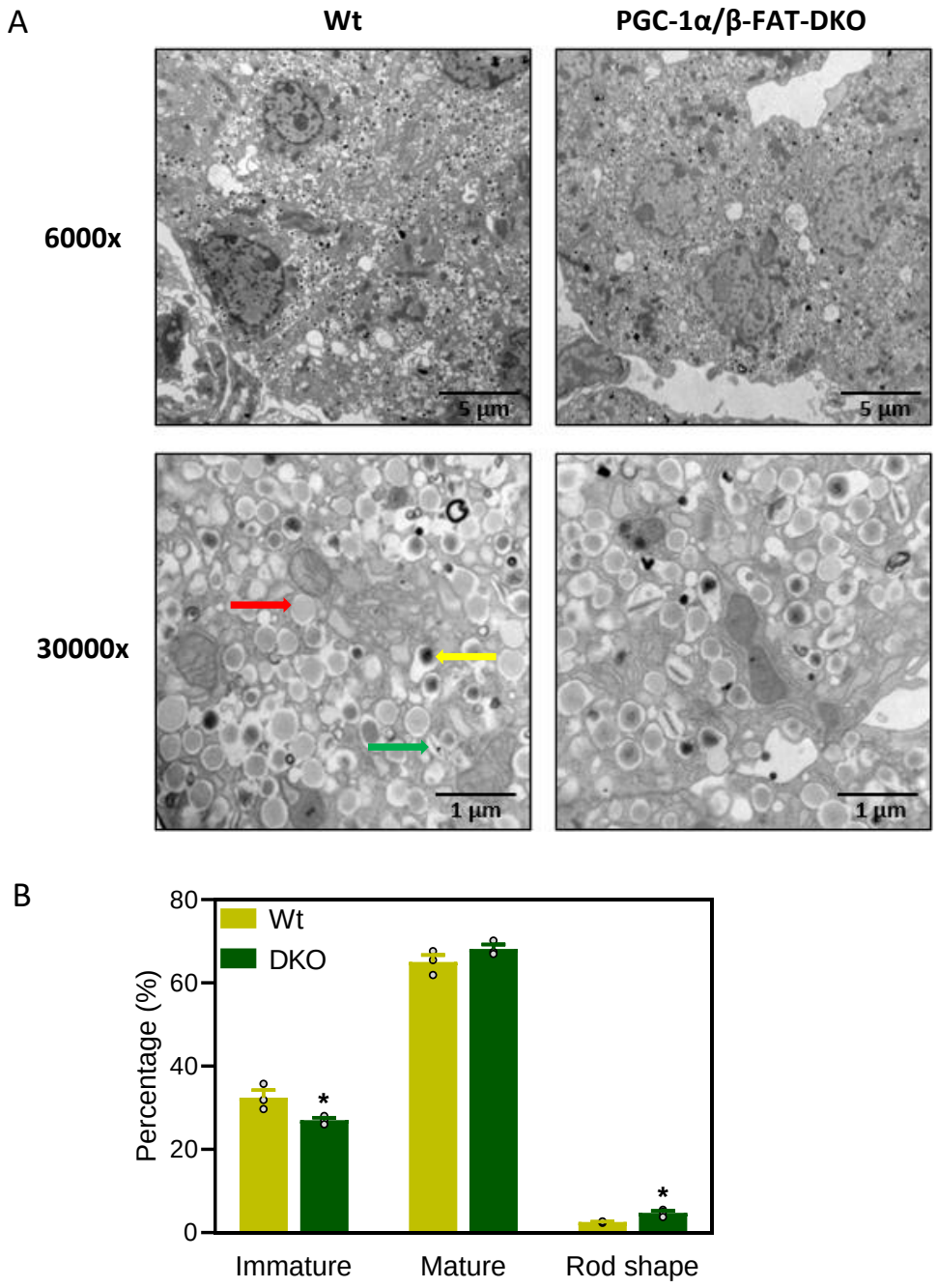


**Figure 4.42. TEM microscopy analysis of pancreatic β-cells and quantification of insulin granules in Wt and PGC-1α/β-FAT-DKO mice fed a HFD60.** At 8 weeks of age, male mice were given a HFD60 for 3 months. Mice were euthanized at the age of 21 weeks. A) TEM images of pancreatic β-cells (6000x) and types of insulin granules (30,000x) inside these cells. Red arrow indicates immature granules; yellow arrow indicates mature granules; and green arrow indicates rod-shaped granules. B) Analysis of the proportion of each insulin granule type within β-cells in Wt and PGC-1α/β-FAT-DKO mice. Student's t-test was applied. Results are expressed as mean ± SEM (n=3 animals/group; 14-21 cells/mouse). * Indicates statistical significance between Wt and PGC-1α/β-FAT-DKO mice. * $P \leq 0.05$.

Quantification and categorization of insulin granules did not consider the localization of these granules inside β-cells. It is well established that pancreatic β-cells contain two types of insulin mature granules pools: reserve pool and readily releasable pool. RRP are really closed to cell membrane and are rapidly secreted upon a glucose stimulus, whilst RP account primary for

the second phase of insulin secretion (62,64). Considering these data, we re-analysed TEM microscopy images to detect whether immature, mature and rod-shaped insulin granules were preferentially associated to RRP than RP granules. To this aim, a *region of interest* (ROI) was established from the cell membrane for up to 500 nm inside the cytoplasm, and insulin granules were quantified in this region (Figure 4.43, A, blue region). From each type of granule located in this area, we distinguished those found touching or bordering the cell membrane (docked) from those that were found deeper inside. Quantification of insulin granules in the region of interest did not report differences in the number of docked and non-docked insulin granules between Wt and PGC-1α/β-FAT-DKO mice (Figure 4.43, B).

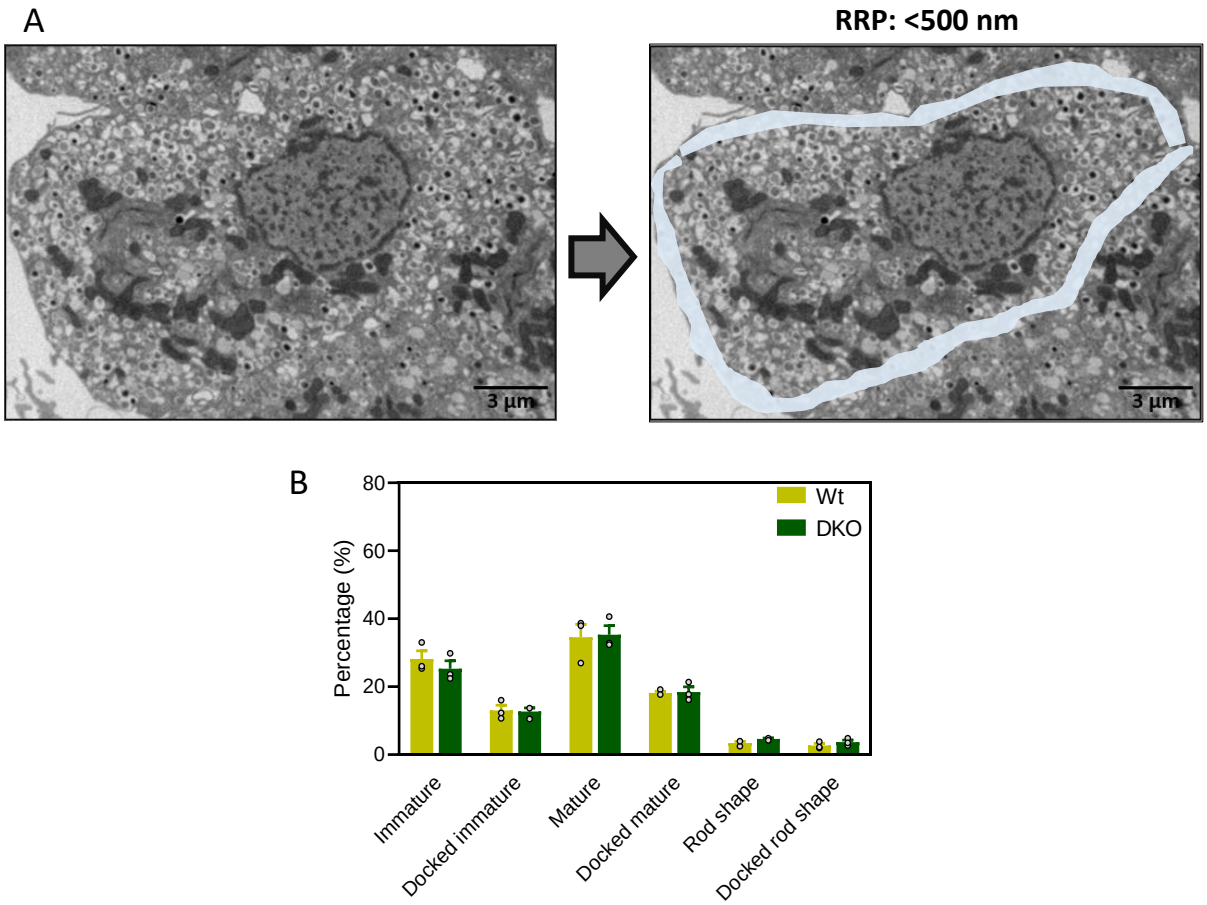


**Figure 4.43. TEM quantification of insulin granules close to cell membrane (up to 500 nm) inside β-cells from Wt and PGC-1α/β-FAT-DKO mice fed a HFD60.** At 8 weeks of age, male mice were given a HFD60 for 3 months. Mice were euthanized at the age of 21 weeks. A) TEM images of a pancreatic β-cell (6,000x) with the region of interest (ROI) coloured in blue. B) Contribution of cell membrane-docked and non-docked granules to total in Wt and PGC-1α/β-FAT-DKO mice. Student's t-test was applied. Results are expressed as mean ± SEM (n=3 animals/group).

Data from the TEM study did not reveal any difference in the degree of maturation of the granules or in the population ready to be secreted that could explain the lower levels of insulin secretion in PGC-1α/β-FAT-DKO mice.

### 4.3.4 Glucose-stimulated insulin secretion (GSIS) assay in pancreatic islets from PGC-1α/β-FAT-DKO mice

Insulin secretion was determined in isolated pancreatic islets from Wt and PGC-1α/β-FAT-DKO male mice fed for 3 months with a HFD60. Islets were exposed to basal (2.8 mM) and stimulated (20 mM) glucose concentrations to evaluate the capacity to sense glucose and secrete insulin. Insulin secreted was evaluated in the culture media and insulin content was directly extracted from β-cells by an acid/ethanol exposure. Both measurements were normalized by DNA concentration from pancreatic islets.

As seen in Figure 4.44, A, pancreatic islets from both Wt and PGC-1α/β-FAT-DKO mice responded to stimulated glucose concentrations by secreting more insulin. The fold induction from basal to stimulated glucose concentrations was similar between genotypes (10.86 in Wt and 12.72 in PGC-1α/β-FAT-DKO mice) (Figure 4.44, B). Despite this, both at basal and stimulated glucose concentrations, pancreatic islets from PGC-1α/β-FAT-DKO mice secreted significantly less insulin than those from Wt control mice (Figure 4.44, A). These results indicated that the responsiveness to a high glucose concentration is maintained in pancreatic islets from Wt and PGC-1α/β-FAT-DKO mice, but that the latter ones secrete less insulin. In the same way, when insulin content from pancreatic islets was evaluated, it was seen that pancreatic islets from PGC-1α/β-FAT-DKO mice contained less insulin than those from Wt littermates (Figure 4.44, C).

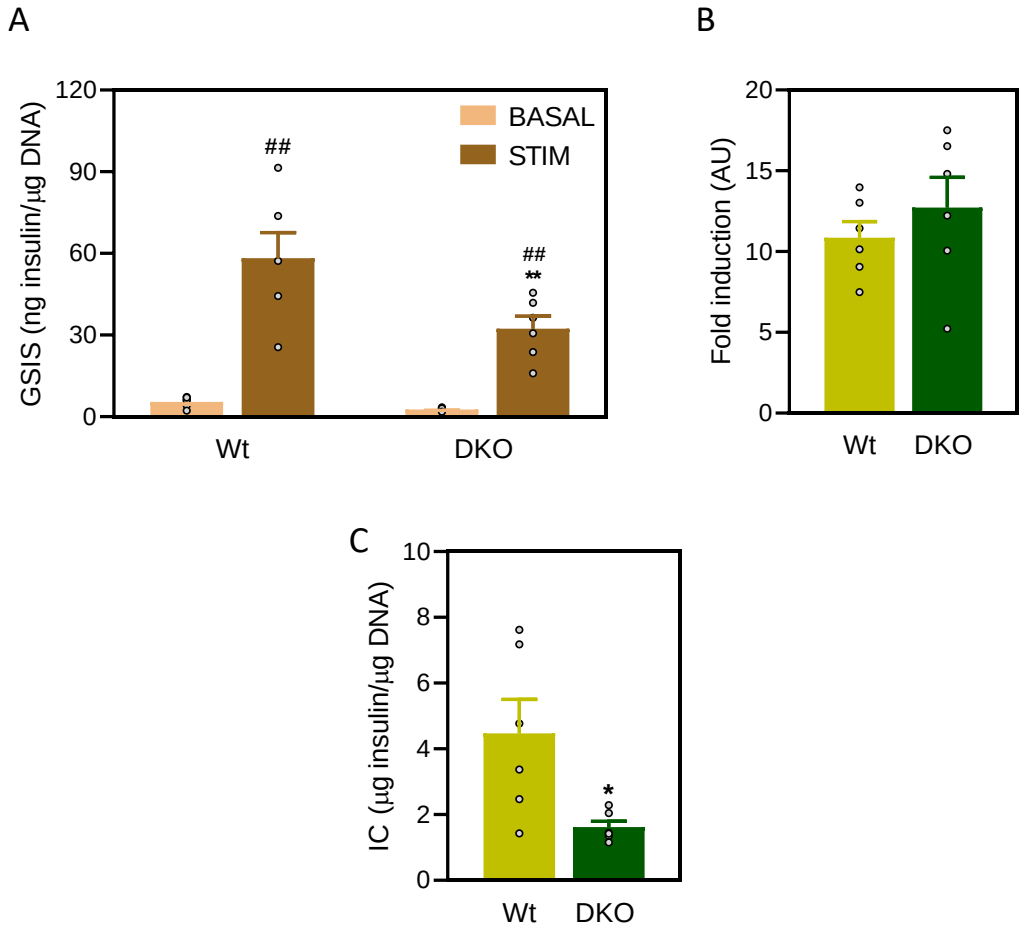

**Figure 4.44. Glucose-stimulated insulin secretion (GSIS) and insulin content in isolated pancreatic islets from Wt and PGC-1α/β-FAT-DKO mice fed a HFD60.** At 8 weeks of age, male mice were given a HFD60 for 3 months. The GSIS assay was performed when mice were 20 weeks of age. A) Pancreatic islets were exposed to basal (2.8 mM) and stimulated (20 mM) glucose concentrations and insulin secretion to the media was assessed by ELISA. B) The fold induction of insulin secretion was evaluated. C) Insulin content within islets was obtained by acid-ethanol exposure and sonication, and then quantified by ELISA. ANOVA test followed by a Tukey's multiple comparison post hoc analysis was applied. Results are expressed as mean ± SEM (n=5-6 animals/group). * Indicates statistical significance between Wt and PGC-1α/β-FAT-DKO mice; # Indicates statistical significance between glucose concentrations. *,# $P \leq 0.05$; **,## $P \leq 0.01$.

GSIS suggested that the lower levels of blood insulin observed in PGC-1α/β-FAT-DKO mice at basal state and after receiving a bolus of glucose was due to a lower insulin content in β-cells rather to a defect in the secretion itself. To confirm this, the experiment was replicated in another cohort of mice that, in addition of mice fed a HFD60, included also a group of mice fed a regular chow diet. In both chow diet and HFD60 fed mice, pancreatic islets responded to glucose by secreting more insulin. (Figure 4.45, A). Long-term exposure to HFD60 resulted in higher basal insulin secretion, which is in agreement with the hyperinsulinemia associated to HFD60-induced insulin resistance. Consequently, the fold induction of glucose-stimulated insulin secretion was lower in HFD60 fed mice compared to chow fed mice, although differences did not reach statistical significance (Figure 4.45, B). Despite the differential effect of the diet on insulin secretion in pancreatic islets from Wt and PGC-1α/β-FAT-DKO mice, contrary to the previous experiment, insulin content in these islets was not modified by the exposure to HFD60 (Figure 4.45, C).

When the effect of the genotype was evaluated, we observed that pancreatic islets from PGC-1α/β-FAT-DKO mice exhibited a tendency to generally secrete more insulin than those from Wt littermates, both when fed a regular chow diet and a HFD60. However, this increment was only significant when pancreatic islets from Wt and PGC-1α/β-FAT-DKO mice fed a HFD60 were exposed to stimulated glucose concentrations. Nevertheless, no differences in the fold induction or insulin content between genotypes were found (Figure 4.45, B and C, respectively).

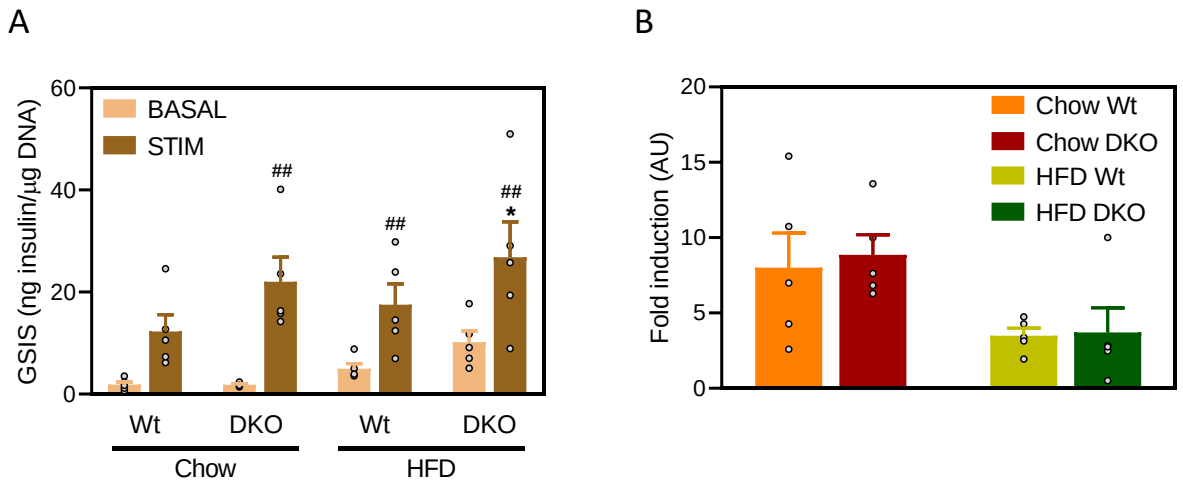

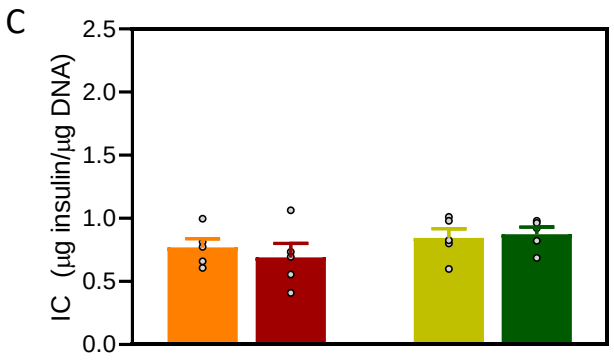


**Figure 4.45. Glucose-stimulated insulin secretion (GSIS) and insulin content in isolated pancreatic islets from Wt and PGC-1α/β-FAT-DKO mice fed either a regular chow or a HFD60.** At 8 weeks of age, male mice were given a HFD60 for 4 months. Parallelly, a cohort group of age-matched mice were fed a regular chow diet. The GSIS assay was performed when mice were 24-26 weeks of age. A) Pancreatic islets were exposed to basal (2.8 mM) and stimulated (20 mM) glucose concentrations and B) the fold induction of secretion was evaluated. C) Insulin content was obtained by acid-ethanol exposure and sonication in Wt and PGC-1α/β-FAT-DKO mice. ANOVA test followed by a Tukey's multiple comparison post hoc analysis was applied. Results are expressed as mean ± SEM (n=4-6 animals/group). * Indicates statistical significance between Wt and PGC-1α/β-FAT-DKO mice; # Indicates statistical significance between glucose concentrations. *,# $P \leq 0.05$; **,## $P \leq 0.01$.

Despite the differences in the two experiments, both were coincident in showing that fold induction of glucose-stimulated insulin secretion was preserved in PGC-1α/β-FAT-DKO mice fed a HFD60, as well as in regular chow diet.

## 4.4. Proteomic analysis of the secretome from adipose tissues of PGC-1α/β-FAT-DKO mice fed a HFD60

Reduced serum c-peptide levels and glucose intolerance found in PGC-1α/β-FAT-DKO mice when exposed to 3 months of HFD60 pointed towards an insulin secretion defect. Hence, considering that PGC-1α/β-FAT-DKO were engineered to be devoid of PGC-1s specifically in adipocytes, but the main phenotypic manifestation indicated a pancreatic functional defect, we speculated that the lack of PGC-1s in adipocytes resulted in the alteration of the adipose-pancreatic crosstalk. We therefore screened the possible molecules behind this crosstalk, focusing on the proteins secreted by adipose tissues that could impact pancreatic insulin secretion. For this, the secretome of adipose tissues, both brown and white, was characterized in Wt and PGC-1α/β-FAT-DKO male mice fed for 3 months with a HFD60.

### 4.4.1 Identification of adipose tissues secretome by *untargeted* proteomics

To identify the secretome of adipose tissues, conditioned media from explants of gonadal WAT, inguinal WAT and BAT from Wt and PGC-1α/β-FAT-DKO mice fed a HFD60 for 3 months was obtained and subsequently analysed by liquid-chromatography-mass spectrometry.

In total, 13,105 peptides and 2,994 proteins were identified at least in one condition. From all of them, 1,893 proteins differed significantly between tissues and genotypes ($P \leq 0.05$) and with a Fold Change greater than 2. The PCA from these data indicated the grade of variability between groups (Figure 4.46). The *principal component 1 (*PC1*)* (45.46%) showed that most

variability was found between adipose tissues. The *principal component 2 (*PC2*)* showed the variability between genotypes in each adipose tissue.

The differential impact of the genotype in the proteins discovered in the conditioned media from adipose tissues was further evaluated specifically for each specific tissue. In conditioned media of BAT, from the 1,741 proteins detected by untargeted proteomics, 667 proteins were differentially found between Wt and PGC-1α/β-FAT-DKO mice (FC>2, $P \leq 0.05$). DAVID bioinformatic tool showed that proteins with a higher abundance in BAT conditioned media from PGC-1α/β-FAT-DKO mice compared to Wt littermates were related to extracellular matrix maintenance, angiogenesis and response to different stimuli, whilst proteins less abundant in PGC-1α/β-FAT-DKO mice involved mitochondria and fatty acid metabolism (Supplementary Table 8.3 and 8.4). Concerning WAT depots, the number of proteins found in media of inguinal and gonadal WAT between Wt and PGC-1α/β-FAT-DKO mice was really low compared to BAT. In gonadal WAT, 1,874 proteins were detected in the conditioned media, from which only 18 proteins were found in different amounts between Wt and PGC-1α/β-FAT-DKO mice. In conditioned media from inguinal WAT, 1,744 proteins were detected, but only the amount of 2 proteins differed between Wt and PGC-1α/β-FAT-DKO mice (Supplementary Table 8.5).

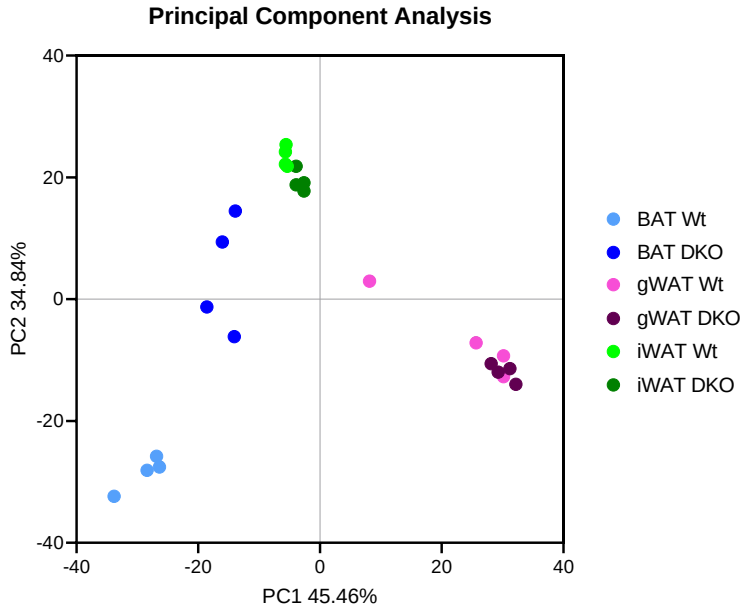


**Figure 4.46. Principal Component Analysis (PCA) of proteins found by *untargeted* proteomics in secreted media from gonadal WAT, inguinal WAT and BAT of Wt and PGC-1α/β-FAT-DKO mice fed a HFD60.** At 8 weeks of age, male mice were given a HFD60 for 3 months. Mice were euthanized at the age of 22-23 weeks. Each dot represents a Wt or PGC-1α/β-FAT-DKO animal which a specific set of proteins found in the conditioned media of adipose tissue. Higher variability between groups is given by PC1, which separates between adipose tissues. PC2 shows differences in the secretome of Wt and PGC-1α/β-FAT-DKO mice regarding each adipose tissue.

### 4.4.2 Filtration workflow for the identification of BAT secreted proteins

The proteins found in the conditioned media of BAT were subjected to a bioinformatics analysis in order to distinguish proteins actively secreted by this tissue from proteins accidentally found in the media as a result of being released by damaged or dead cells. To this

aim, proteins previously identified in the conditioned media were selected based on mass spectrometry parameters: peptide count >1 and confidence score >25, aimed at increasing the confidence in the detection and identification of the proteins. This results in 440 proteins confidently identified as differentially found in conditioned media from Wt and PGC-1α/β-FAT-DKO mice.

Then, these were evaluated using *VerSeDa* platform to identify those proteins known to be secreted or that contained motifs that allowed their secretion by classical and non-classical pathways. SignalIP (threshold set > 0.8), TargetIP (threshold set > 0.8) and Secretome IP (threshold set > 0.7) software tools of the VerSeDa platform were used for this purpose (Figure 4.47). This procedure resulted in 191 proteins filtrated. After a manual curation for mitochondrial and nuclear proteins, a final list of 126 proteins differentially secreted by BAT between Wt and PGC-1α/β-FAT-DKO mice was obtained.

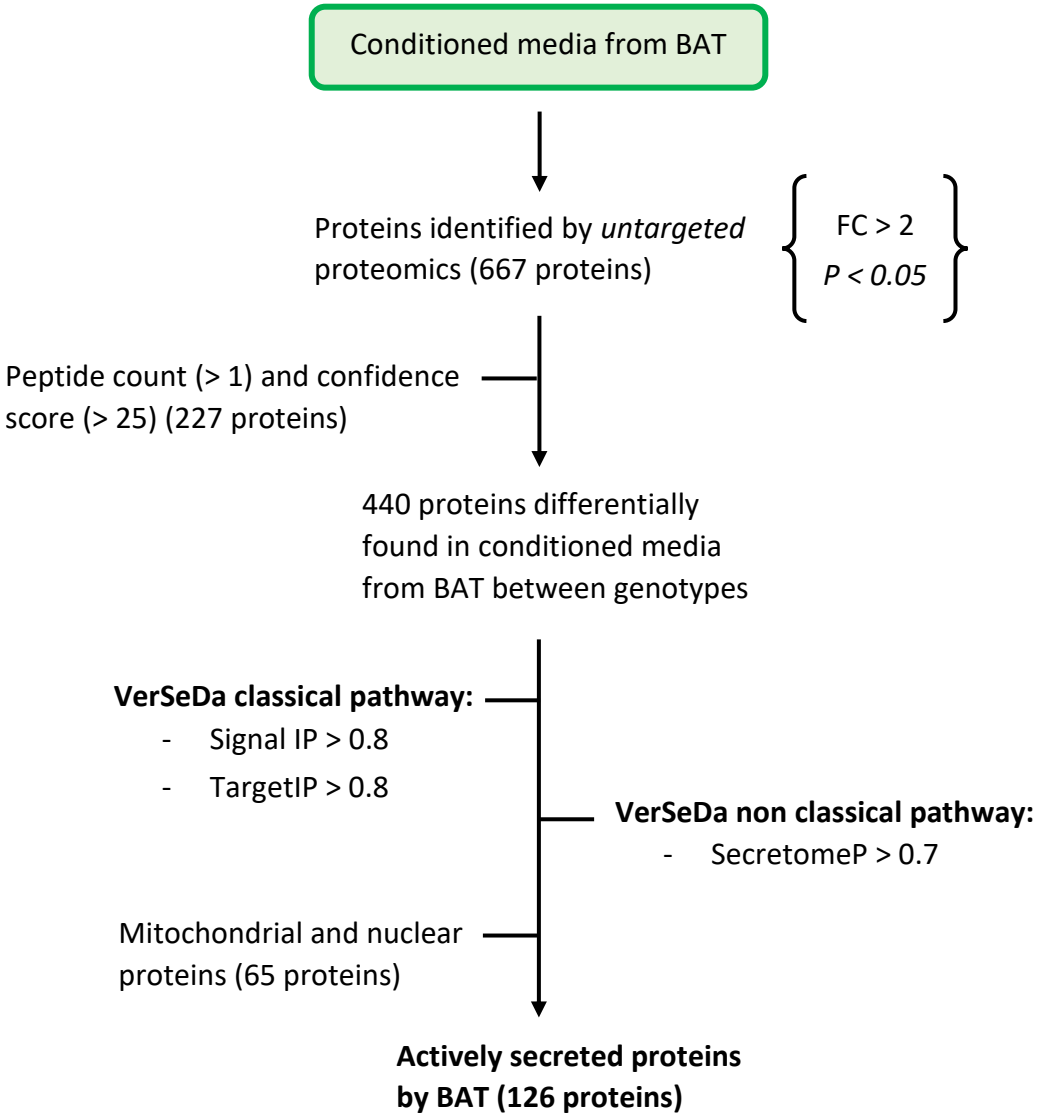


**Figure 4.47. *In silico* workflow for the identification of actively secreted proteins by BAT from Wt and PGC-1α/β-FAT-DKO mice fed a HFD60.** At 8 weeks of age, male mice were given a HFD60 for 3 months. Mice were euthanized at the age of 22-23 weeks**.** Proteins identified by *untargeted proteomics* in the conditional media of BAT secretome were filtrated for Fold Change (FC > 2), *P-value* (< 0.05), Peptide count (> 1) and Confidence Score

(> 25). Using VerSeDa platform, the 440 proteins differently found in conditioned media of BAT between genotypes were subsequently assessed for their probability to be secreted by either classical or non-classical pathways. Then, mitochondrial and nuclear proteins were removed from the resulting list. Finally, 126 proteins were found to be actively and differentially secreted by BAT between Wt and PGC-1α/β-FAT-DKO mice.

The PCA resulting from the comparison of the 126 proteins differentially secreted by BAT indicates a higher heterogenicity in PGC-1α/β-FAT-DKO mice rather than Wt mice (Figure 4.48). The PC1 (82.17%) displayed the variability in the 126 proteins actively secreted between genotypes, whether PC2 (6.93%) showed the variability within each group.

When the same filtration process was applied to secreted proteins by WAT depots, we found that the secretome of inguinal and gonadal WAT depots was very similar between genotypes. In this regard, only 3 actively secreted proteins were found to differ between genotypes in gonadal WAT and 1 in inguinal WAT, thereby indicating a minor effect of WAT secretome (Supplementary Table 8.6).

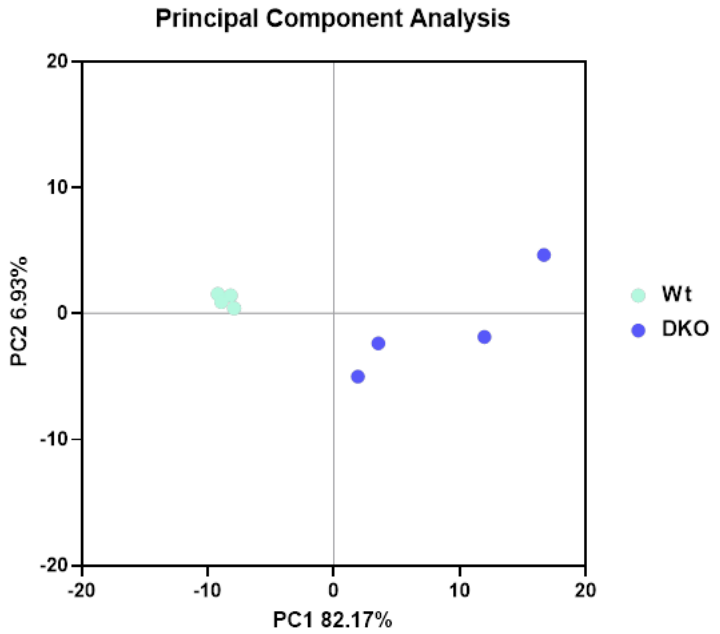


**Figure 4.48. Principal Component Analysis (PCA) of the secreted proteins by BAT from Wt and PGC-1α/β-FAT-DKO mice fed a HFD60.** At 8 weeks of age, male mice were given a HFD60 for 3 months. Mice were euthanized at the age of 22-23 weeks**.** Each dot represents a Wt or PGC-1α/β-FAT-DKO animal which a specific set of secreted proteins. Higher variability between groups is given by PC1, which separates between genotypes. PC2 shows that there is more heterogenicity between PGC-1α/β-FAT-DKO mice than amongst Wt mice.

The list of abundances from the 126 proteins differentially secreted by BAT from Wt and PGC-1α/β-FAT-DKO mice indicated that most proteins were higher secreted by PGC-1α/β-FAT-DKO mice rather than Wt control mice (Figure 4.49).

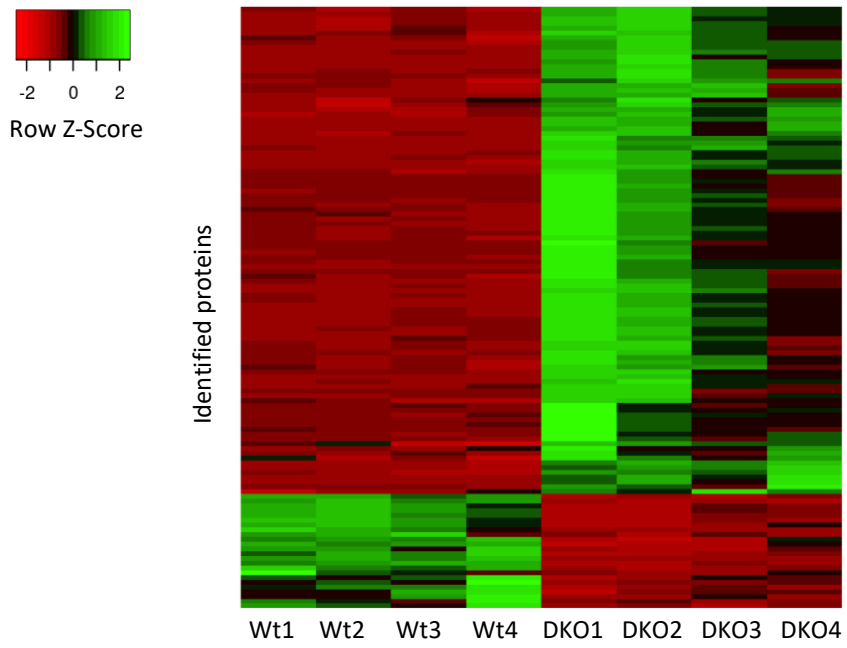


**Figure 4.49. HeatMap of BAT secreted proteins from Wt and PGC-1α/β-FAT-DKO mice fed a HFD60.** At 8 weeks of age, male mice were given a HFD60 for 3 months. Mice were euthanized at the age of 22-23 weeks. HeatMap of Wt and PGC-1α/β-FAT-DKO secretome indicating proteins more secreted (green z-score) or less secreted (red z-score) between groups.

Analysis of proteins filtrated by the DAVID bioinformatic tool showed that the most 10 enriched biological processes involving the proteins higher secreted by BAT from PGC-1α/β-FAT-DKO mice compared to Wt mice were related to the extracellular matrix and the immune system (Table 4.3). These proteins were mainly located in the extracellular space. The molecular function process did not provide relevant information. Regarding the proteins more secreted by BAT from Wt mice, they were principally involved in the metabolism of fatty acids and in the differentiation of brown fat (Table 4.4).

**TABLE 4.3: Gene enrichment analysis of genes that code for proteins higher secreted by BAT from PGC-1α/β-FAT-DKO mice than Wt mice**

| Category | GO term | #Genes | P-Value |
|---|---|---|---|
| **GOTERM_BP** | Extracellular matrix organization | 13 | 1,20E-10 |
| **GOTERM_BP** | Negative regulation of peptidase activity | 11 | 7,80E-10 |
| **GOTERM_BP** | Response to hypoxia | 11 | 8,00E-08 |
| **GOTERM_BP** | Proteolysis | 16 | 1,90E-07 |
| **GOTERM_BP** | Negative regulation of endopeptidase activity | 8 | 2,00E-07 |
| **GOTERM_BP** | Complement activation, alternative pathway | 5 | 5,50E-07 |
| **GOTERM_BP** | Acute-phase response | 6 | 1,00E-06 |
| **GOTERM_BP** | Wound healing | 8 | 1,30E-06 |
| **GOTERM_BP** | Cell adhesion | 14 | 8,20E-06 |
| **GOTERM_BP** | Angiogenesis | 10 | 1,40E-05 |
| **GOTERM_CC** | Extracellular region | 83 | 7,60E-69 |
| **GOTERM_CC** | Extracellular space | 75 | 1,50E-54 |

| | | | |
|---|---|---|---|
| **GOTERM_CC** | Basement membrane | 16 | 1,30E-17 |
| **GOTERM_CC** | Extracellular matrix | 19 | 1,90E-15 |
| **GOTERM_CC** | Lysosome | 16 | 5,80E-09 |
| **GOTERM_CC** | Endoplasmic reticulum | 23 | 7,50E-06 |
| **GOTERM_CC** | Melanosome | 7 | 7,80E-06 |
| **GOTERM_CC** | Smooth endoplasmic reticulum | 5 | 1,60E-05 |
| **GOTERM_CC** | Endoplasmic reticulum lumen | 7 | 1,80E-05 |
| **GOTERM_CC** | Cell surface | 14 | 8,40E-05 |

**Table 4.3. Most significant GO terms obtained from gene enrichment analysis of proteins higher secreted by BAT from PGC-1α/β-FAT-DKO mice than Wt mice using DAVID bioinformatics source.** GOTERM_BP, biological process; GOTERM_CC, cellular component.

**TABLE 4.4: Gene enrichment analysis of genes that code for proteins higher secreted by BAT from Wt than from PGC-1α/β-FAT-DKO mice**

| Category | GO term | #Genes | P-Value |
|---|---|---|---|
| **GOTERM_BP** | Fatty acid metabolic process | 4 | 1,10E-03 |
| **GOTERM_BP** | Long-chain fatty acid transport | 2 | 1,30E-02 |
| **GOTERM_BP** | Fatty acid transport | 2 | 3,30E-02 |
| **GOTERM_BP** | One-carbon metabolic process | 2 | 3,50E-02 |
| **GOTERM_BP** | Brown fat cell differentiation | 2 | 4,10E-02 |
| **GOTERM_CC** | Mitochondrion | 10 | 6,50E-05 |
| **GOTERM_CC** | Cytoplasm | 16 | 1,70E-03 |
| **GOTERM_CC** | Extracellular space | 6 | 4,90E-02 |
| **GOTERM_MF** | Arylesterase activity | 2 | 6,50E-03 |
| **GOTERM_MF** | Long-chain fatty acid binding | 2 | 6,50E-03 |
| **GOTERM_MF** | Lyase activity | 3 | 1,30E-02 |
| **GOTERM_MF** | Carbonate dehydratase activity | 2 | 1,80E-02 |
| **GOTERM_MF** | Long-chain fatty acid transporter activity | 2 | 2,00E-02 |
| **GOTERM_MF** | Hydro-lyase activity | 2 | 2,10E-02 |
| **GOTERM_MF** | Fibronectin binding | 2 | 3,80E-02 |

**Table 4.4. Most significant GO terms obtained from gene enrichment analysis of proteins higher secreted by BAT from Wt mice than PGC-1α/β-FAT-DKO mice using DAVID bioinformatics source.** GOTERM_BP, biological process; GOTERM_CC, cellular component; GOTERM_MF, molecular function.

### 4.4.3 Quantification in serum of proteins differentially secreted by BAT from PGC-1α/β-FAT-DKO mice fed a HFD60

According to our hypothesis, only proteins secreted by BAT that could reach pancreas are good candidates to mediate the BAT-pancreatic crosstalk. For this reason, we aimed at quantifying in serum of Wt and PGC-1α/β-FAT-DKO mice the proteins that we identified as differentially secreted by BAT of these mice. We quantified serum protein concentration by either *targeted* proteomics or ELISA. On the one hand, 156 peptides from 52 proteins were evaluated by *targeted* proteomics (Supplementary Table 8.2). On the other hand, only

selected proteins were quantified by ELISA due to the high cost associated to this assay and the limited availability of robust ELISA assays.

*Targeted* proteomics and ELISA quantification resulted in the identification of two proteins significantly more concentrated ($P \leq 0.05$) in serum of PGC-1α/β-FAT-DKO mice (FC> 1.5) than in Wt serum (Figure 4.50). These proteins were Kininogen-1 (O08677) and Resistin (Q99P87). Moreover, although it did not reach statistical significance ($P = 0.32$), the protein Fibrinogen Gamma Chain (Q8VCM7) was found to be two-fold less concentrated in the serum of PGC-1α/β-FAT-DKO mice than in the serum from Wt mice.

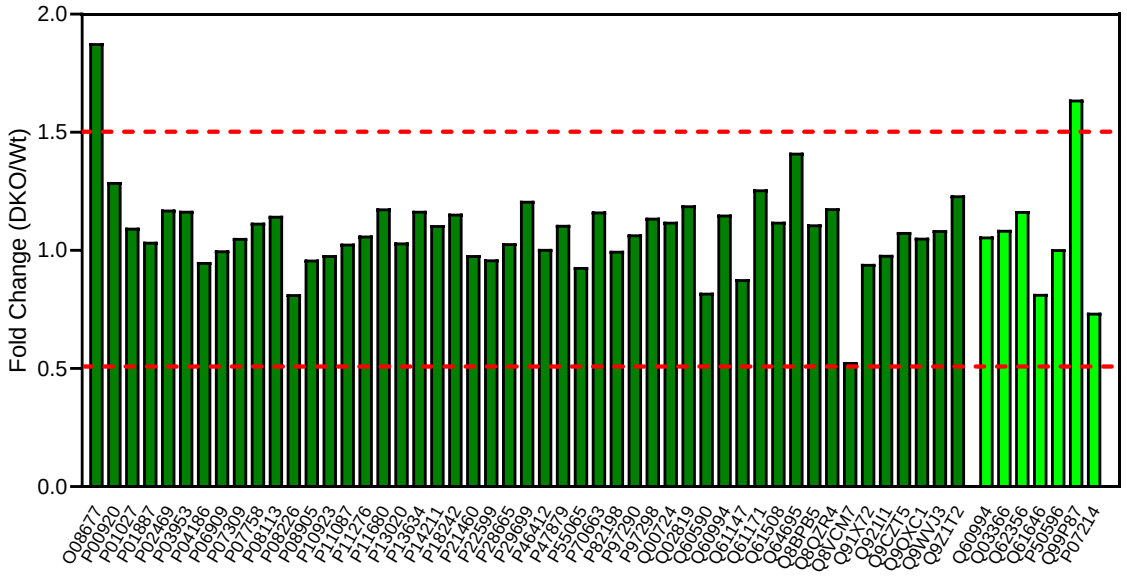


**Figure 4.50. Quantification of BAT secreted proteins in serum from Wt and PGC-1α/β-FAT-DKO mice fed a HFD60.** At 8 weeks of age, male mice were given a HFD60 for 3 months. At the age of 20 weeks, serum from Wt and PGC-1α/β-FAT-DKO mice was collected and concentrations of selected proteins were evaluated by *targeted* proteomics (dark green) or ELISA (light green).

## 4.5. *In* vitro assessment of the effect of resistin on insulin secretion in INS-1 cells

Resistin was found to be up-regulated in the serum of PGC-1α/β-FAT-DKO mice compared to Wt control mice when fed a HFD60 for 3 months. Considering that resistin has been linked to glucose intolerance and IR, we thought that it could be a plausible mediator of the adipose-pancreatic crosstalk leading to an altered insulin secretion in PGC-1α/β-FAT-DKO mice. To test this, we evaluated insulin secretion in INS-1 832/13 cells (hereafter referred as INS-1) after being treated for 24 h with recombinant resistin (50 and 500 ng/mL).

On the one hand, insulin secretagogues (10 mM Leucine and 24 mM KCl) were used as positive controls for insulin secretion. Treatment for 1h with either Leucine or KCl significantly increased the secretion of insulin, indicating that these cells secrete insulin when they were stimulated (Figure 4.51, A). Compared to Leucine, KCl has a higher capacity to promote insulin secretion in INS-1 cells. INS-1 cells also responded well to high concentrations of glucose by

secreting insulin at levels similar to those found when they were treated with leucine (Figure 4.51, B).

Treating cells with increasing concentrations (50 and 500 ng/mL) of recombinant resistin for 24 h resulted in an increment in basal insulin secretion (when incubated with low glucose concentrations of 2.8 mM), regardless of the dose of resistin used (Figure 4.51, B). Still, insulin secretion at basal glucose concentrations was more notorious when cells were treated with 500 ng/mL of recombinant resistin. However, insulin secretion upon stimulation with 16.7 mM of glucose in resistin-treated cells was similar to that of untreated cells (Figure 4.51, B). When expressed as fold induction, insulin secretion was diminished in resistin-treated cells, but this effect appears to be mostly due to the high levels of basal insulin secretion, rather to an impairment of insulin secretion in response to high glucose concentration (Figure 4.51, C).

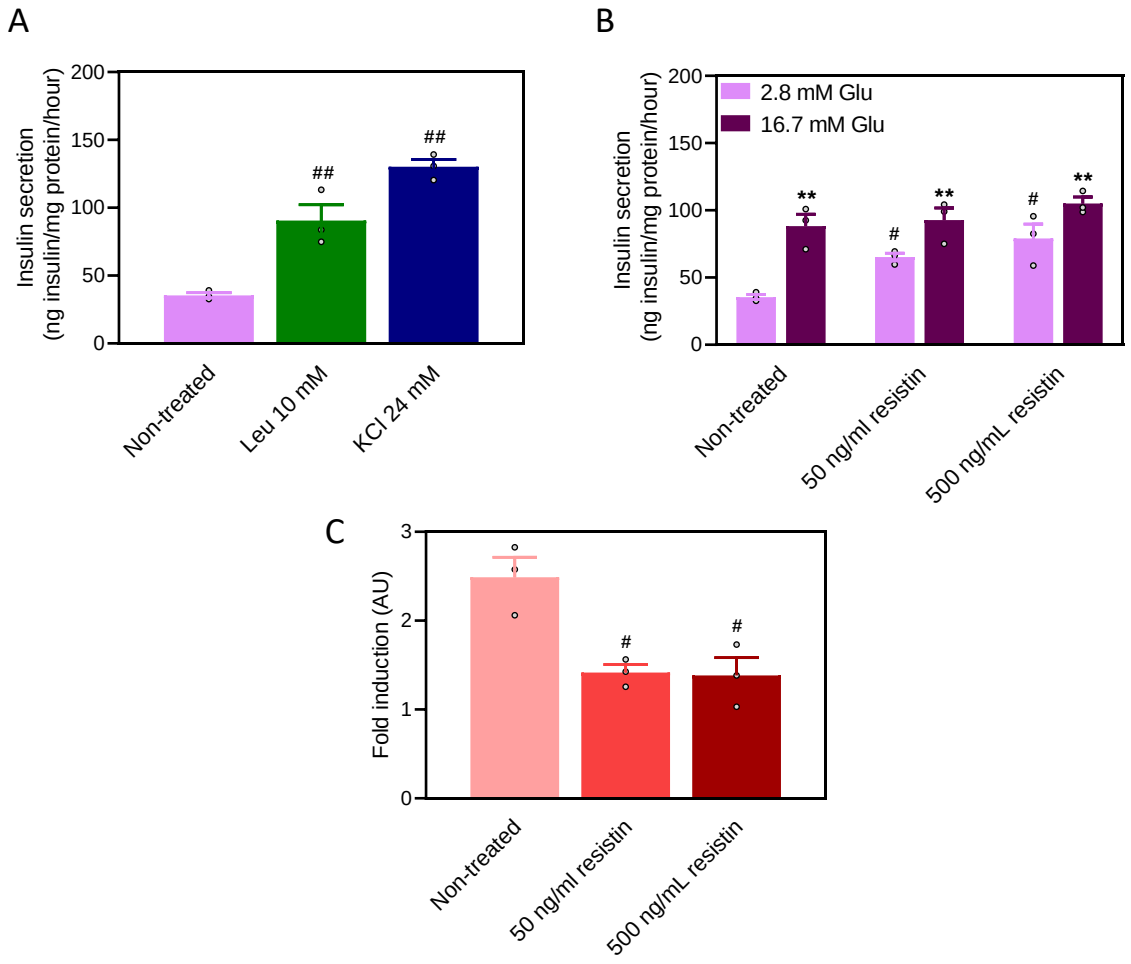


**Figure 4.51. Glucose-stimulated insulin secretion (GSIS) in INS-1 832/13 cell line treated with recombinant resistin.** A) To evaluate the insulin secretory capacity of INS-1 cells, the leucine and KCl secretagogues were used as positive controls in cells incubated with a low (2.8 mM) glucose concentration. B) Prior to the GSIS, INS-1 cells were incubated with 50 or 500 ng/ml of recombinant resistin during 24 hours. Then, a conventional GSIS was conducted in the presence of resistin in INS-1 cells by incubating them with 2.8 mM (basal) or 16.7 mM (stimulated) of glucose. C) Ratio between insulin secretion under basal and stimulated conditions. ANOVA test followed by a Tukey's multiple comparison post hoc analysis was applied. Results are expressed as mean ± SEM (n=3). * Indicates statistical significance between basal and stimulated glucose conditions; # Indicates statistical significance between treatments. *,# $P \leq 0.05$; **,## $P \leq 0.01$.

Insulin content in INS-1 cells was also determined. As shown in Figure 4.52, insulin content was not significantly altered in any condition assayed, including treatment with resistin.

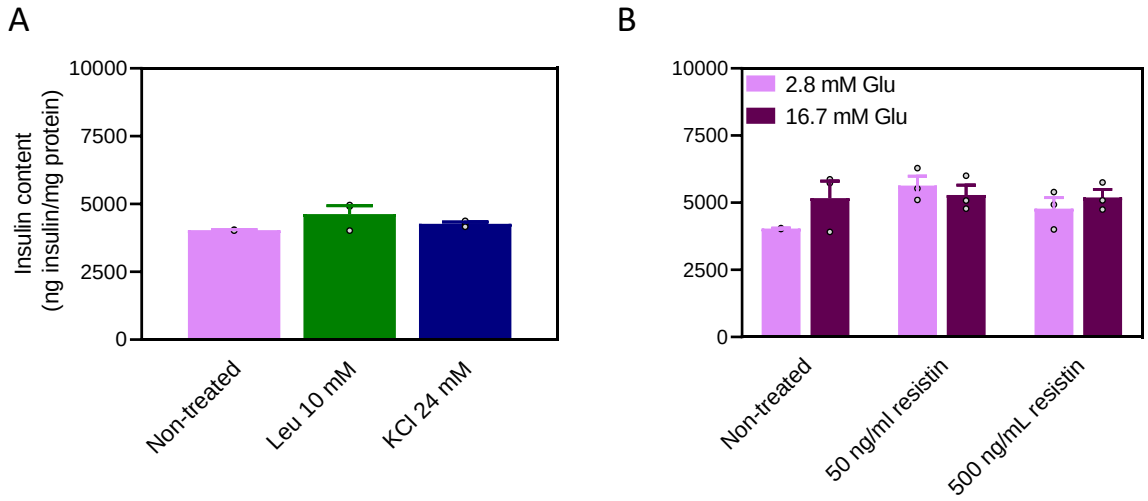


**Figure 4.52. Insulin content in INS-1 832/13 cells treated with recombinant resistin.** A) Insulin content in INS-1 cells after the addition of leucine and KCl positive controls. B) Insulin content in non-treated cells and after 24 h of treatment with 50 or 500 ng/ml of recombinant resistin. ANOVA test followed by a Tukey's multiple comparison post hoc analysis was applied. Results are expressed as mean ± SEM (n=3).

Our studies in INS-1 cells show that resistin treatment increases basal insulin secretion in pancreatic β-cells. Since our observations in mice predict that the molecule (or molecules) mediating BAT-pancreatic function actually impairs basal insulin secretion by β-cells, these results suggest that resistin is not responsible for the reduced circulating insulin levels found in PGC-1α/β-FAT-DKO mice.

# 5. DISCUSSION

## 5.1. Impairment of mitochondrial gene expression in PGC-1α/β-deleted adipose tissues

Obesity is known to be a major factor in the development of insulin resistance, a previous step in the appearance of T2D (3,4). Nowadays, however, the mechanisms behind the promotion of insulin resistance by obesity are still under debate. Amongst the different potential mechanisms postulated, a reduction in mitochondrial mass and function in insulin sensitive tissues has been suggested as an important contributing factor. In this regard, a decrease in mitochondrial mass and oxidative capacity has been observed in adipose tissues and skeletal muscle from diabetic and obese insulin resistant individuals, in both humans and rodents (38-41). Despite these data, it is still unclear to which extent mitochondrial dysfunction in these tissues causes insulin resistance and contributes to the development of T2D.

PGC-1 co-activators are crucial mediators of mitochondrial biogenesis and, therefore, they have gained attention for their relevancy on obesity and T2D, two pathological situations in which their expression levels in WAT and skeletal muscle has been shown to be decreased (138,139). PGC-1s increase mitochondrial mass and modulate gene expression through the interaction with transcription factors such as NRFs, PPARs and ERRs. These factors allow PGC-1s to regulate the replication of mitochondrial DNA or the expression of genes involved in several mitochondrial pathways, like the OxPhos system, TCA and fatty acid oxidation (118). In WAT, PGC-1α is important for the adaptation to different stimuli but it is dispensable for mitochondrial biogenesis (124). Contrarily, adipose-specific deletion of PGC-1β causes a significant decrease in the expression of genes involved in the mitochondrial oxidative functions (187). However, the changes in gene expression observed are not accompanied by a reduction in mtDNA content, suggesting that although PGC-1β has a preponderant role over PGC-1α in the regulation of mitochondrial gene expression, its deficiency is not sufficient to alter mitochondrial mass in WAT, pointing towards a partial compensation by PGC-1α or other transcriptional regulators (188).

Given the link between mitochondrial dysfunction and IR, previous work from our laboratory tried to uncover the effect that impaired mitochondrial function had on glucose homeostasis through the adipose-specific deletion of PGC-1α or PGC-1β (124,188). Although these studies provided evidence for the role of PGC-1s in mitochondrial biogenesis in white adipocytes, particularly PGC-1β (188), they failed to demonstrate a direct impairment of glucose tolerance or insulin sensitivity in mice due to reduced mitochondrial oxidative function in adipose tissue. It must be stated, though, that the reduction in mitochondrial function observed in these models was, at the most, modest. Therefore, one could speculate that the degree of mitochondrial dysfunction achieved using single adipose-specific PGC-1β deletion could not be sufficient to trigger IR. Considering the functional redundancy of PGC-1α and PGC-1β (126), to ensure a more robust effect on mitochondrial biogenesis and function, an adipocyte-specific double knockout mouse model for both co-activators was generated (PGC-1α/β-FAT-DKO mice) (36). In this previous study, white and brown adipose tissues from PGC-1α/β-FAT-DKO mice displayed a reduction in the expression of mitochondrial genes in parallel to a decrease in the protein levels, more severely in BAT. Mitochondrial dysfunction in BAT tissues

was accompanied by a severe accumulation of fat in brown adipocytes, indicative of impaired brown adipocyte functionality, but not noticeable alterations were found in WAT. Although these mice did not show any impairment in glucose homeostasis when fed a chow diet, they exhibited a tendency towards mild glucose intolerance when fed a HFD45, although differences were not statistically significant (36). Nevertheless, PGC-1α/β-FAT-DKO mice maintained both whole body and tissue-specific insulin sensitivity and did not develop obesity (36). Still, the mild glucose intolerance observed prompted us to deepen into the metabolic phenotype of PGC-1α/β-FAT-DKO mice by subjecting them to a diet with an even higher fat content, HFD60, and then studying adipose tissues and glucose homeostasis.

In the experimental set up of the present study, PGC-1α/β-FAT-DKO mice either fed a chow diet or a HFD60 showed a decrease in mitochondrial gene expression in inguinal WAT similar to that previously described when animals were fed a HFD45 (36). Indeed, consistent with the role of PGC-1α and PGC-1β in the control of mitochondrial function and biogenesis, deletion of both co-activators significantly reduced the expression of genes encoding for proteins of the OxPhos system in inguinal WAT depot.

It is interesting to note, that even if PGC-1s co-activators are considered as master regulators of mitochondrial biogenesis, the simultaneous deletion of PGC-1α and PGC-1β in white adipocytes did not result, however, in a complete ablation of mitochondrial gene expression in WAT. These results indicate that other factors contribute to the maintenance of mitochondrial mass in adipocytes and relativize the importance of PGC-1s on the control of mitochondrial gene expression in WAT, in agreement with the lower expression of these co-activators in this tissue compared to others such as BAT, heart or skeletal muscle. In this sense, ERRs, NRFs or PPARs transcription factors could be up-regulated in response to the loss-of-function of PGC-1s co-activators in inguinal WAT in order to maintain mitochondrial function. However, because PGC-1s directly up-regulate their expression, it is unlikely that these transcription factors could be up-regulated with the loss of PGC-1 co-activators. In addition, other members of the PGC-1 family such as PRC, NT-PGC-1α and PGC-1α4 could eventually compensate for the deletion of PGC-1α/β. However, NT-PGC-1α and PGC-1α4 originate from the *Ppargc1a* gene and both contain exons 4 and 5, which are flanked by the *loxP* sequences that *Cre* recombinase recognizes in our mouse model. Therefore, these truncated PGC-1α isoforms are also silenced by Cre recombinase in PGC-1α/β-FAT-DKO mice, making impossible that NT-PGC-1α and PGC-1α4 could compensate for the lack of PGC-1α. Regarding the *Pprc1* gene, whose expression generates the less studied member of PGC-1 family, PRC, it is restricted to the regulation of mitochondrial biogenesis in proliferating cells (121). However, because the PRC function in adult tissues is still unclear, a compensative role of this member of the family cannot be totally ruled out in WAT of PGC-1α/β-FAT-DKO mice.

Since we had already analysed gene expression in PGC-1α/β-FAT-DKO mice under a different fat regime, in the present study, gene expression analysis was only performed in the subcutaneous depot of WAT (inguinal), but not in the visceral depot (gonadal). This analysis was intended as a way to verify that the phenotype with regard to mitochondrial gene expression was preserved in the frame of the new experimental set up. Inguinal WAT was preferred over gonadal WAT owing to the higher amounts of mitochondria that subcutaneous

depots have and for being more prone to browning that the visceral depot. Nevertheless, previous studies from our laboratory ensured that both co-activators were also effective in reducing mitochondrial gene expression levels in gonadal WAT (124,188). On the other hand, although we have not assessed mitochondrial function in adipose tissues of our HFD60-fed mice, we expect it to be decreased to the same extent as in PGC-1α/β-FAT-DKO mice fed a HFD45, since the impact of lacking PGC-1s on mitochondrial gene expression is similar, regardless of the diet used.

Akin to the results observed in inguinal WAT, BAT from PGC-1α/β-FAT-DKO mice showed a decrease in the expression of mitochondrial genes encoding for proteins from the OxPhos system, consistently with the crucial role of PGC-1α and PGC-1β on brown adipocyte maturation and mitochondrial biogenesis (126). However, this reduction in gene expression was greater in BAT than in inguinal WAT, indicating a more relevant role of PGC-1s in controlling mitochondrial biogenesis in brown fat.

BAT main function is non-shivering thermogenesis, a process highly dependent on mitochondria and PGC-1α activity. With cold exposure, this co-activator is induced, thereby prompting heat production (118). However, recent studies support the notion that PGC-1β can also impair adrenergically-stimulated thermogenesis in BAT by influencing the communication between mitochondria and lipid droplets (189). In any case, though, PGC-1α is considered the main driver of the thermogenic response in BAT through the control of *Ucp1* expression. In agreement with the thermogenic role of PGC-1s, the expression of *Ppargc1a* (and in a lesser extent *Ppargc1b*) gene was up-regulated by cold in Wt mice, but it was blunted in PGC-1α/β-FAT-DKO mice. As well, the expression of the thermogenic genes *Ucp1* and *Cidea,* and to a minor extent the expression of genes encoding for components of the OxPhos system and TCA, was increased in Wt mice after cold exposure, but it was severely blunted in PGC-1α/β-FAT-DKO mice. Although at thermoneutrality (30°C) no thermogenic response is required, loss of PGC-1β has been described to affect the basal expression of mitochondrial genes from the OxPhos system and TCA. Exceptionally, the expression of *Adrb3* gene in BAT was up-regulated by cold and by the deletion of PGC-1α/β co-activators, irrespectively of the environmental temperature. This suggests that *Adrb3* may exert an effect beyond non-shivering thermogenesis in BAT from PGC-1α/β-FAT-DKO mice. ADRB3 receptor promotes, together with ADRB1, lipolysis and fatty acid oxidation in BAT (190). Moreover, ADRB receptors have been involved in the expansion of this tissue (191,192). Bearing these data in mind, up-regulated expression of *Adrb3* by the loss of PGC-1α/β co-activators could represent a compensatory mechanism to reverse loss of thermogenic function through the recruitment and activation of new brown adipocytes in BAT from PGC-1α/β-FAT-DKO mice.

Down-regulation of mitochondrial genes in adipose tissues from PGC-1α/β-FAT-DKO mice is probably accompanied by a loss of mitochondrial oxidative function and mitochondrial mass in these mice. Traditionally, mitochondrial dysfunction and a reduced mitochondrial mass have been observed in insulin resistant individuals (30). However, in our previous work, mitochondrial dysfunction observed in PGC-1α/β-FAT-DKO mice did not drive IR in the main insulin-sensing tissues (adipose tissue, liver, skeletal muscle). Moreover, when fed a HFD60, PGC-1α/β-FAT-DKO mice exhibited similar whole body insulin sensitivity than their Wt

counterparts. Accordingly, other studies have also shown that reduced mitochondrial function in skeletal muscle do not impair insulin sensitivity. For instance, in the study of Zechner *et al.,* they demonstrated that global loss of PGC-1α combined with muscle-specific loss of PGC-1β caused a reduction in the mitochondrial function in this tissue, but this did not alter insulin sensitivity and glucose tolerance in these mice (125). Altogether, these data suggest that decreased mitochondrial biogenesis and function, at least in adipose tissues, are not sufficient to bring out a systemic insulin resistant phenotype.

## 5.2. Effects of the lack of PGC-1s on adipose tissues and body weight

PGC-1s integrate environmental and physiological cues that signal high energy demands by increasing mitochondrial biogenesis and oxidative function in many tissues, thereby modulating energy homeostasis. Moreover, mitochondrial activity is decreased in obese and diabetic individuals, suggesting that mitochondrial dysfunction may lead to impaired energy expenditure and by this means contribute to obesity. In this regard, the expression of *Ppargc1a* in adipose tissue has been found reduced in genetically and diet-induced obese mice and human (193,194). Although PGC-1β is principally involved on the basal mitochondrial status, its expression has also been found reduced in obese individuals (195). Likewise, the expression of both PGC-1α and PGC-1β is reduced in skeletal muscle from obese mice (196). All these data suggest that the lack of PGC-1 co-activators in adipose tissues could favour the development of obesity.

However, in our previous work, when mice were fed a HFD with a 45% of Kcal from fat, PGC-1α/β-FAT-DKO mice gained a similar amount of weight than Wt littermates. In the current experimental set-up using a HFD60, body weight of PGC-1α/β-FAT-DKO mice was mildly increased compared to Wt littermates only after 2 months of HFD60 feeding. This gain in body weight correlated with an increase in adiposity, although very modest, represented by an accumulation of fat in adipose tissues, mainly in gonadal WAT depot and in BAT. Compared to males, no differences in body weight were found between Wt and PGC-1α/β-FAT-DKO females.

The disruption of mitochondria appears to have a minor effect on the biology of WAT. Consistent with increased WAT mass in mice fed a HFD60, inguinal white adipocytes from PGC-1α/β-FAT-DKO mice were slightly bigger than those from Wt mice, indicating a modest adipocyte hypertrophy. Such differences in adipocyte size between Wt and PGC-1α/β-FAT-DKO mice were not observed in the gonadal depot. In this regard, one could speculate that the increase in the mass of gonadal fat in PGC-1α/β-FAT-DKO mice is achieved by hyperplasic mechanisms. However, given that HFD has proven to prompt hypertrophy in visceral WAT and hyperplasia in subcutaneous WAT (197), certain grade of hypertrophy would be expected in the gonadal WAT depot. Aside from the mild differences in the size of inguinal white adipocytes observed in PGC-1α/β-FAT-DKO mice, no other morphological alterations were detected in the tissue. Moreover, the expression of the terminal differentiation markers *AdipoQ, Leptin* and *Resistin* did not differ in the inguinal WAT from these mice when fed a

HFD60. These data support the notion that lack of PGC-1 co-activators and the consequent reduction of mitochondrial activity has a minor impact on WAT.

Contrary to the effects observed on WAT, PGC-1α/β deletion had way more severe effects on BAT, already visible when dissecting the tissue, which appeared paler than BAT from Wt littermates. The histological study revealed that brown adipocytes from PGC-1α/β-FAT-DKO mice accumulate more lipids than those from Wt. These results are consistent with the fact that PGC-1α/β deletion in brown adipocytes alters their mitochondrial capacity to oxidate fatty acids, thereby increasing the accumulation of TAG in lipid droplets (reviewed in 198). Accordingly, BAT from 25-week-old PGC-1α/β-FAT-DKO mice fed a regular diet present a higher expression of WAT-like markers (*Igfbp3, AdipoQ, Leptin, Resistin*) than BAT from Wt mice. This, together with reduced mitochondrial content, oxidative capacity and increased lipid accumulation is consistent with the increase in the "whitening" (the acquisition of a WAT phenotype) of BAT that characterise males and females in the process of aging (199,200). In response to the higher stress conditions derived from HFD60 feeding, the expression of WAT markers in BAT from PGC-1α/β-FAT-DKO mice is even more notorious.

In agreement with other studies linking the "whitening" of BAT with its inflammation (201), we observed a notably increase in the expression of inflammatory genes in BAT from PGC-1α/β-FAT-DKO mice. Indeed, the expression of *Cfd* and *Il1b* was notably up-regulated merely by the deletion of PGC-1 co-activators in brown adipocytes. CFD also called adipsin, is known for maintaining adipose tissue homeostasis and glycaemia (202,203) and it is up-regulated during white adipocyte differentiation (204). IL-1β is a well-stablished pro-inflammatory cytokine related to the recruitment of macrophages in adipose tissue that favours fat accumulation in adipocytes (205). Under the effect of the HFD60, though, the expression of *Il1b* was not modulated in BAT from PGC-1α/β-FAT-DKO mice. As HFD is known to promote inflammation in adipose tissues, the lack of modulation of *Il1b* expression could be due to the fact that IL-1β is mainly secreted by adipose macrophages (102), which are in low numbers in BAT compared to WAT. Alternatively, it is plausible that the expression of other inflammatory markers precedes that of *Il1b.* Supporting this, the expression of *Ccl2,* which was increased in our results, has been observed to precede the expression of other macrophage markers during the development of obesity (206). This switch towards a white-like phenotype by brown adipocytes of PGC-1α/β-FAT-DKO mice is also supported by the acquisition of a secretory profile that is more similar to that of WAT, as it will be further discussed.

However, the expression of identity markers for brown adipocytes (*Ucp1, Pdk4, Lhx8, Meox2, Prdm16, Zic1*) was also up-regulated in BAT from PGC-1α/β-FAT-DKO mice concomitant to the increase in the expression of WAT markers. Although it seems inconsistent with the "whitening" of the tissue, it is conceivable to think that both processes could occur at the same time in BAT. On the one side, PGC-1α/β deletion in brown adipocytes alters their mitochondrial capacity to mobilize and oxidate fatty acids, thereby promoting the accumulation of TGA in bigger lipid droplets. At the same time, the lack of PGC-1s impairs the terminal differentiation of brown adipocytes, as indicated by the loss of brown fat markers such as *Ucp1* and a reduction in mitochondrial density and function in this tissue (126). Both processes, lipid accumulation and impaired terminal differentiation contribute to the

acquisition of a WAT-like phenotype in BAT. On the other side, PGC-1α/β-FAT-DKO mice may intend to compensate the impairment in thermogenesis resulting from the "whitening" of brown adipocytes by enhancing the thermogenic program in those brown adipocytes in which recombination did not occur or by activating brown adipogenesis in the tissue. Both processes justify the increased expression of the previous mentioned brown adipocyte markers in BAT from PGC-1α/β-FAT-DKO mice, instead of its down-regulation.

BAT impairment has been associated with increased body weight and the development of obesity in humans and rodents. In mice, reduced BAT mass and UCP-1 levels are found in obese individuals (207,208). Similarly, the amount of BAT is inversely correlated with the *body* BMI in obese humans (209), together with a reduced thermogenic response (210). In fact, some polymorphisms of *Ucp1* have been associated to a defective thermogenic response that correlates with a higher BMI (211). Accordingly, the reduced expression of thermogenic and mitochondrial genes in BAT from PGC-1α/β-FAT-DKO mice led to a completely dysfunctional BAT with impaired non-shivering thermogenesis. Indeed, PGC-1α/β-FAT-DKO mice were unable to sustain body temperature when subjected cold exposure (4°C). Although energy expenditure was not determined, based on results by other authors (212,213), the impairment of BAT thermogenesis it is expected to affect whole body energy expenditure.

In some models of disrupted BAT thermogenesis, the lack of the thermogenic function and the consequent decrease in energy expenditure is accompanied by a body weight gain. Contrarily, activation of BAT thermogenesis is associated with weight loss and prevention of obesity. In mice, adrenergic stimulation of BAT activates UCP-1 and leads to loss of body weight (214). In human, pharmacological activation of BAT also enhances energy expenditure in lean healthy male subjects (215). Given the tight correlation between dysfunctional BAT and energy balance, the increment in body weight observed in PGC-1α/β-FAT-DKO mice fed a HFD60, although mild, is compatible with a positive energy balance resulting from impaired thermogenesis. Arguing these results, the disruption of non-shivering thermogenesis in PGC-1α/β-FAT-DKO mice was not enough to alter body weight in mice fed a chow diet or a HFD45. Moreover, PGC-1α/β-FAT-DKO mice fed a HFD60 and housed at thermoneutrality (30°C) (data not shown) still weighted more than Wt mice, suggesting that disrupted non-shivering thermogenesis does not solely explain the higher weight gain in PGC-1α/β-FAT-DKO mice compared to their Wt littermates. However, these results are likely to be an effect on lipid mobilization rather than an alteration of energy balance.

## 5.3. Detrimental effects of HFD on glucose homeostasis in PGC-1α/β-FAT-DKO mice

Long-term exposure to HFD60 disrupted glucose homeostasis in PGC-1α/β-FAT-DKO mice, as they displayed glucose intolerance already after 2 months of HFD60 feeding. Given the contribution of obesity to the appearance of insulin resistance (216), we confirmed that glucose intolerance observed in PGC-1α/β-FAT-DKO mice was independent of body weight. In this sense, age- and weight-matched PGC-1α/β-FAT-DKO mice were intolerant to glucose compared to Wt mice but maintained similar insulin sensitivity. These results argue the ones

obtained by Kleiner *et al*., in which solely the deletion of PGC-1α in adipose tissues was enough to drive insulin resistance and hyperglycaemia in PGC-1α-KO mice despite conserving body weight (138). In our mouse model, adipose-specific PGC-1α/β deletion preserves, however, insulin sensitivity. In support of the independence of body weight on the development of glucose intolerance in PGC-1α/β-FAT-DKO mice, serum lipidic metabolites were barely changed in these mice, with only a mild but significant reduction in triglycerides. Akin to males, results from females confirmed that PGC-1α/β-FAT-DKO mice were glucose intolerant independently of body weight.

Glucose intolerance in PGC-1α/β-FAT-DKO mice could arise from peripheral or tissue-specific insulin resistance. However, as already mentioned, despite severe glucose intolerance in these mice, both males and females had preserved peripheral insulin sensitivity. In addition, our previous work demonstrated that tissue-specific insulin sensitivity was preserved in adipose tissues, liver and skeletal muscle from PGC-1α/β-FAT-DKO mice (36). Considering that neither dyslipidaemia nor white adipose tissue inflammation are markedly different between Wt and PGC-1α/β-FAT-DKO mice, other causes are behind the glucose intolerance observed in these mice.

Reduced basal serum c-peptide levels were observed in PGC-1α/β-FAT-DKO mice during the time of HFD60 feeding. In response to an oral glucose bolus, PGC-1α/β-FAT-DKO mice also showed less serum c-peptide levels than Wt mice at any age, even before an overt glucose intolerant phenotype appeared. Remarkably, lower fasting insulin levels were observed in PGC-1α/β-FAT-DKO mice after three months fed a HFD45 (36), when these animals already showed a trend towards developing glucose intolerance, demonstrating the consistency of our data. This reduction in serum c-peptide levels in PGC-1α/β-FAT-DKO mice, even before the appearance of an overt glucose intolerance phenotype, pointed towards a pancreatic problem with insulin secretion in these mice, since c-peptide is a surrogate of insulin secretion by pancreatic β-cells. This effect on insulin/c-peptide levels was not observed when mice were fed a chow diet, congruently with the lack of differences in the glucose tolerance between genotypes. Despite this, HFD60 increased the serum levels of c-peptide both in Wt and PGC-1α/β-FAT-DKO mice, as lipidic diets promote the secretion of insulin as a way to counteract insulin resistance induced by this kind of diets (217). Moreover, both in Wt and PGC-1α/β-FAT-DKO mice, fed either a chow or a HFD60, serum c-peptide was increased during the first 15 minutes after the delivery of glucose, an effect strongly observed with an oral administration of the sugar. By contrast, intraperitoneal glucose administration often leads to a low insulin excursion compared to oral administration (218,219).

To disclose the cause of reduced insulin and c-peptide levels in serum from PGC-1α/β-FAT-DKO mice, we evaluated several parameters in pancreas from these mice that are known to affect insulin secretion and influence glucose homeostasis. On the one side, a morphometric analysis of pancreatic islets was conducted. In this analysis, we observed an increment in the density of islets, α-cell mass and β-cell mass both in Wt and PGC-1α/β-FAT-DKO mice after 3 months of HFD60 feeding. This temporary increase in the number and size of islets, and particularly β-cell mass, was expected in response to HFD60, as it is a classical response to overcome the insulin resistance induced by this type of diets by increasing insulin secretion

(220,221). Concerning α-cells, an elevated concentration of glucagon in blood is associated with IR and hyperglycaemia in normal and diabetic individuals (222). However, the lack of differences in α-cell mass and glucagon levels in serum from these mice does not support a significant role of these cells in the phenotype observed. In the same way, the general lack of differences in the density of pancreatic islets and β-cell mass in PGC-1α/β-FAT-DKO mice indicates that they are not the cause of the different insulin/c-peptide levels found in these mice.

This conclusion may underestimate, however, the truly impact of lacking PGC-1s in adipose tissues on pancreatic islets from PGC-1α/β-FAT-DKO mice. In fact, the quantification of insulin did not allow us to discern the dynamics of pancreatic β-cells. Knowing that an event of dedifferentiation of fully mature β-cells into progenitor cells can occur in T2D (reviewed in 223), the presence of less secretory β-cells containing insulin may unmask the identification of fully functional β-cells. In the same extent, other events such as β-cell apoptosis, hypertrophy and proliferation may have some impact on the phenotype observed and, therefore, further studies evaluating β-cells individually would be desirable. Still, considering that β-cell mass is not altered in PGC-1α/β-FAT-DKO mice, it is unlikely that processes such as differential cell death or proliferation may account for the differences observed in insulin levels.

The lack of differences in β-cell mass that could help to explain reduced serum insulin levels in PGC-1α/β-FAT-DKO mice prompt us to assess the expression of genes encoding for proteins involved in different aspects of β-cell function. In particular, we assessed the expression of genes involved in mitochondria, β-cell differentiation, identity markers for islet cell subpopulations, transport and metabolism of glucose, packaging and folding of insulin, fusion of insulin granules with the cell membrane, the UPR and immune genes. Interestingly, compared to chow diet, HFD60 feeding did not seem to modulate the expression of these genes neither in pancreatic islets from Wt nor from PGC-1α/β-FAT-DKO mice. This lack of effect by HFD contrasts with the morphometrical analysis, in which HFD60 significantly increased the number of islets and their cellular composition. Discrepancies between both studies may underlie, however, in the different age of mice fed a chow diet in each study. However, one may expect a similar effect of aging in all conditions. Therefore, it could be just that HFD is not sufficient to modulate the gene expression of pancreatic islets. Alternatively, long-term exposure to HFD60 might stimulate the formation of new pancreatic islets rather than or in addition to promoting the expansion of the ones already present in the pancreas. Therefore, the number of pancreatic islets increases over time of HFD60 feeding but individually collected pancreatic islets display a similar gene expression profile than those from age-matched chow fed mice. This explanation is supported by the increased density of islets observed in our study after long-term HFD60 feeding. In any case, the general lack of differences in gene expression between Wt and PGC-1α/β-FAT-DKO mice, both under chow diet and HFD60 conditions, indicates that other mechanisms beyond an alteration of gene expression in pancreatic islets account for the reduced serum insulin and c-peptide levels observed in PGC-1α/β-FAT-DKO mice.

It is well known that an adequate mitochondrial OxPhos function is absolutely necessary for insulin secretion, as this organelle generates the amount of ATP required to fire the depolarization signal for the cell membrane that drives insulin secretion. In this sense, patients suffering from mitochondrial diabetes, which contain defects in mitochondrial DNA and mitochondrial function in β-cells, among other cell types, display decreased β-cell mass, increased β-cell apoptosis and reduced insulin secretion (224). Since some Cre-driving promoters appear to be "leaky" or not as specific as anticipated, and PGC-1s co-activators are universal regulators of mitochondrial biogenesis in most tissue and cell types, we sought to determine if mitochondrial dysfunction could be occurring in our mouse model as a consequence of the accidental deletion of PGC-1s in pancreatic β-cells. Agreeing with the role of PGC-1s as master regulators of mitochondria biogenesis, deletion of PGC-1α/β in pancreatic β-cells has proven to reduce the amount of insulin secreted in response to glucose (225). However, this does not appear to be the case. First, we confirmed that PGC-1s were not deleted in pancreatic islets. Second, despite *Ppargc1a* is mildly up-regulated in pancreatic islets of PGC-1α/β-FAT-DKO mice fed a chow diet, our data do not indicate a contribution of PGC-1s on the differential release of insulin in β-cells, since the expression of mitochondrial genes encoding for proteins of the OxPhos system was not altered in isolated islets from PGC-1α/β-FAT-DKO mice.

The grade of differentiation and identity of pancreatic β-cells was also assessed in pancreatic islets from PGC-1α/β-FAT-DKO mice. To this aim, we quantified the expression of the transcription factors *Foxo1, Pax6, Mafa* and *Nkx6.1.* FOXO1 and PAX6 are transcription factors present in different cell subpopulations from pancreatic islets, whereas MAFA and NKX6.1 are unique from differentiated β-cells (55,226). However, the correct temporal expression of all these transcriptional factors is crucial to obtain differentiated and fully functional β-cells. In this sense, in the study from Cinti *et al*., they observed a reduced expression in the differentiation markers *Foxo1, Mafa* and *Nkx6.1* and the insulin gene in human pancreatic islets of diabetic individuals, which was accompanied by a diminished insulin secretion in these subjects (227,228). In fact, FOXO1 suppression in β-cells results in the dedifferentiation of these cells, whereas the expression of *Mafa* in the exocrine compartment of pancreas is required to reprogram exocrine cells to a β-cell fate (229,230). Likewise, an abnormal expression of identity markers for α-cells (*Gcg*), β-cells (*Ins1, Ins2*) and δ-cells (*Sst*) is typical from less functional pancreatic islets. For instance, in a diabetic mouse model caused by an induced-pancreatic dysfunction, decreased glucose-stimulated insulin secretion is accompanied by alterations in pancreatic islets and a loss of expression of endocrine markers (231). However, the expression of these genes was not altered in pancreatic islets from PGC-1α/β-FAT-DKO mice, irrespectively of the dietary treatment.

The correct signalling and metabolism of glucose are essential for pancreatic islets to properly secrete insulin when the glucose blood concentration raises (232,233). However, when we evaluated the expression of genes encoding for the receptors of glucose (*Glut1, Glut2*) and glycolytic enzymes (*Gapdh, Gck, Pdk1*), we did not find differences in pancreatic islets from PGC-1α/β-FAT-DKO mice. These results contrast with the ones from other studies in which an up-regulation of glycolytic enzymes were observed in pancreatic islets from diabetic mice. As an example, in the study made by Haythorne *et al.* (234), disruption of the electrical activity

and insulin secretion in pancreatic β-cells up-regulated the expression of glycolytic markers in pancreatic islets from diabetic mice. However, glucose oxidation was reduced in these islets and glycogen deposition highly increased in β-cells, thereby suggesting an inefficient oxidation of glucose and conversion to glycogen in diabetic β-cells. In another study made in INS-1 pancreatic cells, disrupted glucose oxidation and accumulation of glycogen was confirmed *in vitro* (235). Contrarily to these studies, based on gene expression, the metabolism of glucose seems to be preserved in PGC-1α/β-FAT-DKO mice even when subjected to a HFD60. On the other hand, the expression of the incretin receptor *Glp1r* was slightly increased in pancreatic islets from PGC-1α/β-FAT-DKO mice fed a HFD60. Interestingly, GIP insulinotropic action, but not that from GLP-1, has been observed to be diminished in T2D patients and perfused islets of diabetic rats (236,237). Since GIP is assumed to mediate the gross insulinotropic effect of incretins in healthy individuals (238), with GLP-1 having an adding effect, a possible disruption in the signalling of GIP in pancreatic islets of PGC-1α/β-FAT-DKO mice cannot be ruled out. Nevertheless, based on the mild alteration in glucose and GLP-1 pathways observed, it does not seem that GLP-1 signalling could have a gross and differential effect on insulin secretion in PGC-1α/β-FAT-DKO mice.

Additionally, the expression of genes encoding for proteins related to the formation of mature insulin was not altered in pancreatic islets from PGC-1α/β-FAT-DKO mice. Amylin (*Iapp*) is co-secreted with insulin and it participates in the regulation of glucose homeostasis by restricting insulin secretion (239). Pro-convertases 1 and 2 are crucial to convert pro-insulin to insulin and, consequently, their disfunction is associated to a lower generation of functional insulin. In this sense, polymorphisms of *Pcsk1* and *Pcsk2* genes have been related to a higher pro-insulin-to-insulin circulating ratio (240,241). In agreement with these data, pancreatic islets from ob/ob mice express higher levels of proconvertases 1 and 2 than normal islets, which are accompanied by a greater synthesis of proinsulin (242). Therefore, the lack of differences in the gene expression of amylin and pro-convertases 1/2 suggests that the maturation of insulin from proinsulin is conserved in pancreatic islets from PGC-1α/β-FAT-DKO mice. Consistently with the preserved expression of genes encoding for proteins mediating the maturation of insulin secretory granules, we did not observe an alteration in the population of insulin granules in β-cells from PGC-1α/β-FAT-DKO mice when evaluated by TEM microscopy. Granules were classified into immature, mature and with an atypical shape, named rod-shaped granules. Immature granules contain principally dispersed molecules of proinsulin, whereas mature β-granules consist of condensed and crystallized molecules of insulin surrounded by a pale halo. In T2D, there is a decrease in the conversion of immature insulin granules to mature granules, thereby favouring the exocytosis of proinsulin, which compromises basal and glucose-stimulated insulin secretion in pancreatic β-cells (243). However, the percentage of mature insulin granules was preserved in β-cells from PGC-1α/β-FAT-DKO mice. Conversely, they displayed a reduced proportion of immature insulin granules and a higher proportion of rod-shaped granules. Although it is unclear, some studies have suggested that granules adopting a rod shape contain crystallized proinsulin rather than insulin (244), which seems to be caused by a defective insulin crystallisation and release in β-cells (245). These data could indicate that β-cells from PGC-1α/β-FAT-DKO mice have a defective production of mature insulin granules that promotes the accumulation of granules

containing proinsulin. However, the subtle differences in the number of granules between genotypes and the lack of differences in mature granules question the relative contribution of immature and rod-shaped granules to the phenotype observed. Nevertheless, based on these results it would be worth measuring the secretion of proinsulin to determine if a deficient secretion of mature insulin could be the underlying cause of the glucose intolerance observed in PGC-1α/β-FAT-DKO mice.

The shape of insulin secretion phases is not only modulated by the number of mature insulin granules, but also by the availability of these granules to be secreted. From the 10,000 insulin-containing secretory granules usually found within pancreatic β-cells, 6% are docked to cell membrane and a 20% are almost docked (less than 0.5 μm away from the cell membrane). Amongst the docked granules, 15-20% belong to the RRP, which are the ones primed with a fully assembled exocytosis machinery and that are principally secreted in the 1$^{st}$ phase of insulin secretion (246). Bearing this in mind, we quantified the number of each population of insulin granules in a region located less than 0.5 μm away from the cell membrane. By doing this we attempted to unmask differences in the percentage of mature insulin granules in pancreatic β-cells from PGC-1α/β-FAT-DKO mice in the region below the cell membrane, where RRP granules are located. However, we did not find differences between genotypes. Therefore, we can conclude that the number and localisation of insulin granules are not disrupted in PGC-1α/β-FAT-DKO mice and that other factors account for the reduced serum insulin levels observed in these mice.

Still, other studies have shown that a down-regulation on the expression of genes encoding for proteins implicated in the fusion of insulin granules with the cell membrane is translated into a reduction in the secretion of insulin. In this sense, in the study of Andersson *et al.*, they identified lower gene expression and reduced protein levels of syntaxin 1a and members of the synaptotagmin family in human T2D pancreatic islets (247). Pointing towards the same direction, another study displayed a down-regulation in the expression of *Stx1a, Unc13b, Vamp2* and *Syp,* as well as in their protein levels, in pancreatic islets from T2D individuals (248). Analogous to the previous results on the gene expression of pancreatic islets, we did not find differences in the expression of genes encoding for proteins that participate in the fusion of secretory granules with the cell membrane to allow the release of insulin. This argues in favour of a normal dynamics and fusion of insulin granules with the cell membrane in these mice. These results are also supported by our TEM analysis of insulin granules within β-cells, in which the proportion of docked insulin granules was not different between PGC-1α/β-FAT-DKO and Wt mice. Nevertheless, it is possible that mRNA levels do not correlate with actual protein levels of these enzymes, which should be analysed in the future by techniques allowing protein quantification.

Finally, the expression of genes encoding for proteins that participate in the UPR and the immune response was barely affected in pancreatic islets from PGC-1α/β-FAT-DKO mice. It is known that chronic stress in pancreatic β-cells impairs the expression of regulators of β-cell function and identity, thereby disrupting insulin secretion (249). In this sense, in the study from Engin *et al.*, a reduced expression of members of the UPR was found in T2D subjects as well as in diet- and genetic-induced diabetic mice, seen as a failure of β-cells to cope with IR

by producing higher amounts of insulin (250). Moreover, given the importance of the immune system in T1D, a certain grade of inflammation could be expected in pancreatic islets from PGC-1α/β-FAT-DKO mice. Nevertheless, gene expression analysis indicates that the expression of genes participating in UPR and immune response pathways is not significantly altered in PGC-1α/β-FAT-DKO mice.

Previous results concerning the gene expression of proteins that participate in different pathways related to the secretion of insulin were obtained directly on pancreatic islets instead that on isolated β-cells. Thus, some alterations in gene expression might be masked by the compensative effect of other cell populations within pancreatic islets, although this is unlikely because β-cells constitute most of the cellular mass of the islet. Nevertheless, to better evaluate possible alterations specifically in pancreatic β-cells, it would be worth to isolate these cells and reevaluate the expression of genes previously analysed in pancreatic islets.

Although our studies did not report major alterations in pancreatic islets from PGC-1α/β-FAT-DKO mice, reduced insulin and c-peptide levels in serum of these mice were consistent and pointed towards a pancreatic defect on insulin secretion. To confirm this, we directly evaluated insulin secretion in pancreatic islets from Wt and PGC-1α/β-FAT-DKO mice. Due to the complexity of the technique, we performed only two experiments but including hundreds of pancreatic islets from both genotypes. Both studies agreed in demonstrating that the stimulatory capacity of glucose (fold induction of insulin secretion upon glucose stimulation) is preserved in pancreatic islets from PGC-1α/β-FAT-DKO mice, indicating that β-cells from these mice respond similarly to high doses of glucose than those from Wt mice. Nevertheless, the two experiments disagree in the amount of insulin secreted and in the insulin content in both groups of pancreatic islets. Whereas in the first experiment pancreatic islets from PGC-1α/β-FAT-DKO mice secreted less insulin to the culture medium under basal (2.8 mM glucose) and stimulated (20 mM glucose) conditions than those from Wt mice, in the second experiment, the reduction in the insulin content in pancreatic islets from PGC-1α/β-FAT-DKO mice, responsible for the diminished insulin secretion, was not observed. Still, as mentioned, islets from PGC-1α/β-FAT-DKO mice exhibited a secretory response to high glucose concentrations similar to that observed in Wt mice. Beyond these differences between experiments, which remain to be clarified and demand further investigation, we proved that the fold induction in pancreatic islets from PGC-1α/β-FAT-DKO mice fed a HFD60 in response to stimulatory doses of glucose is similar to that from Wt mice, at least *ex-vivo*. Importantly, these results were replicated in pancreatic islets from chow fed mice, confirming the preservation of the glucose stimulatory capacity in PGC-1α/β-FAT-DKO mice. A possible interpretation of these data is that *ex-vivo* the functionality of pancreatic islets from PGC-1α/β-FAT-DKO mice is not compromised, and its impaired capacity to secrete insulin only occurs *in vivo*. In this regard, it is possible to envision a situation in which circulating molecules present in PGC-1α/β-FAT-DKO mice acutely impair insulin secretion without causing persistent damage in β-cells. Thus, once the pancreatic islets are isolated, the noxious effects of this putative molecule are lost and, as a consequence, islets exhibit normal function.

Analysis of pancreatic islets and β-cells from PGC-1α/β-FAT-DKO mice did not clarify the reasons causing these mice to had lower insulin serum levels than their Wt littermates when fed a HFD. In this sense, morphometrical parameters and gene expression of pancreatic islets were conserved in PGC-1α/β-FAT-DKO mice, suggesting no intrinsic defects in these cells. However, the evaluation of insulin granules within β-cells did not include the characterisation of young and old secretory granules or the dynamics of these granules with microtubules and actin in these cells. It is known that microtubule depolymerization is required to enhance insulin secretion, given that in diabetic conditions microtubule density is increased (251). Therefore, an altered event of polymerization and depolymerization of microtubules could prevent the biphasic response of insulin secretion in pancreatic islets from PGC-1α/β-FAT-DKO mice. In addition, despite the percentage of immature and mature insulin granules is preserved in the docking region of β-cells, functional studies assessing the preferential release of mature insulin granules over immature ones should be done. Other factors such as the electrical activity in β-cells could be altered in PGC-1α/β-FAT-DKO mice, even if the stimulatory capacity of glucose in pancreatic islets from these mice is retained.

## 5.6. The BAT-pancreatic crosstalk

Irrespectively of the previous results on insulin secretion, insulin and c-peptide levels were clearly decreased in serum from PGC-1α/β-FAT-DKO mice. Therefore, these data principally point towards a, yet unidentified, pancreatic defect that ultimately impacts insulin secretion and rends these animals glucose intolerant. Given that our mouse model was engineered to disrupt PGC-1s co-activators exclusively in adipose tissues, and that pancreatic islets seem to respond normally to glucose *ex-vivo*, we hypothesize that a disruption of the crosstalk between adipose tissues and β-cells occurs in PGC-1α/β-FAT-DKO mice.

Traditionally, WAT is known for its capacity to secrete factors in response to different cues that regulate diverse processes, such as energy balance and glucose homeostasis. In a context of obesity and IR, the expression of many of these molecules is altered, thereby contributing to the pathological status. For instance, the secretion of leptin, resistin, RBP4, FABP4 and vaspin positively correlates with the occurrence of obesity and IR, whereas that from omentin and adipsin seems to be lower in obese and diabetic individuals (97). Similar to WAT, increasing evidence indicate that BAT can act as a secretory actor beyond its thermogenic function. In this sense, many reports argue that BAT also secretes adipokines that exert important roles, both in health and disease. Interestingly, given the inverse relation of BAT mass and function with the development of insulin resistance and T2D, BAT-secreted molecules are likely to exert beneficial effect on metabolism. In this sense, FGF-21, the most well-known BAT-derived factor, alleviates glycaemia and lipidaemia by promoting glucose uptake and oxidation in many tissues (163,164). Moreover, it activates thermogenesis and promotes the browning of WAT, opposing to the development of T2D (166,167). IL-6 is another batokine increased after BAT transplantation and activation that enhances hepatic gluconeogenesis in conditions of acute physiological stress, independently of BAT thermogenic function (252). Another novel BAT secreted factor, *12,13-dihydroxy-9Z-octadecenoic acid (12,13-diHOME),* a molecule of lipidic nature, is known to increase cardiac

function and cardiomyocyte respiration. In skeletal muscle, 12,13-diHOME increases fatty-acid uptake. Also in muscle, BAT-derived myostatin reduces the exercise capacity of mice (252). All these molecules secreted by BAT are known to signal distant organs and modulate different metabolic functions, thereby regulating glucose homeostasis.

Our hypothesis stated that one or several molecules secreted by adipose tissues are responsible of the glucose intolerance observed in PGC-1α/β-FAT-DKO mice through their action on pancreatic β-cells. Therefore, to study the proteins secreted by adipose tissues, we performed mass spectrometry on conditioned media obtained from WAT and BAT explants. Many other technical approaches have been undertaken to study cell secretome, such as RNA sequencing or *Serial Analysis of Gene Expression (SAGE),* but we chose mass spectrometry for its high resolving power and availability (253), besides the fact that it directly detects secreted proteins and does not rely in the inference from gene or RNA sequences that identify label sequences that target proteins for secretion. In agreement with the selection of this technique, many other studies, both *in vitro* and *in vivo*, have used mass spectrometry approaches to analyse the secretome from cells and tissues. Concerning adipose tissues, some reports have analysed using proteomics the secreted proteins from *in vitro* adipocytes, as well as WAT and BAT secretome from rodents and humans (reviewed in 254).

The study of adipose tissues secretome by *untargeted* proteomics revealed that most differences were given by the different set of proteins found in the conditioned media between adipose tissues. In fact, although the number of proteins found in conditioned media of BAT (1,741) was similar to that of gonadal WAT (1,874) and inguinal WAT (1,744), their abundance was different depending on the tissue. Nevertheless, a great number of the proteins identified in the conditioned media of adipose tissues were identified as intracellular proteins, indicating that a non-negligible number of proteins found in the media were originated from lysed cells. For this reason, to identify actively secreted proteins, the use of specific bioinformatic tools were used.

Proteins found secreted by inguinal and gonadal WAT depots in Wt mice were highly diverse. The biological pathways more enriched in WAT secretome involved processes such as *extracellular matrix (ECM)* organization or immune system, processes important for WAT structure and functionality (data not shown). In inguinal WAT, biological pathways related to lipid metabolism were also highly and selectively enriched, in agreement with its role in the storage of lipids. Classically white secreted factors such as adipsin, adiponectin, dermatopontin, leptin, resistin or SPARCL1, proteins from the ECM such as tenascin, as well as collagens and integrins, were more abundant in inguinal WAT than in gonadal WAT. Contrarily, categories involving immune and inflammatory processes were more enriched in gonadal WAT. In fact, proteins from these biological processes such as CXCL1, CXCL2 or interleukin 1 receptor antagonist were more abundant in gonadal rather than inguinal WAT. Our findings are in line with the data from other studies obtained in white and brown adipocytes from both human and mice. In the study from Kahn *et al.* (255), they observed a higher presence of inflammatory cytokines and adipokines in conditioned media from visceral versus subcutaneous WAT from obese individuals. Alternatively, in a similar study analysing visceral and subcutaneous WAT secretome from obese individuals (256), an enrichment of

proteins that participate in the remodelling of the ECM was observed in both depots. Both studies are in line with the remodelling of ECM in adipose tissues, particularly visceral depots, and their inflammation seen in response to a situation of nutrient excess such as obesity.

Concerning the secretome of BAT in control mice, our study failed to identify some classic "batokines" such as FGF-21, NRG4, NGF, BMP8B, VEGFA, and only IL-6 was detected. Secreted proteins highly abundant in BAT secretome were related to the metabolism of lipids, especially cholesterol, akin to those from inguinal WAT.

BAT from PGC-1α/β-FAT-DKO mice displayed impaired non-shivering thermogenesis and a certain grade of "whitening" compared to BAT from Wt mice. These alterations were accompanied by a shift in the secretome of this tissue towards a WAT-like secretome. In this sense, BAT secretome from PGC-1α/β-FAT-DKO mice was enriched in typical WAT proteins such as adiponectin, leptin, resistin, dermatopontin, IL-6 or RBP-4 compared to that from Wt mice. Moreover, biological processes related to the ECM remodelling and immune response were predominant in BAT secretome from PGC-1α/β-FAT-DKO mice. In accordance with our data, the study of Rangel-Azevedo *et al.* (257), reported that progressive "whitening" of BAT from HFD-fed mice is associated with decreased thermogenic function and altered expression of genes encoding for BAT secreted factors.

It is interesting to highlight that our proteomic analysis of the secretome of adipose tissues revealed that most differences between Wt and PGC-1α/β-FAT-DKO mice were dependent on the adipose tissue depot considered. Thus, whereas most proteins seem to be conserved in the secretome of WAT depots between Wt and PGC-1α/β-FAT-DKO mice, many proteins appeared differently secreted by BAT between genotypes. 126 proteins were found to be distinctly secreted by BAT from PGC-1α/β-FAT-DKO mice. Contrary, the number of proteins differentially secreted by WAT of Wt and PGC-1α/β-FAT-DKO mice was very low: only 3 proteins appeared differentially secreted by gonadal WAT and 1 protein in inguinal WAT. Therefore, our data indicated that deletion of PGC-1s in BAT severely impacted the secretory capacity of the tissue, an effect almost neglected in WAT depots. Given the fact that BAT mass and activity are proven to inversely correlate with obesity and T2D (144,147), these results opened the possibility of a BAT-pancreatic crosstalk that specifically modulates glucose homeostasis.

Amongst the proteins differentially secreted in media by BAT from Wt and PGC-1α/β-FAT-DKO mice, 102 were up-regulated in PGC-1α/β-FAT-DKO mice and 24 proteins were down-regulated in these mice. The proteomic analysis revealed that many of the proteins highly secreted by BAT from PGC-1α/β-FAT-DKO mice were typically related to WAT, including CFD, dermatopontin, resistin, SPARCL-1, adipsin, RBP4 and adiponectin. These results agreed with the acquisition of a WAT-like phenotype by BAT from these mice. According to Villarroya *et al.* (154), BAT activation involves the secretion of molecules that participate in the reorganization of the ECM and the immune system to adapt to the expansion of the tissue. Akin to the study of this author, we found many proteins involving the ECM to be highly secreted by BAT from PGC-1α/β-FAT-DKO mice, such as laminin subunit alpha 4 and beta 1, nidogen-1, fibronectin, SPARC, SPARCL1, fibronectin, collagen proteins or MMP2. As well, we found proteins from the complement such as complement factor B and complement C3, and

inflammatory proteins such as CCL7, CXCL1, CXCL5 and kininogen 1 more secreted in these mice. Despite these coincidences, primary defects in ECM remodelling through the chronic accumulation of fibrotic proteins are sufficient to disrupt BAT recruitment and function. For instance, in the study from Pellegrinelli *et al.* (258), inactive BAT of HFD-fed mice displayed and enrichment of fibro-inflammatory proteins, showing that BAT "whitening" was associated with higher levels of collagen deposition around adipocytes. Hence, the enrichment of proteins from the ECM and the complement system in BAT secreted media from PGC-1α/β-FAT-DKO mice suggests an incapacity of this tissue to accommodate to the nutritional cue, thereby losing functionality and suffering a process of "whitening". Contrarily, the proteins highly secreted by BAT from Wt mice were related to the metabolism and transport of lipids inside brown adipocytes to adapt to the increased amounts of lipids given by the diet. They included: FABP3, FABP4, lysophospholipase, carbonyl reductase 4, carbonic anhydrase 1 and carbonic anhydrase 2.

Amongst the proteins differentially secreted by BAT from PGC-1α/β-FAT-DKO mice, we attempt to identify the ones with a potential endocrine capacity to signal pancreas. For this, we quantified the concentrations of these proteins in serum of these mice either by *targeted* proteomics or ELISA. Unfortunately, *targeted* proteomics has a threshold limit for the detection of proteins of, approximately, 0.1-1 mg/L. Therefore, the lower sensitivity of this technique only allowed us to detect up to 53 proteins from the 126 differentially detected. By contrast, despite ELISA is more sensitive than *targeted* proteomics, the major pitfalls of the technique are their cost, the requirement of higher amounts of serum and the lack of commercially available kits to test all the proteins to be evaluated. These factors limited the number of proteins that we could identify by ELISA, although the study is ongoing and measure of the remaining candidates are in course.

By using both *targeted* proteomics and ELISA, we ended up by identifying 3 proteins differentially found in serum from PGC-1α/β-FAT-DKO compared to Wt mice. Kininogen-1 and resistin were found increased in serum of PGC-1α/β-FAT-DKO mice, whereas fibrinogen gamma chain was decreased.

**Fibrinogen gamma chain** is one of the three polypeptides that form fibrinogen, a compound involved in the blood coagulation cascade through its conversion to fibrin to form the blood clot (259). Serum levels of fibrinogen are increased in diabetic individuals with hyperglycaemia, promoting the formation of blood clots (259,260). Moreover, formation of fibrin from fibrinogen positively correlates with insulin secretion and β-cell mass in cultured pancreatic islets (261). Hence, reduced serum levels of fibrinogen gamma chain in PGC-1α/β-FAT-DKO mice may negatively impact insulin secretion in pancreatic islets from these mice.

**Kininogen-1** participates in the kallikrein-kinin system as a precursor of the kinins bradykinin and kallidin. Aside from the mediation of inflammation, blood pressure and pain, this system seems to enhance glucose uptake and promote insulin and glucagon secretion (262). Accordingly, plasma levels of kininogen-1, kallikrein and bradykinin are reduced in diabetic subjects (263,264). In this regard, it is unlikely that kininogen-1 would mediate the deleterious effects on β-cells to impair insulin secretion in PGC-1α/β-FAT-DKO mice. Some other studies argue, however, that this system mediates the destruction of pancreatic β-cells, thereby

disrupting insulin secretion (265). Hence, although we have not observed and reduction in β-cell mass, we cannot totally rule out the possibility that increased secretion of kininogen-1 in PGC-1α/β-FAT-DKO mice could exert deleterious effects on insulin secretion in pancreatic islets from these mice.

Finally, **resistin** is a classical WAT adipokine highly secreted in HFD-induced obese and T2D individuals, both in human and in mice (266). This molecule promotes the accumulation of fat in adipocytes and induces insulin resistance in many tissues (267). However, insulin resistance appeared to be preserved in PGC-1α/β-FAT-DKO mice. Studies reporting the effect of resistin on insulin secretion are, however, scarce and often contradictory. In the study from Nakata *et al.* (268), the authors found that non-obese mice overexpressing resistin exhibited impaired insulin secretion in response to glucose. These data would be compatible with resistin mediating the pancreatic phenotype observed in PGC-1α/β-FAT-DKO mice. In addition, 24 h of resistin treatment of pancreatic islets induced insulin resistance in the islets and impaired GSIS by elevating basal insulin secretion and supressing glucose-stimulated secretion, an effect that does not align with our observations in PGC-1α/β-FAT-DKO mice, which show low basal insulin secretion. However, these are coincident with our studies in INS-1 cells treated with recombinant resistin, which show high levels of basal insulin secretion. Based on this study, although resistin seems to have a detrimental effect on cultured β-cells, it is unlikely that increase circulating levels in PGC-1α/β-FAT-DKO mice are the main cause of the impaired pancreatic functionality observed in these mice when fed a HFD.

On the other hand, in a study from Wen *et al.* (269) performed in MIN6, a pancreatic β-cell-like cell line, insulin secretion was reduced both at basal and stimulatory concentrations of glucose when a dose of 50 ng/mL of resistin was used. These data, instead, would be compatible with our findings in PGC-1α/β-FAT-DKO mice and one of the experiments using isolated islets, in which basal and glucose-stimulated insulin levels were reduced.

For the study of insulin secretion in PGC-1α/β-FAT-DKO mice both pancreatic islets and INS-1 cells were used. Given the complexity of pancreatic islets compared to cultured cells and the fact that pancreatic islets are continuously exposed to molecules from PGC-1α/β-FAT-DKO mice, isolated pancreatic islets would be a preferred model for being closer to reality. This would contribute to shed some light on the effects that resistin has on β-cells.

To conclude, in this work we have shown that specific deletion of PGC-1 co-activators in adipose tissues leads to a decrease in mitochondrial function both in WAT and BAT. Despite this, BAT from PGC-1α/β-FAT-DKO mice display a more severe phenotype, especially when fed a HFD60. In fact, impaired non-shivering thermogenesis is accompanied by the "whitening" of BAT in these mice, characterised by the accumulation of fat in brown adipocytes and the acquisition of a WAT-like phenotype. When fed a HFD60, PGC-1α/β-FAT-DKO mice gain more body and adipose tissue weight than Wt mice. Moreover, they are glucose intolerance independently from body weight. Although PGC-1α/β-FAT-DKO mice preserve insulin tolerance, they present lower basal and glucose-stimulated insulin levels compared to control mice. To evaluate the pancreatic mechanisms driving this reduction, we have assessed pancreatic islets as well as pancreatic β-cells. However, it is still unclear whether pancreatic islets from PGC-1α/β-FAT-DKO mice secrete less insulin than those from

Wt mice and the molecular and cellular mechanisms involved. Irrespectively of this, BAT secretome, but not WAT, is altered in PGC-1α/β-FAT-DKO mice, identifying up to 126 proteins with the potential to mediate the BAT-pancreatic crosstalk and impact pancreatic function. Amongst these proteins, at least 3 are altered in serum from these mice, but resistin does not seem to influence, solely, pancreatic functionality, at least based on our experiment with cultured INS-1 cells.

Further studies are needed to explore the effects that resistin, kininogen-1 and fibrinogen gamma chain have on insulin secretion. Moreover, the remaining proteins from BAT secretome that have still not been evaluated in serum from PGC-1α/β-FAT-DKO will need to be measured. Irrespectively of this, it also remains to be clarified the precise defect existing in β-cells or pancreatic islets from PGC-1α/β-FAT-DKO mice and whether interruption of the BAT-pancreatic crosstalk only affects insulin secretion or it also disrupts the response to glucose. Nevertheless, our study highlights the relevance of BAT in the control of glucose homeostasis, particularly the relevance that proteins secreted by BAT may have on the adequate function of pancreatic β-cells. The identification of the adipokines secreted by BAT that control insulin secretion opens the door to the development of new therapeutic strategies for the treatment of T2D based on the administration of modified variant of these molecules with capacity to enhance insulin secretion.

# 6. CONCLUSIONS

## 6. Conclusions

1) Lack of PGC-1 co-activators leads to a reduction in the expression of mitochondrial genes in both white and brown adipose tissue.

2) Impaired expression of mitochondrial genes in brown adipose tissue as a result of lacking PGC-1 co-activators leads to impaired thermogenesis and cold sensitivity. Despite impaired BAT function, PGC-1α/β-FAT-DKO mice do not develop obesity or show any sign of altered glucose homeostasis when fed a regular chow diet.

3) When fed with a very high caloric content from fat, PGC-1α/β-FAT-DKO male mice show a higher, although mild, increased in body weight and adiposity compared to Wt littermates.

4) Both male and female PGC-1α/β-FAT-DKO mice develop, independently of body weight, severe glucose intolerance when fed a high fat diet, but maintain similar insulin sensitivity than Wt littermates.

5) Glucose intolerance in PGC-1α/β-FAT-DKO mice appears to be the result of an impaired capacity of pancreatic β-cells to secrete insulin under basal and glucose-stimulated conditions.

6) Despite lower insulin secretion, morphometric analysis of pancreas revealed no differences between Wt and PGC-1α/β-FAT-DKO mice in the density of islets, α-, β- or δ-cell mass, or the maturation of insulin granules.

7) Similarly, no differences were found between Wt and PGC-1α/β-FAT-DKO mice in the expression of genes involved in pathways related with normal or pathogenic secretion of insulin, including β-cell maturation, mitochondrial function, insulin synthesis and secretion or the unfolded protein response.

8) Untargeted proteomic analysis of the secretome from adipose tissue explants revealed that lack of PGC-1 co-activators in adipocytes severely affects the secretory activity of brown adipose tissue, but has a minor impact on the secretome of white adipose tissues.

9) An enrichment analysis proteins revealed that most of the differentially secreted by brown adipose tissue of PGC-1α/β-FAT-DKO mice fit into the categories of proteins related to the extracellular matrix, complement activation or immune response.

10) Targeted proteomics in serum identified 3 potential candidates (resistin, kininigen-1 and figronectin gamma chain) to mediate the crosstalk between brown adipose tissue and β-cells that could be accountable for the decrease insulin secretion and glucose intolerance observed in PGC-1α/β-FAT-DKO mice.

11) Treatment of cultured INS-1 β-cells with resistin increases basal insulin secretion but it does not affect glucose-stimulated insulin secretion. On this basis, it is unlikely that resistin is the molecule responsible for the pancreatic phenotype observed in PGC-1α/β-FAT-DKO mice.

# 7. REFERENCES

## 7. References


1. WHO. Overweight and Obesity [Internet]. 2021. p. 1–2. Available from: https://www.who.int/news-room/fact-sheets/detail/obesity-and-overweight.
2. CDC. Health Effects of Overweight & Obesity [Internet]. 2022. Available from: https://www.cdc.gov/healthyweight/effects/index.html.
3. IDF Diabetes Atlas [Internet]. 2022. Available from: https://diabetesatlas.org/.
4. Barbeau WE. What is the key environmental trigger in type 1 diabetes – Is it viruses, or wheat gluten, or both? Autoimmunity Reviews. 2012; 12(2): 295-299.
5. Oboza P, Ogarek N, Olszanecka-Glinianowicz M, Kocelak P. Can type 1 diabetes be an unexpected complication of obesity? Front Endocrinol (Lausanne). 2023; 14: 1121303.
6. NHS. Overview: gestational diabetis [Internet]. 2022. Available from: https://www.nhs.uk/conditions/gestational-diabetes/.
7. Chatterjee S, Khunti K, Davies MJ. Type 2 diabetes. The Lancet. 2017; 389: 2239-2251.
8. Galicia-Garcia U, Benito-Vicente A, Jebari S, Larrea-Sebal A, Siddiqi H, Uribe K, Ostolaza H, Martín C. Pathophysiology of Type 2 Diabetes Mellitus. Int J Mol Sci. 2020; 21: 6275-6309.
9. Kojta I, Chacińska M, Blachnio-Zabielska A. Obesity, Bioactive Lipids, and Adipose Tissue Inflammation in Insulin Resistance. Nutrients. 2020; 12(5): 1305-1324.
10. Christensen AA, Gannon M. The Beta Cell in Type 2 Diabetes. Curr Diab. Rep. 2019; 19(81).
11. Cerf ME. Beta cell dysfunction and insulin resistance. Front Endocrinol (Lausanne). 2013; 4(37).
12. Wang L, Yu X, Xu X, Ming J, Wang Z, Gao B, Xing Y, Zhou J, Fu J, Liu T, Liu X, Garstka MA, Wang X, Ji Q. The Fecal Microbiota Is Already Altered in Normoglycemic Individuals Who Go on to Have Type 2 Diabetes. Front Cell Infect. Microbiol. 2021; 11: 598672.
13. Dreisbach C, Prescott S, Alhusen J, Dudley D, Trinchieri G, Siega-Riz AM. Association between microbial composition, diversity, and function of the maternal gastrointestinal microbiome with impaired glucose tolerance on the glucose challenge test. PLoS One. 2022; 17(12): e0271261.
14. Wu Z, Zhang B, Chen F, Xia R, Zhu D, Chen B, Lin A, Zheng C, Hou D, Li X, Zhang S, Chen Y, Hou K. Fecal microbiota transplantation reverses insulin resistance in type 2 diabetes: A randomized, controlled, prospective study. Front Cell Infect Microbiol. 2023; 12: 1089991.
15. Samuel VT, Shulman GI. Mechanisms for insulin resistance: common threads and missing links. Cell. 2012; 148(5): 852-71.
16. Da Silva Rosa SC, Nayak N, Caymo AM, Gordon JW. Mechanisms of muscle insulin resistance and the cross-talk with liver and adipose tissue. Physiol Rep. 2020; 8(19): e14607.

17. Zamora M, Villena JA. Targeting mitochondrial biogenesis to treat insulin resistance. Curr Pharm Des. 2014; 20(35): 5527-57.

18. Muoio DM, Newgard CB. Mechanisms of disease: Molecular and metabolic mechanisms of insulin resistance and beta-cell failure in type 2 diabetes. Nat Rev Mol Cell Biol. 2008; 9(3): 193-205.

19. Bunout D, Muñoz C, López M, de la Maza MP, Schlesinger L, Hirsch S, Pettermann M. Interleukin 1 and tumor necrosis factor in obese alcoholics compared with normal-weight patients. Am J Clin Nutr. 1996; 63(3): 373-6.

20. Yudkin JS, Kumari M, Humphries SE, Mohamed-Ali V. Inflammation, obesity, stress and coronary heart disease: is interleukin-6 the link? Atherosclerosis. 2000; 148(2): 209-14.

21. Hotamisligil GS, Shargill NS, Spiegelman BM. Adipose expression of tumor necrosis factor-alpha: direct role in obesity-linked insulin resistance. Science. 1993; 259(5091): 87-91.

22. Weisberg SP, Hunter D, Huber R, Lemieux J, Slaymaker S, Vaddi K, Charo I, Leibel RL, Ferrante AW Jr. CCR2 modulates inflammatory and metabolic effects of high-fat feeding. J Clin Invest. 2006; 116(1): 115-24.

23. Lee SH, Park SY, Choi CS. Insulin Resistance: From Mechanisms to Therapeutic Strategies. Diabetes Metab J. 2022; 46(1): 15-37.

24. Read A, Schröder M. The Unfolded Protein Response: An Overview. Biology (Basel). 2021; 10(5): 384.

25. Ozcan U, Cao Q, Yilmaz E, Lee AH, Iwakoshi NN, Ozdelen E, Tuncman G, Görgün C, Glimcher LH, Hotamisligil GS. Endoplasmic reticulum stress links obesity, insulin action, and type 2 diabetes. Science. 2004; 306(5695): 457-61.

26. Gregor MF, Yang L, Fabbrini E, Mohammed BS, Eagon JC, Hotamisligil GS, Klein S. Endoplasmic reticulum stress is reduced in tissues of obese subjects after weight loss. Diabetes. 2009; 58(3): 693-700.

27. Aguirre V, Uchida T, Yenush L, Davis R, White MF. The c-Jun NH(2)-terminal kinase promotes insulin resistance during association with insulin receptor substrate-1 and phosphorylation of Ser(307). J Biol Chem. 2000; 275(12): 9047-54.

28. Ohoka N, Yoshii S, Hattori T, Onozaki K, Hayashi H. TRB3, a novel ER stress-inducible gene, is induced via ATF4-CHOP pathway and is involved in cell death. EMBO J. 2005; 24(6): 1243-55.

29. Wang D, Wei Y, Pagliassotti MJ. Saturated fatty acids promote endoplasmic reticulum stress and liver injury in rats with hepatic steatosis. Endocrinology. 2006; 147(2): 943-51.

30. Choo HJ, Kim JH, Kwon OB, Lee CS, Mun JY, Han SS, Yoon YS, Yoon G, Choi KM, Ko YG. Mitochondria are impaired in the adipocytes of type 2 diabetic mice. Diabetologia. 2006; 49(4):784-91.

31. Raffaella C, Francesca B, Italia F, Marina P, Giovanna L, Susanna I. Alterations in hepatic mitochondrial compartment in a model of obesity and insulin resistance. Obesity (Silver Spring). 2008; 16(5): 958-64.

32. Kelley DE, He J, Menshikova EV, Ritov VB. Dysfunction of mitochondria in human skeletal muscle in type 2 diabetes. Diabetes. 2002; 51(10): 2944-50.

33. Jheng HF, Tsai PJ, Guo SM, Kuo LH, Chang CS, Su IJ, Chang CR, Tsai YS. Mitochondrial fission contributes to mitochondrial dysfunction and insulin resistance in skeletal muscle. Mol Cell Biol. 2012; 32(2): 309-19.

34. Bach D, Pich S, Soriano FX, Vega N, Baumgartner B, Oriola J, Daugaard JR, Lloberas J, Camps M, Zierath JR, Rabasa-Lhoret R, Wallberg-Henriksson H, Laville M, Palacín M, Vidal H, Rivera F, Brand M, Zorzano A. Mitofusin-2 determines mitochondrial network architecture and mitochondrial metabolism. A novel regulatory mechanism altered in obesity. J Biol Chem. 2003; 278(19): 17190-7.

35. Goldstein BJ, Mahadev K, Wu X, Zhu L, Motoshima H. Role of insulin-induced reactive oxygen species in the insulin signaling pathway. Antioxid Redox Signal. 2005; 7(7-8):1 021-31.

36. Pardo R, Vilà M, Cervela L, de Marco M, Gama-Pérez P, González-Franquesa A, Statuto L, Vilallonga R, Simó R, Garcia-Roves PM, Villena JA. Calorie restriction prevents diet-induced insulin resistance independently of PGC-1-driven mitochondrial biogenesis in white adipose tissue. FASEB J. 2019; 33(2): 2343-2358.

37. Overton DL, Mastracci TL. Exocrine-Endocrine Crosstalk: The Influence of Pancreatic Cellular Communications on Organ Growth, Function and Disease. Front Endocrinol (Lausanne). 2022; 13: 904004.

38. Karpińska M, Czauderna M. Pancreas-Its Functions, Disorders, and Physiological Impact on the Mammals' Organism. Front Physiol. 2022; 13: 807632.

39. El-Gohary Y, Gittes G. Structure of Islets and Vascular Relationship to the Exocrine Pancreas. Pancreapedia. 2018.

40. Xavier GDS. The Cells of the Islets of Langerhans. J Clin Med. 2018; 7(54).

41. Ionescu-Tirgoviste C, Gagniuc PA, Gubceac E, Mardare L, Popescu I, Dima S, Militaru M. A 3D map of the islet routes throughout the healthy human pancreas. Sci Rep. 2015; 5: 14634.

42. Steiner DJ, Kim A, Miller K, Hara M. Pancreatic islet plasticity: interspecies comparison of islet architecture and composition. Islets. 2010; 2(3): 135-45.

43. Kim A, Miller K, Jo J, Kilimnik G, Wojcik P, Hara M. Islet architecture: A comparative study. Islets. 2009; 1(2): 129-36.

44. Dybala MP, Hara M. Heterogeneity of the Human Pancreatic Islet. Diabetes. 2019; 68(6): 1230-1239.

45. Ravi PK, Singh SR, Mishra PR. Redefining the tail of pancreas based on the islets microarchitecture and inter-islet distance: An immunohistochemical study. Medicine (Baltimore). 2021; 100(17): e25642.

46. Walker JT, Saunders DC, Brissova M, Powers AC. The Human Islet: Mini-Organ With Mega-Impact. Endocr Rev. 2021; 42(5): 605-657.

47. Ehses JA, Perren A, Eppler E, Ribaux P, Pospisilik JA, Maor-Cahn R, Gueripel X, Ellingsgaard H, Schneider MK, Biollaz G, Fontana A, Reinecke M, Homo-Delarche F, Donath MY. Increased number of islet-associated macrophages in type 2 diabetes. Diabetes. 2007; 56(9): 2356-70.

48. Radenkovic M, Uvebrant K, Skog O, Sarmiento L, Avartsson J, Storm P, Vickman P, Bertilsson PA, Fex M, Korgsgren O, Cilio CM. Characterization of resident lymphocytes in human pancreatic islets. Clin Exp Immunol. 201; 187(3): 418-427.

49. Pan FC, Brissova M. Pancreas development in humans. Curr Opin Endocrinol Diabetes Obes. 2014; 21(2): 77-82.

50. Marchetti P, Bugliani M, De Tata V, Suleiman M, Marselli L. Pancreatic Beta Cell Identity in Humans and the Role of Type 2 Diabetes. Front Cell Dev Biol. 2017; 5: 55.

51. Yesil P, Lammert E. Islet dynamics: a glimpse at beta cell proliferation. Histol Histopathol. 2008; 23(7): 883-95.

52. Dor Y, Brown J, Martinez OI, Melton DA. Adult pancreatic beta-cells are formed by self-duplication rather than stem-cell differentiation. Nature. 2004; 429(6987): 41-6.

53. Montanya E, Nacher V, Biarnés M, Soler J. Linear correlation between beta-cell mass and body weight throughout the lifespan in Lewis rats: role of beta-cell hyperplasia and hypertrophy. Diabetes. 2000; 49(8): 1341-6.

54. Hunter CS, Stein RW. Evidence for Loss in Identity, De-Differentiation, and Trans-Differentiation of Islet β-Cells in Type 2 Diabetes. Front Genet. 2017; 8: 35.

55. Bensellam M, Jonas JC, Laybutt DR. Mechanisms of β-cell dedifferentiation in diabetes: recent findings and future research directions. J Endocrinol. 2018; 236(2): R109-R143.

56. Ben-Othman N, Vieira A, Courtney M, Record F, Gjernes E, Avolio F, Hadzic B, Druelle N, Napolitano T, Navarro-Sanz S, Silvano S, Al-Hasani K, Pfeifer A, Lacas-Gervais S, Leuckx G, Marroquí L, Thévenet J, Madsen OD, Eizirik DL, Heimberg H, Kerr-Conte J, Pattou F, Mansouri A, Collombat P. Long-Term GABA Administration Induces Alpha Cell-Mediated Beta-like Cell Neogenesis. Cell. 2017; 168(1-2): 73-85.e11.

57. Hauge-Evans AC, King AJ, Carmignac D, Richardson CC, Robinson IC, Low MJ, Christie MR, Persaud SJ, Jones PM. Somatostatin secreted by islet delta-cells fulfills multiple roles as a paracrine regulator of islet function. Diabetes. 2009; 58(2): 403-11.

58. Zhang J, McKenna LB, Bogue CW, Kaestner KH. The diabetes gene Hhex maintains δ-cell differentiation and islet function. Genes Dev. 2014; 28(8): 829-34.

59. Chera S, Baronnier D, Ghila L, Cigliola V, Jensen JN, Gu G, Furuyama K, Thorel F, Gribble FM, Reimann F, Herrera PL. Diabetes recovery by age-dependent conversion of pancreatic δ-cells into insulin producers. Nature. 2014; 514(7523): 503-7.

60. Holzer P, Reichmann F, Farzi A. Neuropeptide Y, peptide YY and pancreatic polypeptide in the gut-brain axis. Neuropeptides. 2012; 46(6): 261-74.

61. Brereton MF, Vergari E, Zhang Q, Clark A. Alpha-, Delta- and PP-cells: Are They the Architectural Cornerstones of Islet Structure and Co-ordination? J Histochem Cytochem. 2015; 63(8): 575-91.

62. Rorsman P, Ashcroft FM. Pancreatic β-Cell Electrical Activity and Insulin Secretion: Of Mice and Men. Physiol Rev. 2018; 98(1): 117-214.

63. Balch WE, McCaffery JM, Plutner H, Farquhar MG. Vesicular stomatitis virus glycoprotein is sorted and concentrated during export from the endoplasmic reticulum. Cell. 1994; 76(5): 841-52.

64. Hou JC, Min L, Pessin JE. Insulin granule biogenesis, trafficking and exocytosis. Vitam Horm. 2009; 80: 473-506.

65. McCulloch LJ, van de Bunt M, Braun M, Frayn KN, Clark A, Gloyn AL. GLUT2 (SLC2A2) is not the principal glucose transporter in human pancreatic beta cells: implications for understanding genetic association signals at this locus. Mol Genet Metab. 2011; 104(4): 648-53.

66. Prentki M, Matschinsky FM, Madiraju SR. Metabolic signaling in fuel-induced insulin secretion. Cell Metab. 2013; 18(2): 162-85.

67. Olofsson CS, Göpel SO, Barg S, Galvanovskis J, Ma X, Salehi A, Rorsman P, Eliasson L. Fast insulin secretion reflects exocytosis of docked granules in mouse pancreatic B-cells. Pflugers Arch. 2002; 444(1-2): 43-51.

68. Yang J, Chi Y, Burkhardt BR, Guan Y, Wolf BA. Leucine metabolism in regulation of insulin secretion from pancreatic beta cells. Nutr Rev. 2010; 68(5): 270-9.

69. Kotarsky K, Nilsson NE, Flodgren E, Owman C, Olde B. A human cell surface receptor activated by free fatty acids and thiazolidinedione drugs. Biochem Biophys Res Commun. 2003; 301(2): 406-10.

70. Chueire VB, Muscelli E. Effect of free fatty acids on insulin secretion, insulin sensitivity and incretin effect - a narrative review. Arch Endocrinol Metab. 2021; 65(1): 24-31.

71. Bollheimer LC, Skelly RH, Chester MW, McGarry JD, Rhodes CJ. Chronic exposure to free fatty acid reduces pancreatic beta cell insulin content by increasing basal insulin secretion that is not compensated for by a corresponding increase in proinsulin biosynthesis translation. J Clin Invest. 1998; 101(5): 1094-101.

72. Ježek P, Jabůrek M, Holendová B, Plecitá-Hlavatá L. Fatty Acid-Stimulated Insulin Secretion vs. Lipotoxicity. Molecules. 2018; 23(6): 1483.

73. Kailey B, van de Bunt M, Cheley S, Johnson PR, MacDonald PE, Gloyn AL, Rorsman P, Braun M. SSTR2 is the functionally dominant somatostatin receptor in human pancreatic β- and α-cells. Am J Physiol Endocrinol Metab. 2012; 303(9): E1107-16.

74. Park SH, Ryu SY, Yu WJ, Han YE, Ji YS, Oh K, Sohn JW, Lim A, Jeon JP, Lee H, Lee KH, Lee SH, Berggren PO, Jeon JH, Ho WK. Leptin promotes K(ATP) channel trafficking by AMPK signaling in pancreatic β-cells. Proc Natl Acad Sci U S A. 2013; 110(31): 12673-8.

75. Capozzi ME, Wait JB, Koech J, Gordon AN, Coch RW, Svendsen B, Finan B, D'Alessio DA, Campbell JE. Glucagon lowers glycemia when β-cells are active. JCI Insight. 2019; 5(16): e129954.

76. Song G, Pacini G, Ahrén B, D'Argenio DZ. Glucagon increases insulin levels by stimulating insulin secretion without effect on insulin clearance in mice. Peptides. 2017; 88: 74-79.

77. Garzilli I, Itzkovitz S. Design principles of the paradoxical feedback between pancreatic alpha and beta cells. Sci Rep. 2018; 8(1): 10694.

78. Hatting M, Tavares CDJ, Sharabi K, Rines AK, Puigserver P. Insulin regulation of gluconeogenesis. Ann N Y Acad Sci. 2018; 1411(1): 21-35.

79. Röder PV, Wu B, Liu Y, Han W. Pancreatic regulation of glucose homeostasis. Exp Mol Med. 2016; 48(3): e219.

80. Rahman MS, Hossain KS, Das S, Kundu S, Adegoke EO, Rahman MA, Hannan MA, Uddin MJ, Pang MG. Role of Insulin in Health and Disease: An Update. Int J Mol Sci. 2021; 22(12): 6403.

81. Malekzadeh BÖ, Erlandsson MC, Tengvall P, Palmquist A, Ransjo M, Bokarewa MI, Westerlund A. Effects of implant-delivered insulin on bone formation in osteoporotic rats. J Biomed Mater Res A. 2018; 106(9): 2472-2480.

82. Singh S, Sharma R, Kumari M, Tiwari S. Insulin receptors in the kidneys in health and disease. World J Nephrol. 2019; 8(1): 11-22.

83. Fonseca VA. Defining and characterizing the progression of type 2 diabetes. Diabetes Care. 2009; 32 Suppl 2(Suppl 2): S151-6.

84. Rahier J, Guiot Y, Goebbels RM, Sempoux C, Henquin JC. Pancreatic beta-cell mass in European subjects with type 2 diabetes. Diabetes Obes Metab. 2008; 10 Suppl 4: 32-42.

85. Weyer C, Tataranni PA, Bogardus C, Pratley RE. Insulin resistance and insulin secretory dysfunction are independent predictors of worsening of glucose tolerance during each stage of type 2 diabetes development. Diabetes Care. 2001; 24(1): 89-94.

86. Anello M, Lupi R, Spampinato D, Piro S, Masini M, Boggi U, Del Prato S, Rabuazzo AM, Purrello F, Marchetti P. Functional and morphological alterations of mitochondria in pancreatic beta cells from type 2 diabetic patients. Diabetologia. 2005; 48(2): 282-9.

87. Gandasi NR, Yin P, Omar-Hmeadi M, Ottosson Laakso E, Vikman P, Barg S. Glucose-Dependent Granule Docking Limits Insulin Secretion and Is Decreased in Human Type 2 Diabetes. Cell Metab. 2018; 27(2): 470-478.e4.

88. Wang W, Zhang C. Targeting β-cell dedifferentiation and transdifferentiation: opportunities and challenges. Endocr Connect. 2021; 10(8): R213-R228.

89. Quesada I, Tudurí E, Ripoll C, Nadal A. Physiology of the pancreatic alpha-cell and glucagon secretion: role in glucose homeostasis and diabetes. J Endocrinol. 2008 Oct;199(1): 5-19.

90. Knudsen JG, Hamilton A, Ramracheya R, Tarasov AI, Brereton M, Haythorne E, Chibalina MV, Spégel P, Mulder H, Zhang Q, Ashcroft FM, Adam J, Rorsman P. Dysregulation of Glucagon Secretion by Hyperglycemia-Induced Sodium-Dependent Reduction of ATP Production. Cell Metab. 2019; 29(2): 430-442.e4.

91. Rosen ED, Spiegelman BM. What we talk about when we talk about fat. Cell. 2014; 156(1-2): 20-44.

92. Gesta S, Kahn CR. Adipose Tissue Biology: Chapter 4. Springer. 2012.

93. Chait A, den Hartigh LJ. Adipose Tissue Distribution, Inflammation and Its Metabolic Consequences, Including Diabetes and Cardiovascular Disease. Front Cardiovasc Med. 2020; 7:22.

94. Karastergiou K, Fried SK. Cellular Mechanisms Driving Sex Differences in Adipose Tissue Biology and Body Shape in Humans and Mouse Models. Adv Exp Med Biol. 2017; 1043: 29-51.

95. Item F, Konrad D. Visceral fat and metabolic inflammation: the portal theory revisited. Obes Rev. 2012; 13 Suppl 2: 30-9.

96. Laurencikiene J, Skurk T, Kulyté A, Hedén P, Aström G, Sjölin E, Rydén M, Hauner H, Arner P. Regulation of lipolysis in small and large fat cells of the same subject. J Clin Endocrinol Metab. 2011; 96(12): E2045-9.

97. Scheja L, Heeren J. The endocrine function of adipose tissues in health and cardiometabolic disease. Nat Rev Endocrinol. 2019; 15(9): 507-524.

98. Pan WW, Myers MG Jr. Leptin and the maintenance of elevated body weight. Nat Rev Neurosci. 2018; 19(2): 95-105.

99. Friedman J. The long road to leptin. J Clin Invest. 2016; 126(12): 4727-4734.

100. Fang H, Judd RL. Adiponectin Regulation and Function. Compr Physiol. 2018; 8(3): 1031-1063.

101. Schwartz DR, Lazar MA. Human resistin: found in translation from mouse to man. Trends Endocrinol Metab. 2011; 22(7): 259-65.

102. Bing C. Is interleukin-1β a culprit in macrophage-adipocyte crosstalk in obesity? Adipocyte. 2015; 4(2): 149-52.

103. Nishio M, Saeki K. The Remaining Mysteries about Brown Adipose Tissues. Cells. 2020; 9(11): 2449.

104. Shinde AB, Song A, Wang QA. Brown Adipose Tissue Heterogeneity, Energy Metabolism, and Beyond. Front Endocrinol (Lausanne). 2021; 12: 651763.

105. Virtanen KA, Lidell ME, Orava J, Heglind M, Westergren R, Niemi T, Taittonen M, Laine J, Savisto NJ, Enerbäck S, Nuutila P. Functional brown adipose tissue in healthy adults. N Engl J Med. 2009; 360(15): 1518-25.

106. Van Marken Lichtenbelt WD, Vanhommerig JW, Smulders NM, Drossaerts JM, Kemerink GJ, Bouvy ND, Schrauwen P, Teule GJ. Cold-activated brown adipose tissue in healthy men. N Engl J Med. 2009; 360(15): 1500-8.

107. Hadi M, Chen CC, Whatley M, Pacak K, Carrasquillo JA. Brown fat imaging with (18)F-6-fluorodopamine PET/CT, (18)F-FDG PET/CT, and (123)I-MIBG SPECT: a study of patients being evaluated for pheochromocytoma. J Nucl Med. 2007; 48(7): 1077-83.

108. De Jong JM, Larsson O, Cannon B, Nedergaard J. A stringent validation of mouse adipose tissue identity markers. Am J Physiol Endocrinol Metab. 2015; 308(12): E1085-105.

109. Townsend KL, Tseng YH. Of mice and men: novel insights regarding constitutive and recruitable brown adipocytes. Int J Obes Suppl. 2015; 5(Suppl 1): S15-20.

110. Gaspar RC, Pauli JR, Shulman GI, Muñoz VR. Browning and Beiging of Adipose Tissue: Its Role in the Regulation of Energy Homeostasis and as a Potential Target for Alleviating Metabolic Diseases. Am J Physiol Endocrinol Metab. 2021; 320: E488-E495.

111. Park J, Shin S, Liu L, Jahan I, Ong SG, Xu P, Berry DC, Jiang Y. Progenitor-like characteristics in a subgroup of UCP1+ cells within white adipose tissue. Dev Cell. 2021; 56(7): 985-999.e4.

112. Shao M, Wang QA, Song A, Vishvanath L, Busbuso NC, Scherer PE, Gupta RK. Cellular Origins of Beige Fat Cells Revisited. Diabetes. 2019; 68(10): 1874-1885.

113. Speakman JR, Keijer J. Not so hot: Optimal housing temperatures for mice to mimic the thermal environment of humans. Mol Metab. 2012; 2(1): 5-9.

114. Villena JA. Brown Adipose Tissue and Control of Body Weight: A New Potential Target for the Treatment of Obesity. 2008.

115. Carpentier AC, Blondin DP, Haman F, Richard D. Brown Adipose Tissue-A Translational Perspective. Endocr Rev. 2023; 44(2): 143-192.

116. McNeill BT, Morton NM, Stimson RH. Substrate Utilization by Brown Adipose Tissue: What's Hot and What's Not? Front Endocrinol (Lausanne). 2020; 11: 571659.

117. Schulz TJ, Tseng YH. Brown adipose tissue: development, metabolism and beyond. Biochem J. 2013; 453(2): 167-78.

118. Villena JA. New insights into PGC-1 co-activators: redefining their role in the regulation of mitochondrial function and beyond. FEBS J. 2015; 282(4): 647-72.

119. Chang JS, Fernand V, Zhang Y, Shin J, Jun HJ, Joshi Y, Gettys TW. NT-PGC-1α protein is sufficient to link β3-adrenergic receptor activation to transcriptional and physiological components of adaptive thermogenesis. J Biol Chem. 2012; 287(12): 9100-11.

120. Lin J, Yang R, Tarr PT, Wu PH, Handschin C, Li S, Yang W, Pei L, Uldry M, Tontonoz P, Newgard CB, Spiegelman BM. Hyperlipidemic effects of dietary saturated fats mediated through PGC-1beta coactivation of SREBP. Cell. 2005; 120(2): 261-73.

121. Andersson U, Scarpulla RC. Pgc-1-related co-activator, a novel, serum-inducible co-activator of nuclear respiratory factor 1-dependent transcription in mammalian cells. Mol Cell Biol. 2001; 21(11): 3738-49.

122. Vercauteren K, Gleyzer N, Scarpulla RC. Short hairpin RNA-mediated silencing of PRC (PGC-1-related co-activator) results in a severe respiratory chain deficiency associated with the proliferation of aberrant mitochondria. J Biol Chem. 2009; 284(4): 2307-19.

123. Puigserver P, Wu Z, Park CW, Graves R, Wright M, Spiegelman BM. A cold-inducible co-activator of nuclear receptors linked to adaptive thermogenesis. Cell. 1998; 92(6): 829-39.

124. Pardo R, Enguix N, Lasheras J, Feliu JE, Kralli A, Villena JA. Rosiglitazone-induced mitochondrial biogenesis in white adipose tissue is independent of peroxisome proliferator-activated receptor γ co-activator-1α. PLoS One. 2011; 6(11): e26989.

125. Zechner C, Lai L, Zechner JF, Geng T, Yan Z, Rumsey JW, Collia D, Chen Z, Wozniak DF, Leone TC, Kelly DP. Total skeletal muscle PGC-1 deficiency uncouples mitochondrial derangements from fiber type determination and insulin sensitivity. Cell Metab. 2010; 12(6): 633-42.

126. Uldry M, Yang W, St-Pierre J, Lin J, Seale P, Spiegelman BM. Complementary action of the PGC-1 co-activators in mitochondrial biogenesis and brown fat differentiation. Cell Metab. 2006; 3(5): 333-41.

127. Zamora M, Pardo R, Villena JA. Pharmacological induction of mitochondrial biogenesis as a therapeutic strategy for the treatment of type 2 diabetes. Biochem Pharmacol. 2015; 98(1): 16-28.

128. Blesa JR, Prieto-Ruiz JA, Abraham BA, Harrison BL, Hegde AA, Hernández-Yago J. NRF-1 is the major transcription factor regulating the expression of the human TOMM34 gene. Biochem Cell Biol. 2008; 86(1): 46-56.

129. Villena JA, Viñas O, Mampel T, Iglesias R, Giralt M, Villarroya F. Regulation of mitochondrial biogenesis in brown adipose tissue: nuclear respiratory factor-2/GA-binding protein is responsible for the transcriptional regulation of the gene for the mitochondrial ATP synthase beta subunit. Biochem J. 1998; 331 ( Pt 1)(Pt 1): 121-7.

130. Gleyzer N, Vercauteren K, Scarpulla RC. Control of mitochondrial transcription specificity factors (TFB1M and TFB2M) by nuclear respiratory factors (NRF-1 and NRF-2) and PGC-1 family co-activators. Mol Cell Biol. 2005; 25(4): 1354-66.

131. Gulick T, Cresci S, Caira T, Moore DD, Kelly DP. The peroxisome proliferator-activated receptor regulates mitochondrial fatty acid oxidative enzyme gene expression. Proc Natl Acad Sci U S A. 1994; 91(23): 11012-6.

132. Rong JX, Qiu Y, Hansen MK, Zhu L, Zhang V, Xie M, Okamoto Y, Mattie MD, Higashiyama H, Asano S, Strum JC, Ryan TE. Adipose mitochondrial biogenesis is suppressed in db/db and high-fat diet-fed mice and improved by rosiglitazone. Diabetes. 2007; 56(7): 1751-60.

133. Patti ME, Butte AJ, Crunkhorn S, Cusi K, Berria R, Kashyap S, Miyazaki Y, Kohane I, Costello M, Saccone R, Landaker EJ, Goldfine AB, Mun E, DeFronzo R, Finlayson J, Kahn CR, Mandarino LJ. Coordinated reduction of genes of oxidative metabolism in humans with insulin resistance and diabetes: Potential role of PGC-1 and NRF1. Proc Natl Acad Sci U S A. 2003; 100(14): 8466-71.

134. Mootha VK, Lindgren CM, Eriksson KF, Subramanian A, Sihag S, Lehar J, Puigserver P, Carlsson E, Ridderstråle M, Laurila E, Houstis N, Daly MJ, Patterson N, Mesirov JP, Golub TR, Tamayo P, Spiegelman B, Lander ES, Hirschhorn JN, Altshuler D, Groop LC. PGC-1alpha-responsive genes involved in oxidative phosphorylation are coordinately down-regulated in human diabetes. Nat Genet. 2003; 34(3): 267-73.

135. Hara K, Tobe K, Okada T, Kadowaki H, Akanuma Y, Ito C, Kimura S, Kadowaki T. A genetic variation in the PGC-1 gene could confer insulin resistance and susceptibility to Type II diabetes. Diabetologia. 2002; 45(5): 740-3.

136. Vimaleswaran KS, Radha V, Ghosh S, Majumder PP, Deepa R, Babu HN, Rao MR, Mohan V. Peroxisome proliferator-activated receptor-gamma co-activator-1alpha (PGC-1alpha) gene polymorphisms and their relationship to Type 2 diabetes in Asian Indians. Diabet Med. 2005; 22(11): 1516-21.

137. Villegas R, Williams SM, Gao YT, Long J, Shi J, Cai H, Li H, Chen CC, Tai ES; AGEN-T2D Consortium; Hu F, Cai Q, Zheng W, Shu XO. Genetic variation in the peroxisome proliferator-activated receptor (PPAR) and peroxisome proliferator-activated receptor gamma co-activator 1 (PGC-1) gene families and type 2 diabetes. Ann Hum Genet. 2014; 78(1): 23-32.

138. Kleiner S, Mepani RJ, Laznik D, Ye L, Jurczak MJ, Jornayvaz FR, Estall JL, Chatterjee Bhowmick D, Shulman GI, Spiegelman BM. Development of insulin resistance in mice lacking PGC-1α in adipose tissues. Proc Natl Acad Sci U S A. 2012; 109(24): 9635-40.

139. Handschin C, Chin S, Li P, Liu F, Maratos-Flier E, Lebrasseur NK, Yan Z, Spiegelman BM. Skeletal muscle fiber-type switching, exercise intolerance, and myopathy in PGC-1alpha muscle-specific knock-out animals. J Biol Chem. 2007; 282(41): 30014-21.

140. Handschin C, Choi CS, Chin S, Kim S, Kawamori D, Kurpad AJ, Neubauer N, Hu J, Mootha VK, Kim YB, Kulkarni RN, Shulman GI, Spiegelman BM. Abnormal glucose homeostasis in skeletal muscle-specific PGC-1alpha knockout mice reveals skeletal muscle-pancreatic beta cell crosstalk. J Clin Invest. 2007; 117(11): 3463-74.

141. Choi CS, Befroy DE, Codella R, Kim S, Reznick RM, Hwang YJ, Liu ZX, Lee HY, Distefano A, Samuel VT, Zhang D, Cline GW, Handschin C, Lin J, Petersen KF, Spiegelman BM, Shulman GI. Paradoxical effects of increased expression of PGC-1alpha on muscle mitochondrial function and insulin-stimulated muscle glucose metabolism. Proc Natl Acad Sci U S A. 2008; 105(50): 19926-31.

142. Eisele PS, Salatino S, Sobek J, Hottiger MO, Handschin C. The peroxisome proliferator-activated receptor γ co-activator 1α/β (PGC-1) co-activators repress the transcriptional activity of NF-κB in skeletal muscle cells. J Biol Chem. 2013; 288(4): 2246-60.

143. Saito M, Okamatsu-Ogura Y, Matsushita M, Watanabe K, Yoneshiro T, Nio-Kobayashi J, Iwanaga T, Miyagawa M, Kameya T, Nakada K, Kawai Y, Tsujisaki M. High incidence of metabolically active brown adipose tissue in healthy adult humans: effects of cold exposure and adiposity. Diabetes. 2009; 58(7): 1526-31.

144. Leitner BP, Huang S, Brychta RJ, Duckworth CJ, Baskin AS, McGehee S, Tal I, Dieckmann W, Gupta G, Kolodny GM, Pacak K, Herscovitch P, Cypess AM, Chen KY. Mapping of human brown adipose tissue in lean and obese young men. Proc Natl Acad Sci U S A. 2017; 114(32): 8649-8654.

145. Green AL, Bagci U, Hussein S, Kelly PV, Muzaffar R, Neuschwander-Tetri BA, Osman MM. Brown adipose tissue detected by PET/CT imaging is associated with less central obesity. Nucl Med Commun. 2017; 38(7): 629-635.

146. Jung RT, Shetty PS, James WP, Barrand MA, Callingham BA. Reduced thermogenesis in obesity. Nature. 1979; 279(5711): 322-3.

147. Shankar K, Kumar D, Gupta S, Varshney S, Rajan S, Srivastava A, Gupta A, Gupta AP, Vishwakarma AL, Gayen JR, Gaikwad AN. Role of brown adipose tissue in modulating adipose tissue inflammation and insulin resistance in high-fat diet fed mice. Eur J Pharmacol. 2019; 854: 354-364.

148. Hanssen MJ, Hoeks J, Brans B, van der Lans AA, Schaart G, van den Driessche JJ, Jörgensen JA, Boekschoten MV, Hesselink MK, Havekes B, Kersten S, Mottaghy FM, van Marken Lichtenbelt WD, Schrauwen P. Short-term cold acclimation improves insulin sensitivity in patients with type 2 diabetes mellitus. Nat Med. 2015; 21(8): 863-5.

149. Chondronikola M, Volpi E, Børsheim E, Porter C, Annamalai P, Enerbäck S, Lidell ME, Saraf MK, Labbe SM, Hurren NM, Yfanti C, Chao T, Andersen CR, Cesani F, Hawkins H, Sidossis LS. Brown adipose tissue improves whole-body glucose homeostasis and insulin sensitivity in humans. Diabetes. 2014; 63(12): 4089-99.

150. Maliszewska K, Kretowski A. Brown Adipose Tissue and Its Role in Insulin and Glucose Homeostasis. Int J Mol Sci. 2021; 22(4): 1530.

151. Villarroya J, Cereijo R, Gavaldà-Navarro A, Peyrou M, Giralt M, Villarroya F. New insights into the secretory functions of brown adipose tissue. J Endocrinol. 2019; 243(2): R19-R27.

152. Ali Khan A, Hansson J, Weber P, Foehr S, Krijgsveld J, Herzig S, Scheideler M. Comparative Secretome Analyses of Primary Murine White and Brown Adipocytes Reveal Novel Adipokines. Mol Cell Proteomics. 2018; 17(12): 2358-2370.

153. Hansen IR, Jansson KM, Cannon B, Nedergaard J. Contrasting effects of cold acclimation versus obesogenic diets on chemerin gene expression in brown and brite adipose tissues. Biochim Biophys Acta. 2014; 1841(12): 1691-9.

154. Villarroya J, Cereijo R, Giralt M, Villarroya F. Secretory Proteome of Brown Adipocytes in Response to cAMP-Mediated Thermogenic Activation. Front Physiol. 2019; 10: 67.

155. Scheele C, Wolfrum C. Brown Adipose Crosstalk in Tissue Plasticity and Human Metabolism. Endocr Rev. 2020; 41(1): 53–65.

156. Néchad M, Ruka E, Thibault J. Production of nerve growth factor by brown fat in culture: relation with the in vivo developmental stage of the tissue. Comp Biochem Physiol Comp Physiol. 1994; 107(2): 381-8.

157. Yamashita H, Sato Y, Kizaki T, Oh S, Nagasawa J, Ohno H. Basic fibroblast growth factor (bFGF) contributes to the enlargement of brown adipose tissue during cold acclimation. Pflugers Arch. 1994; 428(3-4): 352-6.

158. Asano A, Kimura K, Saito M. Cold-induced mRNA expression of angiogenic factors in rat brown adipose tissue. J Vet Med Sci. 1999; 61(4): 403-9.

159. Tseng YH, Kokkotou E, Schulz TJ, Huang TL, Winnay JN, Taniguchi CM, Tran TT, Suzuki R, Espinoza DO, Yamamoto Y, Ahrens MJ, Dudley AT, Norris AW, Kulkarni RN, Kahn CR. New role of bone morphogenetic protein 7 in brown adipogenesis and energy expenditure. Nature. 2008; 454(7207): 1000-4.

160. Villarroya F, Cereijo R, Villarroya J, Giralt M. Brown adipose tissue as a secretory organ. Nat Rev Endocrinol. 2017; 13(1): 26-35.

161. Ahmad B, Vohra MS, Saleemi MA, Serpell CJ, Fong IL, Wong EH. Brown/Beige adipose tissues and the emerging role of their secretory factors in improving metabolic health: The batokines. Biochimie. 2021; 184: 26-39.

162. Mauer J, Chaurasia B, Goldau J, Vogt MC, Ruud J, Nguyen KD, Theurich S, Hausen AC, Schmitz J, Brönneke HS, Estevez E, Allen TL, Mesaros A, Partridge L, Febbraio MA, Chawla A, Wunderlich FT, Brüning JC. Signaling by IL-6 promotes alternative activation of macrophages to limit endotoxemia and obesity-associated resistance to insulin. Nat Immunol. 2014; 15(5): 423-30.

163. Hondares E, Iglesias R, Giralt A, Gonzalez FJ, Giralt M, Mampel T, Villarroya F. Thermogenic activation induces FGF21 expression and release in brown adipose tissue. J Biol Chem. 2011; 286(15): 12983-90.

164. Giralt M, Gavaldà-Navarro A, Villarroya F. Fibroblast growth factor-21, energy balance and obesity. Mol Cell Endocrinol. 2015; 418 Pt 1: 66-73.

165. Li H, Wu G, Fang Q, Zhang M, Hui X, Sheng B, Wu L, Bao Y, Li P, Xu A, Jia W. Fibroblast growth factor 21 increases insulin sensitivity through specific expansion of subcutaneous fat. Nat Commun. 2018; 9(1): 272.

166. Laeger T, Baumeier C, Wilhelmi I, Würfel J, Kamitz A, Schürmann A. FGF21 improves glucose homeostasis in an obese diabetes-prone mouse model independent of body fat changes. Diabetologia. 2017; 60(11): 2274-2284.

167. Fisher FM, Kleiner S, Douris N, Fox EC, Mepani RJ, Verdeguer F, Wu J, Kharitonenkov A, Flier JS, Maratos-Flier E, Spiegelman BM. FGF21 regulates PGC-1α and browning of white adipose tissues in adaptive thermogenesis. Genes Dev. 2012; 26(3): 271-81.

168. Hanssen MJ, Broeders E, Samms RJ, Vosselman MJ, van der Lans AA, Cheng CC, Adams AC, van Marken Lichtenbelt WD, Schrauwen P. Serum FGF21 levels are associated with brown adipose tissue activity in humans. Sci Rep. 2015; 5: 10275.

169. Yoneshiro T, Aita S, Matsushita M, Kayahara T, Kameya T, Kawai Y, Iwanaga T, Saito M. Recruited brown adipose tissue as an antiobesity agent in humans. J Clin Invest. 2013; 123(8): 3404-8.

170. Liu X, Zheng Z, Zhu X, Meng M, Li L, Shen Y, Chi Q, Wang D, Zhang Z, Li C, Li Y, Xue Y, Speakman JR, Jin W. Brown adipose tissue transplantation improves whole-body energy metabolism. Cell Res. 2013; 23(6): 851-4.

171. Zhu Z, Spicer EG, Gavini CK, Goudjo-Ako AJ, Novak CM, Shi H. Enhanced sympathetic activity in mice with brown adipose tissue transplantation (transBATation). Physiol Behav. 2014; 125: 21-9.

172. Stanford KI, Middelbeek RJ, Townsend KL, Lee MY, Takahashi H, So K, Hitchcox KM, Markan KR, Hellbach K, Hirshman MF, Tseng YH, Goodyear LJ. A novel role for subcutaneous adipose tissue in exercise-induced improvements in glucose homeostasis. Diabetes. 2015; 64(6): 2002-14.

173. Stanford KI, Middelbeek RJ, Townsend KL, An D, Nygaard EB, Hitchcox KM, Markan KR, Nakano K, Hirshman MF, Tseng YH, Goodyear LJ. Brown adipose tissue regulates glucose homeostasis and insulin sensitivity. J Clin Invest. 2013; 123(1): 215-23.

174. White JD, Dewal RS, Stanford KI. The beneficial effects of brown adipose tissue transplantation. Mol Aspects Med. 2019; 68: 74-81.

175. Zhang Y, Fonslow BR, Shan B, Baek MC, Yates JR 3rd. Protein analysis by shotgun/bottom-up proteomics. Chem Rev. 2013; 113(4): 2343-94.

176. VerSeDa. Genome Analysis Platform - CIC bioGUNE [Internet]. 2016. Available from: http://genomics.cicbiogune.es/VerSeDa/index.php

177. Sherman BT, Hao M, Qiu J, Jiao X, Baseler MW, Lane HC, Imamichi T, Chang W. DAVID: a web server for functional enrichment analysis and functional annotation of gene lists (2021 update). Nucleic Acids Research. 2022.

178. Desiere F, Deutsch EW, King NL, Nesvizhskii AI, Mallick P, Eng J, Chen S, Eddes J, Loevenich SN, Aebersold R. The PeptideAtlas project. Nucleic Acids Res. 2006; 34(Database issue): D655-8.

179. Uhlén M, Fagerberg L, Hallström BM, Lindskog C, Oksvold P, Mardinoglu A, Sivertsson Å, Kampf C, Sjöstedt E, Asplund A, Olsson I, Edlund K, Lundberg E, Navani S, Szigyarto CA, Odeberg J, Djureinovic D, Takanen JO, Hober S, Alm T, Edqvist PH, Berling H, Tegel H, Mulder J, Rockberg J, Nilsson P, Schwenk JM, Hamsten M, von Feilitzen K, Forsberg M, Persson L, Johansson F, Zwahlen M, von Heijne G, Nielsen J, Pontén F. Proteomics. Tissue-based map of the human proteome. Science. 2015; 347(6220): 1260419.

180. Asfari M, Janjic D, Meda P, Li G, Halban PA, Wollheim CB. Establishment of 2-mercaptoethanol-dependent differentiated insulin-secreting cell lines. Endocrinology. 1992; 130(1): 167-78.

181. Hohmeier HE, Mulder H, Chen G, Henkel-Rieger R, Prentki M, Newgard CB. Isolation of INS-1-derived cell lines with robust ATP-sensitive K+ channel-dependent and -independent glucose-stimulated insulin secretion. Diabetes. 2000; 49(3): 424-30.

182. Maechler P, Kennedy ED, Sebö E, Valeva A, Pozzan T, Wollheim CB. Secretagogues modulate the calcium concentration in the endoplasmic reticulum of insulin-secreting cells. Studies in aequorin-expressing intact and permeabilized ins-1 cells. J Biol Chem. 1999; 274(18): 12583-92.

183. Rak-Mardyła A, Durak M, Lucja Gregoraszczuk E. Effects of resistin on porcine ovarian follicle steroidogenesis in prepubertal animals: an in vitro study. Reprod Biol Endocrinol. 2013; (11)45.

184. McTernan PG, Fisher FM, Valsamakis G, Chetty R, Harte A, McTernan CL, Clark PM, Smith SA, Barnett AH, Kumar S. Resistin and type 2 diabetes: regulation of resistin expression by insulin and rosiglitazone and the effects of recombinant resistin on lipid and glucose metabolism in human differentiated adipocytes. J Clin Endocrinol Metab. 2003; 88(12): 6098-106.

185. Dong ZX, Su L, Brymora J, Bird C, Xie Q, George J, Wang JH. Resistin mediates the hepatic stellate cell phenotype. World J Gastroenterol. 2013; 19(28): 4475-85.

186. Petrovic N, Walden TB, Shabalina IG, Timmons JA, Cannon B, Nedergaard J. Chronic peroxisome proliferator-activated receptor gamma (PPARgamma) activation of epididymally derived white adipocyte cultures reveals a population of thermogenically competent, UCP1-containing adipocytes molecularly distinct from classic brown adipocytes. J Biol Chem. 2010; 285(10): 7153-64.

187. Lelliott CJ, Medina-Gomez G, Petrovic N, Kis A, Feldmann HM, Bjursell M, Parker N, Curtis K, Campbell M, Hu P, Zhang D, Litwin SE, Zaha VG, Fountain KT, Boudina S, Jimenez-Linan M, Blount M, Lopez M, Meirhaeghe A, Bohlooly-Y M, Storlien L, Strömstedt M, Snaith M, Oresic M, Abel ED, Cannon B, Vidal-Puig A. Ablation of PGC-1beta results in defective mitochondrial activity, thermogenesis, hepatic function, and cardiac performance. PLoS Biol. 2006; 4(11): e369.

188. Enguix N, Pardo R, González A, López VM, Simó R, Kralli A, Villena JA. Mice lacking PGC-1β in adipose tissues reveal a dissociation between mitochondrial dysfunction and insulin resistance. Mol Metab. 2013; 2(3): 215-26.

189. Funda J, Villena JA, Bardova K, Adamcova K, Irodenko I, Flachs P, Jedlickova I, Haasova E, Rossmeisl M, Kopecky J, Janovska P. Adipose tissue-specific ablation of PGC-1β impairs thermogenesis in brown fat. Dis Model Mech. 2022; 15(4): dmm049223.

190. Cero C, Lea HJ, Zhu KY, Shamsi F, Tseng YH, Cypess AM. β3-Adrenergic receptors regulate human brown/beige adipocyte lipolysis and thermogenesis. JCI Insight. 2021; 6(11): e139160.

191. Bengtsson T, Cannon B, Nedergaard J. Differential adrenergic regulation of the gene expression of the beta-adrenoceptor subtypes beta1, beta2 and beta3 in brown adipocytes. Biochem J. 2000; 347 Pt 3(Pt 3): 643-51.

192. Bronnikov G, Houstěk J, Nedergaard J. Beta-adrenergic, cAMP-mediated stimulation of proliferation of brown fat cells in primary culture. Mediation via beta 1 but not via beta 3 adrenoceptors. J Biol Chem. 1992; 267(3): 2006-13.

193. Semple RK, Crowley VC, Sewter CP, Laudes M, Christodoulides C, Considine RV, Vidal-Puig A, O'Rahilly S. Expression of the thermogenic nuclear hormone receptor co-activator PGC-1alpha is reduced in the adipose tissue of morbidly obese subjects. Int J Obes Relat Metab Disord. 2004; 28(1): 176-9.

194. Valerio A, Cardile A, Cozzi V, Bracale R, Tedesco L, Pisconti A, Palomba L, Cantoni O, Clementi E, Moncada S, Carruba MO, Nisoli E. TNF-alpha down-regulates eNOS expression and mitochondrial biogenesis in fat and muscle of obese rodents. J Clin Invest. 2006; 116(10): 2791-8.

195. Kamei Y, Ohizumi H, Fujitani Y, Nemoto T, Tanaka T, Takahashi N, Kawada T, Miyoshi M, Ezaki O, Kakizuka A. PPARgamma co-activator 1beta/ERR ligand 1 is an ERR protein ligand, whose expression induces a high-energy expenditure and antagonizes obesity. Proc Natl Acad Sci U S A. 2003; 100(21): 12378-83.

196. Crunkhorn S, Dearie F, Mantzoros C, Gami H, da Silva WS, Espinoza D, Faucette R, Barry K, Bianco AC, Patti ME. Peroxisome proliferator activator receptor gamma co-activator-1 expression is reduced in obesity: potential pathogenic role of saturated fatty acids and p38 mitogen-activated protein kinase activation. J Biol Chem. 2007; 282(21): 15439-50.

197. Joe AW, Yi L, Even Y, Vogl AW, Rossi FM. Depot-specific differences in adipogenic progenitor abundance and proliferative response to high-fat diet. Stem Cells. 2009;27(10): 2563-70**.**

198. Supruniuk E, Mikłosz A, Chabowski A. The Implication of PGC-1α on Fatty Acid Transport across Plasma and Mitochondrial Membranes in the Insulin Sensitive Tissues. Front Physiol. 2017; 8: 923.

199. Rogers NH, Landa A, Park S, Smith RG. Aging leads to a programmed loss of brown adipocytes in murine subcutaneous white adipose tissue. Aging Cell. 2012; 11(6): 1074-83.

200. Gonçalves LF, Machado TQ, Castro-Pinheiro C, de Souza NG, Oliveira KJ, Fernandes-Santos C. Ageing is associated with brown adipose tissue remodelling and loss of white fat browning in female C57BL/6 mice. Int J Exp Pathol. 2017; 98(2): 100-108.

201. Kotzbeck P, Giordano A, Mondini E, Murano I, Severi I, Venema W, Cecchini MP, Kershaw EE, Barbatelli G, Haemmerle G, Zechner R, Cinti S. Brown adipose tissue "whitening" leads to brown adipocyte death and adipose tissue inflammation. J Lipid Res. 2018; 59(5): 784-794.

202. Cook KS, Groves DL, Min HY, Spiegelman BM. A developmentally regulated mRNA from 3T3 adipocytes encodes a novel serine protease homologue. Proc Natl Acad Sci U S A. 1985 Oct;82(19):6480-4.

203. Zhou Q, Ge Q, Ding Y, Qu H, Wei H, Wu R, Yao L, Wei Q, Feng Z, Long J, Deng H. Relationship between serum adipsin and the first phase of glucose-stimulated insulin

secretion in individuals with different glucose tolerance. J Diabetes Investig. 2018; 9(5): 1128-1134.

204. Song NJ, Kim S, Jang BH, Chang SH, Yun UJ, Park KM, Waki H, Li DY, Tontonoz P, Park KW. Small Molecule-Induced Complement Factor D (Adipsin) Promotes Lipid Accumulation and Adipocyte Differentiation. PLoS One. 2016; 11(9): e0162228.

205. Nov O, Shapiro H, Ovadia H, Tarnovscki T, Dvir I, Shemesh E, Kovsan J, Shelef I, Carmi Y, Voronov E, Apte RN, Lewis E, Haim Y, Konrad D, Bashan N, Rudich A. Interleukin-1β regulates fat-liver crosstalk in obesity by auto-paracrine modulation of adipose tissue inflammation and expandability. PLoS One. 2013; 8(1): e53626.

206. Xu H, Barnes GT, Yang Q, Tan G, Yang D, Chou CJ, Sole J, Nichols A, Ross JS, Tartaglia LA, Chen H. Chronic inflammation in fat plays a crucial role in the development of obesity-related insulin resistance. J Clin Invest. 2003; 112(12): 1821-30.

207. Fu P, Zhu R, Jia J, Hu Y, Wu C, Cieszczyk P, Holmberg HC, Gong L. Aerobic exercise promotes the functions of brown adipose tissue in obese mice via a mechanism involving COX2 in the VEGF signaling pathway. Nutr Metab (Lond). 2021; 18(1): 56.

208. Feldmann HM, Golozoubova V, Cannon B, Nedergaard J. UCP1 ablation induces obesity and abolishes diet-induced thermogenesis in mice exempt from thermal stress by living at thermoneutrality. Cell Metab. 2009; 9(2): 203-9.

209. Cypess AM, Lehman S, Williams G, Tal I, Rodman D, Goldfine AB, Kuo FC, Palmer EL, Tseng YH, Doria A, Kolodny GM, Kahn CR. Identification and importance of brown adipose tissue in adult humans. N Engl J Med. 2009; 360(15): 1509-17.

210. Claessens-van Ooijen AM, Westerterp KR, Wouters L, Schoffelen PF, van Steenhoven AA, van Marken Lichtenbelt WD. Heat production and body temperature during cooling and rewarming in overweight and lean men. Obesity (Silver Spring). 2006; 14(11): 1914-20.

211. Sramkova D, Krejbichova S, Vcelak J, Vankova M, Samalikova P, Hill M, Kvasnickova H, Dvorakova K, Vondra K, Hainer V, Bendlova B. The UCP1 gene polymorphism A-3826G in relation to DM2 and body composition in Czech population. Exp Clin Endocrinol Diabetes. 2007; 115(5): 303-7.

212. Liu Y, Qu Y, Cheng C, Tsai PY, Edwards K, Xue S, Pandit S, Eguchi S, Sanghera N, Barrow JJ. Nipsnap1-A regulatory factor required for long-term maintenance of non-shivering thermogenesis. Mol Metab. 2023; 75: 101770.

213. Wijers SL, Saris WH, van Marken Lichtenbelt WD. Cold-induced adaptive thermogenesis in lean and obese. Obesity (Silver Spring). 2010; 18(6): 1092-9.

214. Sell H, Berger JP, Samson P, Castriota G, Lalonde J, Deshaies Y, Richard D. Peroxisome proliferator-activated receptor gamma agonism increases the capacity for sympathetically mediated thermogenesis in lean and ob/ob mice. Endocrinology. 2004; 145(8): 3925-34.

215. Cypess AM, Weiner LS, Roberts-Toler C, Franquet Elía E, Kessler SH, Kahn PA, English J, Chatman K, Trauger SA, Doria A, Kolodny GM. Activation of human brown adipose tissue by a β3-adrenergic receptor agonist. Cell Metab. 2015; 21(1): 33-8.

216. Ferrannini E, Natali A, Bell P, Cavallo-Perin P, Lalic N, Mingrone G. Insulin resistance and hypersecretion in obesity. European Group for the Study of Insulin Resistance (EGIR). J Clin Invest. 1997; 100(5): 1166-73.

217. Roat R, Rao V, Doliba NM, Matschinsky FM, Tobias JW, Garcia E, Ahima RS, Imai Y. Alterations of pancreatic islet structure, metabolism and gene expression in diet-induced obese C57BL/6J mice. PLoS One. 2014; 9(2): e86815.

218. Small L, Ehrlich A, Iversen J, Ashcroft SP, Trošt K, Moritz T, Hartmann B, Holst JJ, Treebak JT, Zierath JR, Barrès R. Comparative analysis of oral and intraperitoneal glucose tolerance tests in mice. Mol Metab. 2022; 57: 101440.

219. Andrikopoulos S, Blair AR, Deluca N, Fam BC, Proietto J. Evaluating the glucose tolerance test in mice. Am J Physiol Endocrinol Metab. 2008; 295(6): E1323-32.

220. Gupta D, Jetton TL, LaRock K, Monga N, Satish B, Lausier J, Peshavaria M, Leahy JL. Temporal characterization of β cell-adaptive and -maladaptive mechanisms during chronic high-fat feeding in C57BL/6NTac mice. J Biol Chem. 2017; 292(30): 12449-12459.

221. Gao R, Fu Q, Jiang HM, Shen M, Zhao RL, Qian Y, He YQ, Xu KF, Xu XY, Chen H, Zhang Q, Yang T. Temporal metabolic and transcriptomic characteristics crossing islets and liver reveal dynamic pathophysiology in diet-induced diabetes. iScience. 2021; 24(4): 102265.

222. Færch K, Vistisen D, Pacini G, Torekov SS, Johansen NB, Witte DR, Jonsson A, Pedersen O, Hansen T, Lauritzen T, Jørgensen ME, Ahrén B, Holst JJ. Insulin Resistance Is Accompanied by Increased Fasting Glucagon and Delayed Glucagon Suppression in Individuals With Normal and Impaired Glucose Regulation. Diabetes. 2016; 65(11): 3473-3481.

223. Khin PP, Lee JH, Jun HS. A Brief Review of the Mechanisms of β-Cell Dedifferentiation in Type 2 Diabetes. Nutrients. 2021; 13(5): 1593.

224. Maassen JA, Janssen GM, 't Hart LM. Molecular mechanisms of mitochondrial diabetes (MIDD). Ann Med. 2005; 37(3): 213-21.

225. Oropeza D, Jouvet N, Bouyakdan K, Perron G, Ringuette LJ, Philipson LH, Kiss RS, Poitout V, Alquier T, Estall JL. PGC-1 co-activators in β-cells regulate lipid metabolism and are essential for insulin secretion coupled to fatty acids. Mol Metab. 2015; 4(11): 811-22.

226. Zhong F, Jiang Y. Endogenous Pancreatic β Cell Regeneration: A Potential Strategy for the Recovery of β Cell Deficiency in Diabetes. Front Endocrinol (Lausanne). 2019; 10: 101.

227. Cinti F, Bouchi R, Kim-Muller JY, Ohmura Y, Sandoval PR, Masini M, Marselli L, Suleiman M, Ratner LE, Marchetti P, Accili D. Evidence of β-Cell Dedifferentiation in Human Type 2 Diabetes. J Clin Endocrinol Metab. 2016; 101(3): 1044-54.

228. Matsuoka TA, Kaneto H, Miyatsuka T, Yamamoto T, Yamamoto K, Kato K, Shimomura I, Stein R, Matsuhisa M. Regulation of MafA expression in pancreatic beta-cells in db/db mice with diabetes. Diabetes. 2010; 59(7): 1709-20.

229. Talchai C, Xuan S, Lin HV, Sussel L, Accili D. Pancreatic β cell dedifferentiation as a mechanism of diabetic β cell failure. Cell. 2012; 150(6): 1223-34.

230. Zhou Q, Brown J, Kanarek A, Rajagopal J, Melton DA. In vivo reprogramming of adult pancreatic exocrine cells to beta-cells. Nature. 2008; 455(7213): 627-32.

231. Davidson EA, Chen Y, Singh S, Orlicky DJ, Thompson B, Wang Y, Charkoftaki G, Furnary TA, Cardone RL, Kibbey RG, Shearn CT, Nebert DW, Thompson DC, Vasiliou V. Endocrine pancreas-specific Gclc gene deletion causes a severe diabetes phenotype. bioRxiv [Preprint]. 2023: 2023.06.13.544855.

232. Ohtsubo K, Chen MZ, Olefsky JM, Marth JD. Pathway to diabetes through attenuation of pancreatic beta cell glycosylation and glucose transport. Nat Med. 2011; 17(9): 1067-75.

233. Haythorne E, Lloyd M, Walsby-Tickle J, Tarasov AI, Sandbrink J, Portillo I, Exposito RT, Sachse G, Cyranka M, Rohm M, Rorsman P, McCullagh J, Ashcroft FM. Altered glycolysis triggers impaired mitochondrial metabolism and mTORC1 activation in diabetic β-cells. Nat Commun. 2022; 13(1): 6754.

234. Haythorne E, Rohm M, van de Bunt M, Brereton MF, Tarasov AI, Blacker TS, Sachse G, Silva Dos Santos M, Terron Exposito R, Davis S, Baba O, Fischer R, Duchen MR, Rorsman P, MacRae JI, Ashcroft FM. Diabetes causes marked inhibition of mitochondrial metabolism in pancreatic β-cells. Nat Commun. 2019; 10(1): 2474.

235. Roche E, Assimacopoulos-Jeannet F, Witters LA, Perruchoud B, Yaney G, Corkey B, Asfari M, Prentki M. Induction by glucose of genes coding for glycolytic enzymes in a pancreatic beta-cell line (INS-1). J Biol Chem. 1997; 272(5): 3091-8.

236. Yamada Y, Miyawaki K, Tsukiyama K, Harada N, Yamada C, Seino Y. Pancreatic and Extrapancreatic Effects of Gastric Inhibitory Polypeptide. Diabetes. 2006; 55(2).

237. Vilsbøll T, Krarup T, Madsbad S, Holst JJ. Defective amplification of the late phase insulin response to glucose by GIP in obese Type II diabetic patients. Diabetologia. 2002; 45(8): 1111-9.

238. Nauck MA, Bartels E, Orskov C, Ebert R, Creutzfeldt W. Additive insulinotropic effects of exogenous synthetic human gastric inhibitory polypeptide and glucagon-like peptide-1-(7-36) amide infused at near-physiological insulinotropic hormone and glucose concentrations. J Clin Endocrinol Metab. 1993; 76(4): 912-7.

239. Mather KJ, Paradisi G, Leaming R, Hook G, Steinberg HO, Fineberg N, Hanley R, Baron AD. Role of amylin in insulin secretion and action in humans: antagonist studies across the spectrum of insulin sensitivity. Diabetes Metab Res Rev. 2002; 18(2): 118-26.

240. Zheng X, Ren W, Zhang S, Liu J, Li S, Li J, Yang P, He J, Su S, Li P. Association of type 2 diabetes susceptibility genes (TCF7L2, SLC30A8, PCSK1 and PCSK2) and proinsulin conversion in a Chinese population. Mol Biol Rep. 2012; 39(1): 17-23.

241. Strawbridge RJ, Dupuis J, Prokopenko I, Barker A, Ahlqvist E, Rybin D, Petrie JR, Travers ME, Bouatia-Naji N, Dimas AS, Nica A, Wheeler E, Chen H, Voight BF, Taneera J, Kanoni S, Peden JF, Turrini F, Gustafsson S, Zabena C, Almgren P, Barker DJ, Barnes D, Dennison EM, Eriksson JG, Eriksson P, Eury E, Folkersen L, Fox CS, Frayling TM, Goel A,

Gu HF, Horikoshi M, Isomaa B, Jackson AU, Jameson KA, Kajantie E, Kerr-Conte J, Kuulasmaa T, Kuusisto J, Loos RJ, Luan J, Makrilakis K, Manning AK, Martínez-Larrad MT, Narisu N, Nastase Mannila M, Ohrvik J, Osmond C, Pascoe L, Payne F, Sayer AA, Sennblad B, Silveira A, Stancáková A, Stirrups K, Swift AJ, Syvänen AC, Tuomi T, van 't Hooft FM, Walker M, Weedon MN, Xie W, Zethelius B; DIAGRAM Consortium; GIANT Consortium; MuTHER Consortium; CARDIoGRAM Consortium; C4D Consortium; Ongen H, Mälarstig A, Hopewell JC, Saleheen D, Chambers J, Parish S, Danesh J, Kooner J, Ostenson CG, Lind L, Cooper CC, Serrano-Ríos M, Ferrannini E, Forsen TJ, Clarke R, Franzosi MG, Seedorf U, Watkins H, Froguel P, Johnson P, Deloukas P, Collins FS, Laakso M, Dermitzakis ET, Boehnke M, McCarthy MI, Wareham NJ, Groop L, Pattou F, Gloyn AL, Dedoussis GV, Lyssenko V, Meigs JB, Barroso I, Watanabe RM, Ingelsson E, Langenberg C, Hamsten A, Florez JC. Genome-wide association identifies nine common variants associated with fasting proinsulin levels and provides new insights into the pathophysiology of type 2 diabetes. Diabetes. 2011 Oct;60(10):2624-34.

242. Martin SK, Carroll R, Benig M, Steiner DF. Regulation by glucose of the biosynthesis of PC2, PC3 and proinsulin in (ob/ob) mouse islets of Langerhans. FEBS Lett. 1994; 356(2-3): 279-82.

243. Alarcon C, Boland BB, Uchizono Y, Moore PC, Peterson B, Rajan S, Rhodes OS, Noske AB, Haataja L, Arvan P, Marsh BJ, Austin J, Rhodes CJ. Pancreatic β-Cell Adaptive Plasticity in Obesity Increases Insulin Production but Adversely Affects Secretory Function. Diabetes. 2016; 65(2): 438-50.

244. Asai Y, Morimoto H, Mabuchi Y, Sakuma E, Shirasawa N, Wada I, Horiuchi O, Herbert DC, Soji T. Influence of Experimental Diabetes Mellitus on Secretary Granules in beta-Cells in the Dog Pancreatic Islet. II. Relationship between the Spherical Granule and the Cored Vesicle. Biomedical Research. 2007; 18 (1): 9-13.

245. Wijesekara N, Dai FF, Hardy AB, Giglou PR, Bhattacharjee A, Koshkin V, Chimienti F, Gaisano HY, Rutter GA, Wheeler MB. Beta cell-specific Znt8 deletion in mice causes marked defects in insulin processing, crystallisation and secretion. Diabetologia. 2010; 53(8): 1656-68.

246. Rorsman P, Renström E. Insulin granule dynamics in pancreatic beta cells. Diabetologia. 2003; 46(8): 1029-45.

247. Andersson SA, Olsson AH, Esguerra JL, Heimann E, Ladenvall C, Edlund A, Salehi A, Taneera J, Degerman E, Groop L, Ling C, Eliasson L. Reduced insulin secretion correlates with decreased expression of exocytotic genes in pancreatic islets from patients with type 2 diabetes. Mol Cell Endocrinol. 2012; 364(1-2): 36-45.

248. Ostenson CG, Gaisano H, Sheu L, Tibell A, Bartfai T. Impaired gene and protein expression of exocytotic soluble N-ethylmaleimide attachment protein receptor complex proteins in pancreatic islets of type 2 diabetic patients. Diabetes. 2006; 55(2): 435-40.

249. Chen CW, Guan BJ, Alzahrani MR, Gao Z, Gao L, Bracey S, Wu J, Mbow CA, Jobava R, Haataja L, Zalavadia AH, Schaffer AE, Lee H, LaFramboise T, Bederman I, Arvan P, Mathews CE, Gerling IC, Kaestner KH, Tirosh B, Engin F, Hatzoglou M. Adaptation to chronic ER stress enforces pancreatic β-cell plasticity. Nat Commun. 2022; 13(1): 4621.

250. Engin F, Nguyen T, Yermalovich A, Hotamisligil GS. Aberrant islet unfolded protein response in type 2 diabetes. Sci Rep. 2014; 4: 4054.

251. Zhu X, Hu R, Brissova M, Stein RW, Powers AC, Gu G, Kaverina I. Microtubules Negatively Regulate Insulin Secretion in Pancreatic β Cells. Dev Cell. 2015; 34(6): 656-68.

252. Yang FT, Stanford KI. Batokines: Mediators of Inter-Tissue Communication (a Mini-Review). Curr Obes Rep. 2022; 11(1): 1-9**.**

253. Mukherjee P, Mani S. Methodologies to decipher the cell secretome. Biochim Biophys Acta. 2013; 1834(11): 2226-32.

254. Gianazza E, Brioschi M, Eligini S, Banfi C. Mass spectrometry for the study of adipocyte cell secretome in cardiovascular diseases. Mass Spectrom Rev. 2022: e21812.

255. Kahn D, Macias E, Zarini S, Garfield A, Zemski Berry K, MacLean P, Gerszten RE, Libby A, Solt C, Schoen J, Bergman BC. Exploring Visceral and Subcutaneous Adipose Tissue Secretomes in Human Obesity: Implications for Metabolic Disease. Endocrinology. 2022; 163(11): bqac140.

256. Roca-Rivada A, Bravo SB, Pérez-Sotelo D, Alonso J, Castro AI, Baamonde I, Baltar J, Casanueva FF, Pardo M. CILAIR-Based Secretome Analysis of Obese Visceral and Subcutaneous Adipose Tissues Reveals Distinctive ECM Remodeling and Inflammation Mediators. Sci Rep. 2015; 5: 12214**.**

257. Rangel-Azevedo C, Santana-Oliveira DA, Miranda CS, Martins FF, Mandarim-de-Lacerda CA, Souza-Mello V. Progressive brown adipocyte dysfunction: "whitening" and impaired nonshivering thermogenesis as long-term obesity complications. J Nutr Biochem. 2022; 105:109002.

258. Pellegrinelli V, Figueroa-Juárez E, Samuelson I, U-Din M, Rodriguez-Fdez S, Virtue S, Leggat J, Çubuk C, Peirce VJ, Niemi T, Campbell M, Rodriguez-Cuenca S, Blázquez JD, Carobbio S, Virtanen KA, Vidal-Puig A. Defective extracellular matrix remodeling in brown adipose tissue is associated with fibro-inflammation and reduced diet-induced thermogenesis. Cell Rep. 2023; 42(6): 112640.

259. Luzak B, Boncler M, Kosmalski M, Mnich E, Stanczyk L, Przygodzki T, Watala C. Fibrinogen Glycation and Presence of Glucose Impair Fibrin Polymerization-An In Vitro Study of Isolated Fibrinogen and Plasma from Patients with Diabetes Mellitus. Biomolecules. 2020; 10(6): 877.

260. Merghani MM, Hassan FM. Coagulation Disturbance among Essential Hypertensive and Diabetes Mellitus Type II Patients - Khartoum State. Bangladesh J. Medical Sci. 2016; 15(3): 424-429.

261. Beattie GM, Montgomery AM, Lopez AD, Hao E, Perez B, Just ML, Lakey JR, Hart ME, Hayek A. A novel approach to increase human islet cell mass while preserving beta-cell function. Diabetes. 2002; 51(12): 3435-9.

262. Yang C, Chao J, Hsu WH. The effect of bradykinin on secretion of insulin, glucagon, and somatostatin from the perfused rat pancreas. Metabolism. 1997; 46(10): 1113-5.

263. Rothschild AM, Reis ML, Melo VL, Foss MC, Gallo L Jr. Increased kininogen levels observed in plasma of diabetic patients are corrected by the administration of insulin. Horm Metab Res. 1999; 31(5): 326-8.

264. Federspil G, Vettor R, De Palo E, Padovan D, Sicolo N, Scandellari C. Plasma kallikrein activity in human diabetes mellitus. Metabolism. 1983; 32(6): 540-2.

265. Zuccollo A, Navarro M, Frontera M, Cueva F, Carattino M, Catanzaro OL. The involvement of kallikrein-kinin system in diabetes type I (insulitis). Immunopharmacology. 1999; 45(1-3): 69-74.

266. Tripathi D, Kant S, Pandey S, Ehtesham NZ. Resistin in metabolism, inflammation, and disease. FEBS J. 2020; 287(15): 3141-3149.

267. Cantley J. The control of insulin secretion by adipokines: current evidence for adipocyte-beta cell endocrine signalling in metabolic homeostasis. Mamm Genome. 2014; 25(9-10): 442-54.

268. Nakata M, Okada T, Ozawa K, Yada T. Resistin induces insulin resistance in pancreatic islets to impair glucose-induced insulin release. Biochem Biophys Res Commun. 2007 Feb; 353(4): 1046-51.

269. Wen F, Yang Y, Sun C, Fang H, Nie L, Li L, Liu Y, Yang Z. RESISTIN INHIBITS GLUCOSE-STIMULATED INSULIN SECRETION THROUGH MIR-494 BY TARGET ON STXBP5. Acta Endocrinol (Buchar). 2017; 13(1): 32-39.

# 8. ANNEX

**SUPPLEMENTARY TABLE 8.1: LIST OF PRIMERS USED IN THIS STUDY FOR REAL-TIME QUANTITATIVE PCR**

| Gene symbol | Entrez ID | Forward primer | Reverse primer |
|---|---|---|---|
| Aco2 | 11429 | TCTCTAACAACCTGCTCATCGG | TCATCTCCAATCACCACCCACC |
| AdipoQ | 11450 | TGTTCCTCTTAATCCTGCCCA | CCAACCTGCACAAGTTCCCTT |
| Adrb3 | 11556 | GGCCCTCTCTAGTTCCCAG | TAGCCATCAAACCTGTTGAGC |
| Atp5b | 11947 | GCAAGGCAGGGACAGCAGA | CCCAAGGTCTCAGGACCAACA |
| Ccl2 | 20296 | CAAGATGATCCCAATGAGTAG | TTGGTGACAAAAACTACAGC |
| Ccl7 | 20306 | GCTGCTTTCAGCATCCAAGTG | CCAGGGACACCGACTACTG |
| Cd11c | 16411 | CTGGATAGCCTTTCTTCTGCTG | GCACACTGTGTCCGAACTCA |
| Cfd | 11537 | TTTAAGCTATCCCAGAATGC | GATTGACACTCTGAGTTGATG |
| Chop | 13198 | CTGGAAGCCTGGTATGAGGAT | CAGGGTCAAGAGTAGTGAAGGT |
| Cidea | 12683 | CCTCGGCTGTCTCAATGTC | GGCTGCTCTTCTGTATGC |
| **Cox7a1** | 12865 | GACAATGACCTCCCAGTACAC | GCCCAGCCCAAGCAGTATAAG |
| **Coxii** | 17709 | TCTCCCCTCTCTACGCATTCTA | ACGGATTGGAAGTTCTATTGGC |
| **Coxiv** | 12857 | CCATGTCACGATGCTGTCTG | GATGCGGTACAACTGAACTTTCT |
| **Cycs** | 13063 | CACGGCTCTCCCTTTCTCAAG | ACAGTTGCCTCCTGGTGGTTA |
| **Dio2** | 13371 | CAGCTTCCTCCTAGATGCCTA | CTGATTCAGGATTGGAGACGTG |
| **Foxo1** | 56458 | AAACACATATTGAGCCACTG | TCTACTCTGTTTGAAGGAGG |
| **Gapdh** | 14433 | TCAACGGGAAGCCCATCA | CTCGTGGTTCACACCCATCA |
| **Gcg** | 14526 | ACCTTTACCAGTGATGTGAG | GTGGCAAGATTATCCAGAATG |
| **Gck** | 103988 | AGGAGGCCAGTGTAAAGATGT | CTCCCAGGTCTAAGGAGAGAAA |
| **Glp1r** | 14652 | ACAGTGGGGTACGCACTTTC | CGGAGGATGAAGGATGCAAAC |
| **Glut1** | 20525 | ATCTCCACACTGTAGTCTTC | AGCTCAGAGTTCGGTATTAG |
| **Glut2** | 20526 | TTGTGCTGCTGGATAAATTC | AAATTCAGCAACCATGAACC |
| **Iapp** | 15874 | CTGAAAGGGATCTTGAGAAATG | GAACGAACCAAAAAGTTTGC |
| **Igfbp3** | 16009 | CTGAATCATCTGAAGTTCCTC | GGCACTGCTTCTTCTTATAG |
| **Il1b** | 16176 | GAAATGCCACCTTTTGACAGTG | TGGATGCTCTCATCAGGACAG |
| **Ins1** | 16333 | GAGGTACTTTGGACTATAAAGC | TTGAAACAATGACCTGCTTG |
| **Ins2** | 16334 | AGCAGGAAGGTTATTGTTTC | ACATGGGTGTGTAGAAGAAG |
| **Leptin** | 16846 | GACACCAAAACCCTCATCAAGAC | GGTGAAGCCCAGGAATGAAGT |
| **Lhx8** | 16875 | GGCAGAAAGGACAGGCTTAAG | GAGGAAGAATGGTTGGGACTG |
| **Mafa** | 378435 | CATCCGACTGAAACAGAAG | ATTTCTCCTTGTACAGGTCC |
| **Mdh2** | 17448 | GCCCAGGAAACCAGGAATG | GATGGGGATGGTGGAGTTCA |
| **Meox2** | 17286 | GAGAAGAGAAGTGGCAGCAAA | TTCTGGAACCACACTTTCACC |
| **Nd2** | 17717 | ATACTTCGTCACACAAGCAACA | GGCCTAGTTTTATGGATAGGGCT |
| **Ndufb9** | 66218 | AAGGTGCTGCGGCTGTATAAG | TACGGCTGAGGATGCTGATTC |
| **Nkx6.1** | 18096 | GAGAGTCAGGTCAAGGTC | TTGTTGTAATCGTCGTCATC |
| **Nos2** | 18126 | TTTTGCATGACACTCTTCAC | ACTGGTTGATGAACTCAATG |
| **Pax6** | 18508 | TTTGAGAGGACCCATTATCC | AACCATACCTGTATTCTTGC |
| **Pcsk1** | 18548 | GAGGCAAACCCAAATCTTAC | TAGCAAGCCAAATCCAAATC |
| **Pcsk2** | 18549 | ACTGCCTTGTATGATGAGAG | TCAGAGTACAGTTGCCATAC |
| **Pdk1** | 228026 | AGGATCTGACTGTGAAGATG | TGGAAGTACTGTGCATAGAG |
| **Pdk4** | 27273 | GTTCCTTCACACCTTCACCAC | CCTCCTCGGTCAGAAATCTTG |
| **Ppargc1a** | 19017 | GGAGCCGTGACCACTGACA | TGGTTTGCTGCATGGTTCTG |
| **Ppargc1b** | 170826 | AGTGGGTGCGGAGACACAGATG | GTATGGAGGTGTGGTGGGTGGC |

| | | | |
|---|---|---|---|
| **Prdm16** | 70673 | AAGATGGAAATCGGGGAGAGG | CAGGAACACGCTACACGGATG |
| **Resistin** | 57264 | AAGAACCTTTCATTTCCCCTCCT | GTCCAGCAATTTAAGCCAATGTT |
| **Sdhb** | 67680 | TACCGATGGGACCCAGACA | CGTGTGCACGCCAGAGTAT |
| **Sst** | 20604 | CAACCAGACAGAGAATGATG | AACAGGATGTGAATGTCTTC |
| **Stx1a** | 20907 | AGATGATTGACAGGATCGAG | GTGGTTTCTATCCAAAGATGC |
| **Syp** | 20977 | AGATCTTCCTAGTTGGTGAC | CTAACTAGCCACATGAAAGC |
| **Tnfa** | 21926 | CTTCTCATTCCTGCTTGTGGC | ACTTGGTGGTTTGCTACGACG |
| **Ucp1** | 22227 | AGCCATCTGCATGGGATCAAA | GGGTCGTCCCTTTCCAAAGTG |
| **Unc13b** | 22249 | ACTCTATGCAGAGTTACGAC | ACTAGAATGAATGGAGTCCC |
| **Uqcr10** | 66152 | CGAGCGAGCCTTCGATCAG | GTTTCCCCTCGTTGATGTGCT |
| **Vamp2** | 22318 | ATCATCGTTTACTTCAGCAC | TGAAAGATATGGCTGAGAGG |
| **Xbp1** | 22433 | GAAGAAGAGAACCACAAACTC | GTGTTCTTAACTCCTGGTTC |
| **Zic1** | 22771 | CCACAAAAGGACACACACAGG | GGGGTGCGTGTAGGACTTATC |

**Supplementary Table 8.1. List of primers used in this study for real-time quantitative PCR.**

**SUPPLEMENTARY TABLE 8.2: LIST OF PEPTIDES ORDERED FOR THE *TARGETED* PROTEOMICS STUDY**

| Protein ID | Peptide sequence | Molecular Weight |
|---|---|---|
| O08677 | AYFP[C(CAM)]IG[C(CAM)]VHAISTDSPDLEPVL(K) | 2,698.13 |
| | EVLGHSIAQLNAENDHPFYY(K) | 2,453.67 |
| | DAEEAATGE[C(CAM)]TATVGK(R) | 1,775.90 |
| P00920 | AVQQPDGLAVLGIFL(K) | 1,677.01 |
| | YAAELHLVHWNT(K) | 1,589.80 |
| | PALQPLLISYD(K) | 1,365.62 |
| P01027 | VDVPAADLSDQVPDTDSET(R) | 2,140.22 |
| | YVTVVANFGETVVE(K) | 1,662.88 |
| | SELEEDIIPEEDIIS(R) | 1,897.04 |
| P01887 | ILAHTEFTPTETDTYA[C(CAM)](R) | 2,136.35 |
| | TPQIQVYS(R) | 1,101.23 |
| | DWSFYILAHTEFTPTETDTYA[C(CAM)](R) | 2,835.08 |
| **P02469** | LHTLGDNLLDS(R) | 1,363.51 |
| | EGFYDLSAEDPYG[C(CAM)](K) | 1,758.87 |
| | YSDIEPSTEGEVIF(R) | 1,751.88 |
| **P03953** | GDSGSPLV[C(CAM)]GDAVEGVVTWGS(R) | 2,215.41 |
| | RPDVLHQL(R) | 1,143.33 |
| | LSQNASLGPHVRPLPLQYED(K) | 2,370.68 |
| **P04186** | YGQTLRPI[C(CAM)]LP[C(CAM)]TEGTT(R) | 2,133.47 |
| | STGSWSDLQT(R) | 1,247.30 |
| | DLEIEEVLFHP(K) | 1,476.68 |
| **P06909** | T[C(CAM)]GDIPELEHGSA(K) | 1,521.67 |
| | [C(CAM)]TAQGWEPEVP[C(CAM)]V(R) | 1,698.94 |
| | IYSHSGEDIEFG[C(CAM)](K) | 1,649.79 |
| **P07309** | TAESGELHGLTTDE(K) | 1,595.67 |
| | TLGISPFHEFADVVFTANDSGH(R) | 2,527.75 |
| | TSEGSWEPFASG(K) | 1,390.46 |
| **P07758** | IFNNGADLSGITEENAPL(K) | 2,011.21 |
| | DQSPASHEIATNLGDFAISLY(R) | 2,415.61 |
| | VINDFVEKGTQG(K) | 1,442.62 |
| **P08113** | ELISNASDALD(K) | 1,283.39 |
| | GVVDSDDLPLNVS(R) | 1,495.62 |
| | EESDDEAAVEEEEEE(K) | 1,874.79 |
| **P08226** | ELEEQLGPVAEET(R) | 1,609.73 |
| | TANLGAGAAQPL(R) | 1,249.41 |
| | LQAEIFQA(R) | 1,085.24 |
| **P08905** | GDQSTDYGIFQINS(R) | 1,710.78 |
| | AVNA[C(CAM)]GIN[C(CAM)]SALLQDDITAAIQ[C(CAM)]A(K) | 2,686.11 |
| | STDYGIFQINS(R) | 1,410.51 |
| **P10923** | LYSLHPDPIATWLVPDPSQ(K) | 2,285.61 |
| | LPVKVTDSGSSEE(K) | 1,483.62 |
| | ESQESADQSDVIDSQASS(K) | 2,019.01 |
| **P11087** | SGEYWIDPNQG[C(CAM)]NLDAI(K) | 2,088.28 |

| | | |
|---|---|---|
| | ALLLQGSNEIEL(R) | 1,465.68 |
| | FTYSTLVDG[C(CAM)]TSHTGTWG(K) | 2,126.33 |
| **P11276** | HALQSASAGSGSFTDV(R) | 1,700.80 |
| | TYLGNALV[C(CAM)]T[C(CAM)]YGGS(R) | 1,802.05 |
| | FLTTTPNSLLVSWQAP(R) | 1,941.23 |
| **P11680** | S[C(CAM)]LHVPV[C(CAM)]KDPEE(K) | 1,705.99 |
| | S[C(CAM)]SAPAPSHQPPGKP[C(CAM)]SGPAYEH(K) | 2,555.84 |
| | VED[C(CAM)][C(CAM)]LNAAYAFQEHDGGL[C(CAM)]QA[C(CAM)](R) | 2,855.19 |
| **P12032** | LESDTH[C(CAM)]LWTDQVLVGSEDYQS(R) | 2,748.95 |
| | HFA[C(CAM)]LP(R) | 910.09 |
| | TYSAG[C(CAM)]GV[C(CAM)]TVFP[C(CAM)]LSIP[C(CAM)](K) | 2,285.75 |
| **P13020** | SGALNSNDAFVL(K) | 1,343.49 |
| | VPVDPATYGQFYGGDSYIILYNY(R) | 2,782.05 |
| | SQHVQVEEGSEPDAFWEALGG(K) | 2,408.55 |
| **P13634** | EIVNVGHSFHVIFDDSSNQSVL(K) | 2,579.84 |
| | YSGELHLVHWNSA(K) | 1,648.82 |
| | TSEANHDSSLKPLSISYNPATA(K) | 2,439.64 |
| **P14211** | VHVIFNY(K) | 1,027.21 |
| | HEQNID[C(CAM)]GGGYV(K) | 1,484.61 |
| | I)DPDAAKPEDWDE(R) | 1,666.74 |
| **P18242** | GG[C(CAM)]EAIVDTGTSLLVGPVEEV(K) | 2,238.55 |
| | YYHGELSYLNVT(R) | 1,624.77 |
| | ILDIA[C(CAM)]WVHH(K) | 1,399.68 |
| **P21460** | ALDFAVSEYN(K) | 1,264.38 |
| | AL[C(CAM)]SFQIYSVPW(K) | 1,606.90 |
| | KAL[C(CAM)]SFQIYSVPW(K) | 1,735.07 |
| **P22599** | LVQIHIP(R) | 985.21 |
| | LSISGDYNL(K) | 1,117.25 |
| | ELDQDTVFALANYILF(K) | 2,008.28 |
| **P28665** | TTLVTIQSTGSFSQ(K) | 1,605.79 |
| | LQVTASPQSL[C(CAM)]GL(R) | 1,539.80 |
| | FSTSQSLPASQT(R) | 1,419.53 |
| **P29699** | PPASVVVGPVVVP(R) | 1,382.68 |
| | HAFSPVASVESASGETLHSP(K) | 2,146.33 |
| | AQNVPLPVSTLVEFVIAATD[C(CAM)]TA(K) | 2,552.98 |
| **P39061** | TETTGATGQASSLLSG(R) | 1,646.74 |
| | VSPVH[C(CAM)]LDEEDDDED(R) | 1,939.97 |
| | GADFQ[C(CAM)]FQQA(R) | 1,337.46 |
| **P46412** | YVRPGGGFVPNFQLFE(K) | 1,963.25 |
| | FLVGPDGIPVM(R) | 1,310.60 |
| | NS[C(CAM)]PPTAELLGSPG(R) | 1,565.75 |
| **P47879** | EEPRPVPQGS[C(CAM)]QSELH(R) | 2,016.21 |
| | THEDLFIIPIPN[C(CAM)]D(R) | 1,850.11 |
| | [C(CAM)]RPPVG[C(CAM)]EELV(R) | 1,481.76 |
| **P55065** | FLEQELETITIPDVYGA(K) | 2,074.34 |
| | TGLQLSQDSSG(R) | 1,258.32 |
| | GVQIPLPEGINFV(R) | 1,548.82 |
| **P70663** | GHQLQLDYFGA[C(CAM)](K) | 1,544.75 |

| | | |
|---|---|---|
| | ILTHSELAPL(R) | 1,259.49 |
| | LLAGDHPIELLL(R) | 1,469.76 |
| **P82198** | IPAETLN(R) | 923.05 |
| | GDELADSALEIF(K) | 1,415.55 |
| | STVISYE[C(CAM)][C(CAM)]PGYE(K) | 1,700.91 |
| **P97290** | GVTSVSQIFHSPDLAI(R) | 1,837.08 |
| | VLGPDSAANLELINTWVAENTNH(K) | 2,614.89 |
| | LSEALTDFSV(K) | 1,217.37 |
| **P97298** | LTFPLDYHLNQPFLFVL(R) | 2,243.65 |
| | ALYYDLITNPDIHSTY(K) | 2,035.25 |
| | LAAAVSNFGYDLY(R) | 1,569.74 |
| **Q00724** | LQNLDGT[C(CAM)]ADSYSFVFS(R) | 2,090.28 |
| | YWGVASFLQ(R) | 1,236.40 |
| | FSGLWYAIA(K) | 1,163.36 |
| **Q02819** | YLQEVINVLETDGHF(R) | 1,943.16 |
| | LSQELDFVSHNV(R) | 1,553.71 |
| | LVTLEEFLASTQ(R) | 1,516.73 |
| **Q60590** | RPDITPEL(R) | 1,106.26 |
| | YEGGVETFAHLIVL(R) | 1,713.96 |
| | ESQTIGDQ[C(CAM)]VYNSTHLGFQ(R) | 2,350.53 |
| **Q60994** | IFYNQQNHYDGSTG(K) | 1,779.86 |
| | AVLFTYDQYQE(K) | 1,512.66 |
| | SAFSVGLET(R) | 1,076.19 |
| **Q61147** | TESSTVVPTLPGEV(R) | 1,581.76 |
| | EDSA[C(CAM)]IPWAYYSTVD(R) | 1,943.09 |
| | DLYSGLIGPLIV[C(CAM)](R) | 1,585.91 |
| **Q61171** | EGGLGPLNIPLLADVT(K) | 1,715.01 |
| | SAPDFTATAVVDGAF(K) | 1,604.77 |
| | LG[C(CAM)]EVLGVSVDSQFTHLAWINTP(R) | 2,710.10 |
| **Q61508** | [C(CAM)][C(CAM)]ELPYPEQA[C(CAM)][C(CAM)]GEEE(K) | 2,167.44 |
| | AGPAVPQEAIPLQ(K) | 1,426.67 |
| | AWEGTLDGY[C(CAM)]E(R) | 1,466.57 |
| **Q64695** | TESGLQIYLTQFESLV(K) | 1,964.23 |
| | TAVWVSGSQEPS(K) | 1,383.51 |
| | YELQEFLQDT[C(CAM)]VEFLENHITTQNM(K) | 3,139.51 |
| **Q80Z24** | VIVNFAPTIQEI(K) | 1,479.77 |
| | DQAGEYE[C(CAM)]SAENDVSFPDV(K) | 2,268.35 |
| | SSIIFAGGD(K) | 1,002.12 |
| **Q91X72** | ELGSPPGISLETIDAAFS[C(CAM)]PGSS(R) | 2,458.72 |
| | GE[C(CAM)]QSEGVLFFQGN(R) | 1,737.90 |
| | SGAQATWTEVSWPHE(K) | 1,821.95 |
| **Q921I1** | AVSSFFSGS[C(CAM)]VP[C(CAM)]ADPVAFP(K) | 2,238.59 |
| | L[C(CAM)]QL[C(CAM)]PG[C(CAM)]G[C(CAM)]SSTQPFFGYVGAF(K) | 2,750.23 |
| | DFQLFSSPLG(K) | 1,246.41 |
| **Q8BPB5** | [C(CAM)]VNHYGGYL[C(CAM)]LP(K) | 1,588.87 |
| | GSFT[C(CAM)]Q[C(CAM)]LPGYQ(K) | 1,553.79 |
| | [C(CAM)]VNHYGGYL[C(CAM)]LP(K) | 1,588.87 |
| **Q8QZR4** | ALEQAELP(R) | 1,036.17 |

| | | |
|---|---|---|
| | SYTFDFYVPQ(K) | 1,402.54 |
| | GQSQFQAL[C(CAM)]FVT(R) | 1,551.77 |
| **Q8VCM7** | YEALLLTHETSI(R) | 1,555.76 |
| | VAQLEAQ[C(CAM)]QEP[C(CAM)](K) | 1,568.81 |
| | DN[C(CAM)][C(CAM)]ILDE(R) | 1,204.35 |
| **Q9CZT5** | TPEGEEA[C(CAM)]GEANTSQAV(R) | 1,916.00 |
| | ENHVVLASPEET(R) | 1,490.61 |
| | HIQPGAFDALD(R) | 1,349.48 |
| **Q9QXC1** | RVLYLPAYN[C(CAM)]TLRPVS(K) | 2,058.47 |
| | GSIQHLPELDDEKPEES(K) | 2,059.21 |
| | LVVLPFPG(K) | 977.24 |
| **Q9WVJ3** | VGAVASLIQSVASFSIYSPHTGIQ(K) | 2,568.94 |
| | LGLLVDTVGP(R) | 1,149.37 |
| | IIVYNQPYTGYE(K) | 1,595.78 |
| **Q9Z1T2** | NPEQNP[C(CAM)]SVHAQ[C(CAM)]IEE(R) | 2,078.27 |
| | DVDIDSYPDEELP[C(CAM)]SA(R) | 1,991.10 |
| | [C(CAM)]GP[C(CAM)]KPGYTGDQT(R) | 1,606.79 |

**Supplementary Table 8.2. List of peptides ordered for *targeted* proteomics.**

**SUPPLEMENTARY TABLE 8.3: GENE ENRICHMENT ANALYSIS OF UP-REGULATED PROTEINS IN BAT SECRETED MEDIA FROM PGC-1α/β-FAT-DKO MICE**

| Category | GO term | #Genes | *P*-Value |
|---|---|---|---|
| **GOTERM_BP** | Extracellular matrix organization | 26 | 2,30E-16 |
| **GOTERM_BP** | Negative regulation of peptidase activity | 18 | 2,40E-11 |
| **GOTERM_BP** | Angiogenesis | 25 | 5,20E-11 |
| **GOTERM_BP** | Wound healing | 16 | 2,90E-10 |
| **GOTERM_BP** | Negative regulation of endopeptidase activity | 14 | 8,10E-10 |
| **GOTERM_BP** | Haemostasis | 11 | 2,40E-09 |
| **GOTERM_BP** | Blood coagulation | 13 | 4,50E-09 |
| **GOTERM_BP** | Proteolysis | 32 | 6,60E-09 |
| **GOTERM_BP** | Cell adhesion | 32 | 1,10E-08 |
| **GOTERM_BP** | Negative regulation of angiogenesis | 13 | 6,90E-08 |
| **GOTERM_BP** | Fibrinolysis | 7 | 7,10E-08 |
| **GOTERM_BP** | Aging | 17 | 9,40E-08 |
| **GOTERM_BP** | Response to mechanical stimulus | 11 | 1,10E-07 |
| **GOTERM_BP** | Response to hypoxia | 16 | 1,30E-06 |
| **GOTERM_BP** | Acute-phase response | 8 | 1,70E-06 |
| **GOTERM_BP** | Positive regulation of ERK1 and ERK2 cascade | 17 | 1,80E-06 |
| **GOTERM_BP** | Inflammatory response | 22 | 1,80E-06 |
| **GOTERM_BP** | Positive regulation of cell migration | 17 | 7,60E-06 |
| **GOTERM_BP** | Negative regulation of fibrinolysis | 5 | 1,30E-05 |
| **GOTERM_BP** | Collagen catabolic process | 7 | 2,10E-05 |
| **GOTERM_CC** | Extracellular region | 156 | 2,50E-75 |
| **GOTERM_CC** | Extracellular space | 151 | 3,30E-67 |
| **GOTERM_CC** | Extracellular matrix | 42 | 2,30E-27 |
| **GOTERM_CC** | Basement membrane | 27 | 1,30E-22 |
| **GOTERM_CC** | Endoplasmic reticulum | 61 | 5,50E-10 |
| **GOTERM_CC** | Collagen trimer | 13 | 4,70E-09 |
| **GOTERM_CC** | Smooth endoplasmic reticulum | 9 | 2,50E-08 |
| **GOTERM_CC** | Melanosome | 13 | 4,80E-08 |
| **GOTERM_CC** | Cell surface | 35 | 8,20E-08 |
| **GOTERM_CC** | Endoplasmic reticulum lumen | 13 | 2,60E-07 |
| **GOTERM_CC** | Lysosome | 25 | 4,10E-07 |
| **GOTERM_CC** | Golgi apparatus | 48 | 1,10E-06 |
| **GOTERM_CC** | Sarcolemma | 13 | 1,80E-06 |
| **GOTERM_CC** | Macromolecular complex | 35 | 3,80E-06 |
| **GOTERM_CC** | Perinuclear region of cytoplasm | 31 | 1,40E-05 |
| **GOTERM_CC** | Caveola | 10 | 1,80E-05 |
| **GOTERM_CC** | External side of plasma membrane | 28 | 2,10E-05 |

| | | | |
|---|---|---|---|
| **GOTERM_CC** | Synapse | 35 | 2,30E-05 |
| **GOTERM_CC** | Endoplasmic reticulum chaperone complex | 5 | 2,60E-05 |
| **GOTERM_CC** | Fibrinogen complex | 4 | 7,30E-05 |

**Supplementary Table 8.3. Gene enrichment analysis of up-regulated proteins in BAT secreted media from PGC-1α/β-FAT-DKO using DAVID bioinformatic source (*P*≤0.05; FC>2).** The "Biological Process" (GOTERM_BP) and "Cellular compartment" (GOTERM_CC) terms are shown. The 20 lowest *P*-value categories from each term are displayed.

**SUPPLEMENTARY TABLE 8.4: GENE ENRICHMENT ANALYSIS OF DOWN-REGULATED PROTEINS IN BAT SECRETED MEDIA FROM PGC-1α/β-FAT-DKO MICE**

| Category | GO term | #Genes | P-Value |
|---|---|---|---|
| **GOTERM_BP** | Mitochondrial ATP synthesis coupled proton transport | 23 | 2,40E-24 |
| **GOTERM_BP** | Aerobic respiration | 23 | 6,80E-23 |
| **GOTERM_BP** | Tricarboxylic acid cycle | 16 | 3,40E-19 |
| **GOTERM_BP** | Mitochondrial respiratory chain complex I assembly | 17 | 8,60E-16 |
| **GOTERM_BP** | Mitochondrial electron transport, NADH to ubiquinone | 11 | 2,60E-12 |
| **GOTERM_BP** | Response to oxidative stress | 17 | 6,60E-10 |
| **GOTERM_BP** | 2-oxoglutarate metabolic process | 8 | 3,10E-09 |
| **GOTERM_BP** | Cellular respiration | 9 | 3,40E-09 |
| **GOTERM_BP** | Fatty acid metabolic process | 19 | 3,70E-09 |
| **GOTERM_BP** | Respiratory electron transport chain | 9 | 4,80E-09 |
| **GOTERM_BP** | Succinate metabolic process | 6 | 1,70E-08 |
| **GOTERM_BP** | Mitochondrial electron transport, ubiquinol to | 7 | 1,90E-08 |
| **GOTERM_BP** | Fatty acid beta-oxidation using acyl-CoA dehydrogenase | 6 | 5,90E-07 |
| **GOTERM_BP** | Succinyl-CoA metabolic process | 5 | 1,80E-06 |
| **GOTERM_BP** | Mitochondrial electron transport, cytochrome c to oxygen | 6 | 1,00E-05 |
| **GOTERM_BP** | Fatty acid beta-oxidation | 8 | 1,00E-05 |
| **GOTERM_BP** | Apoptotic mitochondrial changes | 6 | 2,70E-05 |
| **GOTERM_BP** | NADH metabolic process | 5 | 1,10E-04 |
| **GOTERM_BP** | Fatty acid biosynthetic process | 8 | 1,40E-04 |
| **GOTERM_BP** | Electron transport chain | 5 | 2,20E-04 |
| **GOTERM_CC** | Mitochondrion | 168 | 2,60E-90 |
| **GOTERM_CC** | Mitochondrial inner membrane | 71 | 4,50E-46 |
| **GOTERM_CC** | Respiratory chain | 27 | 1,80E-31 |
| **GOTERM_CC** | Mitochondrial matrix | 38 | 1,90E-26 |
| **GOTERM_CC** | Mitochondrial respiratory chain complex I | 20 | 6,30E-22 |
| **GOTERM_CC** | Myelin sheath | 30 | 7,60E-21 |
| **GOTERM_CC** | Mitochondrial intermembrane space | 21 | 5,90E-17 |
| **GOTERM_CC** | Mitochondrial respiratory chain complex IV | 10 | 3,70E-11 |
| **GOTERM_CC** | Mitochondrial membrane | 15 | 2,40E-07 |
| **GOTERM_CC** | Mitochondrial intermembrane space protein transporter complex | 5 | 2,50E-07 |
| **GOTERM_CC** | Mitochondrial respiratory chain complex III | 6 | 5,40E-07 |
| **GOTERM_CC** | Mitochondrial nucleoid | 7 | 7,90E-05 |
| **GOTERM_CC** | Cortical cytoskeleton | 5 | 1,10E-03 |
| **GOTERM_CC** | Extrinsic component of mitochondrial inner membrane | 4 | 2,00E-03 |
| **GOTERM_CC** | Oxoglutarate dehydrogenase complex | 3 | 2,20E-03 |

| | | | |
|---|---|---|---|
| **GOTERM_CC** | Cytosol | 86 | 2,20E-03 |
| **GOTERM_CC** | Mitochondrial inner membrane protein insertion | 3 | 4,50E-03 |
| **GOTERM_CC** | Pyruvate dehydrogenase complex | 3 | 5,90E-03 |
| **GOTERM_CC** | Mitochondrial pyruvate dehydrogenase complex | 3 | 5,90E-03 |
| **GOTERM_CC** | Perinuclear region of cytoplasm | 23 | 6,20E-03 |

**Supplementary Table 8.4. Gene enrichment analysis of down-regulated proteins in BAT secreted media from PGC-1α/β-FAT-DKO using DAVID bioinformatic source (*P*≤0.05; FC>2).** The "Biological Process" (GOTERM_BP) and "Cellular compartment" (GOTERM_CC) terms are shown. The 20 lowest *P*-value categories from each term are displayed.

**SUPPLEMENTARY TABLE 8.5: PROTEINS DIFFERENTLY FOUND IN SECRETED MEDIA OF GONADAL AND INGUINAL WAT DEPOTS FROM WT AND PGC-1α/β-FAT-DKO MICE**

| Tissue | Proteins ID | Gene symbol | *P*-Value | Fold Change | Highest condition |
|---|---|---|---|---|---|
| Gonadal WAT | **Q8C0D9** | Cep68 | 0.017 | 2.655 | DKO |
| | **Q9JIK5** | Ddx21 | 0.033 | 2.040 | DKO |
| | **O35181** | Nrg3 | 0.015 | 2.257 | WT |
| | **P03953** | Cfd | 0.019 | 52.814 | WT |
| | **P12804** | Fgl2 | 0.024 | 2.759 | WT |
| | **P21460** | Cst3 | 0.035 | 2.081 | WT |
| | **P28862** | Mmp3 | 0.032 | 2.200 | WT |
| | **P45700** | Man1a | 0.019 | 2.942 | WT |
| | **P50228** | Cxcl5 | 0.049 | 3.101 | WT |
| | **P97290** | Serping1 | 0.035 | 2.232 | WT |
| | **Q03350** | Thbs2 | 0.049 | 2.861 | WT |
| | **Q08761** | Pros1 | 0.031 | 3.029 | WT |
| | **Q60994** | Adipoq | 0.043 | 2.322 | WT |
| | **Q8CG14** | C1s1 | 0.045 | 2.098 | WT |
| | **Q9D668** | Arrdc2 | 0.006 | 2.808 | WT |
| | **Q9D9T0** | Dydc1 | 0.006 | 2.241 | WT |
| | **Q9QUR8** | Sema7a | 0.025 | 2.113 | WT |
| | **Q9Z0E6** | Gbp2 | 0.029 | 3.671 | WT |
| Inguinal WAT | **P62334** | Psmc6 | 0.001 | 2.026 | DKO |
| | **P08071** | Ltf | 0.003 | 2.019 | WT |

**Supplementary Table 8.5. Proteins differently found in the secreted media of gonadal and inguinal WAT depots from Wt and PGC-1α/β-FAT-DKO (*P*≤0.05; FC>2).**

**SUPPLEMENTARY TABLE 8.6: ACTIVELY SECRETED PROTEINS BY GONADAL AND INGUINAL WAT DEPOTS FROM WT AND PGC-1α/β-FAT-DKO MICE**

| Tissue | Proteins ID | Gene symbol | SignalP | TargetP | SecretomeP | Highest condition |
|---|---|---|---|---|---|---|
| Gonadal WAT | **P03953** | Cfd | 0.807 | 0.859 | 0.852 | WT |
| | **P21460** | Cst3 | 0.933 | 0.957 | 0.928 | WT |
| | **Q03350** | Thbs2 | 0.818 | 0.839 | 0.74 | WT |
| Inguinal WAT | **P08071** | Ltf | 0.915 | 0.953 | 0.793 | WT |

**Supplementary Table 8.6. Secreted proteins by gonadal and inguinal WAT depots that differ between Wt and PGC-1α/β-FAT-DKO.** Proteins differently found in secreted media of adipose tissues ($P \leq 0.05$; FC>2) were filtrated with the VerSeDa platform (SignalP and TargetP > 0.8; SecretomeP > 0.7) and curated to eliminate mitochondrial and nuclear proteins. Only 3 proteins in gonadal WAT and 1 in inguinal WAT were obtained, all being more secreted by Wt mice.